DISSERTATION

DEVELOPMENT, CHARACTERIZATION, AND DEPLOYMENT OF A HIGH-RESOLUTION TIME-OF-FLIGHT CHEMICAL IONIZATION MASS SPECTROMETER (HR-TOF-CIMS) FOR THE DETECTION OF CARBOXYLIC ACIDS AND TRACE-GAS SPECIES IN THE TROPOSPHERE

Submitted by

Patrick M. Brophy

Department of Chemistry

In partial fulfillment of the requirements

For the Degree of Doctor of Philosophy

Colorado State University

Fort Collins, Colorado

Summer 2016

Doctoral Committee:

Advisor: Delphine Farmer

Elliot R. Bernstein
Brian McNaughton
Jeffery R. Pierce
Akkihebbal R. Ravishankara

ABSTRACT

DEVELOPMENT, CHARACTERIZATION, AND DEPLOYMENT OF A HIGH-RESOLUTION TIME-OF-FLIGHT CHEMICAL IONIZATION MASS SPECTROMETER (HR-TOF-CIMS) FOR THE DETECTION OF CARBOXYLIC ACIDS AND TRACE-GAS SPECIES IN THE TROPOSPHERE

A historical account of the advances leading to modern high-resolution time-of-flight chemical ionization mass spectrometers (HR-TOF-CIMS) for gas-phase measurements is presented. Recent literature detailing the description of the HR-TOF-CIMS is critically evaluated and put into the context of the historical literature. The development of the HR-TOF-CIMS with reagent ion switching capabilities in the negative mode (acetate and iodide reagent ions), and a novel, low-pressure high-flow inlet with online calibration system is shown to work well in the field. Findings from the deployment of this measurement system during the 2013 Southern Oxidant and Aerosol Study are discussed. Subsequent work with voltage scanning methodologies for controlling cluster transmission is presented and applied to potential aerosol mass chamber experiments examining the oxidation of -pinene. The applicability of acetate

chemical ionization to the direct headspace analysis of beer samples is presented. Lastly, the future directions of acetate chemical ionization and voltage scanning are discussed in relation to numerous recent developments related to both gas-phase measurements and new particle formation.

ACKNOWLEDGEMENTS

I would like to thank my friends and family for their unwavering support of my pursuit of education and self-development. I would like to thank my advisor, Dr. Delphine Farmer, for her trust and support in my work both in the field and in laboratory. The opportunity to take part in building her laboratory and research group as her first graduating Ph.D. student has had an immense impact on my view of my relationship toward the work presented here. I would like to thank the various members from the Farmer Group with whom I have had the pleasure of working. Lastly, I would like to acknowledge the various principle investigators, organizers, contributors, and funding agencies involved in the following field and chamber campaigns: The Southern Oxidant and Aerosol Study (SOAS), Focused Isoprene eXperiments at the California Institute of Technology (FIXCIT), The Front Range Air Pollution and Photochemistry Experiment (FRAPPÉ), Diesel Exhaust Fuel and CONtrol (DEFCON), and the seasonal flux experiments at the Manitou Experimental Forest.

DEDICATION

This work is dedicated to the people who continue to shape, influence, and illuminate my view of what it means to live

TABLE OF CONTENTS

CHAPTER 1

INTRODUCTION TO ATMOSPHERIC MEASUREMENTS USING CHEMICAL IONIZATION MASS SPECTROMETRY

1.1 The Early Days of Ambient Ion Measurements and CIMS

Chemical ionization mass spectrometry (CIMS) was first reported outside the realm of atmospheric mass spectrometry in 1966 as an alternative ionization method to electron impact ionization (Munson and Field, 1966). Methane was used as a reagent gas to produce a characteristic mass spectrum of a trace analyte added to the ion source. The authors used a magnetic deflection spectrometer and generate electrons using a hot wire filament to ionize the reagent gas. The background spectrum (methane only) contained a number of significant background or reagent ion peaks which is a consistent feature of CIMS reagent generation methods. The mass spectrum of n-hexadecane ($C_{16}H_{34}$) exhibited a number of fragment peaks with the largest signal coming from the "quasi-parent ion" of n-hexadecane ($C_{16}H_{33}^{+}$). The electron impact mass spectrum had neither parent ion ($C_{16}H_{33}$+) nor quasi-parent ion and consists primarily of lower molecular weight fragments. These first observations remain remarkably consistent with modern day CIMS methodologies.

Early work probing the composition of ions in the atmosphere facilitated many of the developments necessary to realize ambient atmospheric CIMS measurements and predate the original report of CIMS by Munson and Field. The first in situ measurement of both positive and negative ions in the ionosphere occurred in 1958 using Bennett radio-frequency ion-mass spectrometers mounted to Aerobee-Hi rockets launched into the artic ionosphere (Johnson et al.,

1958). Ambient ion measurements in the ionosphere are much simpler than at lower altitudes because of the lower neutral gas pressure leading to longer lived ions, reduced backgrounds, and relatively simple ion composition. Nearly two decades later, the first report of mass spectrometric measurements of positive ions in the stratosphere tentatively identified a number of protonated, positive ions using a rocket mounted quadrupole mass spectrometer (Arnold et al., 1977). Two years later, balloon-born experiments provided the first measurements of negative ions identifying numerous nitric acid containing clusters (Arnold and Henschen, 1978). Both these stratospheric studies suffered from poor quadrupole mass accuracy making the identification of these ions difficult. Moreover, the lack of general compositional measurements throughout the atmosphere makes these measurements all the more impressive.

Early stratospheric work investigating ambient-ion composition led to important discoveries and eventually tropospheric mass spectrometric measurements. Tropospheric ambient-ion measurements are considerably more difficult due to lower concentrations of ambient ions because of the higher neutral-gas density at lower altitudes and the increased ion-ion recombination rate. In a review of flowing afterglow techniques Ferguson states that "tropospheric ion chemistry has been held back by the horrendous technical problem of sampling and mass analyzing ~10^3 ion/cc in a background of ~10^{19} neutrals/cc" (Ferguson, 1992). The development of the flow-opposed drift tube for quadrupole based ambient ion measurements in the troposphere overcame the horrendous technical challenge marking a large step forward in mass spectrometer sophistication (Eisele, 1983). Similar developments were simultaneously occurring at the Max-Plank Institute in Germany (Arnold et al., 1984). Eisele's instrument was first characterized with a Tesla coil and first deployed to Stone Mountain, outside of Atlanta Georgia, USA (Eisele, 1983). Subsequent field deployments occurred at the remote Sapelo

Island in Georgia, USA and then deployed to the University of Denver research laboratory on top of Mt. Evans in Colorado (Perkins and Eisele, 1984). Further instrument development and the use of a collisional dissociation chamber provided a means for fragmenting positive ions (removing mostly water) and increasing the ability to identify these species by decreasing the complexity of the observed mass spectrum (Eisele, 1986). At this point, the Eisele mass spectrometer interface is beginning to resemble modern quadruple-based chemical ionization instrumentation, and this becomes more obvious with the application of a commercial triple quad mass spectrometer (Eisele, 1988). It should be noted that the developments by Eisele and others focus on the development of the first atmospheric pressure interfaces designed specifically for atmospheric sampling. These developments are presented in figure 1.1 as a timeline.

1.2 Chemical Ionization Mass Spectrometry in the Ambient Atmosphere

Electron impact (EI) ionization was reported in 1918 by Arthur J. Dempster for the analysis of positive ions (Dempster, 1918). Typically, EI is conducted with an electron source at 70 eV, which causes substantial, but reproducible, fragmentation patterns. This technique has remained one of the predominant ionization techniques in mass spectrometry because the structure of individual molecules can be elucidated. The substantial amount of fragmentation requires chromatographic pre-separation to prevent multiple compounds from simultaneously entering the ion source and producing overlapping fragmentation patterns. Thus, the rate at which compounds can be measured from the ambient atmosphere is severely limited by the chromatographic separation. Additionally, the molecular identity of the original compound is often lost in electron impact studies, and this motivated the work by Munson and Field (1966) to develop a method where fragmentation is minimized or eliminated entirely. The complexities of tropospheric chemistry necessitate using soft ionization (no fragmentation) when no

chromatographic separation is performed. Moreover, the large number of individual species in the atmosphere (>10^5 (Goldstein and Galbally, 2007)) requires not only soft ionization, but it also requires selective ionization where only a few molecules out of the thousands are ionized by gas-phase chemical reactions in order to simplify the observed mass spectrum. This is contrasted by EI where nearly any molecule can be ionized due to the high energy of the electron beam relative to the ionization potential of most molecules.

Selective chemical ionization applied to ambient atmospheric sampling of neutral species first appears in the work of Arnold and Hauck at the Max-Plank Institute using water clusters in the positive mode to detect acetonitrile (CH_3CN), acetone ($(CH_3)_2CO$), ammonia (NH_3), and acetaldehyde (CH_3CHO) in the lower stratosphere (Arnold and Hauck, 1985). These techniques were further described by Arnold and Knop in subsequent publications (Arnold and Knop, 1987). A variety of reagent ions were employed by Arnold and Knop for stratospheric measurements including CO_3^--hydrates in the negative mode for the detection of nitric acid (Knop and Arnold, 1985). CO_3^--hydrates are not suitable for tropospheric measurements due to water and ozone interferences, and this remains a prevalent challenge of modern CIMS measurements.

Eisele and Tanner measured the gas-phase concentration of sulfuric acid (H_2SO_4), methane sulfonic acid (CH_3SO_3H), and malonic acid ($CH_2(COOH)_2$) at ground level using nitrate-nitric acid clusters (Eisele and Tanner, 1993). This work was predated by the measurement of OH using, essentially, the same technique to detect sulfuric acid produced from the oxidation of SO_2 by OH (Eisele and Tanner, 1991). Here, we again see the influence of the earlier stratospheric work where sulfuric acid was found to react with nitric acid clusters (R1.1) (Viggiano et al., 1982). This chemistry was directly applied to the ion source by Eisele and

Tanner in the form of a nitrate-based chemical ionization source to selectively ionize a small number of molecules with gas-phase acidity greater than nitric acid (1991; 1993). This technique highlights one of the main requirements for selecting reagent ions: chemical selectivity. Few molecules are more acidic than nitric acid, and thus, only sulfuric acid, methane sulfonic acid, and malonic acid are reported as detectible species in this original publication (Eisele and Tanner, 1993).

$$NO_3^-(HNO_3)_n + H_2SO_4 \rightarrow HSO_4^-(HNO_3)_n + HNO_3 \quad \text{(R1.1)}$$

The selectivity requirements lead to the realization that multiple reagent ions are necessary to measure a vast suite of neutral species in the atmosphere. Laboratory studies discuss this need; Hanson and Ravishankara use an ice-covered neutral flow tube to study the reaction of $ClONO_2$ and N_2O_5 on ice surfaces using a CIMS as a detector motivated by the need to understand ozone depleting mechanisms in the polar stratosphere (Hanson and Ravishankara, 1991). The authors use two reagent ions (I^- and F^-). I^- reacts with $ClONO_2$ and N_2O_5 to produce NO_3^-. Nitric acid will not react with I^- to produce NO_3^- allowing for the detection of $ClONO_2$ and N_2O_5 in the presence of nitric acid. F^- detects a number of other species of interest. The use of multiple reagent analysis in the laboratory highlights the need for the development and characterization of many reagent ions. This work also demonstrates the power of CIMS to selectively ionize specific compounds from within a complex matrix containing known interferences.

The studies discussed here paved the way for quadrupole CIMS developments using a number of reagent ions in the 1990s which are reviewed by Huey (2007). Many of the original reagent ions were selected because they had been previously studied or observed in the atmosphere (Möhler and Arnold, 1991). Additionally, the emergence of proton-transfer reaction

mass spectrometry (PTR-MS) revolutionized atmospheric trace gas detection (Lindinger and Jordan, 1998; Lindinger et al., 1998). PTR-MS marks a notable departure from previous CIMS work because of the use of a drift tube to prevent the formation and subsequent reaction of clusters with analytes. An electric field is applied across the drift tube to accelerate ions and ion-neutral clusters causing collisional dissociation to occur in the reaction chamber. This limits the extent to which water clusters can react with trace gases compared to hydronium (H_3O^+). PTR-MS techniques and findings have been extensively reviewed (de Gouw and Warneke, 2006).

Limited technological developments improved CIMS techniques though the 1990s. The continued use of a collisional dissociation chamber (Eisele, 1986) and the study of its effects on CIMS measurements (Tanner and Eisele, 1995; Tanner et al., 1997) has remained an important consideration for developing and understanding many CIMS techniques. Additionally, new ion guides helped to improve the sensitivity of CIMS measurements following a flurry of publications describing multipole ion guides (Szabo, 1986) and the octopole ion guide (Hägg and Szabo, 1986). Numerous other CIMS methodologies were investigated during the 1990's building off existing techniques (Huey and Lovejoy, 1996; Huey et al., 1995; 1996). The nitrate-cluster based CIMS method for detecting sulfuric acid was improved upon to allow the reaction (R1.1) to reach equilibrium such that sulfuric acid could be directly quantified (Mauldin et al., 1998). The acetate reagent ion was developed in the late 2000s for the selective detection of carboxylic acids (Veres et al., 2008). The quadrupole based mass spectrometers used in these studies limited these methodologies to targeted measurements examining only a handful of atmospherically relevant molecules.

1.3 Time-of-Flight Mass Spectrometry and CIMS

Time-of-flight mass spectrometry was first conceived by W. E. Stephens (Stephens, 1946), and the first experimental report of an working time-of-flight mass spectrometer (called an "ion-velocitron") appeared two years later (Cameron and Eggers, 1948). Large improvements in mass resolution occurred with the invention of the reflectron grid (Mamyrin et al., 1973). Later, orthogonal extraction was implemented with continuous ion sources (Laiko et al., 1994). These developments, which have produced the modern time-of-flight mass spectrometers, are discussed in detail in an excellent and recent review (Radionova et al., 2015).

The more recent application of CIMS and PTR-MS to time-of-flight mass spectrometers (TOF-MS) has had one of the largest impacts on the field of atmospheric chemistry; these developments coincide with aerosol mass spectrometer development (Jayne et al., 2000; Jimenez, 2003) and the coupling of these techniques to TOF-MS by Aerodyne Research Inc. (DeCarlo et al., 2006). The application of time-of-flight mass analyzers with sufficient resolution to determine molecular composition marks a paradigm shift for analytical mass spectrometry. Totally unanticipated chemistry and molecular material can be observed without much knowledge of the sample or target analytes. The most recent developments with time-of-flight mass analyzers demonstrate the concept of non-targeted analysis of atmospheric material (Stark et al., 2015). These types of analysis have appeared in recent laboratory studies and field studies using HR-TOF-CIMS (Aljawhary et al., 2013; Chhabra et al., 2015; Ehn et al., 2014; Friedman et al., 2016; Krechmer et al., 2015; Lopez-Hilfiker et al., 2014; Yatavelli et al., 2012; 2014). This is, however, not without precedent when considering the historical developments of atmospheric mass spectrometry. The early rocket flights with mass spectrometer payloads launched into the atmosphere to probe ion composition were genuinely non-targeted ion measurements.

Application of TOF-MS to PTR-MS and CIMS was directly facilitated by private sector development of TOF-MS technology. The first report of PTR-TOF-MS used ion transfer optics and a TOF-MS manufactured by Kore Technologies (Ely, UK) but suffered from unreasonably low sensitivities, limited mass resolution (m/Dm) of >1000, and a radioactive ^{241}Am source (Blake et al., 2004). Improvements were made to the ion source eliminating the radioactive materials and simultaneously improving the sensitivity of the PTR-TOF-MS, but the PTR-TOF-MS still suffered from poor sensitivity compared to quadrupole systems (Ennis et al., 2005). Further ion source development increased PTR-TOF-MS sensitivity to limits of detection below 1 ppb (Inomata et al., 2006). In 2009 the PTR-TOF-MS was realized in its modern form by IONICON (Innsbruck, Austria) , using a TOF-MS manufactured by Tofwerk (Thun, Switzerland), with ultra-high sensitivity (low pptv) and fast time-response (<100 ms) essentially ushering in the PTR-TOF-MS as the dominant instrument for atmospheric trace gas sampling in the 21st century (Jordan et al., 2009).

The commercialization of TOF-MS instruments by the private business sector continued to be important in facilitating the most recent developments discussed in the latter sections of this introduction. Specifically, the Tofwerk high-resolution TOF-MS (HR-TOF-MS), compact TOF-MS (C-TOF-MS), and later the atmospheric pressure interface (API) for these time-of-flight mass analyzers are key technological developments which required substantial engineering and development in their own right. The API coupled to an HR-TOF brings the story full circle as this original development was intended to measure ambient ions and is known as the API-TOF (Junninen et al., 2010). Significant development and inter-comparison studies have been conducted with this instrument (Ehn et al., 2011). Interesting measurements of gas-phase arsenic cations in real time have been made with this system in the field (Faust et al., 2016). Extensive

non-targeted analysis of atmospheric clustering have also been performed with outstanding success in both field (Ehn et al., 2010a) and chamber studies. (Kirkby et al., 2011; Kürten et al., 2014; Praplan et al., 2015; Schobesberger et al., 2015)

The API-TOF has revolutionized our ability to understand the composition of ambient ions and related clusters (Kulmala et al., 2014), but it should be noted that many of these realizations were foreshadowed by the original quadrupole based measurements. Specifically, the observation of high molecular weight cations with semi-periodic structure observed at Mt. Evans in 1986 (Eisele, 1988) is extremely consistent with the observation of high molecular weight clusters identified with the API-TOF both in the field (Ehn et al., 2010b) and in the Cosmics Leaving OUtdoor Droplets (CLOUD) chamber studies at CERN (Praplan et al., 2015; Schobesberger et al., 2015). The ambient ion measurements using API-TOF ushered in TOF-CIMS for the measurement of neutral trace gases and neutral clusters. This development mirrors the initial ambient ion measurements of the 1970s and early 1980s leading to the early CIMS measurements.

The initial development and application of the Tofwerk API to a C-TOF-MS (Bertram et al., 2011) lead to the modern HR-TOF-CIMS being sold by Aerodyne Research Inc. The HR-TOF-CIMS (Yatavelli et al., 2012) was first used as a backend detector for the previously developed micro orifice volatilization impactor (MOVI) (Yatavelli and Thornton, 2010) for the analysis of both gas and particle composition. It is interesting to note that what has become known as the "TOF-CIMS" community first applied the HR-TOF-CIMS to a far more complex front end (MOVI) for particle and gas analysis without really characterizing the details of chemical ionization occurring in the instrument. This is understandable because most of the major developers were coming from the aerosol mass spectrometer field and were looking for

soft ionization techniques for studying the molecular composition of atmospheric aerosol. Simultaneously, the API-TOF was outfitted with an atmospheric pressure nitrate ion source for sulfuric acid and neutral cluster measurements termed the CI-API-TOF (Jokinen et al., 2012). The major difference between the CI-API-TOF and the HR-TOF-CIMS is that the front end ion sources are operated at atmospheric pressure and reduced pressure, respectively.

A long history of quadrupole based measurements using various CIMS techniques and reagent ions exist in the literature providing substantial precedent *that these techniques work.* The HR-TOF-MS, as claimed earlier, marks a paradigm shift that requires rethinking CIMS as it is being applied to more complex problems under the guise of non-targeted analysis and, especially, non-targeted quantification. The CIMS methods described in the past should act as landmarks for TOF-CIMS development, but to assume that the technical details are understood appears to be a dangerous oversimplification. Fundamental instrument development needs to be perused. CIMS methods that have been shown to detect specific molecules will be easily applied to HR-TOF-CIMS and CI-API-TOF, but to assume that these CIMS methods should extend to all observed high-resolution signals in the mass spectrometer is naive at best; the chemistry is simply not understood.

The TOF-CIMS characterization focusing on chemical ionization is only beginning to catch up as researchers slowly simplify their systems. Multiple reagents (iodide, acetate, and protonated water clusters) were evaluated on a HR-TOF-CIMS by collecting a-pinene oxidation products on a filter, dissolving these products in water, photo-oxidizing the solution with a UV-B lamp, and the atomizing the solution though a heated tube into the HR-TOF-CIMS (Aljawhary et al., 2013). While this experiment is not simple or particularly controlled, the authors show that a large diversity of products are detected with each reagent ion. The time resolved evolution of the

photo-oxidation experiment also shows differences in what is observable with each reagent ion because each reagent ionizes different species to a different extent. Various other comparisons are made, but the underlying ion chemistry is not being questioned or evaluated with careful calibrations. Again, rather than simplifying the measurement, the authors are pursuing non-targeted quantification without first studying instrument responses from basic calibrations!

Careful studies aimed at non-targeted analysis and quantification with iodide-adduct CIMS are slowly being conducted with significant success (Lee et al., 2014). Computational work (Iyer et al., 2016) coupled with laboratory calibrations (Lopez-Hilfiker et al., 2016) have begun to show that non-targeted quantification may be impressively close to being realized. Discrepancies do, however, exist. Iodide-adduct CIMS is a clustering method where some ambient species (X) forms an ion-neutral cluster with iodide via a ligand switching reaction with iodide-water clusters (R1.2-1.3). These reactions are humidity dependent (Lee et al., 2014), but this humidity dependence is not discussed in the attempts to constrain the sensitivity of iodide to a large number of compounds without direct calibration (Lopez-Hilfiker et al., 2016). This suggests a lack of understanding with respect to the actual reaction(s) occurring and leading to the observed iodide-adducts.

$$I^- + H_2O \rightarrow [I{+}H_2O]^- \qquad \text{(R1.2)}$$

$$[I{+}H_2O]^- + X \rightarrow [I{+}X]^- + H_2O \qquad \text{(R1.3)}$$

Nitrate based clustering CIMS methods (CI-API-TOF) have also undergone significant characterization (Jokinen et al., 2012) with the discovery of extremely low volatility organic compounds (ELVOC) (Ehn et al., 2014). Similar low-volatility compounds have also been observed from isoprene oxidation using the same instrument (Krechmer et al., 2015). Nitrate has likewise been used to observe peroxy radical species formed from the ozonolysis of alkenes

(Mentel et al., 2015). Neutral clusters can be efficiently charged by nitrate clustering reactions (Jokinen et al., 2012; Kürten et al., 2014). Computational studies have been conducted modeling the charging of ELVOC-type compounds with nitrate-clusters (Hyttinen et al., 2015). Nitrate CIMS has also been applied in conjunction with two API-TOF (positive and negative mode) measurements at the CLOUD chamber to provide a comprehensive picture of the composition of positive, negative and neutral clusters from a-pinene oxidation under ambient conditions (Praplan et al., 2015).

CLOUD chamber work has facilitated the development of other TOF-CIMS methods as well. For example, bisulfate cluster CIMS methods applied to the CI-API-TOF nitrate source for the detection of amines further demonstrates the power of these instruments for ultra-trace gas detection (Sipilä et al., 2015). The bisulfate-cluster method reports <100 ppqv ambient limits of detection for simple amines. This clustering method points out some of the difficulties with clustering methods in general because each detected amine appears in the mass spectrum multiple times clustered to different numbers of sulfuric acid molecules. Field deployment of these systems will inevitably suffer from complex spectrum. The authors also note difficulties in determining a meaningful background and do not discuss relative humidity dependences.

HR-TOF-CIMS is not (and should not solely be) relegated to the lofty goals of quantifying everything via non-targeted analysis and non-targeted quantification. The Wennberg Group at The California Institute for Technology has applied CF_3O^- CIMS to a C-TOF instrument (Crounse et al., 2006) for targeted analysis and eddy covariance flux measurements (Nguyen et al., 2015). They have also applied the same methods to triple quad mass spectrometers (Clair et al., 2010) for targeted analysis and isomeric speciation of isoprene epoxydiols (IEPOX) and isoprene hydroxy hydroperoxides (ISOPOOH) (Nguyen et al., 2014).

This highlights the complementary nature of triple quad mass spectrometry with HR-TOF-CIMS methods because of their ability to distinguish isomers.

Years after the publication and characterization of the API-TOF, CI-API-TOF, and HR-TOF-MS, IONICON replaced their ion transfer optics on the PTR-TOF-MS with the Tofwerk API (the first quadrupole and vacuum stage removed) to create an powerful PTR system termed the proton transfer reaction quadrupole interface time-of-flight mass spectrometer (PTR-QiTOF) (Sulzer et al., 2014). This system reports mass resolution maximum >10,000 (m/Dm) and maximum sensitivity of about 4700 cps/ppb leading to 20 pptv limits of detection with 100 ms integration or 750 ppqv with 1 min integration time. This development points towards our lack of understanding with respect to the atmospheric pressure interfaces on mass spectrometers and the ion source in general. The numbers reported for the PTR-QiTOF call into question the use of relatively high-pressure chemical ionization methods which have been used to increase sensitivity at the cost of kinetic control and complex humidity dependent clustering reactions. Moreover, the generation of less energetic ions or efficient methods to decrease the ion kinetic energy leaving the ion source remains poorly understood when comparing the PTR-QiTOF to various other HR-TOF-CIMS systems. These poorly understood energy differences probably explain the increase in mass resolution in the PTR system compared to CIMS methods relying on radioactive sources but decoupling the differences in the ion transfer optics complicates the discrepancies. The TOF systems and select operational parameters described herein are summarized in table 1.1 along with the publications relevant to the development of the TOF system.

1.4 Work Presented in this Dissertation: general comments

We have made substantial efforts to carefully characterize and calibrate the HR-TOF-CIMS using, primarily, the acetate reagent ion (Veres et al., 2008). Acetate CIMS operates in a declustered mode, which is distinct from the iodide, nitrate, and bisulfate methods discussed above. The acetate reagent ion deprotonates carboxylic acids that have a larger gas-phase acidity than acetate (Veres et al., 2008). Acetate has the lowest gas-phase acidity of the abundant atmospheric acids making it a nearly universal reagent ion for carboxylic acid detection. The chemistry of the acetate ion makes it unique in that specific classes of compounds (carboxylic acids, or other species with acidic protons such as nitrated phenols (Mohr et al., 2013)) are ionized rather than individual species. The concept of acetate CIMS was to target a functional group based on known reactivity. Thus, non-targeted analysis is aided by knowing that carboxylic acids are primarily ionized when no chromatography or MS/MS is conducted to elucidate the structure. Carboxylic acids are of great interest to the field of atmospheric chemistry because they are implicated in SOA production (Zhang et al., 2007). These species also appear to be rapidly produced in urban (Veres et al., 2011) and anthropogenic influenced rural environments (Brophy and Farmer, 2015) and track the photochemical production of nitric acid. It is also known that these species (like most oxygenated volatile organic compounds) are poorly understood and poorly explained by atmospheric chemistry models as shown by formic acid (Millet et al., 2015).

Our first deployment of this instrument was during the Southern Oxidant and Aerosol Study in 2013. The main aim of this deployment was to calibrate the instrument using a variety of methods in the field to understand instrument stability and sensitivity while looking for interferences. We also used a low-pressure high-flow inlet system that has since been

successfully used for trailer based eddy-covariance flux measurements at the Manitou Experimental Forest near Woodland Park, CO (ongoing work briefly presented in Chapter 5). Various data analysis tools were developed for data handling and ensuring that observed signals are (1) actually arising from the ambient atmosphere, and (2) statistically significant.

Laboratory studies examining the relative humidity dependence of acetate CIMS and underlying ion chemistry were conducted using authentic standards. The API was used to investigate the underlying acetate-cluster and ion-neutral chemistry occurring in the ion source and ion molecule reaction chamber by collisional dissociation scanning. This marks the first attempt to characterize the electric field dependences in the API which has been described as a serious challenge to the community (Sipilä et al., 2015). Analytical tools were also developed for determining whether an observed signal is a cluster or deprotonated-declustered ion. This second study should set the groundwork for operating acetate CIMS with the intention of non-targeted analysis, but non-targeted quantification with acetate CIMS remains a difficult challenge. The methods and findings are broadly applicable to all HR-TOF-CIMS, CI-API-TOF, and API-TOF work with implications for understanding cluster binding energy, cluster stability, instrument sensitivity, and decreasing the ambiguity of non-targeted measurements.

1.4.1 SRI-HR-TOF-CIMS and SOAS[1]

The Southern Oxidant and Aerosol Study (SOAS) near Brent, Alabama was conducted during the summer of 2013. We deployed and developed a HR-TOF-CIMS with switchable reagent ion (SRI) capabilities for measuring trace gases in the negative mode using both acetate and iodide (Brophy and Farmer, 2015). The calibration system and reduced pressure gas-phase

[1] Brophy, P. and Farmer, D. K.: A switchable reagent ion high resolution time-of-flight chemical ionization mass spectrometer for real-time measurement of gas phase oxidized species: characterization from the 2013 southern oxidant and aerosol study, Atmospheric Measurement Techniques, 8(7), 2945, doi:10.5194/amt-8-2945-2015, 2015

inlet were characterized. The average limit of detection and limit of quantification for formic acid during SOAS were 82 ppt and 863 ppt, respectively, corresponding to an average sensitivity of 13 +/- 5 Hz ppt^{-1}. Hourly background determinations and calibrations were shown to be essential for tracking instrument performance and accurately quantifying formic acid. Maximum daytime formic acid concentrations of 10 ppb were observed during SOAS. A strong diel cycle was observed leading to night time concentrations below the limit of quantification. Other species measured exhibit diel behavior similar to formic acid. The concept of the mass defect enhancement plot and the use of signal-to-noise are described in detail as a method for investigating HR-TOF-CIMS spectra in an effort to reduce data complexity.

1.4.2 Acetate CIMS methodology and API Cluster Control[2]

We present a comprehensive characterization of cluster control and transmission through the Tofwerk atmospheric pressure interface installed on various chemical ionization time-of-flight mass spectrometers using authentic standards. This characterization of the atmospheric pressure interface allows for a detailed investigation of the acetate chemical ionization mechanisms and the impact of controlling these mechanisms on sensitivity, selectivity, and mass spectral ambiguity with the aim of non-targeted analysis. Chemical ionization with acetate reagent ions is controlled by a distribution of reagent ion-neutral clusters that vary with relative humidity and the concentration of acetic anhydride precursor. We show that the majority, if not all, ion-neutral chemistry occurs in the ion molecule reactor where incoming sample air mixes with the output of the ion source. Deprotonated carboxylic acids are primarily detected only if sufficient declustering is employed inside the atmospheric pressure interface. The configuration

[2] Brophy, P. and Farmer, D. K.: Clustering, Methodology, and Mechanistic Insights Into Acetate Chemical Ionization Using High-Resolution Time-of-Flight Mass Spectrometry. Submitted to Atmospheric Measurement Techniques Discussion for publication in Atmospheric Measurement Techniques

of a high-resolution time-of-flight chemical ionization mass spectrometer (HR-TOF-CIMS) using an acetate chemical ionization source for non-targeted analysis is discussed. Recent approaches and studies characterizing acetate chemical ionization as it applies to the HR-TOF-CIMS are evaluated in light of the work presented herein.

1.4.3 HR-TOF-CIMS Headspace Analysis

Headspace analysis has been conducted with PTR-MS and a large literature of these experiments exists. Major problems with ethanol containing beverages and PTR-MS are addressed in the literature because high ethanol concentrations produce numerous ethanol containing reagent ion clusters. These clusters completely change the observed PTR-MS chemistry. Various methodologies have been developed to overcome these limitations, but the underlying problem is that the H_3O^+ reagent ion is very sensitive to ethanol which acts as an interference. The acetate reagent ion is insensitive to alcohols in general. We demonstrate that headspace analysis of beer can be conducted with acetate CIMS to produce distinct mass spectrum which can be differentiated based on principal component analysis. Visual inspection of the mass defect plots for each beer sample shows substantial differences due to brewing processes.

1.4.4 Future Directions

The future directions and applications of HR-TOF-CIMS and voltage scanning are discussed with respect to ongoing work related to gas-phase measurement and particle nucleation studies. The challenge and current state of quantification with acetate CIMS is discussed, and recommendations are made regarding the obvious next steps in characterizing acetate ion chemistry are discussed. The complexities of acetate CIMS make characterization challenging compared to other popular methods, such as iodide-adduct CIMS. Recent work at the CLOUD

chamber at CERN and ambient ion measurements with the API-TOF are discussed with respect to voltage scanning and understanding the chemical nature of initially nucleated clusters and small particles (<5 nm).

1.5 Chapter 1 Figures

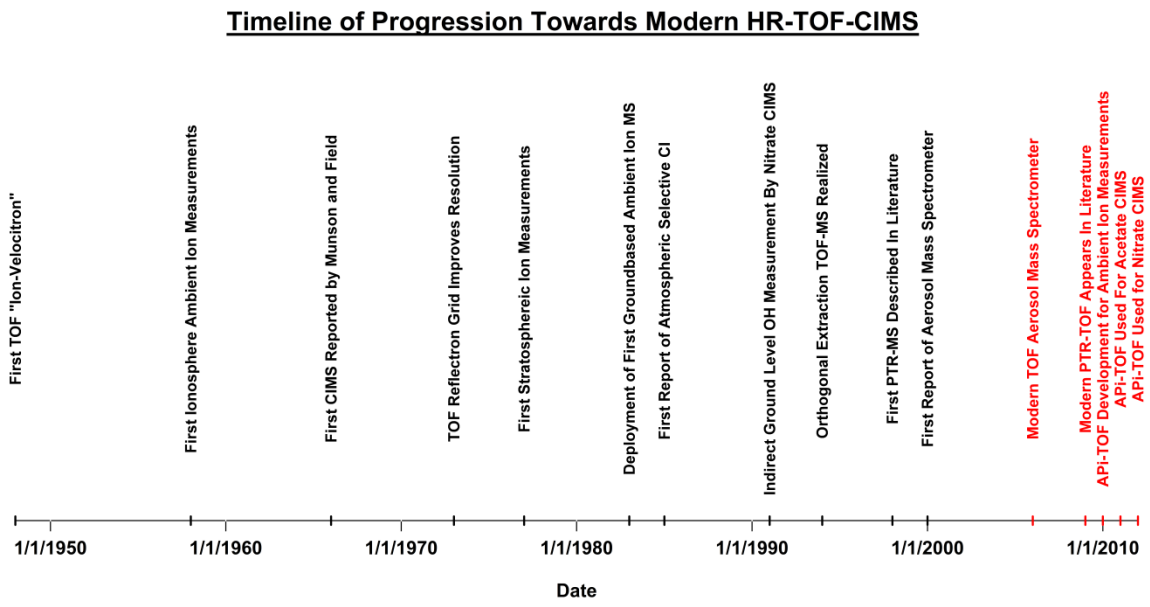

FIGURE 1.1TIMELINE TOWARDS MODERN HR-TOF-CIMS:

Major events in the progression of atmospheric mass spectrometry beginning with quadrupole measurements (black text and markers) leading to time-of-flight mass spectrometer based measurements

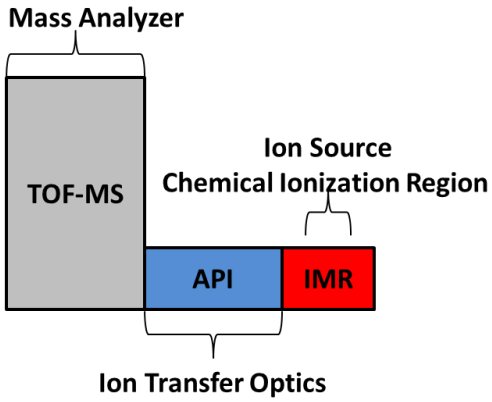

FIGURE 1.2 GENERALIZED CIMS SCHEMATIC

1.6 Chapter 1 Tables

TABLE 1.1 TOF INSTRUMENT SUMMARY:

Front End	Ion Source (Operation Pressure)	Target Analytes by Reagent	References
API-TOF (referred to as APi-TOF in literature)			
API	No Ion Source (Atmospheric Pressure)	+/- Ambient Ions/Ambient Ion-neutral clusters	(Junninen et al., 2010)
CI-API-TOF (referred to as CI-APi-TOF in literature)			
API	Transverse Ion Source (Atmospheric Pressure)	NO_3^-: H2SO4, MSA, Malonic acid, neutral clusters, ELVOCs, peroxy radicals	(Jokinen et al., 2012)
TOF-CIMS			
API	IMR (Reduced Pressure, ~80-120 mbar)	I^- (adduct): Biogenic oxidation products, acids, ELVOC $C_2H_3O_2^-$ (deprotonated): carboxylic acids, nitrated phenols Bisulfate (adduct): amines CF_3O^-: peroxides	C-TOF ($C_2H_3O_2^-$): (Bertram et al., 2011) C-TOF (CF_3O^-): (Crounse et al., 2006) HR-TOF ($C_2H_3O_2^-$): (Brophy and Farmer, 2015; Yatavelli et al., 2012) HR-TOF (I^-): (Lee et al., 2014) HR-TOF (bisulfate): (Sipilä et al., 2015)
(SRI)-PTR-TOF			
Ionicon Ion Funnel	PTR Drift Tube (Reduced Pressure, ~2.3 mbar)	H_3O^+: Molecules with proton affinity > water (Hydrocarbons (MVK, MCAR, etc), aromatics (BTEX), biogenic hydrocarbons (isoprene, terpenes, sesquiterpenes) NO^+/O_2^+: Molecules with proton affinity <water	(Jordan et al., 2009)
PRTQi-TOF			
API (no SSQ)	PTR Drift Tube (Reduced Pressure, ~3.8 mbar)	See Above	(Sulzer et al., 2014)

REFERENCES

Aljawhary, D., Lee, A. K. Y. and Abbatt, J. P. D.: High-resolution chemical ionization mass spectrometry (ToF-CIMS): application to study SOA composition and processing, Atmospheric Measurement Techniques, 6(11), 3211, doi:10.5194/amt-6-3211-2013, 2013.

Arnold, F. and Hauck, G.: Lower stratosphere trace gas detection using aircraft-borne active chemical ionization mass spectrometry, Nature, 315(6017), 307, doi:10.1038/315307a0, 1985.

Arnold, F. and Henschen, G.: First mass analysis of stratospheric negative ions, Nature, 275(5680), 521, doi:10.1038/275521a0, 1978.

Arnold, F. and Knop, G.: Stratospheric trace gas detection using a new balloon-borne acims method, International Journal of Mass Spectrometry and Ion Processes, 81, 33, doi:10.1016/0168-1176(87)80004-6, 1987.

Arnold, F., Heitmann, H. and Oberfrank, K.: First composition measurements of positive ions in the upper troposphere, Planetary and Space Science, 32(12), 1567, doi:10.1016/0032-0633(84)90026-6, 1984.

Arnold, F., KRANKOWSKY, D. and MARIEN, K. H.: First mass spectrometric measurements of positive ions in the stratosphere, Nature, 267(5606), 30, doi:10.1038/267030a0, 1977.

Bertram, T. H., Kimmel, J. R., Crisp, T. A., Ryder, O. S., Yatavelli, R. L. N., Thornton, J. A., Cubison, M. J., Gonin, M. and Worsnop, D. R.: A field-deployable, chemical ionization time-of-flight mass spectrometer, Atmospheric Measurement Techniques, 4(7), 1471, doi:10.5194/amt-4-1471-2011, 2011.

Blake, R. S., Whyte, C., Hughes, C. O., Ellis, A. M. and Monks, P. S.: Demonstration of proton-transfer reaction time-of-flight mass spectrometry for real-time analysis of trace volatile organic compounds, Anal Chem, 76(13), 3841–3845, doi:10.1021/ac0498260, 2004.

Brophy, P. and Farmer, D. K.: A switchable reagent ion high resolution time-of-flight chemical ionization mass spectrometer for real-time measurement of gas phase oxidized species: characterization from the 2013 southern oxidant and aerosol study, Atmospheric Measurement Techniques, 8(7), 2945, doi:10.5194/amt-8-2945-2015, 2015.

Cameron, A. E. and Eggers, D. F.: An Ion ``Velocitron'', Review of Scientific Instruments, 19(9), 605, doi:10.1063/1.1741336, 1948.

Chhabra, P. S., Lambe, A. T., Canagaratna, M. R., Stark, H., Jayne, J. T., Onasch, T. B., Davidovits, P., Kimmel, J. R. and Worsnop, D. R.: Application of high-resolution time-of-flight chemical ionization mass spectrometry measurements to estimate volatility distributions of α-

pinene and naphthalene oxidation products, Atmospheric Measurement Techniques, 8(1), 1, doi:10.5194/amt-8-1-2015, 2015.

Clair, J. M. S., McCabe, D. C., Crounse, J. D., Steiner, U. and Wennberg, P. O.: Chemical ionization tandem mass spectrometer for the in situ measurement of methyl hydrogen peroxide, Rev Sci Instrum, 81(9), 094102, doi:10.1063/1.3480552, 2010.

Crounse, J. D., McKinney, K. A., Kwan, A. J. and Wennberg, P. O.: Measurement of gas-phase hydroperoxides by chemical ionization mass spectrometry, Anal Chem, 78(19), 6726–6732, doi:10.1021/ac0604235, 2006.

DeCarlo, P. F., Kimmel, J. R., Trimborn, A., Northway, M. J., Jayne, J. T., Aiken, A. C., Gonin, M., Fuhrer, K., Horvath, T., Docherty, K. S., Worsnop, D. R. and Jimenez, J. L.: Field-deployable, high-resolution, time-of-flight aerosol mass spectrometer, Anal Chem, 78(24), 8281–8289, doi:10.1021/ac061249n, 2006.

Dempster, A. J.: A new Method of Positive Ray Analysis, Physical Review, 11(4), 316, doi:10.1103/physrev.11.316, 1918.

Ehn, M., Junninen, H., Petäjä, T., Kurtén, T., Kerminen, V. M., Schobesberger, S., Manninen, H. E., Ortega, I. K., Vehkamäki, H., Kulmala, M. and Worsnop, D. R.: Composition and temporal behavior of ambient ions in the boreal forest, Atmospheric Chemistry and Physics, 10(17), 8513, doi:10.5194/acp-10-8513-2010, 2010a.

Ehn, M., Junninen, H., Petäjä, T., Kurtén, T., Kerminen, V. M., Schobesberger, S., Manninen, H. E., Ortega, I. K., Vehkamäki, H., Kulmala, M. and Worsnop, D. R.: Composition and temporal behavior of ambient ions in the boreal forest, Atmospheric Chemistry and Physics, 10(17), 8513, doi:10.5194/acp-10-8513-2010, 2010b.

Ehn, M., Junninen, H., Schobesberger, S., Manninen, H. E., Franchin, A., Sipilä, M., Petäjä, T., Kerminen, V.-M., Tammet, H., Mirme, A., Mirme, S., Hõrrak, U., Kulmala, M. and Worsnop, D. R.: An Instrumental Comparison of Mobility and Mass Measurements of Atmospheric Small Ions, Aerosol Science and Technology, 45(4), 522, doi:10.1080/02786826.2010.547890, 2011.

Ehn, M., Thornton, J. A., Kleist, E., Sipilä, M., Junninen, H., Pullinen, I., Springer, M., Rubach, F., Tillmann, R., Lee, B., Lopez-Hilfiker, F., Andres, S., Acir, I.-H., Rissanen, M., Jokinen, T., Schobesberger, S., Kangasluoma, J., Kontkanen, J., Nieminen, T., Kurtén, T., Nielsen, L. B., Jørgensen, S., Kjaergaard, H. G., Canagaratna, M., Maso, M. D., Berndt, T., Petäjä, T., Wahner, A., Kerminen, V.-M., Kulmala, M., Worsnop, D. R., Wildt, J. and Mentel, T. F.: A large source of low-volatility secondary organic aerosol, Nature, 506(7489), 476–479, doi:10.1038/nature13032, 2014.

Eisele, F. L.: Direct tropospheric ion sampling and mass identification, International Journal of Mass Spectrometry and Ion Processes, 54(1-2), 119, doi:10.1016/0168-1176(83)85011-3, 1983.

Eisele, F. L.: Identification of tropospheric ions, Journal of Geophysical Research: Atmospheres, 91(D7), 7897, doi:10.1029/jd091id07p07897, 1986.

Eisele, F. L.: First tandem mass spectrometric measurement of tropospheric ions, Journal of Geophysical Research, 93(D1), 716, doi:10.1029/jd093id01p00716, 1988.

Eisele, F. L. and Tanner, D. J.: Ion-assisted tropospheric OH measurements, Journal of Geophysical Research, 1991.

Eisele, F. L. and Tanner, D. J.: Measurement of the gas phase concentration of H2SO4 and methane sulfonic acid and estimates of H2SO4 production and loss in the atmosphere, Journal of Geophysical Research, 1993.

Ennis, C. J., Reynolds, J. C., Keely, B. J. and Carpenter, L. J.: A hollow cathode proton transfer reaction time of flight mass spectrometer, International Journal of Mass Spectrometry, 247(1-3), 72, doi:10.1016/j.ijms.2005.09.008, 2005.

Faust, J. A., Junninen, H., Ehn, M., Chen, X., Ruusuvuori, K., Kieloaho, A.-J., Bäck, J., Ojala, A., Jokinen, T., Worsnop, D. R., Kulmala, M. and Petäjä, T.: Real-Time Detection of Arsenic Cations from Ambient Air in Boreal Forest and Lake Environments, Environmental Science & Technology Letters, 3(2), 42, doi:10.1021/acs.estlett.5b00308, 2016.

Ferguson, E. E.: A Personal history of the early development of the flowing afterglow technique for ion-molecule reaction studies, J Am Soc Mass Spectrom, 3(5), 479–486, doi:10.1016/1044-0305(92)85024-E, 1992.

Friedman, B., Brophy, P., Brune, W. H. and Farmer, D. K.: Anthropogenic Sulfur Perturbations on Biogenic Oxidation: SO2 Additions Impact Gas-Phase OH Oxidation Products of α- and β-Pinene, Environmental Science & Technology, 50(3), 1269–1279, doi:10.1021/acs.est.5b05010, 2016.

Goldstein, A. H. and Galbally, I. E.: Known and Unexplored Organic Constituents in the Earth's Atmosphere, Environmental Science & Technology, 41(5), 1514, doi:10.1021/es072476p, 2007.

Hanson, D. R. and Ravishankara, A. R.: The reaction probabilities of ClONO2and N2O5on polar stratospheric cloud materials, Journal of Geophysical Research, 96(D3), 5081, doi:10.1029/90jd02613, 1991.

Huey, L. G. and Lovejoy, E. R.: Reactions of SiF 5− with atmospheric trace gases: ion chemistry for chemical ionization detection of HNO 3 in the troposphere, International journal of mass spectrometry and ion …, 1996.

Huey, L. G., Hanson, D. R. and Howard, C. J.: Reactions of SF6- and I- with Atmospheric Trace Gases, The Journal of Physical Chemistry, 99(14), 5001, doi:10.1021/j100014a021, 1995.

Huey, L. G., Villalta, P. W. and Dunlea, E. J.: Reactions of CF3O-with atmospheric trace gases, The Journal of …, 1996.

Hyttinen, N., Kupiainen-Määttä, O., Rissanen, M. P., Muuronen, M., Ehn, M. and Kurtén, T.: Modeling the Charging of Highly Oxidized Cyclohexene Ozonolysis Products Using Nitrate-Based Chemical Ionization, J Phys Chem A, 119(24), 6339–6345, doi:10.1021/acs.jpca.5b01818, 2015.

Hägg, C. and Szabo, I.: New ion-optical devices utilizing oscillatory electric fields. III. Stability of ion motion in a two-dimensional octopole field, International Journal of Mass Spectrometry and Ion Processes, 73(3), 277, doi:10.1016/0168-1176(86)80003-9, 1986.

Inomata, S., Tanimoto, H., Aoki, N., Hirokawa, J. and Sadanaga, Y.: A novel discharge source of hydronium ions for proton transfer reaction ionization: design, characterization, and performance, Rapid Commun Mass Spectrom, 20(6), 1025–1029, doi:10.1002/rcm.2405, 2006.

Iyer, S., Lopez-Hilfiker, F., Lee, B. H., Thornton, J. A. and Kurtén, T.: Modeling the Detection of Organic and Inorganic Compounds Using Iodide-Based Chemical Ionization, J Phys Chem A, 120(4), 576–587, doi:10.1021/acs.jpca.5b09837, 2016.

Jayne, J. T., Leard, D. C., Zhang, X., Davidovits, P., Smith, K. A., Kolb, C. E. and Worsnop, D. R.: Development of an Aerosol Mass Spectrometer for Size and Composition Analysis of Submicron Particles, Aerosol Science and Technology, 33(1-2), 49, doi:10.1080/027868200410840, 2000.

Jimenez, J. L.: Ambient aerosol sampling using the Aerodyne Aerosol Mass Spectrometer, Journal of Geophysical Research, 108(D7), doi:10.1029/2001jd001213, 2003.

Johnson, C. Y., Meadows, E. B. and Holmes, J. C.: Ion composition of the arctic ionosphere, Journal of Geophysical Research, 63(2), 443, doi:10.1029/jz063i002p00443, 1958.

Jokinen, T., Sipilä, M., Junninen, H., Ehn, M., Lönn, G., Hakala, J., Petäjä, T., Mauldin, R. L., Kulmala, M. and Worsnop, D. R.: Atmospheric sulphuric acid and neutral cluster measurements using CI-APi-TOF, Atmospheric Chemistry and Physics, 12(9), 4117, doi:10.5194/acp-12-4117-2012, 2012.

Jordan, A., Haidacher, S., Hanel, G., Hartungen, E., Herbig, J., Märk, L., Schottkowsky, R., Seehauser, H., Sulzer, P. and Märk, T. D.: An online ultra-high sensitivity Proton-transfer-reaction mass-spectrometer combined with switchable reagent ion capability (PTR+SRI−MS), International Journal of Mass Spectrometry, 286(1), 32, doi:10.1016/j.ijms.2009.06.006, 2009.

Junninen, H., Ehn, M., Petäjä, T., Luosujärvi, L., Kotiaho, T., Kostiainen, R., Rohner, U., Gonin, M., Fuhrer, K., Kulmala, M. and Worsnop, D. R.: A high-resolution mass spectrometer to

measure atmospheric ion composition, Atmospheric Measurement Techniques, 3(4), 1039, doi:10.5194/amt-3-1039-2010, 2010.

Kirkby, J., Curtius, J., Almeida, J., Dunne, E., Duplissy, J., Ehrhart, S., Franchin, A., Gagné, S., Ickes, L., Kürten, A., Kupc, A., Metzger, A., Riccobono, F., Rondo, L., Schobesberger, S., Tsagkogeorgas, G., Wimmer, D., Amorim, A., Bianchi, F., Breitenlechner, M., David, A., Dommen, J., Downard, A., Ehn, M., Flagan, R. C., Haider, S., Hansel, A., Hauser, D., Jud, W., Junninen, H., Kreissl, F., Kvashin, A., Laaksonen, A., Lehtipalo, K., Lima, J., Lovejoy, E. R., Makhmutov, V., Mathot, S., Mikkilä, J., Minginette, P., Mogo, S., Nieminen, T., Onnela, A., Pereira, P., Petäjä, T., Schnitzhofer, R., Seinfeld, J. H., Sipilä, M., Stozhkov, Y., Stratmann, F., Tomé, A., Vanhanen, J., Viisanen, Y., Vrtala, A., Wagner, P. E., Walther, H., Weingartner, E., Wex, H., Winkler, P. M., Carslaw, K. S., Worsnop, D. R., Baltensperger, U. and Kulmala, M.: Role of sulphuric acid, ammonia and galactic cosmic rays in atmospheric aerosol nucleation, Nature, 476(7361), 429–433, doi:10.1038/nature10343, 2011.

Knop, G. and Arnold, F.: Nitric acid vapour measurements in the troposphere and lower stratosphere by chemical ionisation mass spectrometry, Planetary and Space Science, 33(8), 983, doi:10.1016/0032-0633(85)90111-4, 1985.

Krechmer, J. E., Coggon, M. M., Massoli, P., Nguyen, T. B., Crounse, J. D., Hu, W., Day, D. A., Tyndall, G. S., Henze, D. K., Rivera-Rios, J. C., Nowak, J. B., Kimmel, J. R., Mauldin, R. L., Stark, H., Jayne, J. T., Sipilä, M., Junninen, H., Clair, J. M. S., Zhang, X., Feiner, P. A., Zhang, L., Miller, D. O., Brune, W. H., Keutsch, F. N., Wennberg, P. O., Seinfeld, J. H., Worsnop, D. R., Jimenez, J. L. and Canagaratna, M. R.: Formation of Low Volatility Organic Compounds and Secondary Organic Aerosol from Isoprene Hydroxyhydroperoxide Low-NO Oxidation, Environmental Science & Technology, 49(17), 10330–10339, doi:10.1021/acs.est.5b02031, 2015.

Kulmala, M., Petäjä, T., Ehn, M. and Thornton, J.: Chemistry of atmospheric nucleation: on the recent advances on precursor characterization and atmospheric cluster composition in connection with atmospheric new …, Annual review of …, 2014.

Kürten, A., Jokinen, T., Simon, M., Sipilä, M., Sarnela, N., Junninen, H., Adamov, A., Almeida, J., Amorim, A., Bianchi, F., Breitenlechner, M., Dommen, J., Donahue, N. M., Duplissy, J., Ehrhart, S., Flagan, R. C., Franchin, A., Hakala, J., Hansel, A., Heinritzi, M., Hutterli, M., Kangasluoma, J., Kirkby, J., Laaksonen, A., Lehtipalo, K., Leiminger, M., Makhmutov, V., Mathot, S., Onnela, A., Petäjä, T., Praplan, A. P., Riccobono, F., Rissanen, M. P., Rondo, L., Schobesberger, S., Seinfeld, J. H., Steiner, G., Tomé, A., Tröstl, J., Winkler, P. M., Williamson, C., Wimmer, D., Ye, P., Baltensperger, U., Carslaw, K. S., Kulmala, M., Worsnop, D. R. and Curtius, J.: Neutral molecular cluster formation of sulfuric acid-dimethylamine observed in real time under atmospheric conditions, Proc Natl Acad Sci USA, 111(42), 15019–15024, doi:10.1073/pnas.1404853111, 2014.

Laiko, V. V., Dodonov, A. F. and Cotter, R. J.: Resolution and spectral-line shapes in the reflecting time-of-flight mass spectrometer with orthogonally injected ions, Rapid Communications in Mass Spectrometry, 8(9), 720, doi:10.1002/rcm.1290080912, 1994.

Lee, B. H., Lopez-Hilfiker, F. D., Mohr, C., Kurtén, T., Worsnop, D. R. and Thornton, J. A.: An iodide-adduct high-resolution time-of-flight chemical-ionization mass spectrometer: application to atmospheric inorganic and organic compounds, Environmental Science & Technology, 48(11), 6309–6317, doi:10.1021/es500362a, 2014.

Lindinger, W. and Jordan, A.: Proton-transfer-reaction mass spectrometry (PTR–MS): on-line monitoring of volatile organic compounds at pptv levels, Chem Soc Rev, 27(5), 347, doi:10.1039/a827347z, 1998.

Lindinger, W., Hansel, A. and Jordan, A.: On-line monitoring of volatile organic compounds at pptv levels by means of proton-transfer-reaction mass spectrometry (PTR-MS) medical applications, food control and environmental research, International Journal of Mass Spectrometry and Ion Processes, 173(3), 191, doi:10.1016/s0168-1176(97)00281-4, 1998.

Lopez-Hilfiker, F. D., Iyer, S., Mohr, C., Lee, B. H., DaposAmbro, E. L., Kurtén, T. and Thornton, J. A.: Constraining the sensitivity of iodide adduct chemical ionization mass spectrometry to multifunctional organic molecules using the collision limit and thermodynamic stability of iodide ion adducts, Atmospheric Measurement Techniques, 9(4), 1505, doi:10.5194/amt-9-1505-2016, 2016.

Lopez-Hilfiker, F. D., Mohr, C., Ehn, M., Rubach, F., Kleist, E., Wildt, J., Mentel, T. F., Lutz, A., Hallquist, M., Worsnop, D. and Thornton, J. A.: A novel method for online analysis of gas and particle composition: description and evaluation of a Filter Inlet for Gases and AEROsols (FIGAERO), Atmospheric Measurement Techniques, 7(4), 983, doi:10.5194/amt-7-983-2014, 2014.

Mamyrin, B. A., Karataev, V. I., Shmikk, D. V. and Zagulin, V. A.: The mass-reflectron, a new nonmagnetic time-of-flight mass spectrometer with high resolution, Zh Eksp Teor Fiz, 1973.

Mauldin, R. L., Tanner, D. J. and Eisele, F. L.: A new chemical ionization mass spectrometer technique for the fast measurement of gas phase nitric acid in the atmosphere, Journal of Geophysical Research: Atmospheres, 103(D3), 3361, doi:10.1029/97jd02212, 1998.

Mentel, T. F., Springer, M., Ehn, M., Kleist, E., Pullinen, I., Kurtén, T., Rissanen, M., Wahner, A. and Wildt, J.: Formation of highly oxidized multifunctional compounds: autoxidation of peroxy radicals formed in the ozonolysis of alkenes – deduced from structure–product relationships, Atmospheric Chemistry and Physics, 15(12), 6745, doi:10.5194/acp-15-6745-2015, 2015.

Millet, D. B., Baasandorj, M., Farmer, D. K., Thornton, J. A., Baumann, K., Brophy, P., Chaliyakunnel, S., de Gouw, J. A., Graus, M., Hu, L., Koss, A., Lee, B. H., Lopez-Hilfiker, F. D., Neuman, J. A., Paulot, F., Peischl, J., Pollack, I. B., Ryerson, T. B., Warneke, C., Williams, B. J. and Xu, J.: A large and ubiquitous source of atmospheric formic acid, Atmospheric Chemistry and Physics, 15(11), 6283, doi:10.5194/acp-15-6283-2015, 2015.

Mohr, C., Lopez-Hilfiker, F. D., Zotter, P., Prévôt, A. S. H., Xu, L., Ng, N. L., Herndon, S. C., Williams, L. R., Franklin, J. P., Zahniser, M. S., Worsnop, D. R., Knighton, W. B., Aiken, A. C., Gorkowski, K. J., Dubey, M. K., Allan, J. D. and Thornton, J. A.: Contribution of nitrated phenols to wood burning brown carbon light absorption in Detling, United Kingdom during winter time, Environmental Science & Technology, 47(12), 6316–6324, doi:10.1021/es400683v, 2013.

Munson, M. S. B. and Field, F. H.: Chemical Ionization Mass Spectrometry. I. General Introduction, Journal of the American Chemical Society, 88(12), 2621, doi:10.1021/ja00964a001, 1966.

Möhler, O. and Arnold, F.: Flow reactor and triple quadrupole mass spectrometer investigations of negative ion reactions involving nitric acid: Implications for atmospheric HNO3 detection by …, Journal of Atmospheric Chemistry, 1991.

Nguyen, T. B., Coggon, M. M., Bates, K. H., Zhang, X., Schwantes, R. H., Schilling, K. A., Loza, C. L., Flagan, R. C., Wennberg, P. O. and Seinfeld, J. H.: Organic aerosol formation from the reactive uptake of isoprene epoxydiols (IEPOX) onto non-acidified inorganic seeds, Atmospheric Chemistry and Physics, 14(7), 3497, doi:10.5194/acp-14-3497-2014, 2014.

Nguyen, T. B., Crounse, J. D., Teng, A. P., Clair, J. M. S., Paulot, F., Wolfe, G. M. and Wennberg, P. O.: Rapid deposition of oxidized biogenic compounds to a temperate forest, Proc Natl Acad Sci USA, 112(5), E392–401, doi:10.1073/pnas.1418702112, 2015.

Perkins, M. D. and Eisele, F. L.: First mass spectrometric measurements of atmospheric ions at ground level, Journal of Geophysical Research, 89(D6), 9649, doi:10.1029/jd089id06p09649, 1984.

Praplan, A. P., Schobesberger, S., Bianchi, F., Rissanen, M. P., Ehn, M., Jokinen, T., Junninen, H., Adamov, A., Amorim, A., Dommen, J., Duplissy, J., Hakala, J., Hansel, A., Heinritzi, M., Kangasluoma, J., Kirkby, J., Krapf, M., Kürten, A., Lehtipalo, K., Riccobono, F., Rondo, L., Sarnela, N., Simon, M., Tomé, A., Tröstl, J., Winkler, P. M., Williamson, C., Ye, P., Curtius, J., Baltensperger, U., Donahue, N. M., Kulmala, M. and Worsnop, D. R.: Elemental composition and clustering behaviour of α-pinene oxidation products for different oxidation conditions, Atmospheric Chemistry and Physics, 15(8), 4145, doi:10.5194/acp-15-4145-2015, 2015.

Radionova, A., Filippov, I. and Derrick, P. J.: In pursuit of resolution in time-of-flight mass spectrometry: A historical perspective, Mass Spectrom Rev, doi:10.1002/mas.21470, 2015.

Schobesberger, S., Franchin, A., Bianchi, F., Rondo, L., Duplissy, J., Kürten, A., Ortega, I. K., Metzger, A., Schnitzhofer, R., Almeida, J., Amorim, A., Dommen, J., Dunne, E. M., Ehn, M., Gagné, S., Ickes, L., Junninen, H., Hansel, A., Kerminen, V. M., Kirkby, J., Kupc, A., Laaksonen, A., Lehtipalo, K., Mathot, S., Onnela, A., Petäjä, T., Riccobono, F., Santos, F. D., Sipilä, M., Tomé, A., Tsagkogeorgas, G., Viisanen, Y., Wagner, P. E., Wimmer, D., Curtius, J., Donahue, N. M., Baltensperger, U., Kulmala, M. and Worsnop, D. R.: On the composition of ammonia–sulfuric-acid ion clusters during aerosol particle formation, Atmospheric Chemistry and Physics, 15(1), 55, doi:10.5194/acp-15-55-2015, 2015.

Sipilä, M., Sarnela, N., Jokinen, T., Junninen, H., Hakala, J., Rissanen, M. P., Praplan, A., Simon, M., Kürten, A., Bianchi, F., Dommen, J., Curtius, J., Petäjä, T. and Worsnop, D. R.: Bisulfate – cluster based atmospheric pressure chemical ionization mass spectrometer for high-sensitivity (, Atmospheric Measurement Techniques, 8(10), 4001, doi:10.5194/amt-8-4001-2015, 2015.

Stark, H., Yatavelli, R. L. N., Thompson, S. L., Kimmel, J. R., Cubison, M. J., Chhabra, P. S., Canagaratna, M. R., Jayne, J. T., Worsnop, D. R. and Jimenez, J. L.: Methods to extract molecular and bulk chemical information from series of complex mass spectra with limited mass resolution, International Journal of Mass Spectrometry, 389, 26, doi:10.1016/j.ijms.2015.08.011, 2015.

Stephens, W. E.: Proceedings of the American Physical Society, Physical Review, 69(11-12), 674, doi:10.1103/physrev.69.674, 1946.

Sulzer, P., Hartungen, E., Hanel, G., Feil, S., Winkler, K., Mutschlechner, P., Haidacher, S., Schottkowsky, R., Gunsch, D., Seehauser, H., Striednig, M., Jürschik, S., Breiev, K., Lanza, M., Herbig, J., Märk, L., Märk, T. D. and Jordan, A.: A Proton Transfer Reaction-Quadrupole interface Time-Of-Flight Mass Spectrometer (PTR-QiTOF): High speed due to extreme sensitivity, International Journal of Mass Spectrometry, 368, 1, doi:10.1016/j.ijms.2014.05.004, 2014.

Szabo, I.: New ion-optical devices utilizing oscillatory electric fields. I. Principle of operation and analytical theory of multipole devices with two-dimensional electric fields, International Journal of Mass Spectrometry and Ion Processes, 73(3), 197, doi:10.1016/0168-1176(86)80001-5, 1986.

Tanner, D. J. and Eisele, F. L.: Present OH measurement limits and associated uncertainties, Journal of Geophysical Research, 100(D2), 2883, doi:10.1029/94jd02609, 1995.

Tanner, D. J., Jefferson, A. and Eisele, F. L.: Selected ion chemical ionization mass spectrometric measurement of OH, Journal of Geophysical Research: Atmospheres, 102(D5), 6415, doi:10.1029/96jd03919, 1997.

Veres, P. R., Roberts, J. M., Cochran, A. K., Gilman, J. B., Kuster, W. C., Holloway, J. S., Graus, M., Flynn, J., Lefer, B., Warneke, C. and de Gouw, J.: Evidence of rapid production of organic acids in an urban air mass, Geophysical research letters, 38(17), n/a, doi:10.1029/2011gl048420, 2011.

Veres, P., Roberts, J. M., Warneke, C., Welsh-Bon, D., Zahniser, M., Herndon, S., Fall, R. and de Gouw, J.: Development of negative-ion proton-transfer chemical-ionization mass spectrometry (NI-PT-CIMS) for the measurement of gas-phase organic acids in the atmosphere, International Journal of Mass Spectrometry, 274(1-3), 48, doi:10.1016/j.ijms.2008.04.032, 2008.

Viggiano, A. A., Perry, R. A., Albritton, D. L., Ferguson, E. E. and Fehsenfeld, F. C.: Stratospheric negative-ion reaction rates with H2SO4, Journal of Geophysical Research, 87(C9), 7340, doi:10.1029/jc087ic09p07340, 1982.

Yatavelli, R. L. N. and Thornton, J. A.: Particulate Organic Matter Detection Using a Micro-Orifice Volatilization Impactor Coupled to a Chemical Ionization Mass Spectrometer (MOVI-CIMS), Aerosol Science and Technology, 44(1), 61, doi:10.1080/02786820903380233, 2010.

Yatavelli, R. L. N., Lopez-Hilfiker, F., Wargo, J. D., Kimmel, J. R., Cubison, M. J., Bertram, T. H., Jimenez, J. L., Gonin, M., Worsnop, D. R. and Thornton, J. A.: A Chemical Ionization High-Resolution Time-of-Flight Mass Spectrometer Coupled to a Micro Orifice Volatilization Impactor (MOVI-HRToF-CIMS) for Analysis of Gas and Particle-Phase Organic Species, Aerosol Science and Technology, 46(12), 1313, doi:10.1080/02786826.2012.712236, 2012.

Yatavelli, R. L. N., Stark, H., Thompson, S. L., Kimmel, J. R., Cubison, M. J., Day, D. A., Campuzano-Jost, P., Palm, B. B., Hodzic, A., Thornton, J. A., Jayne, J. T., Worsnop, D. R. and Jimenez, J. L.: Semicontinuous measurements of gas–particle partitioning of organic acids in a ponderosa pine forest using a MOVI-HRToF-CIMS, Atmospheric Chemistry and Physics, 14(3), 1527, doi:10.5194/acp-14-1527-2014, 2014.

Zhang, Q., Jimenez, J. L., Canagaratna, M. R., Allan, J. D., Coe, H., Ulbrich, I., Alfarra, M. R., Takami, A., Middlebrook, A. M., Sun, Y. L., Dzepina, K., Dunlea, E., Docherty, K., DeCarlo, P. F., Salcedo, D., Onasch, T., Jayne, J. T., Miyoshi, T., Shimono, A., Hatakeyama, S., Takegawa, N., Kondo, Y., Schneider, J., Drewnick, F., Borrmann, S., Weimer, S., Demerjian, K., Williams, P., Bower, K., Bahreini, R., Cottrell, L., Griffin, R. J., Rautiainen, J., Sun, J. Y., Zhang, Y. M. and Worsnop, D. R.: Ubiquity and dominance of oxygenated species in organic aerosols in anthropogenically-influenced Northern Hemisphere midlatitudes, Geophysical research letters, 34(13), n/a, doi:10.1029/2007gl029979, 2007.

de Gouw, J. and Warneke, C.: Measurements of volatile organic compounds in the earth's atmosphere using proton-transfer-reaction mass spectrometry, Mass Spectrom Rev, 26(2), 223–257, doi:10.1002/mas.20119, 2006.

CHAPTER 2

A SWITCHABLE REAGENT ION HIGH-RESOLUTION TIME-OF-FLIGHT CHEMICAL IONIZATION MASS SPECTROMETER FOR REAL-TIME MEASUREMENT OF GAS PHASE OXIDIZED SPECIES: CHARACTERIZATION FROM THE 2013 SOUTHERN OXIDANT AND AEROSOL STUDY[1]

2.1 Introduction

Chemical ionization mass spectrometry (CIMS) remains an active area of research and development despite its long history of atmospheric application. CIMS instrumentation continues to increase the number and diversity of quantifiable compounds in both the gas and aerosol phase due, primarily, to advances in mass spectrometry. The choice of reagent ion is paramount to detecting atmospherically relevant compounds with a high degree of sensitivity without interference from other species (Huey, 2007). The concept of CIMS relies on selectively ionizing a subset of the molecular species present in the sampled air in order to simplify analysis and reduce isobaric interferences. This is the key to quadrupole based mass spectrometers, which do not provide sub-unit mass resolution and can suffer from isobaric interferences when analyzing complex mixtures without separation. High-resolution time-of-flight chemical ionization mass spectrometers (HR-TOF-CIMS) capable of determining molecular composition help to alleviate this problem with species differing slightly in exact mass, but they cannot directly distinguish between conformational isomers (Nozière et al., 2015). As such, reagent ion selectivity remains

[1]Brophy, P., Farmer, D.K.: A Switchable Reagent Ion High-Resolution Time-of-Flight Chemical Ionization Mass Spectrometer for real-time measurement of gas phase oxidized species: Characterization from the 2013 Southern Oxidant and Aerosol Study, Atmos. Meas. Tech., 8, 2945-2959, 2015, DOI: 10.5194/amt-8-2945-2015

the key to unambiguously analyzing atmospheric samples by CIMS regardless of the detector resolution. Conversely, reagent ion selectivity also limits the amount of information one can obtain from an atmospheric sample. Multiple reagent analysis maintains the benefit of selectivity while increasing the number of detectible species.

Multiple reagent analysis in CIMS provides a wealth of information and allows investigators to observe the system of interest using different ionization schemes; each reagent ion softly, little to no fragmentation of neutral species upon ionization, ionizes different species to a different degree providing the analyst with different sets of information. The proton-transfer-reaction mass spectrometry (PTR-MS) community implements this approach to a limited extent through the use of hollow cathode technology to produce not only H_3O^+ but also NO^+ and O_2^+ (Jordan et al., 2009). NO^+ is known to be a soft ionizer like H_3O^+, and O_2^+ is less soft and can provide another option for ionizing species of interest. Selected ion flow tube mass spectrometry (SIFT-MS) using H_3O^+, NO^+, and O_2^+ reagents is well studied, and rapidly switching the reagent ion and simultaneous use of two reagent ions at once are reported with promising results (Smith et al., 2005). The major limitation noted in these studies is peak overlap on a quadrupole based mass spectrometer. Laboratory examples using multiple reagent analysis are limited. Investigations of the aqueous-phase photooxidaiton of levoglucosan (Zhao et al., 2014) and the ozonolysis of α-pinene (Aljawhary et al., 2013) use multiple reagent ions (iodide, protonated water clusters, and acetate) in their analysis. These different ionization schemes provide very different mass spectra and a more comprehensive picture of the underlying chemistry. The fact that few studies use multiple reagent analysis is not surprising. Recent commercialization of the field-deployable HR-TOF-CIMS has started to transition the CIMS field from thinking about

individual compounds, primarily due to hardware limitations of quadrupole based systems, to ensembles of compounds detected across a large mass range (Chhabra et al., 2015).

Typical CIMS measurements utilize one reagent ion throughout a measurement campaign or various regent ions in controlled laboratory settings where experiments can be repeated; the latter case provides a broader suite of compounds than the use of a single reagent ion. Reagent ions are generated from two component gas mixtures (usually nitrogen and a precursor reagent molecule) and exposed to either a radioactive source (Po-210 or Am-241) or a hollow cathode source. The reagent ion flow mixes with ambient sample and selectively ionizes neutral species. Matrix effects can alter ionization efficiency in different ways for different reagent ions. For example, iodide ionization of organic acids exhibits a strong dependence on relative humidity but not necessarily the same dependence for every analyte (Kercher et al., 2009; Mielke et al., 2011; Lee et al., 2014; Woodward-Massey et al.,2014). High backgrounds are also a problem for CIMS measurements. Wentzel et al. (2014) report high formic acid backgrounds using the acetate reagent ion preventing the measurement of formic acid during chamber studies. This highlights two problems with CIMS measurements: the preparation of clean air without detectible concentrations of species of interest for reproducible background measurements, and the production of reagent ion gas mixtures without numerous side products that contribute to instrument background. Both issues affect instrument backgrounds and can increase the limit of detection.

Five reagent ions outside the PTR-MS and SIFT-MS field have seen recent application to ambient atmospheric measurements: protonated water clusters $(H_2O)_nH^+$, iodide water clusters $I(H_2O)_n^-$, nitrate NO_3^-, CF_3O^-, and acetate $CH_3CO_2^-$. These reagents and the relevant literature are summarized by Aljawhary et al. (2013). Effectively implementing a reagent ion scheme involves

tuning the mass spectrometer voltages to optimize the detection of the product ions or clusters. For example, the acetate ion requires strong declustering electric fields such that all detectable species (M) are observed as deprotonated ions (R2.1a) and not as clusters (R2.1b) (Chhabra et al., 2015).

$$H\text{-}M + CH_3C(O)O^- \rightarrow CH_3C(O)OH + M^- \quad \text{(R2.1a)}$$

$$H\text{-}M + CH_3C(O)O^- \rightarrow [CH_3C(O)O^- \cdot M\text{-}H] \quad \text{(R2.1b)}$$

Alternatively, the use of iodide water clusters requires the opposite treatment of the electric fields. Species detected by iodide appear primarily as clusters (R2.2), and their efficient transfer to the time-of-flight region of the instrument is crucial to maintain high sensitivity (Lee et al., 2014).

$$I\text{-}H_2O^- + M \rightarrow I\text{-}M^- + H_2O \quad \text{(R2.2)}$$

In modern instrumentation, voltages associated with the mass spectrometer's transfer optics to increase or decrease clustering can be modified rapidly (<1 s). Changing the polarity of the instrument to detect negative and positive ions is relatively slow (>1 minute). The ion molecule reactor and radioactive source used for water cluster, iodide, CF_3O^-, and acetate CIMS is the same, but nitrate systems have substantially different reactors. Water cluster CIMS operates in positive mode, while the others operate in negative mode. The storage and preparation of CF_3O^- remains challenging compared to the other methods (Crounse et al., 2006). For these reasons, this paper proposes online switching between iodide and acetate CIMS, with the added benefit that acetate's sensitivity to acids is independent of water vapor (Veres et al., 2008). Here, we describe the switchable reagent ion (SRI) HR-TOF-CIMS, characterize its background, sensitivity and stability, and use ambient measurements taken during the Southern Oxidant and Aerosol Study to describe a method for examining the bulk high-resolution data.

2.2 Site Description

The Southern Oxidant and Aerosol Study (SOAS) set out to understand the interactions of biogenic and anthropogenic emissions in the southeastern United States. The SOAS ground supersite, located in Brent, Alabama (32.903016^0, -87.250104^0) included gas, aerosol, and meteorological instruments. The site is located in a cleared field on top of a hill surrounded by dense hardwood and pine forests in a rural landscape. High temperature (24.7 ^{0}C average, 32.7 ^{0}C max, 17.4 ^{0}C min) and high relative humidity (81.8% RH average, 100% RH max, 37.9% RH min) characterize the summer months. The SRI-HR-TOF-CIMS was housed in an air conditioned trailer located on top of the cleared hill. The instrument inlet was positioned above the trailer roof at a height of 6 m with a total length of approximately 7.5 m.

2.3 Instrument Description

We demonstrate online reagent ion switching for gas phase field measurements during the SOAS campaign in an effort to measure a broader suite of compounds and utilize the advantages associated with a high-resolution time-of-flight mass spectrometer.

2.3.1 The HR-TOF-CIMS

The HR-TOF-CIMS (Tofwerk AG and Aerodyne Research, Inc.) (Figure 2.1, S2.I1) is described extensively in the literature (DeCarlo et al., 2006; Bertram et al., 2011; Yatavelli et al. 2012; Lee et al., 2014), and we offer a brief description here. The HR-TOF-CIMS can sample at or below atmospheric pressure using an atmospheric pressure interface (APi) that reduces the pressure through a series of four sequential pressure drops leading to the high vacuum time-of-flight chamber (Junninen et al., 2010). In a chemical ionization (CI) configuration, ambient air enters the ion molecule reactor (IMR) and mixes with the CI reagent ion. IMR pressure is independently controlled by a single scroll SH-110 pump (Agilent Technologies). Ions generated

in the IMR pass through two sets of segmented, RF-only quadrupoles and a lens stack prior to entering the orthogonal extraction region of the time-of-flight mass spectrometer.

The first segmented quadrupole is the short segmented quadrupole (SSQ) located after the IMR in a separate vacuum region held at 2 mbar by a Triscroll 600 pump (Agilent Technologies). The segmented quadrupole provides a linear voltage drop across the length of the quadrupole, and it helps to control both the transmission of ion-neutral clusters through the APi and contributes to the mass-to-charge (m/z) dependent transmission efficiency of the instrument. Subsequent vacuum regions housing the second set of segmented quadrupoles, lens stack, and time-of-flight chamber are pumped by a split-flow turbomolecular pump (Pfeiffer Vacuum Technology AG) backed by an MD-1 diaphragm pump (Vaccubrand, Inc.). The second, larger set of segmented, RF-only quadrupoles (the 'big segmented quadrupole', BSQ) has similar functionality as the SSQ. Lastly, the lens stack helps to align the ion trajectory into the orthogonal extraction region, affecting the resolution ($m/\Delta m$) and the shape of the observed high-resolution peak.

Ion counts detected on the micro channel plate detector (Photonis Inc) are amplified and pre-averaged on the analogue to digital converter (ADQ1600, SP Devices) before being sent to the computer (Dell Power Edge R220) via a high speed USB connection. Online mass calibration occurs simultaneously with the data acquisition but requires additional post-processing. The instrument regularly achieves high mass accuracy (<20 ppm) with mass resolution >4000. Mass spectra are acquired at an extraction frequency of 17 kHz corresponding to a mass-to-charge (m/z) range of 15-1026 in the negative mode at 1 second resolution.

2.3.2 Ion Generation

Iodide and acetate reagent ions are chosen for this experiment for a variety of reasons:

1. Both ions are acquired in the negative mode making APi voltage switching fast
2. Acetate and iodide are commonly used in ambient field measurements
3. The two reagent ions provide different sets of measureable compounds
4. Iodide has humidity dependence, but acetate does not
5. The methods of generating iodide and acetate ions are simple

Acetate (also referred to as negative-ion proton-transfer CIMS (NI-PT-CIMS) or acid-CIMS) provides a method for softly ionizing gas phase organic and inorganic acids (Veres et al., 2008; Roberts et al., 2010; Veres et al., 2011; Yatavelli et al., 2012) and nitrated phenols (Mohr et al., 2013) with a high degree of sensitivity. Iodide measures oxidation products from isoprene and terpene species, acids, and various inorganic species (Huey et al., 1995; Slusher et al., 2004; Kercher et al., 2009; Aljawhary et al., 2013; Lee et al., 2014; Woodward-Massey et al., 2014). Together, the two CI methods provide measurements of gas phase species that are generally more oxidized than those observed using PTR-TOF-MS, but neither acetate nor iodide appear to provide measurements of extremely low volatility organic compounds (ELVOCs) that are observed using nitrate CI (Aljawhary et al., 2013; Ehn et al., 2014). CF_3O^- provides another interesting reagent ion choice that could be implemented on this system, but the difficulties associated with producing and storing the precursor pose a significant challenge compared to the facile methods of producing iodide and acetate reagent ions (Crounse et al., 2006).

Iodide ion generation on this instrument is similar to methods described in the literature (Slusher et al., 2004; Lee et al., 2014). Briefly, a home built methyl iodide (Sigma Aldrich, 99% Reagent Plus) permeation device constructed from ¼'' perfluoroalkoxy (PFA) tubing is placed

inside a glass tube surrounded by a temperature controlled aluminum block held at 40 ^{0}C. Ultra high purity (UHP) nitrogen is flown over the permeation device at a rate of 2 standard liters per min (SLPM). Acetate ions are generated following the design presented by Veres et al. (2008). A 0.5 L electropolished stainless steel cylinder (Swagelok) filled with 300 mL of acetic anhydride (Sigma Aldrich, ≥99% Reagent Plus) is placed inside an aluminum block and heated to 50 ^{0}C. UHP nitrogen delivered to the headspace of the cylinder at a rate of 5 standard cubic centimeters per minute (sccm) mixes with the diluting flow to provide a total flow of approximately 2 SLPM.

Both sources are switched on and off by activating an inline stainless steel solenoid valve (Parker Hannifin Corp, Model 009-0272-900) using home built circuitry and a CoolCube (Parker Hannifin Corp) to prevent the valves from overheating during prolonged operation. Each source uses only stainless steel tubing and separate Po-210 ionizers (NRD, 10 mCi) to reduce contamination between sources. The output of the ion sources (1 SLPM) mix with incoming ambient air (2 SLPM) in the IMR. The IMR is held at 60 ^{0}C and 100 mbar for the duration of the study.

2.3.3 Source Switching

Switching the reagent ion mode requires changing the mass spectrometer voltages associated with the ion transfer optics in the APi in order to change the extent to which clustering occurs. A custom LabVIEW (National Instruments, LabVIEW 2013) interface is implemented using Tofwerk's Application Programing Interface (Tofwerk AG, Version 1.94) to control the instrument's data acquisition system, set voltages associated with the ion transfer optics, and synchronize all online automation. External devices and data streams are acquired using Labjack data acquisition devices (Labjack, model U12). Iodide voltage set points are optimized by maximizing the $[I{\bullet}H_2O]^-$ cluster relative to I^- in an attempt to efficiently transfer iodide adducts

to the ToF analyzer (Lee et al., 2014). Acetate voltage set points were optimized by minimizing the acetate acetic acid cluster, $[Ac•AcH]^-$, relative to the acetate ion. The ratio between the acetate-acetic acid cluster and acetate is 0.02, which is similar to the values reported by Mohr et al. (2013), using the Aerodyne HR-TOF-CIMS. This value greatly differs from the value (0.2) reported by Chhabra et al. (2015) using the same instrument. Careful tuning to minimize the $[Ac•AcH]^-$ is likely important for maintaining sensitivity, minimizing clustering with the acetate reagent ion via reaction R1b, and avoiding mass spectral misinterpretation (Chhabra et al., 2015).

The LabVIEW program begins by switching the necessary valves to introduce and interrupt the appropriate reagent ion flows, and sends the associated voltage set points to the mass spectrometer's power supply and control hardware. Next, data acquisition is triggered from within the LabVIEW program starting the TOF extraction pulses and triggering the acquisition of data. Instrument acquisition parameters such as run time, m/z range, and preaveraging are preset. Once data acquisition is initiated from LabVIEW, the TOF data acquisition recorder runs until the acquisition runtime is met. LabVIEW and the associated Tofwerk Application Programing Interface monitor whether acquisition is active, and at the end of the run the program restarts by selecting the appropriate reagent configuration. Calibrations and external device control are typically initiated at the beginning of acquisition, but this is user selectable and customizable.

2.3.4 Data Analysis and High-Resolution Processing

Data are analyzed with Tofware (Aerodyne Research, Inc. and Tofwerk AG) and Igor Pro (Wavemetrics). The different reagent ion chemistries necessitate different data treatment in order to properly determine single ion peak shape, the masses used to determine instrument resolution, and ions suitable for mass calibration. Iodide mass calibration is conducted on O_2^-, Cl^-, NO_2^-, I^-,

IH_2O^-, $IHNO_3^-$, and I_3^-. Acetate mass calibration is conducted on O_2^-, Cl^-, NO_2^-, $C_2H_3O_2^-$, NO_3^-, $C_2F_3O_2^-$, and $C_4H_7O_4^-$. In both cases, these ions provide a stable mass calibration over time. Both mass calibrations use a three parameter fit ($a*m^c+b$) included as an option within Tofware (DeCarlo et al., 2006). Baseline calculations use a pre-averaging algorithm for both iodide and acetate, which captures the baseline properly for most ions of interest. A TOF duty cycle correction is applied to the largest reagent ion signal, acetate or iodide, which corrects for the inherent mass-to-charge bias introduced from orthogonal extraction. High-resolution (HR) analysis requires two separate lists of ion molecular formula for fitting, which differ significantly between ion sources. The SOAS data set undergoes preaveraging from the original 1 Hz data to 0.1 Hz to expedite HR fitting calculations. After processing the HR ion fits, the data are normalized to the reagent ion signal (I^- and CH_3COO^-). The HR fit of iodide and acetate are used to normalize all ions detected with iodide and acetate, respectively. The subsequent treatment of the processed HR normalized data is completed using code written specifically for the analysis of the SOAS field campaign given the timing of hourly, automated calibrations and zeros.

2.3.5 Fast Flow, Reduced Pressure Inlet with Integrated Atmospheric Pressure Calibration Source

A fast flow, reduced pressure borosilicate glass inlet with particle skimming geometry based off the work of Ellis et al. (2010) is used for SOAS measurements (Figure 2.2, SI2.2). Limited examples of particle skimming inlets exist in the literature but characterization remains lacking (Kercher et al., 2009).

2.3.5.1 Reduced Pressure Inlet

Significant modifications to the original design make the inlet suitable for interfacing to a mass spectrometer designed for trace gas detection. Ambient air (including both gases and

particles) enter a 1'' OD, thick walled glass tube at atmospheric pressure before passing through a 1.0 mm glass critical orifice. This orifice limits the flow to the pump and reduces the pressure of the inlet system. A large bypass flow pumps the inlet in line with the air passing through the critical orifice, and the sampling flow pulls air orthogonally to the flow crossing the critical orifice in an attempt to eliminate particles from contacting the IMR and sampling lines. The bypass line and sampling line reconnect after the IMR interface. Flow is monitored just after the IMR and after the two lines reconnect by means of two analogue mass flow meters (MKS Instruments), thus providing a measure of total flow to the pump. Pressure monitoring with a Baratron (MKS Instruments, Model 750C) occurs after both flow meters, and pressure is controlled using a fast-acting bidirectional electronic needle valve (Aalborg Instruments and Controls, Inc, Model SMV20) and a proportional integral derivative loop (PID) run at 10 Hz from within the Labview software.

Pressure control is crucial for this inlet system because of the observed instability of the diaphragm pump (Vaccubrand Inc., Model: MD-4) and the use of a critical orifice to separate the IMR from the reduced pressure system. If pressure changes in the sampling line, then the sample flow to the IMR will change, and thus, the ratio of the reagent flow to the sample flow becomes unstable complicating quantification. Two other major modifications from the original design include a lack of heating on the glass inlet to minimize shifts in gas-particle partitioning, and an increase in the total flow through the system.

2.3.5.2 Integration of Atmospheric Pressure Calibration Source

We integrate a permeation based calibration system into the low pressure inlet system for online calibrations with both zero air and ambient air. Calibrations conducted in zero air are *external standard calibrations,* and calibrations conducted in ambient air are *standard addition*

calibrations. Instrument zeros and calibrations are conducted hourly at the beginning of each acquisition period (Figure 2.3). The inlet design includes a port for zero air overflows and an additional port for inlet calibrations. The ultra-zero air overflow is controlled using a high pressure, normally closed solenoid valve (NResearch, Inc., Model: HP648T012) and a critical orifice (O'Keefe Controls, Inc., C_v=0.031) to provide a >20 SLPM overflow at the glass inlet. All gas lines leading from the high-purity stainless steel regulator (Matheson TRIGAS Corp.) are 1/8'' OD instrument grade stainless steel (Restek Corp.).

The calibration port is not used for this study due to the difficulty associated with transporting sticky calibration gases from permeation ovens (VICI Metronics, Dynacalibrator Model 150) through long lengths of tubing to the glass inlet. Iodide and acetate reagent ions are sensitive to the fluorinated compounds that outgas from PFA and FEP tubing, and these fluorinated compounds are known interferences for nitrate CIMS (Ehn et al., 2012). Attempts to use the calibration port in the field with long PFA transfer lines from the permeation oven to the inlet lead to the complete titration of the acetate reagent ion by fluorinated acidic compounds (trifluoroacetic acid and related compounds) outgassing from the tubing. Titration of the reagent ion makes calibration impossible. Instead, we introduce calibration gases into the reduced pressure inlet by interfacing a normally closed solenoid shutoff valve on the vent (NResearch Inc.), three way valves onto each permeation oven, and a PFA flow restricting needle valve (Swagelok, P/N: PFA-4RPS4) between the low pressure inlet line near the IMR entrance and the atmospheric pressure permeation source (Figure 2.2). This setup allows calibration gas to flow into the low pressure inlet at controlled rates over a large range (~1 mL/min to 1 L/min) when the system is activated. The flow over the permeation device(s) is never interrupted and excess flow is vented during calibrations. An additional, controllable dilution of the permeation tube

output by mass flow controller (MKS Instruments) can occur prior to introducing the flow to the low pressure inlet providing a method for producing a multipoint calibration curve over a very large calibration range. Complete formic acid calibration curves (1-10 ppb) were conducted offline each day during the campaign as both external standard and standard addition calibrations.

2.4 Results

2.4.1 Instrument Performance

The SRI-HR-TOF-CIMS SOAS dataset includes six days of data with the instrument operating in switching mode and 18 days operating in acetate mode only. Switching occurs hourly between acetate and iodide. The inlet system maintains a constant 350 mbar sampling pressure (Figure SI2.3) and calibration system provides stable calibration and zero air for the entire measurement period. The instrument, however, exhibits variable sensitivity to the zeros and calibrations over the entire measurement period regardless of mode of operation. The hourly background measurements of formic acid using acetate vary by a relative standard deviation (RSD) of 153%, and the standard addition calibrations and the external standard calibrations vary by a relative standard deviation of 50% and 41%, respectively over the entire campaign. The limit of detection (LOD) and limit of quantification (LOQ) take into account both background count rate and sensitivity providing a better metric for evaluating instrument performance than sensitivity alone. The LOD and LOQ for formic acid during the entire measurement period using acetate vary by only 20% RSD. The average LOD and LOQ are 82 ppt and 863 ppt, respectively, corresponding to an average sensitivity of 13 ± 5 Hz ppt^{-1}. This sensitivity is consistent with other reported sensitivities to formic acid when adjusted for extraction frequency (Chhabra et al., 2015, Mohr, et al., 2013, Yatavelli et al., 2012). A time series of the LOD and

LOQ calculated each hour in acetate mode is provided (Figure 2.4).Variability in formic acid background, sensitivity, and calculated limits of detection and quantification decrease when operating in switching mode compared to operation in dedicated acetate mode but likely reflects the length of time each mode operated during the campaign. The observed background variation during acetate mode is not limited to formic acid. Figure 2.5 shows the relative change in background counts for every HR ion fit plotted over the course of the entire SOAS campaign.

Background variation for iodide mode shows similar variability, and while representative of general instrument stability these backgrounds do not capture the true background due to the use of dry zero air (Lee et al., 2014). During switching mode the iodide background for formic acid varies by 49% RSD, and acetate mode varies by 27% RSD. Higher variability is also observed for formic acid calibrations using iodide (20% RSD) compared to acetate (5% RSD). Variability in the background across the mass spectra is also observed for iodide as seen with acetate (Figure 2.5).

Ambient data during acetate mode calibrated using the standard addition method and the external standard method are tightly correlated (r^2=0.986) with a slope of 0.97 exhibiting a nearly 1:1 relation (Figure 2.6). The correlation between the two methods for calibration using iodide disagree by a factor of 1.75, likely due to the issues associated with humidity and ionization efficiency (Figure 2.7).

2.4.2 Quantified Ambient Formic Acid Data Using the Acetate Reagent Ion

Three distinct time periods are observed in the formic acid time series (Figure 2.8). The first and last time periods from June 22 to July 3 and from July 8 to July 16, respectively, exhibit strong diel trends. The ambient temperatures from July 4 to July 7 were lower and coincident with daily rainfall, leading to lower gas phase concentrations often below the limit of

quantification. The maximum observed formic acid concentration of 10 ppb occurred on June 27 in the early evening (~6pm, local time). The maximum daily formic acid concentration from June 22 to July 3 and from July 8 to July 16 both occur at approximately 6 pm local time. At night, concentrations consistently drop below the limit of quantification. Three other sets of acids are provided to show the temporal behavior of various acids but calibrations are not currently available (Figure 2.9a-c).

2.4.3 Mass Defect Enhancement Plots

Numerous other acids present in the ambient acetate data show similar temporal behavior as formic acid with subtle differences depending on the species (Figure 2.9a-c), but the number of species detected exceeds what is reasonable to publish as time series. Thus, figure 2.10a shows a mass defect plot of a normalized and background corrected one hour average on the afternoon of June 27, 2013 between 3:00 PM and 4:00 PM local time of all the ions detected with acetate and assigned a HR ion fit. Figure 2.10b shows the effect of filtering the data by signal-to-noise ratio and shows only the species with S/N>3. The mass defect (d_m) is the difference between the nominal mass and the exact mass of the detected ion. The mass defect of detected species plotted against the mass-to-charge ratio provides one space to examine complex, high-resolution time-of-flight mass spectral data. The signal-to-noise ratio is defined as the ratio of one ion signal during ambient sampling divided by the standard deviation of that ion at some confidence level (typically 3σ) measured in zero air. Normally, signal-to-noise would be reported at some specific concentration, but calibration factors are not available for the majority of the species measured; this use of signal-to-noise criteria helps to filter out background ions and detected species that if we knew the calibration factor would still be below the statistically

significant limit of detection. Of the 621 ions fit in the HR spectra, 423 are eliminated by imposing the signal-to-noise cutoff.

CIMS measurements are characterized by high background signal, and we note that frequent online zeros are essential for examining data in this space due to background measurement instability. These frequent zeros can either directly provide an enhancement ratio or help to provide trustworthy enhancement ratios by constraining background variability. The enhancement ratio is defined as the ambient signal of the ion subtracted by the background signal and divided by the ambient signal expressed as a percent. Alternatively, if strong diel behavior is observed or if plumes are intercepted at an instrument's inlet, an enhancement ratio can be defined by a time of high or low signal acting as ambient or background signal, respectively. This type of analysis may be broadly useful for measurement techniques like HR-TOF-CIMS that have high background signal as it clarifies which signals are truly present in ambient data. This approach is of particular interest for chamber studies where hundreds, or even thousands, of compounds are detected but many remain unchanged over the course of the experiment. Figure 2.10c shows the effect of applying the enhancement ratio cut off to eliminate species that change less than 5% from background using the same signal-to-noise filtered data as in figure 2.10b; this additional filtering eliminates 94 ions from the 198 ions meeting the signal-to-noise criteria. The diel method is also presented; figure 2.10d shows the mass defect enhancement plot of background subtracted data where the average signal during the photochemical minimum, occurring between 1:55 AM and 2:45 AM on June 27th, is used as the background and the photochemical maximum, occurring between 5:05 PM and 5:55 PM on June 27th, is used as the signal. Thus, the diel approach to mass defect plots quantifies the enhancement in signal in daytime over nighttime.

Representative time series are presented for iodide mode highlighting isoprene related oxidation species detected as clusters with iodide (Figure 2.11). Signal-to-noise criteria do not help to filter iodide data due to overall higher signal-to-noise ratios compared to acetate mode data. As such, a mass defect plot showing the species that change by more than 5% from 6:00 AM on June 22 to 6 PM on June 22, 2013 is presented and colored by the calculated percent change (Figure 2.12). Out of 556 HR ion fits between 32 and 328 m/z, 162 ions change by less than 5%.

Lastly, additional dimensions of data can aid in the interpretation of these enhancement mass defect plots. For example, one can perform cross correlation calculations on the ions of interest and color the enhancement mass defect plot by the correlation coefficient (r) (SI2.4). The correlation coefficient can be calculated for any species of interest against all other species or even calculated using auxiliary instrument data (wind direction, $[O_3]$, ambient temperature, etc.) against all ions present on the enhancement mass defect plot. HR-TOF mass spectrometers have the added advantage of providing elemental composition. This can provide another descriptive parameter for exploring the enhancement mass defect plot; the oxygen to carbon ratio of ions with S/N ratio >3 are presented in the supplementary information (SI2.5).

2.4.4 Mass Defect Enhancement Plots to Evaluate Inlet Performance

The mass defect enhancement plot is used to examine data collected during the characterization of the low pressure inlet system deployed during SOAS. A nitrogen gas overflow of the inlet under normal operating conditions is used to determine the time constant associated with detected species meeting the criteria of having a signal-to-noise ratio >3 and decreasing by at least 5%. Molecular oxygen acts as a marker for the non-sticky component of ambient air sampled through the inlet. An offset exponential regression is performed on the time

series of all species meeting the criteria during the nitrogen overflow to determine the time constant, τ. This experiment was performed during the last night of SOAS at 10:45 PM local time on July 15th. Of the 621 ions fit in the HR spectra only 43 species meet the criteria and are plotted as a mass defect plot. The data are sized by signal-to-noise ratio and colored by the time constant derived from regression (Figure 2.13). Oxygen has a time constant of 1.2 s in the system.

2.5 Discussion

2.5.1 Rapid Reagent Switching Performance

Switching quickly between acetate and iodide reagent sources every 10 minutes shows minimal reagent ion hysteresis (Figure 2.14a). The primary source of the equilibration behavior observed immediately after switching sources is the time associated with pressure stabilization and the stabilization of the RF fields across the quadrupoles. Laboratory studies show that pressure stabilization takes 40 seconds after switching either source and corresponds to a pressure change of 10 mbar. SSQ and BSQ RF stabilization takes significantly longer (~2 minutes) and is indirectly observed by examining the cluster distribution of acetate+acetic acid cluster $[Ac•AcH]^-$ and iodide+water cluster $[I•H_2O]^-$.

The ratio of the primary reagent ions for each mode, iodide and acetate, to the $[I•H_2O]^-$ and $[Ac•AcH]^-$ cluster, respectively, shows the significant difference in clustering caused by voltage switching (Figure 2.14b). The acetate signal is more than 100 times greater than the first cluster, while iodide is only 5 times greater than the corresponding $[I•H_2O]^-$ cluster; this also shows the time needed to reestablish the cluster distribution inside the IMR, which requires about 3 minutes to equilibrate at 100 mbar with voltage switching but without IMR pressure control.

A potential problem with switching reagent ions is cross talk – the possibility that residual reagent from the previous mode can act as a reagent ion while operating in the alternative mode. We do not observe any direct evidence of this occurring for two reasons. First, the detection of iodide clusters is nearly impossible with acetate's strong declustering voltage settings, and we are currently focused on iodide clusters $[I+M]^-$ while operating in iodide mode. Iodide mode does produce numerous deprotonated, declustered species that are likely peroxycarboxylic acid-containing species, but the interpretation of this region of the mass spectra remains suspect due to a lack of authentic standards (Mielke et al., 2012). Second, ambient acetate calibration and background data show no obvious difference in variability due to operating in switching mode during the beginning of SOAS compared to operating the instrument in dedicated acetate mode for the latter part of SOAS. While not the focus of this study, detection of acetic acid and hydroiodic acid using iodide CIMS and acetate CIMS, respectively, in a reagent switching setup may suffer a larger cross talk problem because the detected species are the reagent ions in the complementary mode. The use of hourly zeros, or zeros immediately after switching reagents, may counteract these effects but would require investigation.

The hourly calibrations conducted during acetate mode CIMS show consistent agreement between standard addition calibrations and external standard calibrations during both switching mode and dedicated acetate mode (Figure 2.6). This suggests that switching reagents does not introduce additional matrix effects that alter the sensitivity of formic acid calibrated in zero air relative to ambient air. If reagent ion switching changed the underlying ion-molecule chemistry in the IMR, we would expect to see variability in the background measurements with zero air for acetate mode during switching versus acetate mode in a dedicated acetate-only mode. The

backgrounds, however, remain consistently variable between the switching and acetate-only time periods (Figure 2.5). Most species exhibit significant changes in background to the same extent over time regardless of whether or not reagent switching is occurring. This is also the case with the LOD and LOQ calculated for formic acid (Figure 2.4); both show changes over time, but no abrupt changes occur when dedicated acetate mode is used compared to switching mode. Thus, rapid switching appears to be a robust technique for accessing a larger variety of analyte molecules with a single instrument.

2.5.2 The Importance of Instrument Zeros and Calibrations

The hourly determination of instrument zeros during SOAS is essential for accurately quantifying formic acid and tracking the behavior of other gas phase acids using acetate reagents. Figure 2.15 demonstrates the effect of background subtracting formic acid after applying hourly calibration factors and shows that the absolute value and temporal behavior of formic acid changes depending on the background subtraction method. Applying a single background value to formic acid across the sampling period is insufficient for accurate or precise measurement, and will lead to over- or under-estimation of the instrument background and absolute concentration. The effect of background subtracting by a single value compared to hourly background subtraction can be investigated by correlating the ambient data using the two background approaches. A slope of 1.29, a y-intercept of -0.29, and an r^2=0.79 suggests that a single background subtraction causes a systematic bias. The direction of the bias will depend on the timing of the single background; in this example, concentrations are overestimated by ~30%. The effect of no background subtraction is also investigated using linear regression which produces the same slope and correlation, but with a much larger y-intercept of 2.33, indicative of an overestimate.

Calibrations in zero air and ambient air vary to a lesser extent than the observed variation in background but remain important (section 2.4.1). The agreement between the two calibration methods, as described above, is excellent (r^2= 0.98), suggesting that no matrix effects, including relative humidity, affect the ionization efficiency of formic acid using acetate as a reagent ion.

This type of systematic instability in sensitivity to formic acid using acetate as a reagent ion is also reported for an HR-TOF-CIMS operating with a micro-orifice volatilization impactor (MOVI) for aerosol sampling (Mohr et al., 2013). Frequent zeros are not presented making it difficult to address whether this instability is actually arising from background fluctuations, a true change in instrument sensitivity to formic acid, or both. Mohr et al. (2013) suggest this instability arises from changes in trailer temperature, which were similar to SOAS operating conditions. Regardless, these two examples of reported instability highlight the importance of hourly calibration and measurement of instrument backgrounds when deploying these instruments in unstable environments typically encountered during field operation.

Unlike acetate, the iodide reagent ion exhibits a humidity dependent sensitivity to formic acid (Lee et al., 2014; Woodward-Massey et al., 2014). The background signal obtained for formic acid in zero air does not represent the true background of the system because of the use of dry zero air. Despite the use of standard additions during iodide acquisition, the quantification of formic acid remains suspect due to our inability to constrain representative background. Iodide backgrounds in dry zero air show similar variability as the acetate backgrounds across the entire mass range (Figure 2.5). This provides some evidence that much of the observed variability in the two data sets arises from instrument parameters that are influenced by environmental operating conditions, such as the trailer temperature.

Previous studies using iodide CI have implemented acid scrubbers to remove formic acid (Le Breton et al., 2012). While this technique works for formic acid, it would be unlikely to remove other relevant species such as isoprene epoxide (IEPOX) or isoprene hydroxyhydroperoxide (ISOPOOH). Catalytic conversion using a heated catalyst has also been used to generate zero air from ambient air, but incomplete conversion remains a problem as the oxygenated byproducts of incomplete conversion are often detected by CI methods (Lee et al., 2014). The production of zero air and the determination of instrument background remains a challenge that can lead to artificially high LOD and LOQ when compounds of interest are not completely absent.

2.5.3 Inlet Performance for Oxygenated VOC Detection

We limit our analysis of inlet performance to ions that have S/N>3 and decrease by at least 5% from ambient during a nitrogen overflow of the inlet (Figure 2.13). Most of the species analyzed have residence times between 1 and 2 seconds, but longer residence times (~3.5 s) do exist for Cl^- and $C_8H_{11}O_4^-$. Recent work characterizing Teflon chambers shows that chemistry dependent wall losses occur (Zhang et. al., 2014). Similar surface chemistry is likely occurring inside the PFA tubing of the inlet and contributes to the observed distribution of residence time. Unfortunately, this experiment occurs at 10:45 PM EST during SOAS, corresponding to a minimum in number and concentration of species in ambient air. This inherently limits our analysis to a small subset of nighttime species, but does demonstrate that different species behave differently in the inlet.

2.5.4 Formic Acid Measurements During SOAS

The formic acid time series obtained during the SOAS campaign exhibits very strong diel variation resembling the behavior of nitric acid (Figure 2.8). Nitric acid is produced through

secondary photochemical reactions, and a strong correlation between nitric acid and formic acid would suggest that formic acid primarily arises from secondary photochemical processing. Detailed analysis of this data set shows that nitric acid and formic acid are well correlated (r^2=0.78) suggesting both may have similar sources and sinks at SOAS (Millet et al. 2015).

This correlation is contrasted by recent airborne (Le Brenton et al. 2014) and ground based measurements (Bannan et al. 2014) during the Winter ClearfLo Campaign over the United Kingdom using a quadrupole CIMS implementing the iodide reagent ion for the detection of formic and nitric acid. In that study, airborne measurements of formic acid and nitric acid are less correlated (r^2=0.59), and the ground based measurements show very low correlation (r^2=0.14). This difference between SOAS and the ClearFlo campaign suggest a difference in sources, and potentially sinks, between regions dominated by anthropogenic versus biogenic emissions. Direct formic acid emissions may dominate regions with high anthropogenic emissions while secondary sources may dominate regions with primarily biogenic influences (Paulot et al. 2011). In the biogenic-dominated SOAS dataset, rapid photochemical sources and rapid sinks are required to explain the diel profile. There is no evidence for such rapid sinks in the ClearFlo datasets, suggesting a less rapid sink of formic acid, potentially due to seasonal or land-cover differences.

Ground based gas phase acid measurements during CalNex 2010 in Pasadena, California with an acetate CIMS showed significant enhancement of formic acid from night to day (Veres et al. 2011). Nitric acid correlates with formic acid (r^2=0.59) and is similar to what is found over the United Kingdom during the winter. Formic acid peaks at noon during the CalNex study, but peak formic acid occurs around 3 PM local time at SOAS. In both cases, formic acid continually decreases overnight.

2.5.5 Other Acids Detected During SOAS

Numerous ions detected using acetate have high signal-to-noise ratios providing direction for future investigations using HR-TOF-CIMS. Out of the 621 ions fit in the acetate spectra, 198 HR ions fit from 32-320 m/z have S/N >3 and 57 ions have S/N>10 during the peak photochemical hour on June 28th of the SOAS study. Formic (CH_2O_2), acrylic ($C_3H_4O_2$), propanoic ($C_3H_6O_2$), methacrylic ($C_4H_6O_2$), and the sum of pyruvic ($C_3H_4O_3$) and butyric ($C_4H_8O_2$) acid concentrations are reported during the CalNex study (Veres et al. 2011). These acids all follow the general trend observed for formic acid during that study with strong daytime enhancement relative to nighttime concentrations. Similar behavior for many of the species occurs during SOAS, although authentic calibration for each compound was not conducted (Figure 2.9a). The use of a HR-TOF-CIMS allows for the molecular composition of each ion to be determined, and in the case of pyruvic and butyric acid, HR fitting allows for the separation of the isobaric species.

Glycolic ($C_2H_4O_3$) acid and lactic acid ($C_3H_6O_3$) (possibly the sum of lactic acid and hydroxy-propanoic acid) are detectable species and have the potential for permeation tube based calibration (Veres et al. 2008) (Figure 2.9b). Isocyanic acid (HNCO) is of great interest for public health and air quality, and calibration methods exist using a thermal decomposition-diffusion source (Roberts et al. 2010, Wentzell et al. 2013, Woodward-Massey et al 2014). 2,2-Dihydroxy acetic acid ($C_2H_4O_4$) exhibits an interesting time series in which ion signal at low concentration drops to zero due to the complete absence of background signal during zero air measurements. This provides one of the few examples where background count rates do not influence the measurement. Numerous other oxidized species exist in the data, and HR analysis provides some insight to these molecules. However, this analysis is complicated by the presence

of isobaric isomers. For example, $C_4H_4O_3$ could be a number of different compounds including various oxo-butenoic acids, hydroxy-butynoic acids, or a hydroxy-furanone.

Biogenic oxidation products with carboxylic acid functionality behave similarly to formic acid (Figure 2.9c). Methacrylic acid epoxide (MAE, $C_4H_6O_3$) is detected with high signal-to-noise and is a known oxidation product of isoprene under high NO_x conditions arising from hydroxyl radial oxidation of MPAN (Lin et al. 2013). MAE is highly correlated with formic acid (r^2=0.92). Various examples of terpene related oxidation products also exhibit good signal and temporal variability that is consistent with the smaller acids. Ketopinic acid ($C_{10}H_{14}O_3$), pinonic acid ($C_{10}H_{16}O_3$), pinic acid ($C_9H_{14}O_4$), and an unknown compound ($C_9H_{14}O_5$) are presented as examples. Commercially available standards of ketopinic and pinonic acid exist but only in certain isomeric forms.

This discussion leads to two directions of future study. Performing and developing calibrations for as many of these compounds as possible will provide quantitative, speciated data to modelers; it should be acknowledged that knowing the temporal behavior without quantification is also of importance. Even for the simple case of formic acid, current models cannot capture the observed diel cycle observed at SOAS with the known sources and sinks (Millet et al 2015). Thus, it is questionable how providing a long list of quantified species will aid the current understanding of atmospheric oxidation. Alternatively, placing these CIMS measurements into a frame work for examining bulk gas phase trends needs to be explored and developed. Many frameworks exist for understanding aerosol chemistry, but it is not clear that these frameworks are appropriate for analysis of gas phase CIMS data. The mass defect enhancement plot presented in this paper offers one possible approach, but the interpretation of this space across multiple CIMS methods or locations remains a challenge (Figure 2.10a-d).

Aljawhary et al. (2013) use a similar method where direct subtraction of mass defect plots is applied and referred to as the "difference mass defect plot."

2.5.6 Species Detected with Iodide

The mass defect enhancement plot acquired in iodide mode shows the 394 species that change by at least 5% between a one hour average at 6 AM and a one hour average at 6 PM on June 22nd, highlighting the complexity of the mass spectra obtained by the HR-TOF-CIMS (Figure 2.12). Given the limited usefulness of the hourly zero air measurements during iodide mode (section 2.4.1) we compare the changes in ambient diel data rather than calculating the mass defect enhancement plot from zero air spectra. Six time series of species clustered with iodide are provided to show the temporal variability of species of interest (Figure 2.11). These include known isoprene oxidation products hydroxyhydroperoxide (ISOPOOH) and isoprene epoxide (IEPOX), which are detected as a single ion $[I{\bullet}C_5H_{10}O_3]^-$ (Paulot, et al., 2009a). Additional oxidation products following the pattern of $C_5H_{10}O_n$ also appear in the data and correspond to the successive addition of oxygen, likely proceeding via direct OH oxidation or by autooxidation (Crounse et al., 2013). Recent study of the photooxidation of levoglucosan using a HR-TOF-CIMS observes similar additions of oxygen to levoglucosan producing a series of oxidation products (Zhao, et al., 2014). Isoprene hydroxy-nitrate ($C_5H_9NO_4$) is observed along with isoprene peroxy nitrate ($C_5H_9NO_5$) (Perring, et al, 2009; Paulot et al, 2009b). Measurements of isoprene hydroxy-nitrate by CF_3O^- during the BEARPEX 2009 study exhibit strong variation from night to day as observed at SOAS (Beaver et al., 2012).

2.6 Conclusion

Ambient formic acid measurements in the South Eastern United States are presented using a novel configuration of the HR-TOF-CIMS. The average LOD and LOQ for formic acid

are 82 ppt and 863 ppt, respectively, corresponding to an average sensitivity of 13 ± 5 $Hzppt^{-1}$ corresponding to an extraction frequency of 17 kHz. Instrument backgrounds during SOAS are highly variable, and hourly zeros are essential for quantification. Online switching between acetate and iodide reagent ions does not change the underlying ionization chemistry and shows negligible cross-contamination, thus providing a promising route to measuring a greater number of species in the field with a single mass spectrometer. The low pressure fast flow inlet and the associated calibration source show little hysteresis, have short residence times for most compounds (<2 s), and generate stable sampling conditions over long periods of time with no maintenance. Frequent (i.e. hourly) zeroing and calibration of the CIMS is essential for accurately quantifying gas phase species in the ambient atmosphere. Overflowing the inlet with high purity zero air works well for determining background signals for acetate CI, but the need to replicate ambient humidity conditions prevents this from being a useful method for determining iodide CI background.

Quantification of a large suite of species remains quite challenging due to the difficulties associated with generating gas phase standards of low volatility, high O/C species, and identifying the complex humidity dependence observed with iodide CI. Standards for many of the species either do not exist, or exist in limited forms. Many of the complex species of interest are detected as a single ion, but the ions reaching the detector are an ensemble of isomers that are detected with different sensitivities making analysis complex. Tandem mass spectrometers or ion mobility mass spectrometers coupled to an HR-TOF provide a route to deconvolving these complex spectra. The SRI-HR-TOF-CIMS may be able to deconvolve some of the complex signals consisting of multiple isomeric species because each reagent has different sensitivities to different compounds, with some compounds being detected in only one reagent ion. For

example, methacrylic and acrylic acid are detected by acetate CIMS, but only methacrylic acid is detected by iodide CIMS.

Bulk analysis of HR CIMS data needs further work, but the mass defect enhancement plotting method outlined here provides one route for eliminating most of the background ions detected on CIMS instruments. This reduces the number of individual species one must sort through, and draws attention to the species most easily detected for a specific experiment.

2.7 Chapter 2 Figures

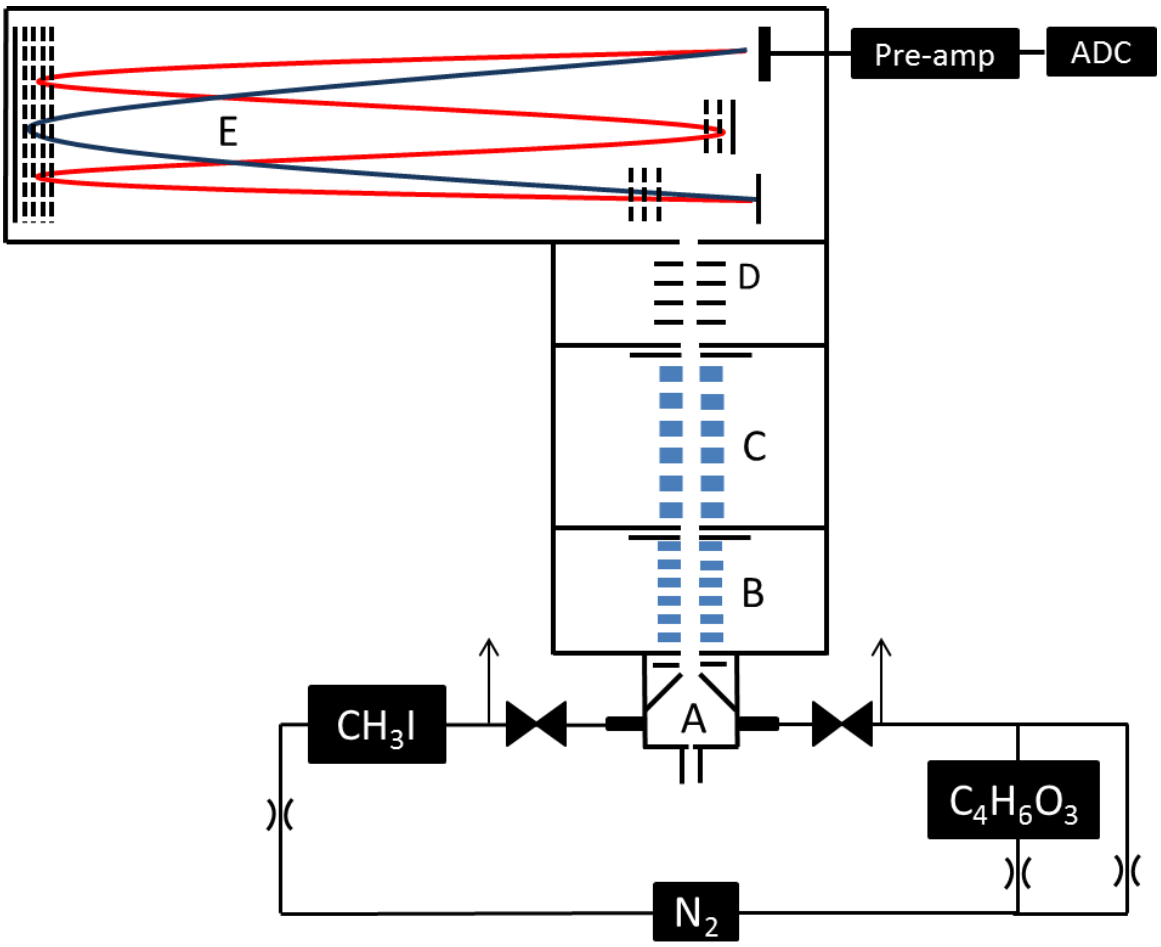

FIGURE 2.1 THE SRI-HR-TOF-CIMS:

Schematic of the SRI-HR-TOF-CIMS including the different regions of the atmospheric pressure interface. Reagent ions enter the IMR (A) and mix with incoming ambient air. The first RF-only short segmented quadrupole (SSQ, B) guides ions through the second reduced pressure region into the third stage housing the second RF-only big segmented quadrupole (BSQ, C). Ions pass through a lens stack (D) prior to being orthogonally extracted into the time-of-flight chamber (E).

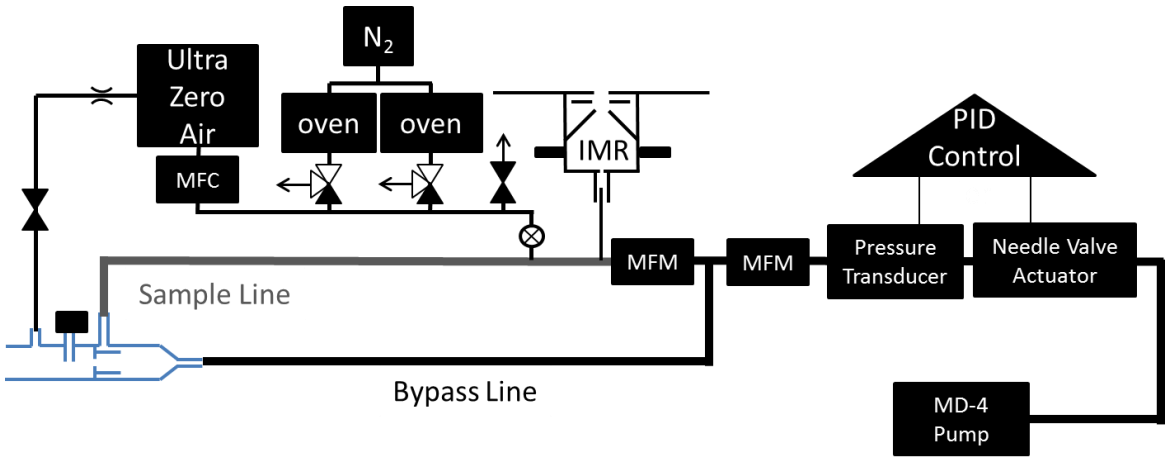

FIGURE 2.2 REDUCED PRESSURE CALIBRATION SETUP:

Schematic of the sampling and calibration setup during SOAS. The reduced pressure inlet and associated controls include two mass flow meters (MFM), a pressure transducer, needle valve actuator, pump, and computer PID controls. Valves show flow direction during ambient sampling.

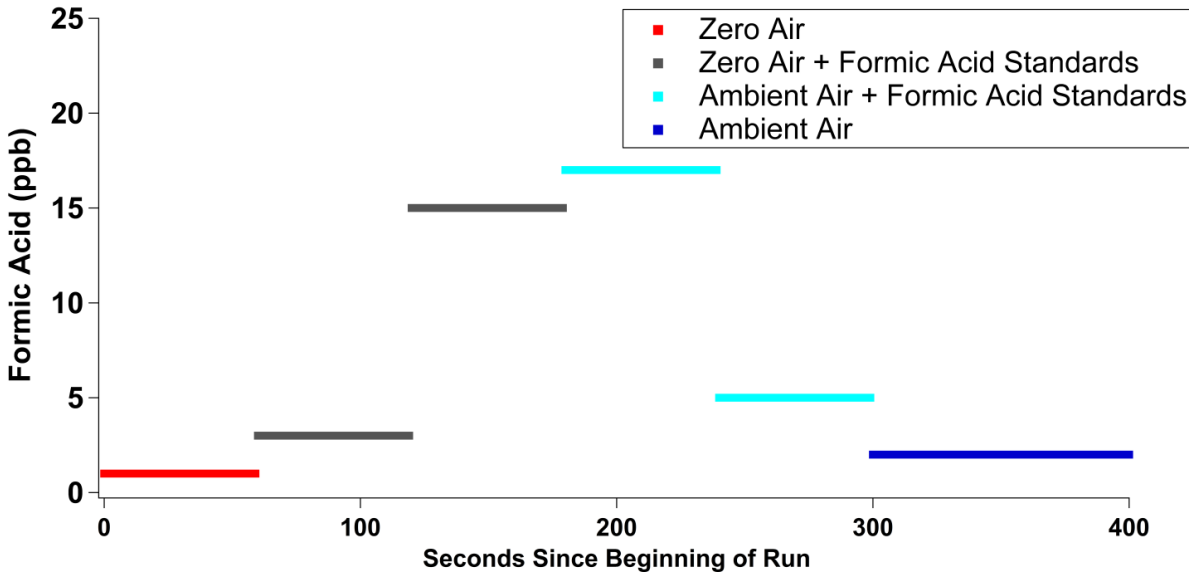

FIGURE 2.3 IN-FIELD ON-LINE CALIBRATION PROCEDURE:

The calibration regimen was conducted hourly during SOAS, and allowed for calibration of formic acid in both dry Ultra Zero air (total hydrocarbon content <0.01 ppm) and ambient air.

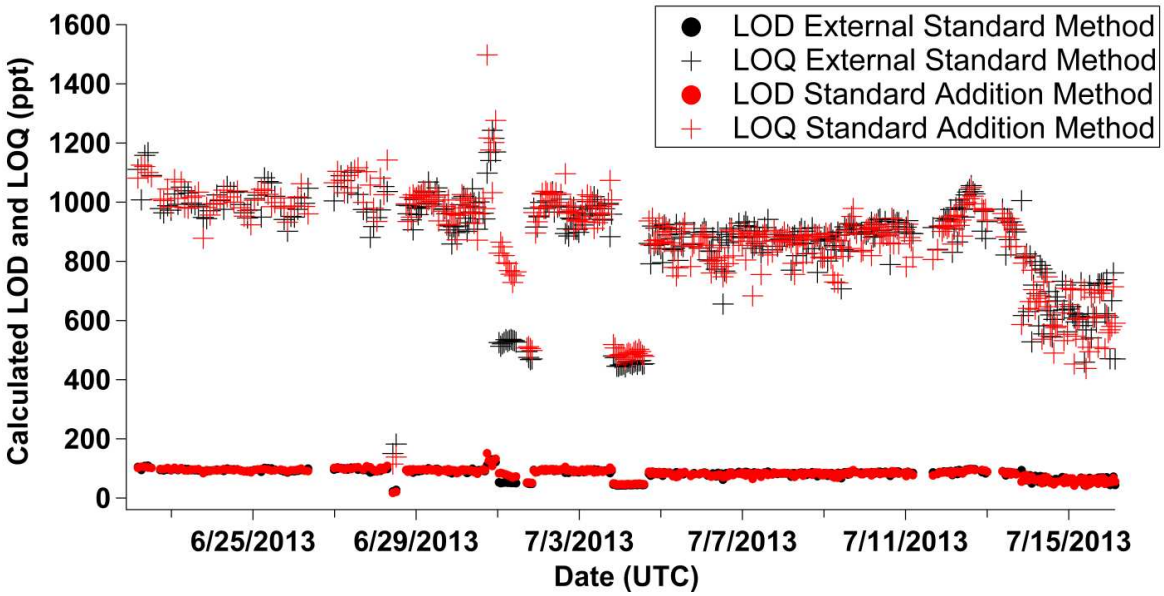

FIGURE 2.4 LOD AND LOQ METHOD TIME SERIES:

Time series of calculated limit of detection (LOD, circles) and limit of quantification (LOQ, crosses) for formic acid during hourly external standard (black) and standard addition (red) calibrations at SOAS while operating the instrument in acetate mode. The consistency between standard addition and external standard calibration demonstrates the lack of matrix effects from variation in relative humidity or other interferences.

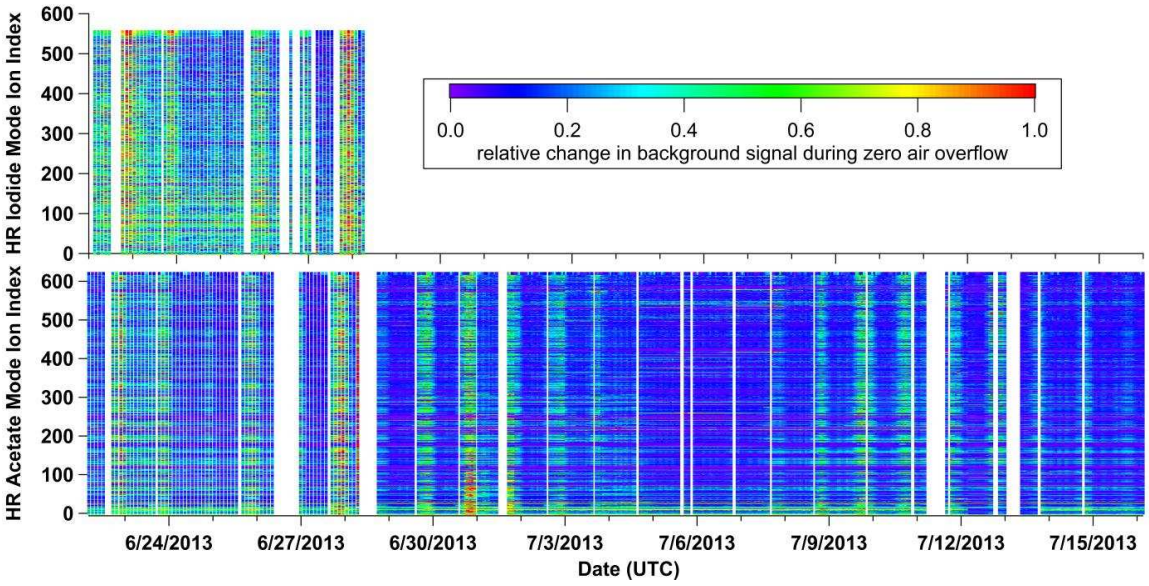

FIGURE 2.5 SRI-HR-TOF-CIMS BACKGROUND VARIATION:

The relative change in the hourly background for every high-resolution ion fit in both iodide mode and acetate mode demonstrates substantial differences in backgrounds for different ions, and the high degree of variability in backgrounds throughout the field deployment.

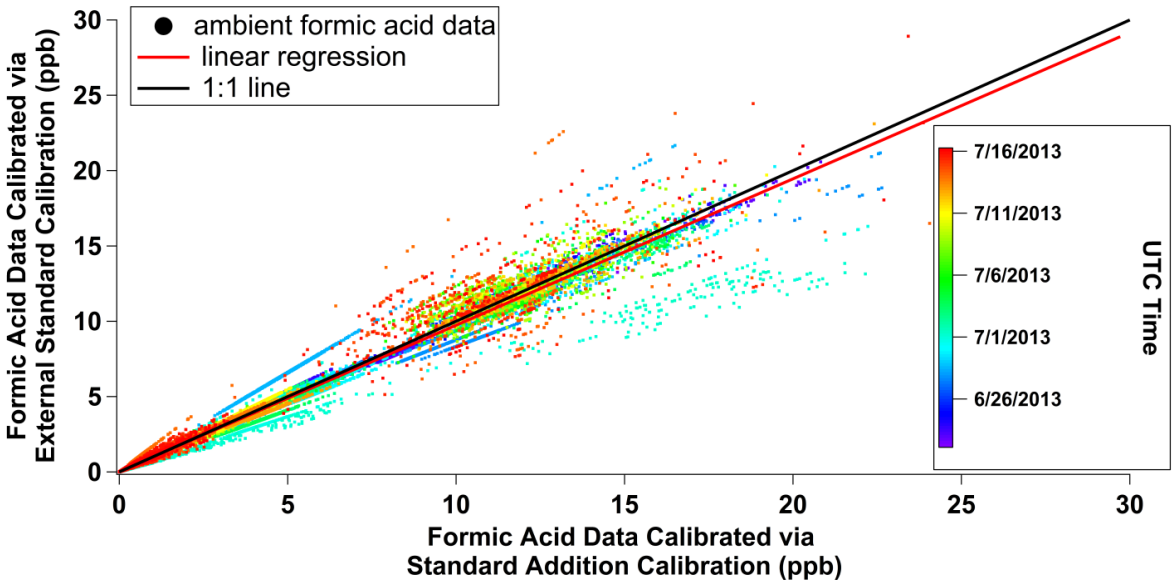

FIGURE 2.6 FORMIC ACID ACETATE CIMS CALIBRATION COMPARISON:

Scatter plot comparison of formic acid calibrated by standard addition and external standard during acetate mode.

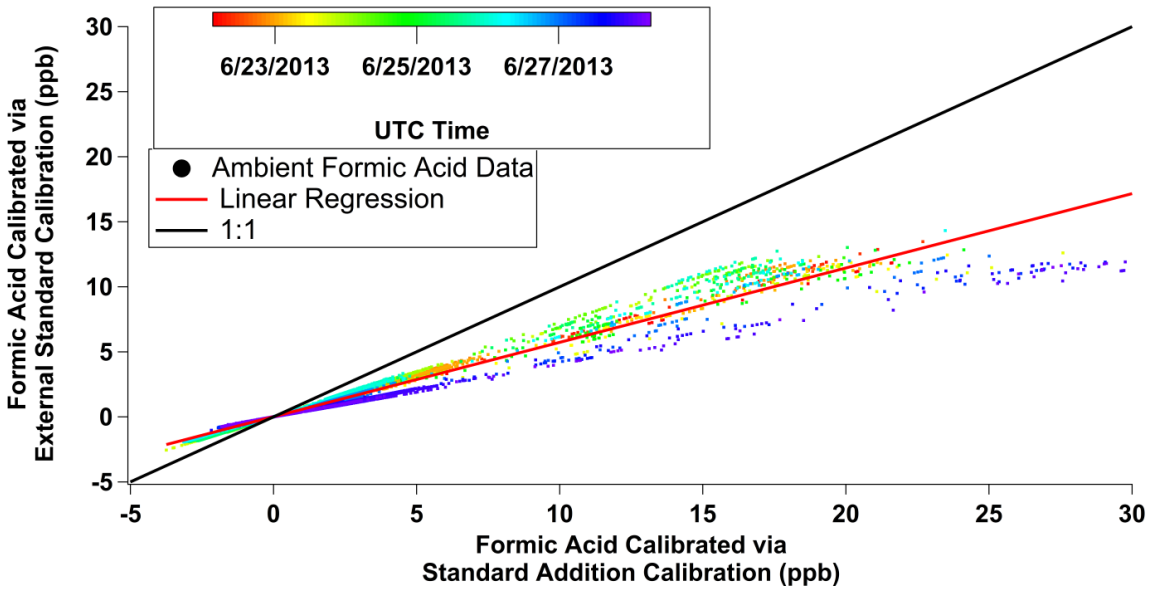

FIGURE 2.7 FORMIC ACID IODIDE CIMS COMPARISON:

Scatter plot comparison of formic acid calibrated by standard addition and external standard during iodide mode. Linear regression of the data gives a slope of 0.57 consistent with the humidity-dependence of iodide ionization causing underestimation of formic acid when calibrated in dry air.

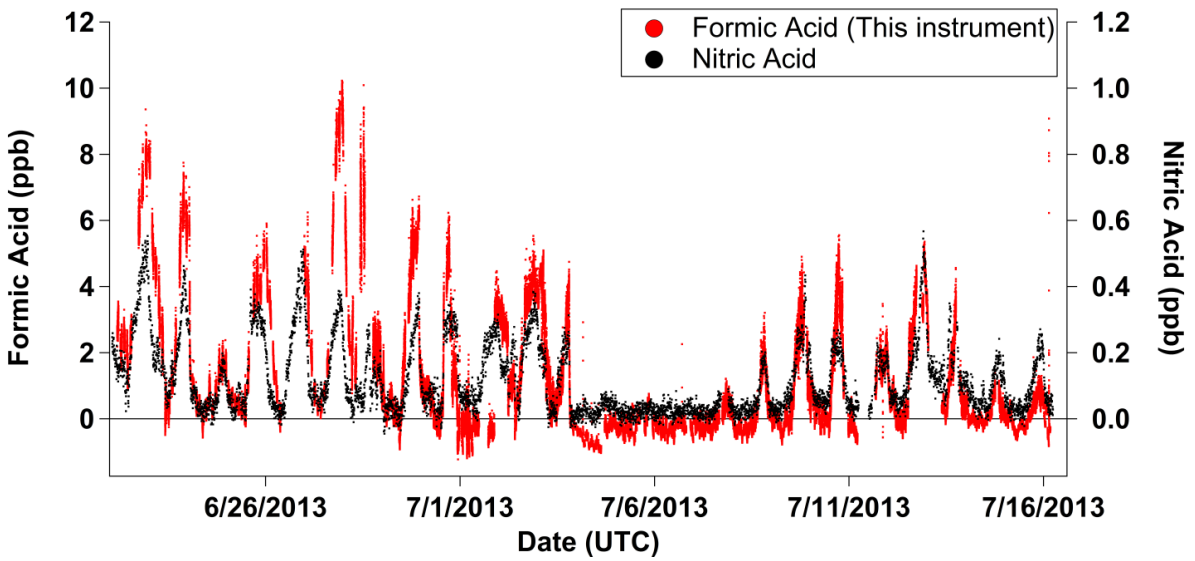

FIGURE 2.8 FORMIC ACID TIME SERIES:

Formic acid time series (this instrument) showing strong diel cycle from day to night. The behavior is strikingly similar to nitric acid which is produced through secondary photochemistry and lost through rapid dry deposition. Nighttime formic acid concentrations consistently decrease below the limit of quantification with day time maximums in the 2-10 ppb range, consistent with fast photochemical production and rapid sinks.

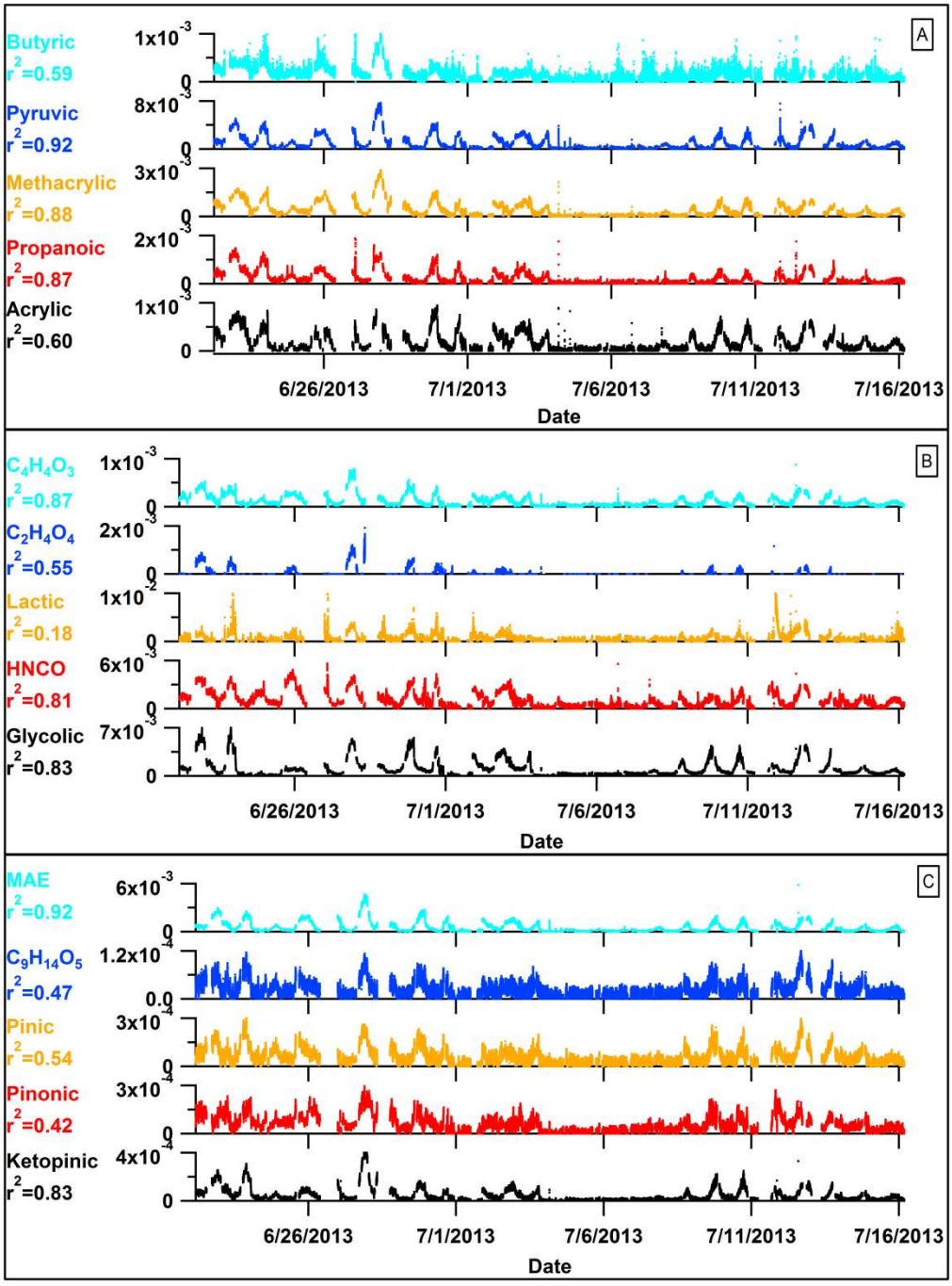

FIGURE 2.9 OTHER ACIDS DURING SOAS:

Time series of other acids observed with acetate ionization during SOAS. These compounds were not directly calibrated during the deployment, so signals are presented as counts per second normalized by the total reagent ion signal (acetate), and the correlation coefficient with formic acid is provided. (a) acids commonly measured using acetate (b) species of interest (c) biogenic oxidation products with carboxylic acid functionality

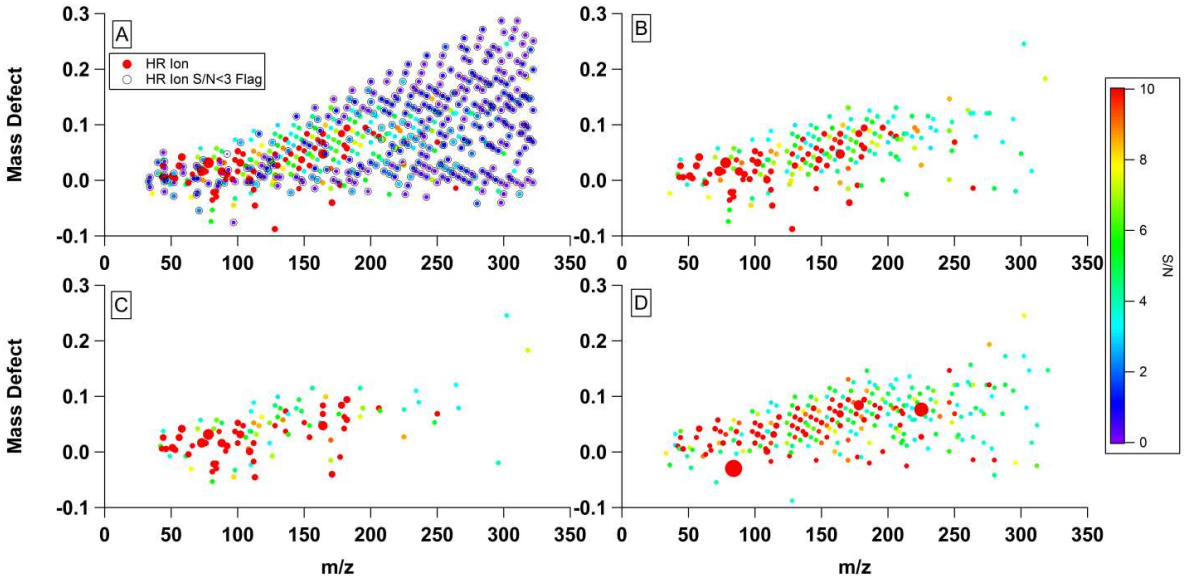

FIGURE 2.10 MASS DEFECT ENHANCEMENT PLOTS:

Mass defect enhancement plots showing the HR ion fits in acetate mode. (A-C) utilize the zero air method for defining background and signal between 3:00 PM and 4:00 PM local time on June 27, 2013. (A) All HR ion fits colored by S/N with ions having a S/N<3 flagged. (B) HR ion fits with S/N>3 only. (C) HR ion fits with S/N>3 and change by at least 5% compared to the zero. (D) Utilizes the diel method for defining background (average mass spectrum during nighttime minimum) and signal (average mass spectrum during photochemical peak) and is also colored by S/N ratio. These data are also filtered by S/N>3 and change by 5%.

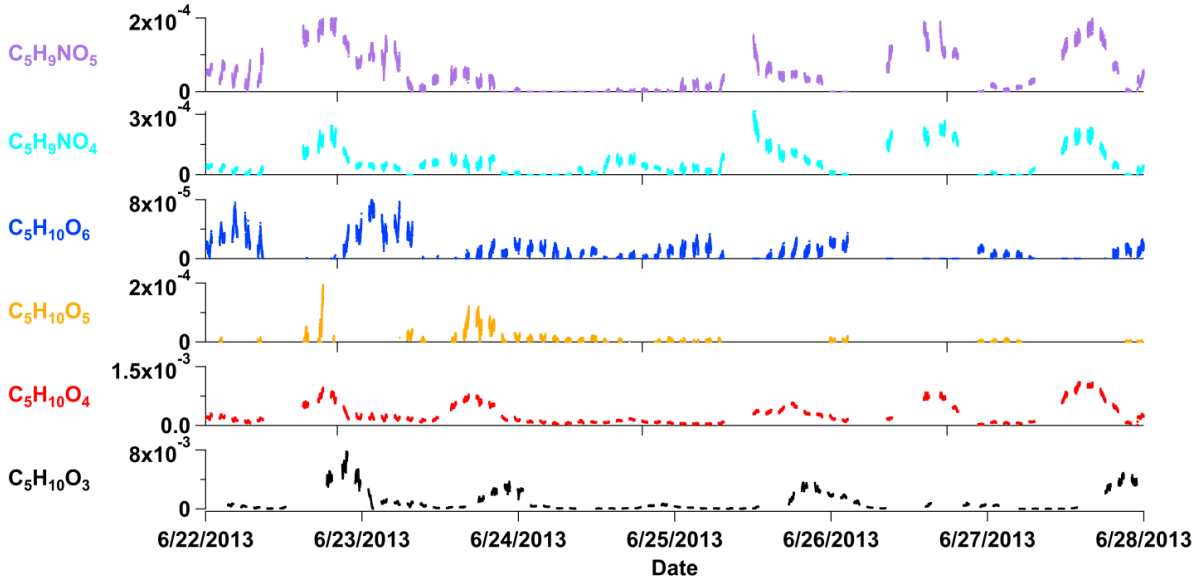

FIGURE 2.11 SELECT IODIDE TIME SERIES:

Select iodide species without direct calibration exhibit trends occurring on different time scales. Signals are in counts per second normalized by total reagent ion (I^-).

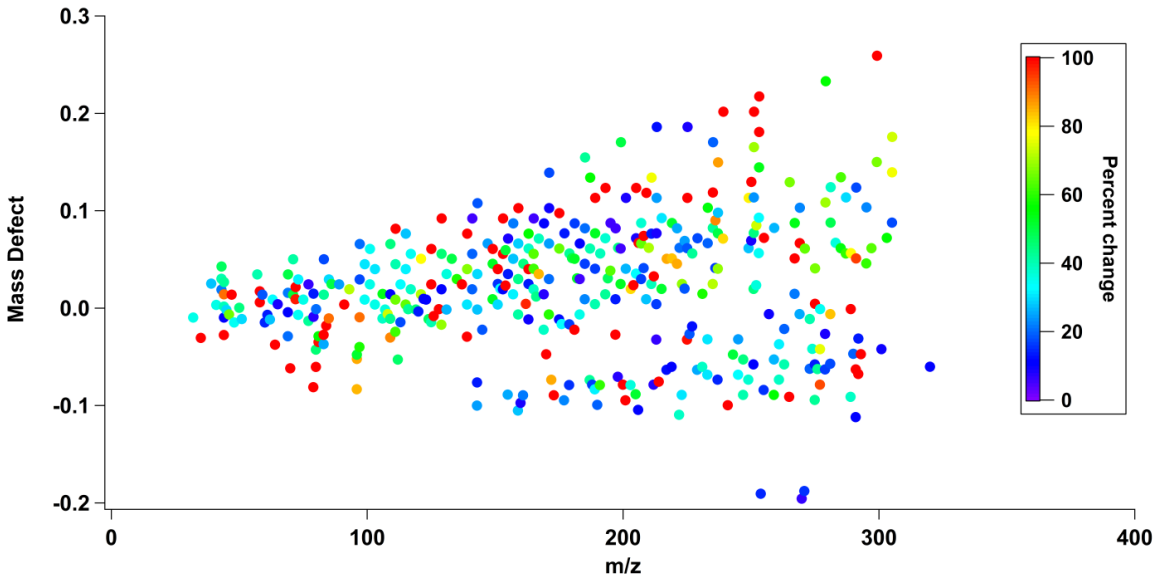

FIGURE 2.12 MASS DEFECT ENHANCEMENT IODIDE PLOT:

Mass defect plot of the iodide spectra colored by percent change from 6:00 AM on June 22 to 6 PM on June 22, 2013 and showing only species that change by >5%

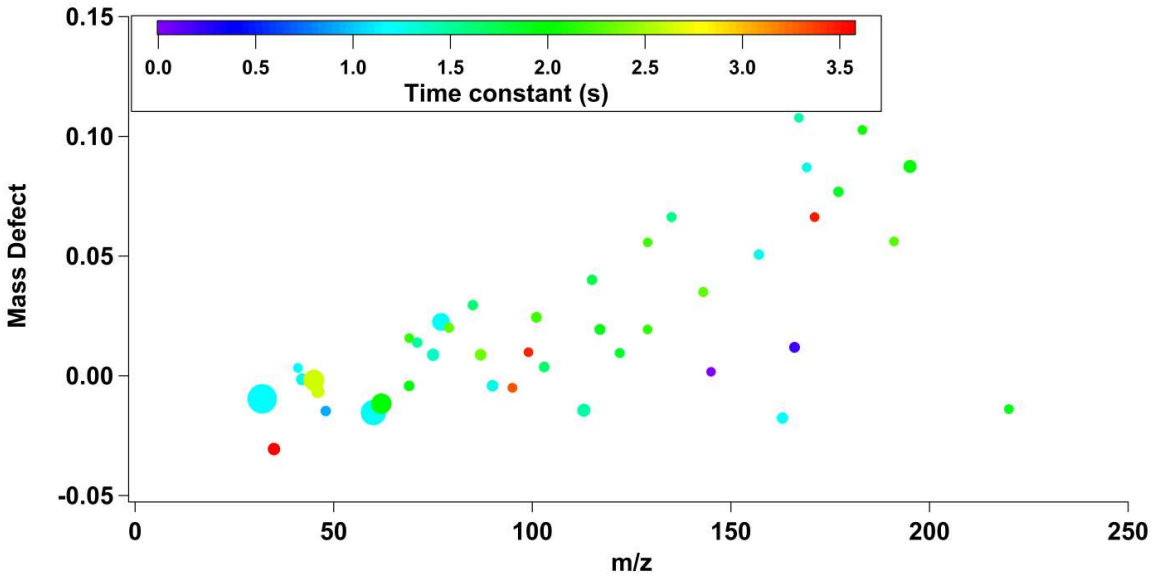

FIGURE 2.13 MASS DEFECT ENHANCEMENT INLET PLOT:

Mass defect enhancement plot for inlet characterization. Only ions with S/N>3 that decrease by at least 5% when overflowing the inlet with nitrogen are displayed. Points are colored by the time constant obtained from exponential fit analysis. The three ions with the longest residence times include $C_8H_{11}O_4^-$ (3.48 s), $C_4H_3O_3^-$ (3.43 s), and Cl^- (3.58 s).

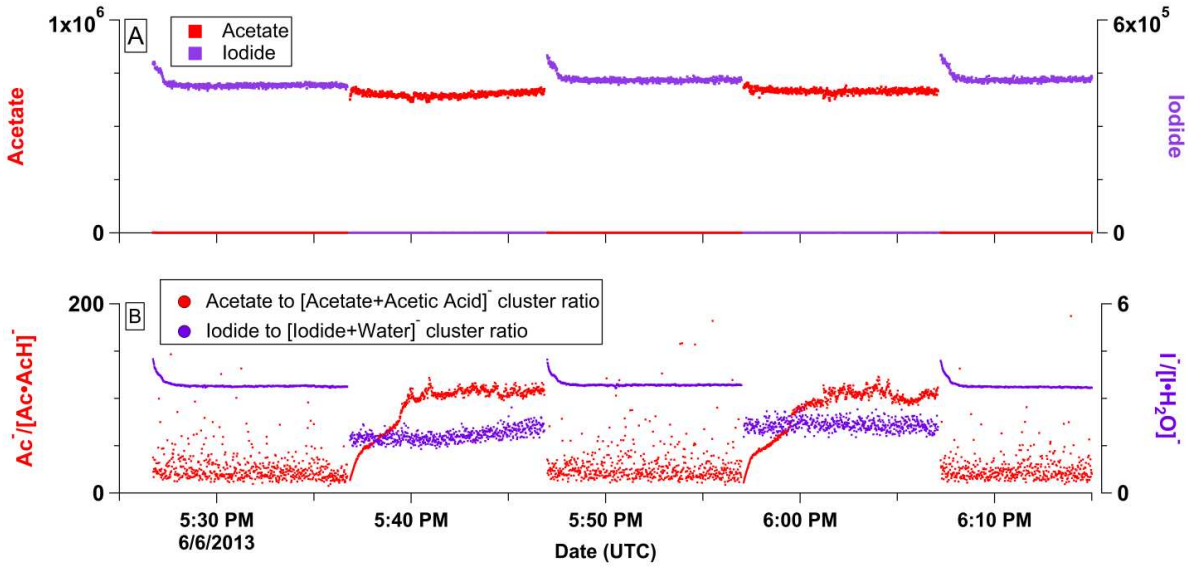

FIGURE 2.14 REAGENT SWITCHING:

Rapid reagent switching between acetate and iodide with voltage switching. (A) Primary reagent ions (B) ratio between primary reagent ion and corresponding cluster of interest

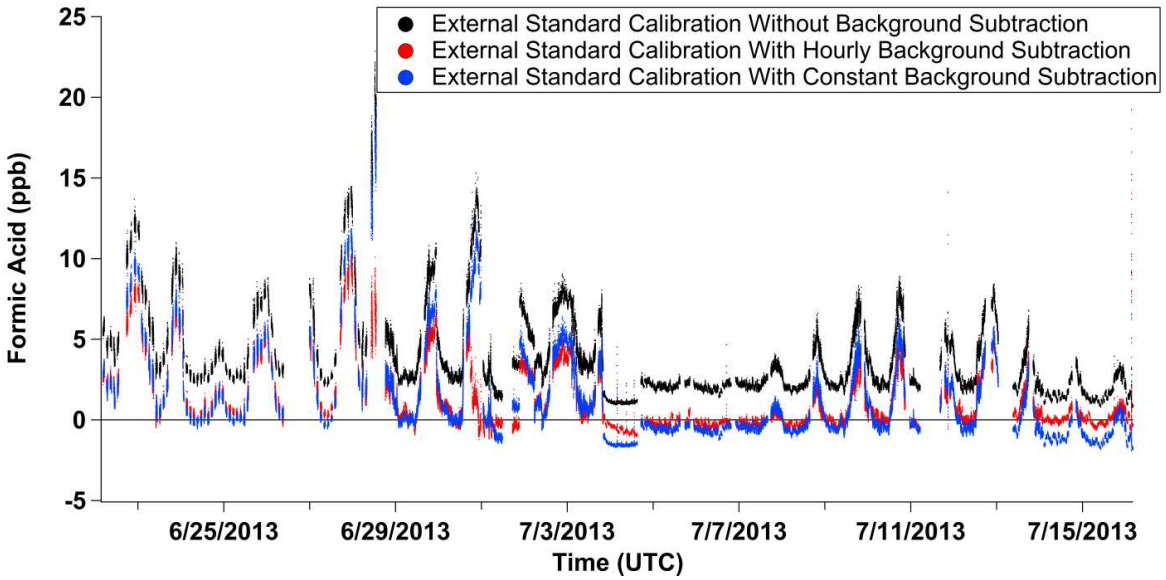

FIGURE 2.15 BACKGROUND SUBTRACTION EFFECTS:

Effect of background subtraction on ambient calculated concentration

2.8 Chapter 2 Supplementary Information (SI2)

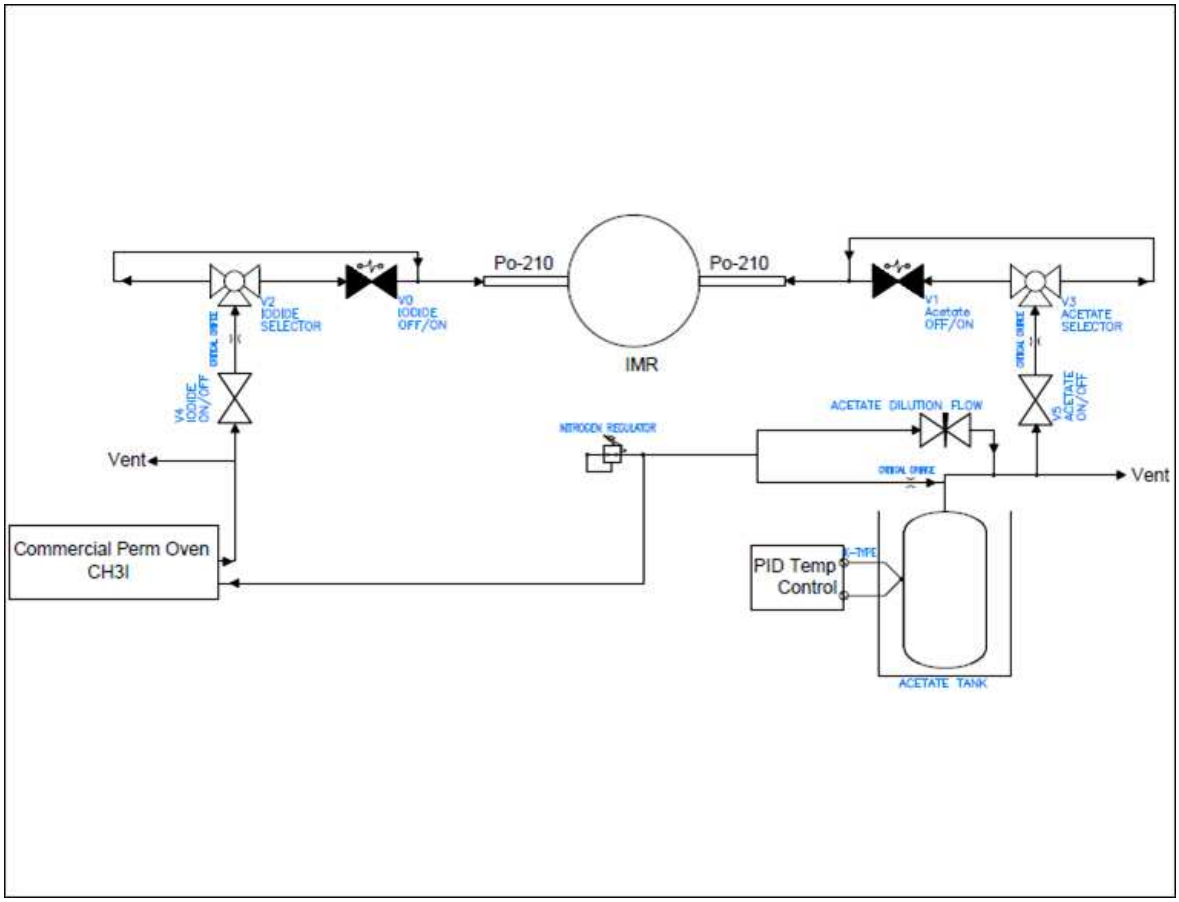

FIGURE SI2.1 FIELD SETUP:

Schematic diagram showing the setup for reagent switching with selectable flow path for automatic switching driven by solenoid valves or manual control.

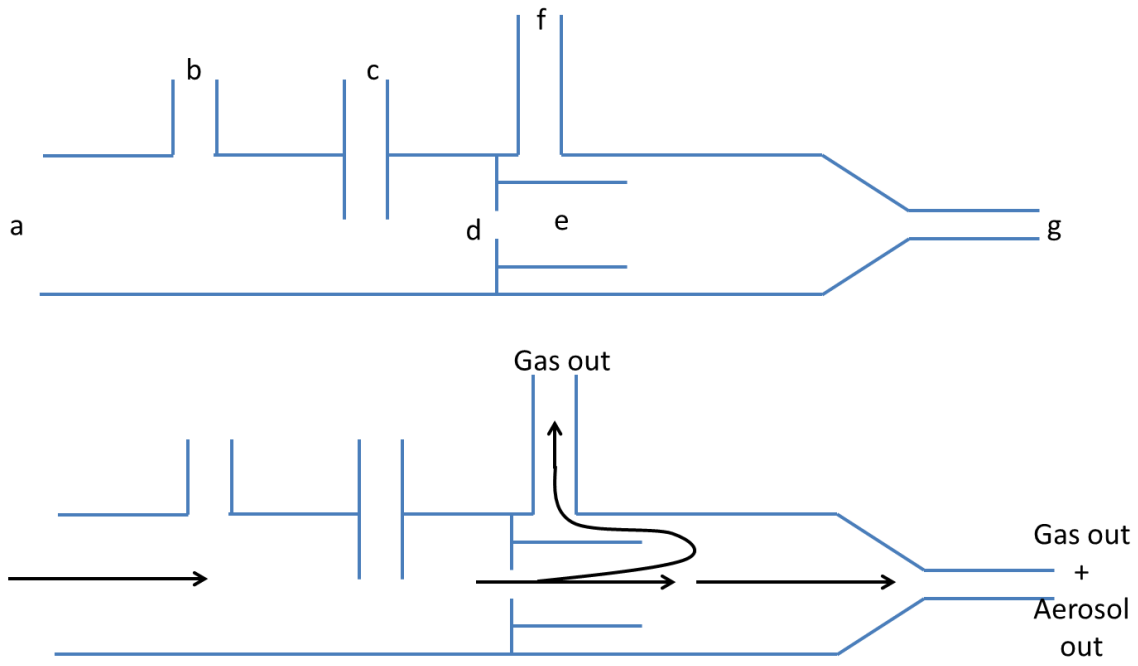

FIGURE SI2.2 GLASS INLET:

Glass inlet design (a) aerosol and gas inlet; (b) zero air overflow port; (c) calibration port (not used in this study); (d) critical orifice; (e) glass particle skimmer and flow director; (f) gas sampling port at reduced pressure; (g) bypass line at reduced pressure

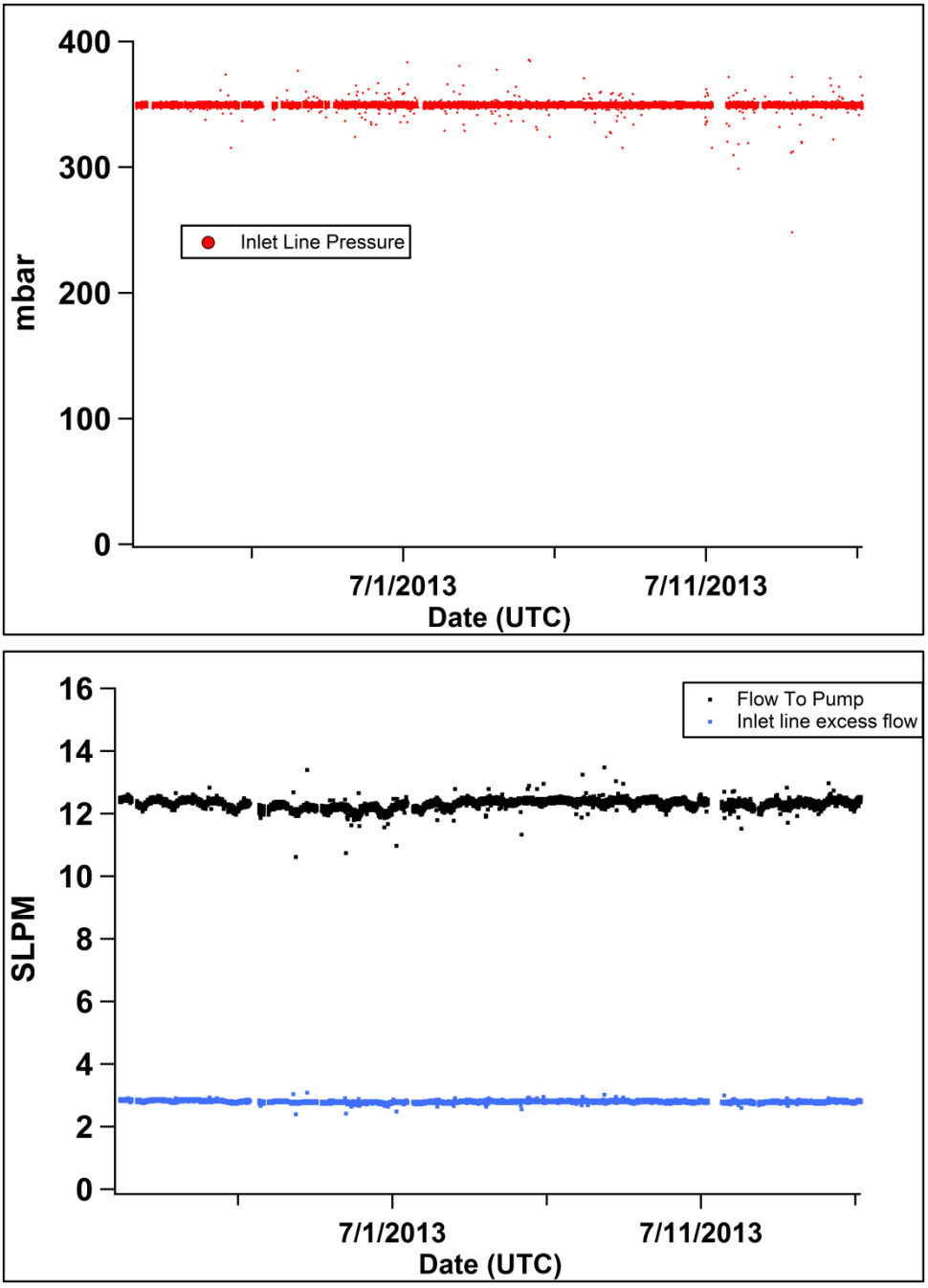

FIGURE SI2.3 INLET PERFORMANCE:

Diagnostic inlet performance showing the pressure stability, the total flow through the gas sampling line, and the total flow to the pump during SOAS.

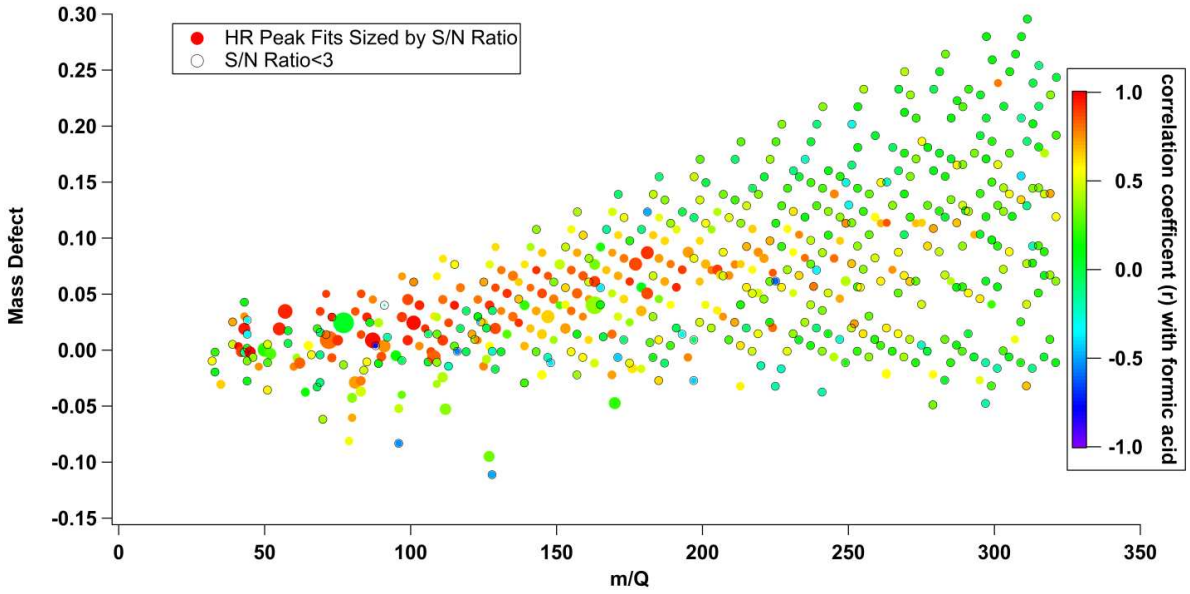

FIGURE SI2.4 MASS DEFECT PLOT OF HR IONS:

Mass defect plot showing all HR ion fits. Each ion fit is colored by the correlation coefficient with formic acid and sized by S/N ratio. Ions with a S/N<3 are marked with a black circle outline.

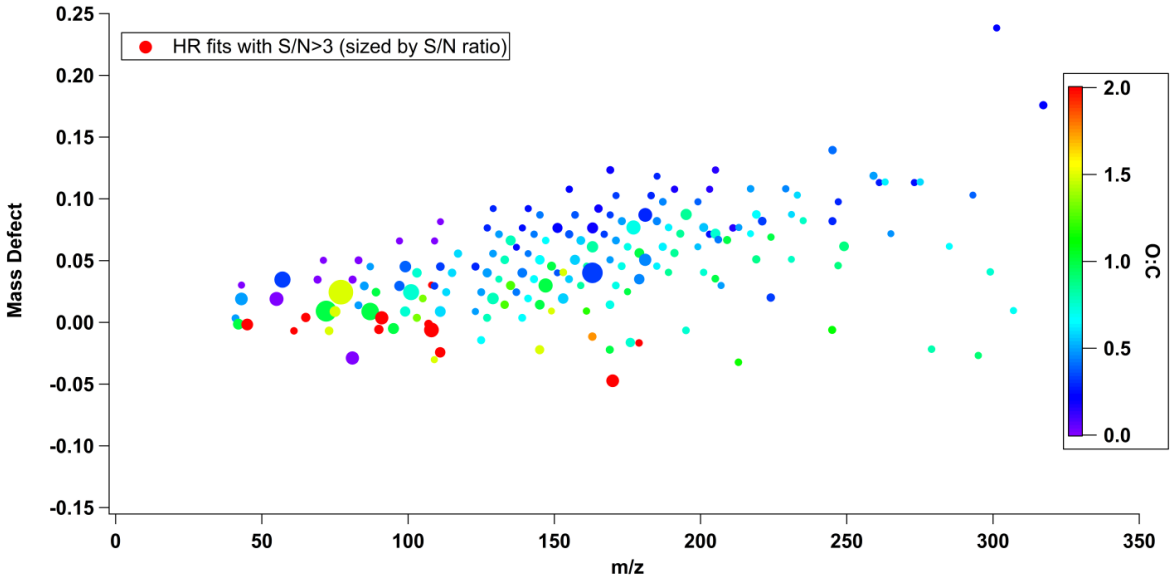

FIGURE SI2.5 MASS DEFECT ENHANCEMENT PLOT:

Mass defect enhancement plot showing all species with S/N>3 and colored by oxygen:carbon ratio as determined from the HR ion fits.

REFERENCES

Aljawhary, D., Lee, A. K. Y., and Abbat, J. P. D.: High-resolution chemical ionization mass spectrometry (ToF-CIMS): Applications to study SOA composition and processing, Atmos. Meas. Tech. 6, 3211-3224, 2013.

Bannan, T. J., Bacak, A., Muller, J. B. A., Booth, A. M., Jones, B., Le Breton, M., Leather, K. E., Ghalaieny, M., Xiao, P., Shallcross, D. E., Percival, C. J.: Importance of direct anthropogenic emissions of formic acid measured by a chemical ionization mass spectrometer (CIMS) during the Winter ClearfLo Campaign in London, January 2012, Atmos. Environ., 83, 301-310, 2014

Beaver, M. R., St. Clair, J. M., Paulot, F., Spencer, K. M., Crounse, J. D., LaFranchi, B. W., Min, K. E., Pusede, S. E., Wooldridge, P. J., Schade, G. W., Park, C., Cohen, R. C., Wennberg, P. O.: Importance of biogenic precursors to the budget of organic nitrates: observation of multifunctional organic nitrates by CIMS and TD-LIF during BEARPEX 2009, Atmos. Chem. Phys., 12, 5773-5785, 2012

Bertram, T. H., J. R. Kimmel, T. A. Crisp, O. S. Ryder, R. L. N. Yatavelli, J. A. Thornton, M. J. Cubison, M. Gonin, and D. R. Worsnop: A field-deployable, chemical ionization time-of-flight mass spectrometer, Atmos. Meas. Tech., 4, 1471-1479, 2011.

Crounse, J. D., McKinney, K. A., Kwan, A. J., and Wennberg, P. O.: Measurement of gas-phase hydroperoxides by chemical ionization mass spectrometry, Anal. Chem., 78, 6726-6732, 2006.

Crounse, J. D., Nielsen, L. B., Jørgensen, S., Kjaergaard, H. G., Wennberg, P. O.: Autoxidation of organic compounds in the atmosphere, J. Phys. Chem. Lett., 4, 3513-3520, 2013

Chhabra, P. S., Lambe, A. T., Canagaratna, M. R., Stark, H., Jayne, J. T., Onasch, T. B., Davidovits, P., Kimmel, J. R., Worsnop, D. R.: Application of high-resolution time-of-flight chemical ionization mass spectrometry measurements to estimate volatility distributions of α-pinene and naphthalene oxidation products, Atmos. Meas. Tech., 8, 1-18, 2015.

DeCarlo, P. F., Kimmel, J. R., Trimborn, A., Northway, M. J., Jayne, J. T., Aiken, A. C., Gonin, M., Fuhrer, K., Horvath, T., Docherty, K. S., Worsnop, D. R., Jimenez, J. L.: Field-deployable, high-resolution, time-of-flight aerosol mass spectrometer, Anal. Chem., 78, 8281-8289, 2006.

Ehn, M., Kleist, E., Junninen, H., Petäjä, T., Lönn, G., Schobesberger, S., Dal Maso, M., Trimborn, A., Kulmala, M., Worsnop, D. R., Wahner, A., Wildt, J., Mentel, Th. F.: Gas phase formation of extremely oxidized pinene reaction products in chamber and ambient air, Atmos. Chem. Phys., 12, 5113-5127, 2012

Ehn, M., Thornton, J. A., Kleist, E., Sipilä, M., Junninen, H., Pullinen, I., Springer, M., Rubach, F., Tillman, R., Lee, B., Lopez-Hilfiker, F., Andres, S., Acir, I., Rissanen, M., Jokinen, T., Schobesberger, S., Kangasluoma, J., Kontkanen, J., Nieminen, T., Kurtén, T.,Nielsen, L. B., Jørgensen, S., Kjaergaard, H. G., Canagaratna, M., Dal Maso, M., Berndt, T., Petäjä, T., Wahner,

A., Kerminen, V., Kulmala, M., Worsnop, D. R., Wildt, J., and Mentel, T. F.: A large source of low-volatility secondary organic aerosol, Nature, 506, 476-479, 2014.

Ellis, R. A., Murphy, J. G., Pattey, E., van Haarlem, R., O'Brien, J. M., Herndon, S. C.: Characterizing a quantum cascade tunable infrared laser differential absorption spectrometer (QC-TILDAS) for measurements of atmospheric ammonia, Atmos. Meas. Tech., 3, 297-406, 2010.

Huey, G. L.: Measurement of trace atmospheric species by chemical ionization mass spectrometry: speciation of reactive nitrogen and future directions, Mass Spectrom. Rev., 26, 166-184, 2007

Huey, G. L., Hanson, D. R., and Howard, C. J.: Reactions of SF_6^- and I^- with atmospheric trace gases, J. Phys. Chem., 99, 5001-5008, 1995

Jordan, A., Haidacher, S., Hanel, G., Hartungen, E., Herbig, J., Märk, L., Schottkowsky, R., Shauser, H., Sulzer, P., Märk, T.D.: An online ultra-high sensitivity proton-transfer-reaction mass-spectrometer combined with a switchable reagent ion capability (PTR+SRI-MS), Int. J. Mass Spectrom., 286, 32-38, 2009.

Junninen, H., Ehn, M., Petäjä, T., Luosujärvi, L., Kotiaho, T., Kostiainen, R., Rohner, U., Gonin, M., Fuhrer, K., Kulmala, M., and Worsnop, D.R.: A high-resolution mass spectrometer to measure atmospheric ion composition, Atmos. Meas. Tech., 3, 1039-1053, 2010.

Kercher, J. P., Riedel, T. P., Thornton J. A.: Chlorine activation by N_2O_5: Simultaneous, in situ detection of $ClNO_2$ and N_2O_5 by chemical ionization mass spectrometry, Atmos. Meas. Tech., 2, 193-204, 2009.

Le Breton, M., McGillen, M. R., Muller, J. B. A., Bacak, A., Shallcross, D. E., Xiao, P., Huey, L. G., Tanner, D., Coe, H., and Percival, C. J.: Airborne observations of formic acid using a chemical ionization mass spectrometer, Atmos. Meas. Tech., 5, 3029-3039, 2012

Le Brenton, M., Bacak, A., Muller, J. B. A., Xiao, P., Shallcross, B. M. A., Batt, R., Cooke, M. C., Shallcross, D. E., Bauguitte, S. J.-B., Percival, C. J.: Simultaneous airborne nitric acid and formic acid measurements using a chemical ionization mass spectrometer around the UK: analysis of primary and secondary pathways, Atmos. Environ., 83, 166-175, 2014.

Lee, B. H., Lopez-Hilfiker, F. D., Mohr, C., Kurtén, T., Worsnop, D. R., and Thornton, J. A.: An iodide-adduct high-resolution time-of-flight chemical-ionization mass spectrometer: applications to atmospheric inorganic and organic compounds, Environ. Sci. Technol., 48, 6309-6317, 2014.

Lin, Y., Zhang, H., Pye, H. O. T., Zhang, Z., Marth, W. J., Park, S., Arashiro, M., Cui, T., Budisulistiorini, S. H., Sexton, K. G., Vizuete, W., Xie, Y., Luecken, D. J., Piletic, I. R., Edney, E. O., Bartolotti, L. J., Gold, A., Surratt, J. D.: Epoxide as a precursor to secondary organic aerosol formation from isoprene photooxidation in the presence of nitrogen oxides, PNAS, 110, 6718-6723, 2013.

Mielke, L. H., Furgeson, A., Osthoff, H. D.: Observation of $ClNO_2$ in a mid-continental urban environment, Environ. Sci. Technol., 45, 8889-8896, 2011.

Mielke, L. H., Osthoff, H. D.: On quantitative measurements of peroxycarboxylic nitric anhydride mixing ratios by thermal dissociation chemical ionization mass spectrometry, Int. J. Mass Spectrom., 310, 1-9, 2012.

Millet, D. B., Baasandorj, M., Farmer, D. K., Thornton, J. A., Baumann, K., Brophy, P., Chaliyakunnel, S., de Gouw, J. A., Graus, M., Hu, L., Koss, A., Lee, B.H., Lopez-Hilfiker, F. D., Neuman, J. A., Paulot, F., Peischl, J., Pollack, I. B., Ryerson, T. B., Warneke, C., Williams, B. J., Xu, J.: A large and ubiquitous source of atmospheric formic acid, Atmos. Chem. Phys. Discuss., 15, 4537-4599, 2015.

Mohr, C., Lopez-Hilfiker, F. D., Zotter, P., Prévôt, A. S. H., Xu, L., Ng, N. L., Herndon, S. C., Williams, L. R., Franklin, J. P., Zahniser, M. S., Worsnop, D. R., Knighton, W. B., Aiken, A. C., Gorkowski, K. J., Dubey, M. K., Allan, J. D., Thornton, J. A.: Contribution of nitrated phenols to wood burning brown carbon light absorption in Detling, United Kingdom during winter time, Environ. Sci. Technol., 47, 6316-6324, 2013.

Nozière, B., Kalberer, M., Claeys, M., Allan, J., D'Anna, B., Decesari, S., Finessi, E., Glasius, M., Grgić I., Hamilton, J. F., Hoffmann, T., Iinuma, Y., Jaoui, M., Kahnt, A., Kampf, C. J., Kourtchev, I., Maenhaut, W., Marsden, N., Saarikoski, S., Schnelle-Kreis, J., Surratt, J., Szidat, S., Szmigielski, R., Wisthaler, S.: The molecular identification of organic compounds in the atmosphere: state of the art and challenges, Chem. Rev., Article ASAP, 2015, DOI: 10.1021/cr5003485

Paulot, F., Crounse, J. D., Kjaergaard, H. G., Kürten, A., St. Clair, J. M., Seinfeld, J. H., Wennberg, P. O.: Unexpected epoxide formation in the gas-phase photooxidation of isoprene, Science, 325, 730-733, 2009a.

Paulot, F., Crounse, J. D., Kjaergaard, H. G., Kroll, J. H., Seinfeld, J. H., Wennberg, P. O.: Isoprene photooxoidation: new insights into the production of acids and organic nitrates, Atmos. Chem. Phys., 9, 1479-1501, 2009b.

Paulot, F., Crounse, J. D., Toon, G. C., Millet, D. B., DeCarlo, P. F., Vigouroux, C., Deutscher, N. M., González Abad, G., Notholt, J., Warneke, T., Hannigan, J. W., Warneke, C., de Gouw, J. A., Dunlea, E. J., De Mazière, M., Griffith, D. W. T., Bernath, P., Jimenez, J. L., Wennberg, P. O.: Importance of secondary sources in the atmospheric budgets of formic and acetic acids, Atmos. Chem. Phys., 11, 1989-2013, 2011

Perring, A. E., Wisthaler, A., Graus, M., Wooldridge, P. J., Lockwood, A. L., Mielke, L. H., Shepson, P. B., Hansel, A., Cohen, R. C.: A product study of the isoprene+NO_3 reaction, Atmos. Chem. Phys., 9, 4945-4956, 2009

Roberts, J. M., Veres, P., Warneke, C., Neuman, J. A., Washenfelder, R. A., Brown, S. S., Baasandorj, M., Burkholder, Burling, I. R., Johnson, T. J., Yokelson, R. J., and de Gouw, J.: Measurement of HONO, HNCO, and other inorganic acids by negative-ion proton-transfer

chemical-ionization mass spectrometry (NI-PT-CIMS): application to biomass burning emissions, Atmos. Meas. Tech., 3, 981-990, 2010.

Smith, D., Španěl, P.: Selected ion flow tube mass spectrometry (SIFT-MS) for on-line trace gas analysis, Mass Spectrom. Rev., 24, 661-700, 2005.

Slusher, D. L., Huey, L. G., Tanner, D. J, Flocke, F. M., and Roberts, J. M.: A thermal dissociation-chemical ionization mass spectrometry (TD-CIMS) technique for the simultaneous measurement of peroxyacyl nitrates and dinitrogen pentoxide, J. Geophys. Res., 109, D19315, 2004.

Veres, P., Roberts, J. M., Warneke, C., Welsh-Bon, D., Zahniser, M., Herndon, S., Fall, R., and de Gouw, J.: Development of negative-ion proton-transfer chemical-ionization mass spectrometry (NI-PT-CIMS) for the measurement of gas-phase organic acids in the atmosphere, Int. J. Mass Spectrom., 274, 48-55, 2008.

Veres, P., Roberts, J. M., Cochran, A. K., Gilman, J. B., Kuster, W. C., Holloway, J. S., Graus, M., Flynn, J., Lefer, B., Warneke, C., de Gouw, J.: Evidence of rapid production of organic acids in an urban air mass, Geophys. Res. Lett., 38, 17, L17807, 2011.

Wentzell, J. J. B., Liggio, J., Li, S., Vlasenko, A., Staebler, R., Lu, Gang., Poitras, M., Chan, T., Brook, J. R.: Measurements of gas phase acids in diesel exhaust: a relevant source of HNCO?, Environ. Sci. Technol., 47, 7663-7671, 2013.

Woodward-Massey, R., Taha, Y. M., Moussa, S. G., Osthoff, H. D.: Comparison of negative-ion proton-transfer with iodide ion chemical ionization mass spectrometry for quantification of isocyanic acid in ambient air, Atmos. Environ., 92, 693-703, 2014

Yatavelli, R. L. N., Lopez-Hilfiker, F. Wargo, J. D., Kimmel, J. R., Cubison, M. J., Bertram, T. H., Jimenez, J. L., Gonin, M., Worsnop, D. R. and Thorton, J. A.: A chemical ionization high-resolution time-of-flight mass spectrometer coupled to a micro orifice volatilization impactor (MOVI-HRToF-CIMS) for analysis of gas and particle-phase organic species, Aerosol Sci. Tech., 46:12, 1313-1327, 2012.

Zhang, X., Cappa, C. D., Jathar, S. H., McVay, R. C., Ensberg, J. J., Kleeman, M. J., Seinfeld, J. H.: Influence of vapor wall loss in laboratory chambers on yields of secondary organic aerosol, PNAS, 11, 16, 5802-5807, 2014.

CHAPTER 3

CLUSTERING, METHODOLOGY, AND MECHANISITC INSIGHTS INTO ACETATE CHEMICAL IONIZATION USING HIGH-RESOLUTION TIME-OF-FLIGHT MASS SPECTROMETRY[1]

3.1 Introduction

Recent commercialization and packaging of time-of-flight chemical ionization mass spectrometers (TOF-CIMS) into field deployable packages by Aerodyne Research Inc. and Tofwerk AG has led to the wide-spread use of these instruments (Aljawhary et al., 2013; Bertram et al., 2011; Brophy and Farmer, 2015; Chhabra et al., 2015; Ehn et al., 2010; 2011; 2014; Faust et al., 2016; Friedman et al., 2016; Jokinen et al., 2012; Junninen et al., 2010; Krechmer et al., 2015; Lee et al., 2014; Lopez-Hilfiker et al., 2016; 2015; 2014; Mohr et al., 2013; Sipilä et al., 2015; Yatavelli et al., 2012; 2014; Zhao et al., 2014). Any chemical ionization (CI) source, or more generally any near-atmospheric pressure ion source, can be installed on the front end of the mass spectrometer providing a flexible TOF instrument platform. The design and operation of the ion source effects the sensitivity of the instrument, but the fundamental ion chemistry is the key consideration to designing a CI source that is both sensitive and selective. Thus, the selection of an appropriate reagent ion for detecting the compound, or class of compounds, of interest is important (Huey, 2007). The ions observed in the TOF mass spectrum do not necessarily represent the distribution of ions generated in the ion source due to collisional

[1]Brophy, P., Farmer, D. K., Clustering, Methodology, and Mechanistic Insights Into Acetate Chemical Ionization Using High-Resolution Time-of-Flight Mass Spectrometry. Submitted to Atmospheric Measurement Techniques Discussion for publication in Atmospheric Measurement Techniques

dissociation (Bertram et al., 2011) and mass-dependent transmission effects (Heinritzi et al., 2016). Collisional dissociation simplifies the observed mass spectrum and has a long history of use dating back to the original developments of tropospheric CIMS measurements (Eisele, 1986). Controlling the extent of collisional dissociation can be used to investigate the ion-neutral chemistry occurring in the ion source. The TOF-CIMS uses a tunable multistate atmospheric pressure interface (API) that can eliminate or transmit clusters, but the operational details of this interface have not been investigated with systematic rigor.

TOF-CIMS represents a distinct departure from traditional quadrupole CIMS methodologies in which specific species are targeted for quantification. TOF-CIMS collect a continuous mass spectrum at high (<1 Hz) acquisition rates, whereas quadrupole detectors collect a limited number of ions due to limitations on sensitivity and time resolution due to duty cycle effects. Additionally, high-resolution TOF-CIMS (HR-TOF-CIMS) enables the assignment of a molecular formula to every observed mass peak. These two features of the HR-TOF-CIMS provide an opportunity to examine CI ion chemistry. Moreover, users can identify and observe the temporal behavior of compounds that have not previously known to exist or calibrated in a non-targeted approach (Ehn et al., 2014). Quadrupole systems contrast this approach. Ideally, quadrupole CI is deployed with the intent of measuring specific species with readily available authentic calibration standards and well-characterized interferences. Calibrations are typically conducted for a limited number of compounds, but interferences are difficult to address until they are identified through instrument intercomparisons and careful study. The recent identification of the decomposition of isoprene hydroxy-hydroperoxides (ISOPOOH) to methyl vinyl ketone (MVK) and methacrolein (MACR) in both gas chromatograph instruments and

proton-transfer reaction mass spectrometers (PTR-MS) highlights this challenge as both techniques have a long history of MVK and MACR measurements (Rivera-Rios et al., 2014).

Both TOF and quadrupole detectors remain subject to misinterpretation of the mass spectrum in the absence of complex interferences. Quadrupole systems with unit mass resolution can suffer from attributing the signal from a single mass to charge ratio (*m/z*) to a single species and potentially miss isobaric interferences at the same nominal, or unit, mass. Recent intercomparisons between co-located quadrupole PTR-MS and time-of-flight PTR-MS instruments highlight the power of high-resolution analysis in the identification of multiple overlapping peaks (Warneke et al., 2015)**.** HR-TOF systems can separate closely spaced peaks, but knowing the actual identity of ion signals from their exact mass and extracting the high-resolution information remains challenging (Cubison and Jimenez, 2015; Stark et al., 2015). Improving the knowledge of the ion chemistry, ionization mechanisms, and instrument performance is paramount to correctly interpreting the mass spectrum because CI relies on selectively ionizing specific compounds or classes of compounds. Quantitative and qualitative non-targeted analysis in the complex chemical space of the atmosphere using HR-TOF-CIMS necessitates characterization of the chemistry occurring within the ion source and the instrument's subsequent control over the transmission, clustering, and fragmentation of those ions.

Acetate CIMS, originally termed negative-ion proton-transfer chemical ionization, is conventionally thought to selectively ionize carboxylic acids and some inorganic acids by proton abstraction (R3.1) (Veres et al., 2008). Other compounds, such as nitrated phenols, are detectable with acetate CIMS due to their high gas phase acidity relative to the acetate ion (Mohr et al., 2013). However, acetate can also form adducts with levoglucosan, which are detected as

[levoglucosan + acetate]$^-$ clusters and not deprotonated due to their low gas phase acidity relative to the acetate ion (R3.2-R3.3) (Zhao et al., 2014). Similarly, isoprene epoxydiols (IEPOX) and ISOPOOH have also been reported to cluster with acetate (Budisulistiorini et al., 2015). Perhaps due to this wide array of potential analytes, acetate CIMS is extensively applied to TOF-CIMS platforms under a variety of experimental configurations (Aljawhary et al., 2013; Brophy and Farmer, 2015; Budisulistiorini et al., 2015; Chhabra et al., 2015; Lopez-Hilfiker et al., 2014; 2015; Mohr et al., 2013; Wentzell et al., 2013; Yatavelli et al., 2012; 2014; Zhao et al., 2014). Using an acetate CI source coupled to the Tofwerk API, Bertram et al. demonstrated that a distribution of acetate clusters exist but can be collisionally dissociated during their transfer through the API by applying stronger electric fields across the ion optics (2011). Potential ion-molecule reactions occurring between the reagent ion and analyte (R-H) are thus:

Proton abstraction

$$CH_3C(O)O^- + R\text{-}H \rightarrow CH_3C(O)OH + R^- \quad \text{(R3.1)}$$

Cluster reaction

$$CH_3C(O)O^- + R\text{-}H \rightarrow [CH_3C(O)O + R\text{-}H]^- \quad \text{(R3.2)}$$

We note, however, that two other types of reactions may be occurring:

Ligand exchange

$$[CH_3C(O)O + R\text{-}H]^- + R'\text{-}H \rightarrow [CH_3C(O)O + R'\text{-}H]^- + CH_3C(O)OH \quad \text{(R3.3)}$$

Declustering via collisional dissociation

$$[CH_3C(O)OH + R]^- + E_{CDC} \rightarrow CH_3C(O)OH + R^- \quad \text{(R3.4)}$$

While rare, fragmentation reactions are also known to occur within CIMS instrumentation

$$R + E_{CDC} \rightarrow r_1^- + r_2 \quad \text{(R3.5)}$$

In light of recent studies detecting nitrated phenols as deprotonated products (Mohr et al., 2013) and detecting levoglucosan (Zhao et al., 2014) and IEPOX/ISOPOOH (Budisulistiorini et al., 2015) as acetate clusters, we suggest that these reaction should be more generalized to include other molecules with various functional groups and non-acidic protons. Reactions R3.1 and R3.2 have been reported in the literature for acetate CIMS assuming that carboxylic acids are detected (Bertram et al., 2011). Ligand exchange reactions (R3.3) have not directly been identified to occur with acetate CIMS, but the chemistry appears to be very similar to iodide adduct CIMS where $[I + H_2O]^-$ reacts in a ligand exchange reaction with some analyte (X) to produce $[I + X]^-$ (Lee et al., 2014). The declustering reaction R3.4 is implicitly discussed by Bertram *et al.* (2011). Lastly, fragmentation in PTR-MS instruments is known to be an extensive feature. A study of atmospheric sesquiterpenes ($C_{15}H_{24}$) identifies seven fragment ions where the specific sesquiterpene will contribute to each fragment to a different extent due to structural differences (Kim et al., 2009).

Acetate CIMS can be contrasted to iodide adduct CIMS, another rapidly developing chemical ionization method being applied to TOF-CIMS platforms (Aljawhary et al., 2013; Friedman et al., 2016; Lee et al., 2014; Lopez-Hilfiker et al., 2014; 2016; Zhao et al., 2014). Iodide adduct CIMS predominantly forms iodide adducts with neutral species due to its high electronegativity; iodide is not expected to substantially abstract protons or transfer electrons (Iyer et al., 2016). Once ion-neutral clusters are formed, the ion optics of the mass spectrometer must efficiently transmit these clusters to the mass analyzer. The lack of proton abstraction or charge transfer allows this CIMS method to be operated in a cluster mode because the iodide ion holds the vast majority of the negative charge. Thus, the dominant clustering mechanism involves iodide. The dominant clustering mechanism with acetate CIMS involves the acetate ion,

but the prevalence of proton abstraction produces stable anions that will also undergo clustering reactions.

The Tofwerk API enables users to control and vary the extent of collisional dissociation, allowing for more representative descriptions of ion source chemistry. The Tofwerk API consists of two segmented RF-only quadrupoles: the “Short Segmented Quadruple” (SSQ) and the “Big Segmented Quadrupole” (BSQ). These components are housed in two differentially pumped vacuum chambers and contain various skimmers and entrance plates (Figure 3.1). Between the entrance of the API and the last skimmer after the BSQ, there are nine individually controllable voltage components and the two RF-only segmented quadrupoles making the task of optimally tuning the API a serious undertaking. This task is made more complex by the realization that instrument resolution, ion transmission efficiency, and extent of collisional dissociation are all interrelated.

Previous studies have examined these components with regard to controlling and/or understanding the transmission of ions and clusters to the TOF (Bertram et al., 2011; Heinritzi et al., 2016). The original description of the Tofwerk API uses no ion source and describes ambient ions and ion-neutral clusters in the atmosphere (Junninen et al., 2010). The authors characterize the ion transmission efficiency of the API-TOF tuned to transmit clusters using an electrospray source emitting tetra-heptyl ammonium bromide. Ion transmission efficiency is defined as the fraction of ions at the inlet or in the ion source that make it to the detector. No attempts to systematically characterize or optimize the API components are presented, although the authors note that ion transmission efficiency is strongly dependent on the voltage settings in the API. A comparison of methods for experimentally determining mass-dependent ion transmission

efficiency has also been reported, but no evaluation of the voltage settings, their relationships, and their effect on clustering or transmission efficiency is reported (Heinritzi et al., 2016).

The application of the Tofwerk API to a C-TOF configured as an acetate CI instrument provides some more insight to understanding the relationships between various API components as they relate to cluster transmission and collisional dissociation (Bertram et al., 2011). Here, the authors suggest that collisional dissociation of ion-neutral clusters occurs between the exit of the SSQ and the entrance of the BSQ vacuum stage. This claim appears to be in slight contrast to the recent results describing the use of voltage scanning to determine instrument sensitives with the iodide reagent ion (Lopez-Hilfiker et al., 2016). The authors scan the API voltages to increase the difference between the BSQ front and the last skimmer after the SSQ and lens skimmer (Figure 3.1 and Table 3.1). Ion transmission efficiency is maintained by floating all components upstream of the last skimmer more negative as the voltage difference between these two components is increased. Systematic floating of API components to change the voltage difference between two components maintains the electric field strengths between all other components. This approach also prevents changing the axial-electric field across the RF-only segmented quadrupoles; changing the axial-electric field will result in changes in ion transmission efficacy which must be avoided so that a mass spectrum collected under one voltage setting is comparable to results collected using a different voltage configuration.

Previous work comparing the iodide adduct, acetate, and water cluster CIMS methodologies using a HR-TOF-CIMS highlights the need for significant characterization of collisional dissociation in the API (Aljawhary et al., 2013). The authors tune a HR-TOF-CIMS to “weak-field mode” for iodide adduct and water cluster CIMS operation. A “strong-field mode” is used while operating in acetate mode. Comparing the negative ion mode voltage configurations

under strong-field and weak-field operation presented in the supplementary information shows numerous voltage relationships that may lead to subtle differences in relative ion transmission efficiency. This problem is not unique, and authors rarely publish exact voltage configurations as the exact voltages needed to tune the API will vary across instruments. The lack of careful study when configuring the API is obvious in the available HR-TOF-CIMS literature using acetate CI where reported [acetate + acetic acid] to acetate ratios (referred to here after as the acetate cluster ratio) vary by orders of magnitude (Brophy and Farmer, 2015). For example, Bertram *et al.*(2011) report an acetate cluster ratio of 2.6×10^{-3}, Mohr *et al.* (2013) report an acetate cluster ratio of 0.07, Brophy and Farmer (2015) report an acetate cluster ratio of 0.02, and Chhabra *et al.* (2015) report an acetate cluster ratio of 0.2.

We present a comprehensive characterization of the Tofwerk API. This characterization of the API allows for a detailed investigation of the acetate ionization mechanisms and the impact of controlling for these mechanisms on sensitivity, detection limits, selectivity, and mass spectral ambiguity with the general aim of non-targeted analysis. We show that the majority, if not all, ion-neutral chemistry occurs in the ion molecule reactor (IMR) where incoming sample air mixes with the output of the ion source. Lastly, we provide insight on configuring these HR-TOF-CIMS systems for non-targeted analysis and the detection of clusters.

3.2 Methods

3.2.1 Instrument Description and Chemical Ionization Source

The HR-TOF-CIMS (Tofwerk AG and Aerodyne Research, Inc.) is described extensively in the literature (Bertram et al., 2011; Brophy and Farmer, 2015; DeCarlo et al., 2006; Jokinen et al., 2012; Junninen et al., 2010; Lee et al., 2014). The instrument described herein is operated in the negative ion mode with acetate reagent ions. The configuration is described in detail by

Brophy and Farmer (2015). Notable differences include the use of a larger SH-112 single scroll pump (Agilent Technologies, Inc.) backing the IMR, a custom built quartz glass reservoir with metal to quartz fittings for holding the reagent precursor, and the use of the standard IMR critical orifice for sampling from atmospheric pressure at 1900 sccm. Mass spectra are acquired at an extraction frequency of 25.0 kHz and pre-averaged to 1 s mass spectra over a mass range from 2 to 494 *m/z* using an analog to digital converter (ADQ1600 SP Devices). Instrument resolution is >5000 for peaks above ~100 *m/z*. A TofDaq recorder is used to configure TOF acquisition parameters (Tofwerk AG, ToFDaq Version 1.97) and record mass spectra.

The quartz glass reagent reservoir is filled with acetic anhydride (Sigma-Aldrich, ≥99% ReagentPlus Grade) and the headspace is continually flushed with ~10 sccm UHP N_2 from a cryogenic dewar (Airgas, Inc.) using a 50 sccm mass flow controller (MKS Instruments, Inc. 1179A) and analogue controller (MKS Instruments, Inc. 247D). All connections to and from the reagent reservoir are made with instrument grade 1/8'' stainless steel instrument-grade lines (Restek, Inc.) and stainless steel Swagelok fittings and ferrules. The saturated headspace is mixed with a diluting UHP N_2 flow (~2000 sccm) controlled with a stainless steel needle valve (Swagelok). Approximately 900 sccm of the N_2-acetic anhydride mixture is subsampled through a critical orifice (O'Keefe Controls) into a Po-210 ionizer (NRD Static Controls LLC). A short, ¼'' outer diameter piece of PEEK tubing (Vici Metronics) separates and electrically isolates the stainless steel line from the Po-210 ionizer that is directly threaded into the IMR body. The glass reservoir, stainless steel lines, and Po-210 ionizer are held at 40 ^{0}C with a PID temperature controller and heating tape (Omega Engineering, Inc.). The IMR is held at 50 ^{0}C using the temperature controls onboard the HR-TOF-CIMS.

3.2.2 Experimental Setup

Gas phase standards of formic (CH_2O_2), propionic ($C_3H_6O_2$), butyric ($C_4H_8O_2$), methacrylic ($C_4H_6O_2$), nitric (HNO_3), and hydrochloric acid (HCl) are generated using permeation tubes (KIN-TEK Laboratories, Inc.) and custom built permeation ovens. The ovens are continually flushed with UHP N_2 at a constant flow of ~50 sccm and resistively headed to a constant temperature using PID temperature controllers (Omega Engineering, Inc.). The permeation rate of each species is determined by monitoring the mass loss of the permeation tubes over the course of months. Ultra zero grade air (Airgas Inc.) is mixed with the output of the permeation tubes to create single component alkanoic acid standards in clean air. The same source of ultra zero grade air is also used for instrument zeros and humidified air. Humidification of zero air is accomplished by passing the air through a series of large volume glass, custom built water bubblers filled with LCMS grade water (Sigma-Aldrich). The humidity system operates at a constant flow and varies the relative humidity (RH) using two mass flow controllers (MKS Instruments, Inc. 1179A) and a PID loop controlling the RH from an inline RH sensor (Omega Engineering HX71-V1). The sum of two mass flow controllers is held constant by the PID control loop and the ratio of the flows are changed to produce a large range of humidified air (0-90%). All additional flows are controlled with mass flow controllers (MKS Instruments, Inc. 1179A). The gas sample flow is sent to the HR-TOF-CIMS through a 3-way solenoid valve (NResearch, Inc) positioned upstream from the humidified air system. The total humidified flow is set below the sampling flow of the HR-TOF-CIMS (2 SLPM) and either zero air or a calibration mixture is subsampled through the 3-way valve to makeup the remaining sample flow (Figure SI3.1).

All components of this system are automated to allow for comprehensive calibrations of the six authentic acid standards under different instrument settings and different RH conditions. LabVIEW scripts (LabVIEW 2014 Version 14.0f1, National Instruments, Inc.) control the gas flows using pre-determined sets of flow rates, humidity settings, and instrument voltage configurations. Multiple data acquisition devices (Labjack Inc, U12) are implemented to record all flows, RH sensor output, and valve states. The HR-TOF-CIMS is controlled using the Tofwerk Application Programing Interface (Tofwerk AG, Version 1.97) from within the LabVIEW environment. All data streams read by the data acquisition devices are logged to the Tofwerk HDF files along with the HR-TOF-CIMS data.

Two general modes of operation exist for this experimental setup: full calibration mode and voltage scanning mode. Briefly, operating in full calibration mode produces one background-subtracted multi-point calibration curve at each specified RH setting. Next, LabVIEW changes the instrument voltage settings and repeats the experiment. One file is created for each instrument zero and calibration step in order to simplify data processing by averaging entire files of a fixed length. Voltage scanning mode utilizes the same flow system but maintains all the flows while switching instrument voltages. Again, a separate data file is created for each voltage configuration.

3.2.3 Data Analysis

Post-processing is performed in Igor Pro (WaveMetrics Inc, Version 6.3.7.2) running Tofware (Tofwerk AG, Aerodyne Research, Inc. Version 2.5.3). Tofware is used to process, fit, and then extract HR-TOF data and auxiliary data generated from the experimental setup. Once the integrated high-resolution time series are extracted, scrips developed in Igor Pro process all of the experimental data to produce calibration curves summaries and statistics. TOF duty cycle

corrections are made at *m/z* 59 for all data collected. Mass calibration is conducted using a three parameter fit available within Tofware using O_2^-, $^{35}Cl^-$, $^{37}Cl^-$, CHO_2^-, NO_2^-, $C_2H_3O_2^-$, and NO_3^- as mass calibration peaks. Additionally, $C_4H_7O_4^-$, the [acetic acid + acetate] cluster, is also included for mass calibration when operating in clustering modes where sufficient signal from this species is detected.

Calibration experiments are normalized by the ratio of the total ion signal at each calibration step relative to the total ion signal in zero air. Traditionally, normalization is conducted using the acetate reagent ion. Under declustered settings, acetate accounts for most of the total ion signal (>80%). These calibration experiments are complicated by voltage scanning of the API. Clustered settings retain the acetate clusters, which can contribute more of the total ion signal than acetate. Thus, the use of total ion signal is appropriate to maintain consistency in normalization procedures across a large range of clustering conditions. Experiments where only zero air is used are normalized by simply dividing the individual ion signals by the total ion signal and expressing the observed signals as a fraction of total signal.

3.2.4 Voltage Set Determination with Thuner

Exploration of the API component relations provide additional insight to the operation of these complex instruments. Very large sets of voltages (>40,000 configurations) are produced using Thuner (Tofwerk AG, Version 1.9.11.0), a design of experiment optimization software produced by Tofwerk. Thuner enables the user to establish relationships between various API components and set performance targets (resolution, sensitivity, peak shape). These component relations are used to set voltages in the API and optimize voltage settings based on the performance target criteria. For example, to optimize the instrument in a clustered mode (i.e. maintaining low electric field strengths through the API), the voltage difference between last

skimmer of the SSQ and the BSQ front can be set to a small range (0-2 V), allowing Thuner to test the impact of tuning each region of the API on desired parameters. Increasing the voltage difference between the skimmer and BSQ front (2-4 V, 4-6 V, etc.) moves the instrument stepwise from a cluster transmitting regime to a declustering regime. The SSQ and BSQ RF-frequency and amplitude are held constant at 2.65 MHz and 4.26 MHz with an amplitude of 200 V and 400 V, respectively.

Maintaining instrument and sample stability is essential during these experiments, particularly when comprehensive (>7 days) Thuner experiments are conducted. For this reason, the instrument samples ultra zero air throughout the entire Thuner experiment. Further details from these experiments are presented in the supplemental information (SI3.8.2). Ultimately, a single voltage configuration at a voltage difference of 1 V between the last skimmer and BSQ front are chosen by filtering for sensitivity, resolution, and the acetate cluster ratio using the Thuner XML output and various scripts written in Igor Pro. This voltage starting point is used to create all the voltage set point files for the voltage scanning experiments (Table SI3.1). Seven component relations are defined between adjacent components (Figure 3.1 and Table 3.1). The component nearest the TOF is held constant while all components upstream are floated together including the IMR body itself.

3.2.5 Voltage Scanning and Cluster Detection

We use non-linear least-squares sigmoidal regression following the work by Lopez-Hilfiker *et al.* to describe declustering voltage scans and determine the characteristic voltage (dV_{50}) at half signal maximum (Lopez-Hilfiker et al., 2016). The work by Lopez-Hilfiker *et al.* (2016) focuses on the sensitivities for iodide ion-neutral clusters and only examines declustering scans of species initially clustered with iodide that fall apart upon increasing the electric field

strength between two components. In contrast, acetate CIMS produces both ion-neutral clusters with acetate (and other negatively charged ions) and deprotonated-declustered ions. This more complex case means that ion signals may either increase or decrease as the electric field strength increases during a voltage scan. As such, we introduce another parameter to further describe the behavior of ions detected in the high-resolution mass spectrum: positive and negative change. Figure 3.2 details the fitting procedure and quantification of this change. A stable region at low voltage differences (low electric filed strength, high cluster transmission) is averaged and compared to a stable region at high voltage differences (high electric field strength, low cluster transmission) using a Student's T-Test. If the null hypothesis (the two populations are the same) is rejected, then the percent change is calculated. This allows for the dV_{50} to be converted into a positive or negative number.

Lopez-Hilfiker *et al.* (2016) filter their fits based on the criteria that if the mean square residual is >10%, the fit is rejected. This is insufficient for our purposes of characterizing this more complex set of voltage scans. Instead, we first reject unreasonable dV_{50} values where the calculated dV_{50} is greater than twice the scan range. Next, we use the output of the Student's T-Test to remove voltage scans with start and end points that likely belong to the same population (3s certainty). Lastly, linear least-squares cross correlation is performed on the high-resolution time series to identify correlation with the acetate reagent ion and the $[\text{acetate + acetic acid}]^-$ cluster. The acetate reagent ion follows an increasing sigmoidal shape due to the declustering of various acetate (or other anion) containing clusters and thus acts as a model shape for deprotonated-declustered species. The opposite is true for the $[\text{acetate + acetic acid}]^-$ cluster: the decluster scan follows a decreasing sigmoidal shape characteristic of clusters breaking apart. The sum of the correlation coefficients of the species of interest vs acetate and the species of interest

vs the [acetate + acetic acid]$^-$ provides a final cutoff ($r^2_{sum} \geq 1.5$). Most sigmoidal fits that remain follow anticipated declustering or clustering shapes.

3.3. Results

3.3.1 Typical Mass Spectrum and Voltage Scanning

The overall effect of voltage scanning on the observed mass spectrum using acetate CIMS is partially described in previous work characterizing the application of the Tofwerk API with a C-TOF-CIMS (Bertram et al., 2011). Our use of a HR-TOF-CIMS enables further identification of dominant peaks in the mass spectrum and a more comprehensive analysis of tuning effects and ionization chemistry. Figure 3.3 shows both the log-scale mass spectrum and linear-scale mass spectrum collected while flowing ultra zero air into the inlet and changing the voltage difference between the skimmer and BSQ front (component relation 5). The mass spectrum collected under high electric field strength (dV=12) is dominated by the acetate reagent ion (*m/z* 59.014, 80.1 % total signal) with a small contribution from O_2^- (3.2% total signal), CHO_2^- (2.4% total signal), and $C_2HO_4^-$ (4.7% total signal). Decreasing the voltage difference by half (dV=6) decreases the acetate reagent ion contribution (67.8% total signal) while enabling the appearance of the [acetic acid + acetate]$^-$ cluster (*m/z* 119.035, 7.9% total signal) and contributing a small amount of $C_2H_4O_4^-$ (1.85% total signal) and [acetate + $C_2H_3O_5$]$^-$ (*m/z* 166.012, 2.1% total signal). The most clustered settings (dV=2) completely change the reagent ion distribution. The acetate reagent ion decreases significantly (28% total signal) and both the [acetic acid + acetate]$^-$ cluster and [acetate + $C_2H_3O_5$]$^-$ cluster increase drastically (35.2% and 19.3%, respectively).

The appearance of $C_2H_3O_5$ clustered with acetate is unanticipated. We suggest this cluster is a radical fragment from the reagent precursor (acetic anhydride) that rapidly undergoes auto-

oxidation with two O_2 molecules (SI3.8.3). Overflowing the IMR with UHP N_2 and eliminating O_2 completely removes this observed cluster. Bertram *et al.* observe even more clustering than herein, with the higher order cluster [(acetic acid)$_2$ + acetate]$^-$ nearly equal to the acetate ion. Another interesting feature of the mass spectrum presented by Bertram *et al.* is the presence of a peak at *m/z* 166, potentially corresponding to the [acetate + $C_2H_3O_5$]$^-$ cluster. Despite observing a large abundance of the [(acetic acid)$_2$ + acetate]$^-$ cluster, [acetate + $C_2H_3O_5$]$^-$ remains quite small and may point to other operational differences such as the amount of acetic anhydride added to the Po-210 ionizer. The effect of the amount of acetic anhydride remains an open question in the literature, but we present preliminary experiments addressing this variable in the supplement (SI3.8.4).

3.3.2 API Component Relations

Voltage scans and cluster control have been discussed in terms of the voltage difference between the skimmer and the BSQ front (component relation 5), but numerous other component relations exist that may be suitable for controlling collisional dissociation. To address other component relations, dry ultra zero air is flown into the instrument inlet, and acetate and the first cluster, [acetic acid + acetate]$^-$, are examined as model compounds for deprotonated-declustered species and cluster species, respectively (See Section 3.2.5). Figure 3.4 shows the voltage scans for adjacent components in the API. It is apparent that while the dV_{50} for acetate and the [acetic acid + acetate]$^-$ cluster is extremely similar for any given set of component voltages, the dV_{50} for these species varies substantially across components. This is due to differences in both component spacing and pressure in the two regions of the API (BSQ, SSQ), resulting in different electric field strengths at the same voltage difference. Also displayed in figure 3.4 are the [acetic acid + acetate]$^-$ to acetate ratio. This ratio is reported in a number of acetate CIMS publications

(discussed in the Introduction) and provides a direct comparison between instruments to describe the extent of clustering. Converting the applied voltage differences into units of Townsend (Td) (i.e. electric field strength, E, normalized to the number density, N) show orders of magnitude variability in the fitted dV_{50} values for acetate and the [acetic acid + acetate]$^-$ cluster. Thus, the E/N formulation fails to explain the collisional dissociation energies between various components in this system.

If the voltage difference between adjacent components is set with a voltage difference of 0 V, ion flow through these components is controlled by fluid mechanics alone, and a decrease in ion transmission efficiency is observed. Thus, there is a lower limit to how gently one can transmit ions through these components while maintaining an electric field and high ion transmission efficiency. Deviations from the sigmoidal fit are observed at higher voltage differences for the axial voltage component on the BSQ (component relation 6). This field is applied between the BSQ back and BSQ front, but this deviation is attributable to ion transmission effects through the BSQ. This feature does not appear with the SSQ (component relation 2) because sufficiently high voltages needed to complete the curve could not be achieved due to voltage limits applied to the API to prevent electrical discharge. Another interesting feature is observed when scanning the second skimmer, located after the BSQ, and the BSQ back (component relation 7). Here, the cluster never reaches zero and the acetate signal remains correspondingly low in comparison to other components.

The exit of the SSQ to the lens skimmer (component relation 3) provides a promising region for cluster control compared to the choice of components used in previous studies (Lopez-Hilfiker et al., 2016), which are unable to directly resolve the dV_{50} of the [iodide + water] cluster and limited in their ability to directly resolve the dV_{50} for the [iodide + formic acid] cluster.

Similar to that study, scanning the BSQ front and skimmer relation (component relation 5) for the relevant acetate ions and ion-neutral clusters results in the identical problem described by Lopez-Hilfiker *et al.* (2016) when attempting to resolve the entire sigmoidal curve: we are unable to generate sufficiently low electric fields needed to transmit weakly bound clusters. In contrast, the exit of the SSQ to lens skimmer (component 3) better allows us to quantify stable cluster and decluster regions; this greatly improves our ability to detect clusters during non-targeted voltage switching experiments because there exists stable regions that can be defined as clustered and declustered (see sections 3.2.5 and 3.3.6).

3.3.3 Acetate CIMS Ion Chemistry

Operating the HR-TOF-CIMS with acetate reagent ions in a clustering mode provides a more representative view of the ion-neutral chemistry occurring in the IMR than the declustered mode. One interesting observation is that despite the relatively high pressure in the SSQ region (2 mbar) ion-neutral clusters do not appear to form in this region. One can attribute all the ion-neutral clustering chemistry to either reactions in the IMR or cluster condensation during the jet expansion from the IMR into the SSQ. This is inferred because clustering can be controlled between the SSQ entrance plate and the SSQ front (component relation 1). After passing through this region, the ions must make it through the entire length of the SSQ and subsequent skimmers making up most of the residence time through this region.

RH effects on the reagent ions are investigated while operating the HR-TOF-CIMS in both cluster mode (component relation 5, dV=2) and declustered mode (component relation 5, dV=20) (Figure 3.5). Using dry ultra zero air, the abundances of acetate, [acetate + acetic acid]$^-$ cluster, [acetate + $C_2H_3O_5$]$^-$ radical cluster are quite similar. Upon the addition of water, these abundances drastically change with the appearance of an [acetate + water]$^-$ cluster. The [acetate

+ water]$^-$ cluster competes with the other clusters while the sum total of acetate, [acetate + acetic acid]$^-$, [acetate + $C_2H_3O_5$]$^-$, and [acetate + water]$^-$ remains unchanged. We note that the [acetate + water]$^-$ cluster is observed to increase under the highly declusterd settings (component relation 5, dV=20), although it only makes up a small fraction of the total signal (~0.01% total ion signal) compared to the clustered settings (~17% total ion signal) at the highest RH (80% RH).

Although Veres *et al.* (2008) note that a collisional dissociation chamber is important to "dissociate weakly bound cluster ions such as $CH_3C(O)O^-(H_2O)_n$", neither the [acetate + $C_2H_3O_5$]$^-$ nor [acetate + water]$^-$ clusters have been directly identified in previous studies. This may be due to most acetate CIMS experiments being run under relatively declustered settings. The large abundance of acetate clusters observed in this study suggests that instead of a single reagent ion, chemical ionization in acetate CIMS is controlled by a distribution of reagent ion-neutral clusters that vary with RH and the concentration of acetic anhydride precursor. This is a consistent observation with Bertram *et al*., in which their comparison between the observed mass spectra under low and high electric field strengths leads to the realization that numerous acetate clusters exist and are involved in ionizing reactions (2011).

3.3.4 Comprehensive Calibrations

Calibrations of six acid standards exhibit similar RH and voltage dependences for both the deprotonated-declustered ions and ion-neutral clusters (Figure 3.6, SI3.8.5). All voltage scans are conducted between the skimmer and the BSQ front (component relation 5). Propionic acid is exemplary of the behavior of the carboxylic acids. In cluster mode, the dominant ions are the deprotonated-declustered conjugate base of the acid (R^-), the acetate cluster [acetate + R-H]$^-$, the water cluster [H_2O + R-H]$^-$, and the self-cluster [R-H + R]$^-$. The self-cluster is not observed for methacrylic acid (Figure SI3.5-SI3.9). All of these clusters are suppressed by operating the

instrument in a declustered mode. We reiterate that while the detection of these clusters can be eliminated, the cluster chemistry is still occurring in the IMR. Operation in clustered mode produces linear calibration curves for all species presented. In clustered mode, the most sensitive ion for the four carboxylic acids is the acetate cluster, although the sensitivities for this cluster rapidly decrease as the electric field strength is increased and the clusters are broken up. Increasing the electric field strength simultaneously increases the calculated sensitivity of all the acids at their deprotonated-declustered mass to a point where either ion transmission effects or fragmentation begin to occur and lower the sensitivity. The most sensitive ion for the two inorganic acids in cluster mode (hydrochloric acid and nitric acid) is the deprotonated-declustered ion. The [nitrate+nitric acid]$^-$ self cluster also shows high sensitivity for nitric acid.

The RH dependence of these clusters proceeds in the same manner as the reagent clusters. Increasing water vapor concentration in the IMR (or RH in the sample line) decreases the [acetate + R-H]$^-$ cluster by forming the associated water cluster. Thus, the water cluster and acetate cluster have opposite RH effects. The same effect is observed for the self-cluster. The deprotonated-declustered ion is more difficult to reconcile. Under dry conditions, the deprotonated-declustered ion exhibits the lowest sensitivity. Increasing the water vapor content leads to an initial increase in sensitivity, followed by a suppression of sensitivity at the highest water vapor content.

These effects can be clearly observed by examining a single voltage set corresponding to a vertical slice of Figure 3.6. Figure 3.7 shows this picture at dV=2 and examines the change in sensitivity as a function of IMR water content. Here, the sensitivity with water vapor is normalized to the sensitivity under dry conditions following the work by Lee *et al.* (2014). The change in sensitivity to the [propanoate + H_2O]$^-$ cluster increases 149 fold while the sensitivity of

the self-cluster and acetate cluster decrease by a factor of 5 and 1.6, respectively. For all analyte acids, the sensitivity of the deprotonated-declustered ions changes by, at most, a factor of 2 as a function of water vapor concentration, indicating a robust signal.

Acetate CIMS measurements are characterized by high background count rates which affect the limit of detection (LOD). The LOD is calculated for all calibration curves (SI3.8.5.3). The LODs of propionic acid ions detected in cluster mode are plotted in figure 3.7. The high sensitivity to the [acetate + R-H]$^-$ clusters leads to a very low 1 s LOD (S/N=3) below 10 ppt for the alkanoic acids detected as clusters. The same acids have higher LODs operating in declustered mode ~50-100 ppt examining the deprotonated-declustered ions. The lower sensitivity towards the inorganic acids produces much higher LODs. Deprotonated-declustered nitric acid and hydrochloric acid have 1 s LOD (S/N=3) of 2-4 ppb and <8 ppb, respectively.

These low LODs for the [acetate + R-H]$^-$ carboxylic acid clusters are attributable to the lower background count rates observed at higher *m/z* and the higher sensitivity of the [acetate + R-H]$^-$ carboxylic acid clusters. Increasing the voltage difference decreases the sensitivity to these clusters so that we calculate very high LODs. Under normal field operating conditions, these clusters will not contribute substantially to the observed mass spectrum. This greatly improves our ability to identify and extract molecular information by decreasing mass spectral complexity; artifacts like water clusters and self- or cross-clustering reactions are eliminated. The Supplementary Information (SI3.8.5.3) provides a more detailed presentation of the LODs for all calibrated species.

3.3.5 Evidence of Fragmentation

Molecular fragmentation can occur at high electric field strengths. Specific ions observed in the mass spectrum enable investigation of the voltages at which fragmentation onsets. We

investigate fragmentation between the SSQ back and the lens skimmer (component relation 3) and between the skimmer and BSQ front (component relation 5). We identify at least 6 ions (O_2^-, C_2HO^-, $C_2H_3O^-$, HO_2^-, $C_3H_3^-$, $C_3H_3O^-$) with very high dV_{50} values and molecular formulae consistent with fragmentation (Figure 3.8). Fragmentation must be considered when configuring a CIMS experiment to avoid destroying compounds of interest. Scanning component relation 3 exhibits a clear fragmentation curve, with most dV_{50} values occurring at dV=40. This is about twice as large as the dV_{50} values observed for the [acetate + acetic acid]$^-$ cluster. The sigmoidal fits for component relation 5 are less obvious, but calculated dV_{50} values for the fragment ions are nearly four times as large as observed for the [acetate + acetic acid]$^-$ cluster. The possibility of molecular fragmentation may explain some of the observed decreases in sensitivity at the higher dV values for the deprotonated-declustered ions (Figure 3.6). It remains challenging to separate the fragmentation effect from ion transmission effects that may dominate under very high electric field strengths (dv > 40 V Component Relation 3, dV>15 V Component Relation 5).

3.3.6 Complex Sample Declustering and Implications for Ambient Atmospheric Data

We use a potential aerosol mass (PAM) chamber to create a complex mixture of oxidized organic species in high concentrations from the oxidation of α-pinene by OH. The purpose of this experiment is not to make any claims about α-pinene + OH chemistry but instead to generate a complex mixture of oxygenated organic molecules that is not currently possible to obtain through authentic standards. The configuration of the PAM chamber is described in detail by Friedman *et al.* (2016). Briefly, a flow of ~65 ppbv α-pinene is oxidized by 2.8 x 10^6 molecules cm^{-3} OH (or ~1.9 days equivalent OH exposure) in a 13.1 L PAM chamber in ~2 minutes. Declustering scans between the SSQ back and lens skimmer (component relation 3) change the observed mass spectrum and is best observed in mass defect space (Figure 3.9). The dV_{50} values

obtained for the clustered ions shows an increasing trend with increasing mass, consistent with Lopez-Hilifiker et al. (2016)'s observation that large multifunctional nitrates and large oxygenated species exhibit high dV_{50} values.

Bulk descriptive values are calculated by Tofware using the ion signal intensity to weight the contribution of each individual ion to the total signal (Figure 3.10). This approach is frequently conducted with the HR-TOF-CIMS, either without correcting for differences in sensitivity (Friedman et al., 2016), or by applying the sensitive of one species (typically formic acid) to every species (Chhabra et al., 2015). The main finding is that the average oxygen to carbon ratio (O:C), hydrogen to carbon ratio (H:C), oxidation state, and carbon number (# carbons) all change significantly as a function of applied voltage difference. The average # carbons per ion decreases by ~1.7 carbon atoms per ion at the most declustered voltages. This is consistent with primarily removing or declustering acetate containing clusters; other species are simultaneously declustered, but acetate is the most abundant ion and thus comprises the dominant cluster. The average oxidation state decreases with declustering voltage with three distinct regions: low (0-18 V), intermediate (18-30 V), and high (>30 V) dV values. Little declustering is observed at low dV. The observed average oxidation state remains stable and is consistent with the behavior of other bulk metrics. Acetate clusters and other ion-neutral clusters dissociate in the intermediate dV range, causing the steep change observed in average oxidation state. Calculated bulk oxidation state continues to decrease at high dV values and is either due to the onset of fragmentation or the continued dissociation of strongly bound clusters.

dV_{50} values obtained by scanning component relation 3 using authentic standards are compared to the dV_{50} values of the same ions observed during the declustering PAM experiment (Table 3.2). The dV_{50} values determined for the disappearance of acetate clusters using authentic

standards in zero air are similar to the dV_{50} values obtained during the PAM scans (Figure 3.11). However, the PAM declustering scan consistently shows larger dV_{50} values for the deprotonated-declustered ions of all alkanoic acids. We present two hypotheses to account for this observation: (1) the complex mix of species produces cluster not only with acetate, but also with other abundant ions. This is consistent with the observation of self-clusters and clusters with background ions during the single component comprehensive calibrations (section 3.4). If these clusters are more strongly bound than the acetate containing cluster, then the destruction of the more strongly bound clusters will continue as the voltage difference increases and lead to the observed increase in dV_{50} values. (2) The difference in dV_{50} for deprotonated-declustered ions between the standards and PAM mixture may be the result of fragmentation of multi-functional oxygenated hydrocarbons that are decomposing to ions that are isobaric with the alkanoic acids.

The shape of the declustered-deprotonated ions during the PAM declustering scan is different from the behavior of these species during single component declustering scans in zero air. When individual authentic standards are added to zero air and declustering depletes the acetate-carboxylic acid cluster, the corresponding deprotonated-declustered ion ceases to change. In contrast, PAM declustering scans show continually increasing signal for the C3-C5 alkanoic acids with declustering. The signal intensity of the C3-C5 alkanoic acids during the PAM experiment is quite low in comparison to formic acid. Thus, the amount of fragmentation or declustering from strongly bound clusters must be substantial to actually observe this effect for formic acid.

3.4. Discussion: Acetate CIMS

Acetate CIMS ionizes analytes by both proton abstraction (R3.1) and ion-neutral clustering reactions (R3.2-R3.3). Detected ions are observed as deprotonated-declustered ions

because of the collisional dissociation that occurs during the transfer of the ions from the ion source to the mass analyzer (R3.4). The original development of this method by Veres *et al.* (2008) overlooks the importance of clustering in the ion source due to the use of a quadrupole mass spectrometer, limited mass scan range, and a collisional dissociation chamber (CDC). The idea that acetate CIMS is selective towards carboxylic acids is true, but the two ionization pathways (clustering vs direct proton abstraction) complicate mass spectral interpretation and efficient declustering with a CDC is necessary. Thus, the selectivity of acetate towards acids is really a function of both ion-neutral chemistry and instrument operation.

We find that the acetate CIMS reagent ions and reagent ion clusters behave similarly to the detected species in both clustering behavior and effects of API declustering. The observed clustering behavior of the reagent ions with water (Figure 3.5) explains the sensitivity dependence on RH (Figure 3.6-3.7, SI3.8.4). During calibration, the analyte-containing clusters are shifting in abundance as a function of water vapor concentration leading to differences in collisional dissociation efficiency and proton-abstraction efficiency. This is inconsistent with previous quadrupole acetate CIMS experiments that indicate no humidity dependence for formic acid (Veres et al., 2008). However, the ions most susceptible to humidity effects are the ion-neutral clusters; these species are rarely detected because of the operation of the API on the HR-TOF-CIMS in a declustered mode and the use of a CDC on quadrupole instruments. Collisional dissociation both simplifies the observed mass spectrum and eliminates the observation of acetate containing ion-neutral clusters. Effective collisional dissociation is the key to predominantly detecting proton-abstraction reaction products and maintaining the level of selectivity desired with chemical ionization. Ambient detection of IEPOX and ISOPOOH using

acetate clusters (Budisulistiorini et al., 2015) will likely suffer from severe humidity effects leading to large changes in sensitivity.

Similar humidity dependences are observed with iodide adduct CIMS (Lee et al., 2014). Acetate CIMS may be simpler because the sensitivities for the deprotonated-declustered ions follow approximately the same trend at a given voltage configuration in the API. In contrast, species clustered with iodide exhibit different RH dependences in both magnitude and shape for iodide adduct CIMS. We observe similarly complex RH dependencies in acetate and iodide reagent ions when run in a clustering mode (Figure 3.7). The observation of carboxylic acids clustering with water and other ions has been observed using quadrupole instruments with atmospheric pressure ion sources (Viidanoja et al., 1998).

The role of water on acetate CIMS chemistry remains difficult to reconcile. Propionic acid sensitivities are the lowest under dry and very wet conditions (Figure 3.6), but other trends exist for other deprotonated-declustered acids (SI3.8.5.1). The formation of the water-, acetate-, and self-clusters show identical RH dependence for all the calibration compounds: the addition of water shifts the cluster distribution as water is incorporated into acetate clusters.

Controlling for clustering reactions by operating the API on the HR-TOF-CIMS under declustered settings is obvious, but the API voltage configurations do not exist as a binary system of "clustered" and "declustered" operation, making the choice of voltages a balancing act. The data presented herein indicate that operating with an acetate cluster ratio of ~$1x10^{-2}$ is sufficient to eliminate the contribution of all clusters with carboxylic acids directly investigated here under ambient conditions. This corresponds to a dV at component relation 5 of ~15 V and a dV at component relation 3 of ~35 V. However, these exact voltage differences may be instrument-dependent, making the acetate cluster ratio an important operational parameter that

should be reported when using acetate CIMS as suggested in previous publications from this group (Brophy and Farmer, 2015). The effect of acetate precursor, acetic anhydride, concentrations on sensitivity warrants further study. Acetic anhydride is a difficult reagent precursor to work with because it is difficult to quantify the mass entering the Po-210 ionizer. It is even more difficult to constrain how efficiently acetate is produced from the α particle flux and comparison between instruments and ion sources remains nebulous.

Acetate CIMS requires significant declustering for ambient atmospheric measurement. The sensitivity to propionic acid detected as propanoate is maximized for component relation 5 at a dV of 10-12 V (Figure 3.6), although the LOD and relative contribution of each cluster versus the deprotonated-declustered species remains surprisingly high at these voltages (see SI3.8.5 for additional compounds, LODs, and sensitivity ratios). Increasing the dV at component relation 5 causes the relative contribution of each cluster to drop and decreases the sensitivity of the deprotonated-declustered ions (SI3.8.5.2). However, these high voltage differences lead to the formation of potential fragment ions at low *m/z* (Figure 3.8). We note that the average bulk parameters (O:C, H:C, # carbons, oxidation state) continually change as a function of applied voltage difference (Figure 3.10). The experiments calculating bulk parameters scan component relation 5, and distinct changes appear at a dV of 30 V. This may support the hypothesis that fragmentation is occurring because at dV = 30 V, the average H:C increases while the average O:C decreases, consistent with multifunctional oxygenate fragmentation. Increasing the voltage difference between adjacent components decreases the probability of transmitting a cluster through the API, although the clusters will be detectable at sufficiently high concentrations as shown by the calculated LODs (SI3.8.5.3).

Chhabra et al. (2015) present a method to account for clustering, or adduct formation, in a study of α-pinene and naphthalene oxidation products using a PAM chamber and acetate HR-TOF-CIMS. However, this method underestimates the complexity of the clustering problem by assuming that clustering reactions proceed only via adducts between acetate and a non-clustered ion (R-H) forming acetate clusters, $[R\text{-}H + acetate]^-$. The acetate-cluster mechanism is the most dominant clustering mechanism for the carboxylic acids studied in this work because there is a very high concentration of acetate ions relative to any other species in the IMR. Nitric acid, however, provides one exception to this hypothesis. The $[nitric\ acid + acetate]^-$ cluster and deprotonated declustered nitrate ion are less sensitive (i.e. contribute less to the mass spectrum total signal) relative to the [nitrate + nitric acid] self-cluster under all voltage differences and RH conditions (SI3.8.5.2, Figure SI3.17). Thus, this approach neglects self-clustering, water-clustering, and other cross-species clustering reactions which occur, albeit to a lesser extent than acetate clustering, in the system described herein. We evaluate the Chhabra *et al.* methodology for accounting for acetate clusters (SI3.8.6), and find that propionic acid clustering with acetate is underestimated by a factor of 15.5-26 depending on RH. Formic acid is accurately addressed under dry conditions, but is underestimated by a factor of 15 with the addition of water. Butyric acid is under estimated by a factor of 17-26, and methacrylic acid is underestimated by a factor of 5-12 depending on RH. The findings described herein further emphasize the importance of accounting for RH dependences of the reagent ion and thus cluster distribution.

We note two challenges in quantifying the impact of clustering on observed bulk properties or mass. (1) The presence of self-clusters and clusters formed with other ions present in the background spectrum during single component calibrations suggests that complex mixtures will be impacted by clustering from other species; for example, ambient formic acid

may form formate ions that cluster with other carboxylic acids. In situ standard additions are one approach for identifying this problem of secondary chemical ionization. (2) RH changes the ratio of clustered analyte to deprotonated-declustered analyte (Figure 3.7, SI3.8.5.2), further complicating quantification in ambient field measurements. However, controlling cluster interference in observed mass spectra by collisional dissociation is a straightforward approach to the complexity of acetate CIMS. Other formulations proposed in the literature may oversimplify this problem.

Quantification of complex mixtures with acetate CIMS is a complex problem. Clustering is the key mechanism for abstracting protons from carboxylic acids. Proton-abstracted declustered ions are predominantly observed if clusters are collisionally dissociated during transmission from the IMR to the detector. This suggests that some combination of both cluster binding energy and gas phase acidity control the extent to which the analyte species retains a charge upon declustering. The prevalence of cross-clustering reactions also demonstrates that secondary ion chemistry is occurring to an appreciable extent. The challenge of quantification when sensitivity varies by both analyte and RH may be further complicated by IMR design and ion transmission through the ion optics. With all these considerations, it is remarkable that such good agreement has been found between acetate CIMS measurements and aerosol mass spectrometer data suggesting that despite the complexities and unknowns, acetate CIMS captures an important fraction of the gas phase chemistry relevant to secondary organic aerosol production and evolution (Aljawhary et al., 2013; Chhabra et al., 2015; Lopez-Hilfiker et al., 2016).

3.5 Conclusion

Non-targeted analysis using HR-TOF-CIMS with no pre-separation is challenging, but remains a promising technique to understand atmospherically relevant species at low (<1 ppb) concentrations. We characterize numerous operational parameters using authentic standard calibrations that drastically improve our ability to understand and interpret the acetate CIMS mass spectrum. Tuning the HR-TOF-CIMS to a declustered mode in which the acetate ratio is $\leq 1x10^{-2}$ eliminates the clusters formed in the IMR. Further, we investigate the efficiency of declustering by applying the voltage scanning tools described herein to a complex mixture of α-pinene oxidation products. These tools provide a convenient approach to identifying whether alkanoic acid signals, for example, are solely due to the organic acid, or also the product of clustering or fragmentation reactions.

Iodide adduct and nitrate adduct CIMS may also benefit from routinely operating in a voltage scanning mode for non-targeted analysis. The iodide CIMS mass spectrum contains a poorly understood region that is separated in mass defect space from the iodide-cluster region by the "iodide valley" (Lee et al., 2014). This region is thought to contain peroxyacids (R-C(O)OOH) which appear as carboxylic acids upon increasing the applied voltage difference in the API. Thus, under normal iodide adduct CIMS operation, species in this region will exist as a complex mixture of ion-neutral clusters without iodide. Upon declustering, the iodide adducts will fall apart along with any of the non-iodide containing ion-neutral clusters observed in the more positive mass defect region. This would provide an additional set of information that can be compared to the results obtained in a clustered mode where only the iodide containing clusters are evaluated. Lastly, if the lessons learned here about acetate CIMS apply to deprotonated-

declustered anions in general, one may decrease the RH dependence observed with the iodide adducts by operating in a declustered mode and examining declustered species.

The API characterization presented herein may impact the analysis of atmospheric ions and new–particle formation under both ambient and laboratory conditions, such as the Cosmics Leaving OUtdoor Droplets (CLOUD) facility. Recent publications detailing CLOUD chamber measurements show stable clusters containing up to 17 sulfuric acid molecules clustered with other species (Schobesberger et al., 2015). The authors note that water is absent from most observed clusters due to evaporation inside the API-TOF, and that other species may also fragment (Olenius et al., 2013). The literature surrounding the API-TOF further acknowledges that declustering inside the instrument is poorly understood, and that fragmentation is highly related to instrument settings (Ehn et al., 2011; Junninen et al., 2010; Olenius et al., 2013). The scanning procedures presented herein may be of particular use to API-TOF instruments, in determining both the strength of these clusters, and API control/bias on observed cluster size and composition.

The observed mass spectrum acquired using acetate CIMS is the combined result of CI occurring in the IMR and declustering occurring throughout the instrument. Ignoring clustering will result in an underestimation of the average H:C ratio and overestimation of the average O:C ratio, average oxidation state, and average number of carbons. Clustering is efficiently controlled using API component relations, and clusters can be identified using non-linear least-squares sigmoidal regression and dV_{50} detection. The techniques and considerations described herein will be relevant for a wide variety of API-TOF users.

3.6 Chapter 3 Tables

TABLE 3.1 COMPONENT RELATIONS:

Component relationships defined by adjacent components in the API. (See Figure 3.1 for API schematic)

Component Relation	**Component A**	**Component B**
1	Q1 EP	SSQ Front
2	SSQ Front	SSQ Back
3	SSQ Back	Lens Skimmer
4	Lens Skimmer	Skimmer
5*	Skimmer	BSQ Front
6	BSQ Front	BSQ Back
7	BSQ Back	Skimmer 2
*Component relation used by Lopez-Hilfiker *et. al.* (2016)		

TABLE 3.2 COMPARISON OF CLUSTER SCANS WITH AUTHENTIC STANDARDS AND COMPLEX MATRIX SCANS:

Alkanoic acid species scanning results during authentic standard API scanning (left column) and PAM chamber scanning (right column). dV_{50} values are reported for the deprotonated-declustered ions (increasing signal with increasing dV) and for the acetate-clustered ions (decreasing signal with increasing dV).

	Standard Scans (dV_{50})		PAM Scans (dV_{50})	
Species	Primary Ions (appearance)	Acetate Cluster (disappearance)	Primary Ion (appearance)	Acetate Cluster (disappearance)
Formic Acid ($CH(O)OH$)	23.02 +/- 0.9	22.62 +/- 0.4	24.00 +/- 0.1	22.86 +/- 0.03
Propionic Acid ($C_2H_5C(O)OH$)	24.56 +/- 0.2	25.02 +/- 0.9	30.15 +/- 0.8	25.37 +/- 0.7
Butyric Acid ($C_3H_7C(O)OH$)	25.65 +/- 0.2	26.09 +/- 0.1	29.67 +/- 0.6	25.81 +/- 0.3
Pentanoic Acid ($C_4H_9C(O)OH$)	NA	NA	30.15 +/- 0.8	25.37 +/- 0.71
Hexanoic Acid ($C_5H_{11}C(O)OH$)	NA	NA	33.27 +/- 3.3	(23.97 +/- 1.0)[1]
Acetate Reagent ($C_2H_5C(O)OH$)	23.87 +/- 0.03	24.05 +/- 0.02	24.03 +/- 0.05	24.25 +/- 0.03

3.7 Chapter 3 Figures

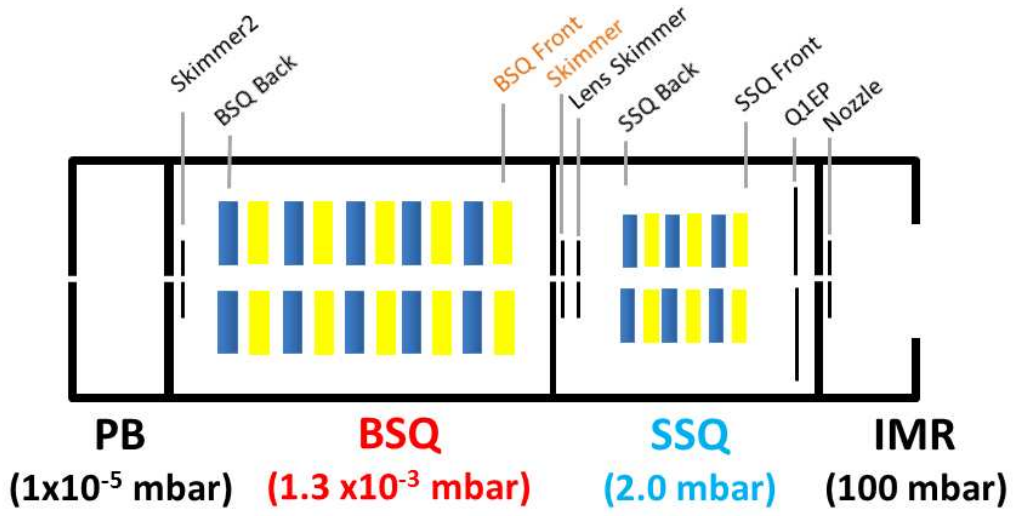

FIGURE 3.1 TOFWERK API SCHEMATIC:

Schematic of the Tofwerk atmospheric pressure interface (API) showing where the IMR mounts on the API, the short segmented quadrupole (SSQ), the big segmented quadrupole (BSQ), and the primary beam (PB) region.

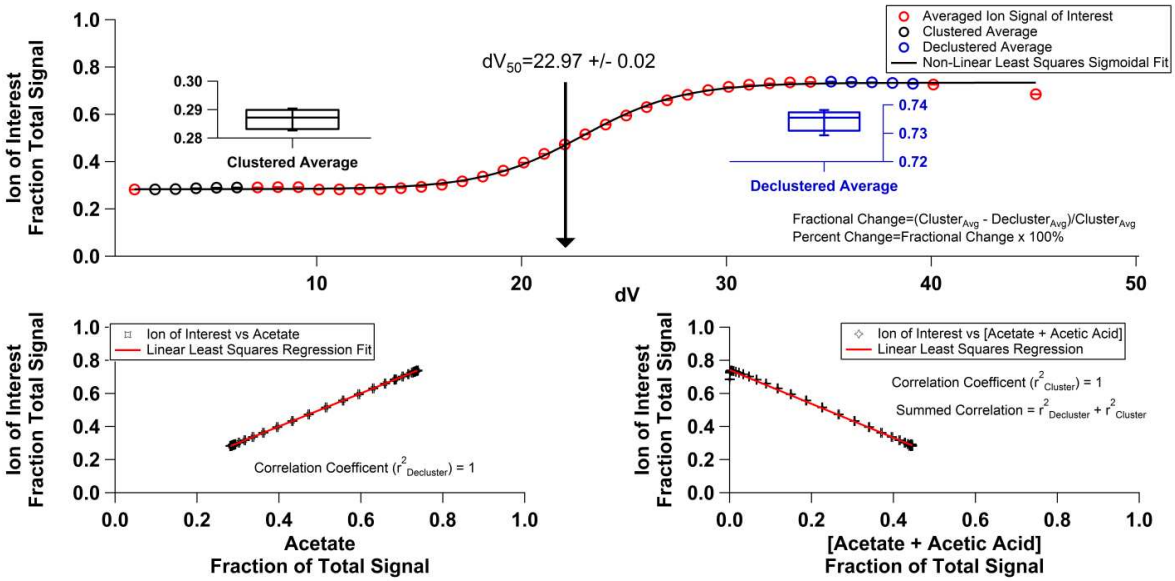

FIGURE 3.2 NON-LINEAR LEAST-SQUARES SIGMOIDAL REGRESSION AND CLUSTER DETECTION SCHEME:

Top panel: An ion of interest is normalized to the total ion signal and plotted against the voltage difference for some component relation (component relation 3 is shown here). The black circles show the portion of the curve used to average the signal of the ion during operation under weak (clustered) electric field strength with an inset box-and-whisker plot representing the clustered-average. Blue circles show the portion of the curve used to average the signal of the ion during operation under strong (declustered) electric field strength with an inset box-and-whisker plot representing the declustered-average. The dV_{50} value obtained from the non-linear least-squares sigmoidal fit is also displayed.

Bottom: The correlation scatter plots of the ion of interest with acetate and the [acetic acid +acetate] cluster. Linear regression produces an r^2 correlation coefficient for the ion of interest vs acetate (used as the model for a declustered-deprotonated species) and the ion of interest vs [acetic acid + acetate]. These two correlation coefficients are summed and used as criteria for including or excluding declustering scans.

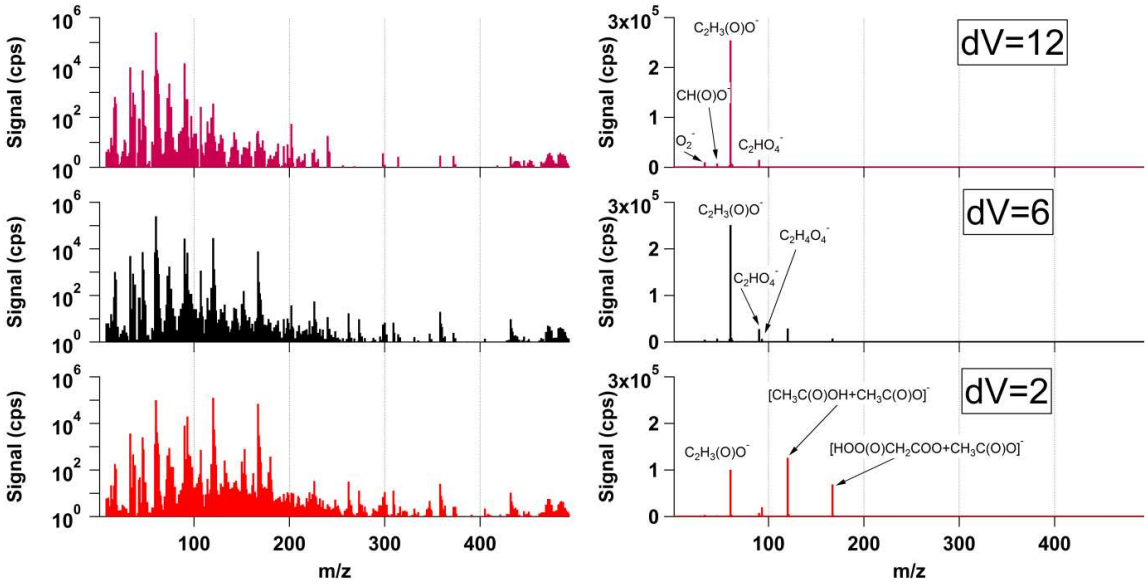

FIGURE 3.3 REPRESENTATIVE MASS SPECTRA AS FUNCTION OF DV:

A representative background mass spectrum obtained by overflowing the IMR with zero air is shown at three voltage differences (component relation 5). Both the log scale mass spectrum (left column) and linear scale (right column) mass spectrum are displayed. Dominant peaks related to the reagent ion chemistry are labeled.

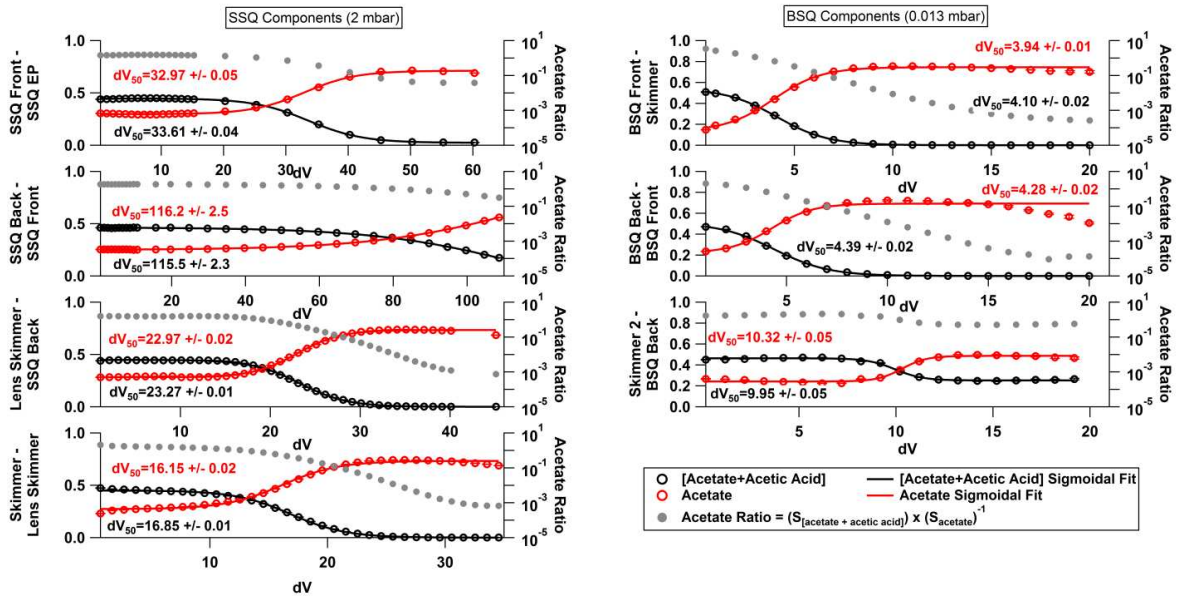

FIGURE 3.4 COMPONENT SCANS:

Voltage scan results conducted between the 7 component relations in the API. Acetate (red dots) and the [acetic acid + acetate] cluster (black dots) are plotted on the left axis. Fitted dV_{50} values for acetate (red trace) and the [acetic acid + acetate] cluster (black trace) are included along with the least-squares sigmoidal fit. The acetate ratio (grey dots) is plotted on the right axis as a log scale. Left column: components housed in the vacuum chamber containing the SSQ (2 mbar). Right column: components housed in the vacuum chamber containing the BSQ (0.013 mbar).

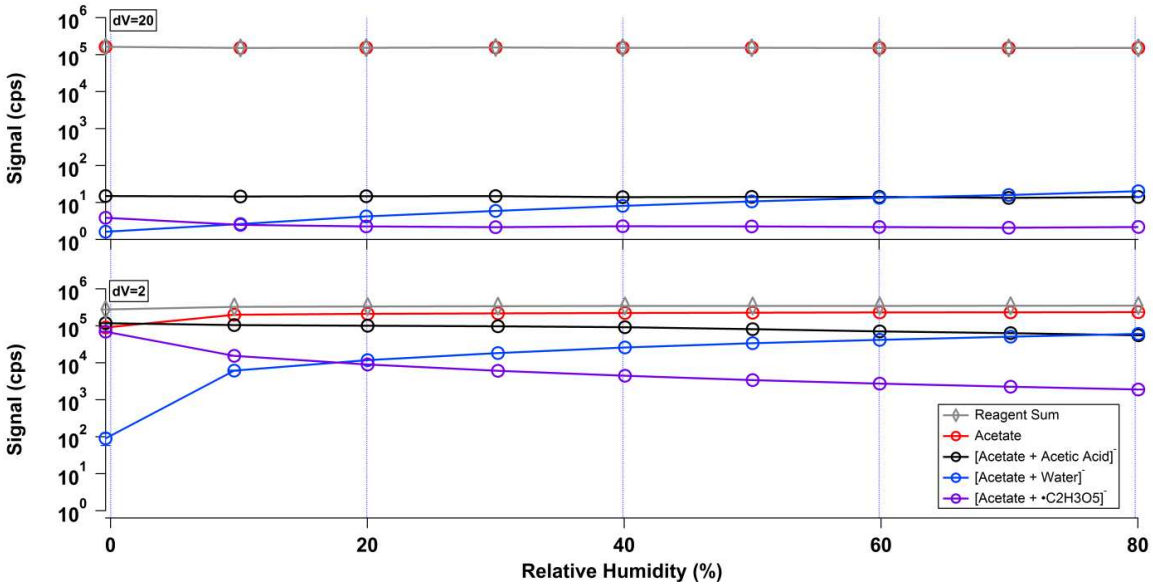

FIGURE 3.5 REAGENT IONS AND RELATIVE HUMIDITY:

The effect of water vapor on various reagent ions is shown under two voltage settings dV=2 (clustered) and dV=20 (declustered) at component relation 5.

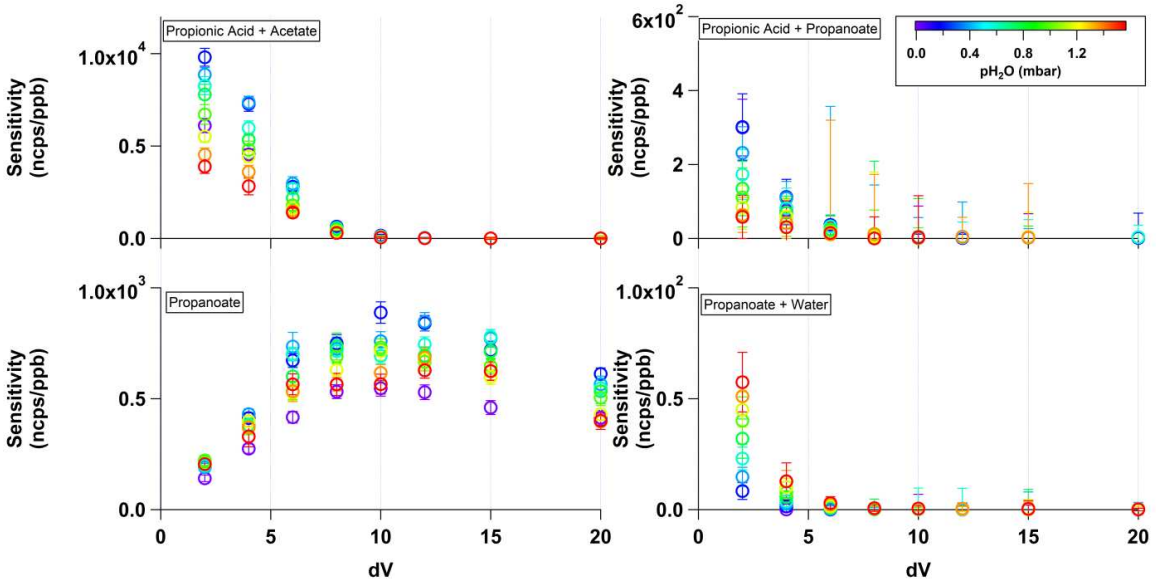

FIGURE 3.6 RH DEPENDENCE AND CLUSTER CONTROL ON PROPIONIC ACID SENSITIVITY:

The sensitivity to propionic acid and related clusters is plotted against the voltage difference applied between the skimmer and BSQ front (component relation 5) in units of normalized counts per second per ppb (ncps/ppb). The points are colored by the calculated water vapor content in the IMR corresponding to changing the relative humidity from 0% to 80% under laboratory conditions.

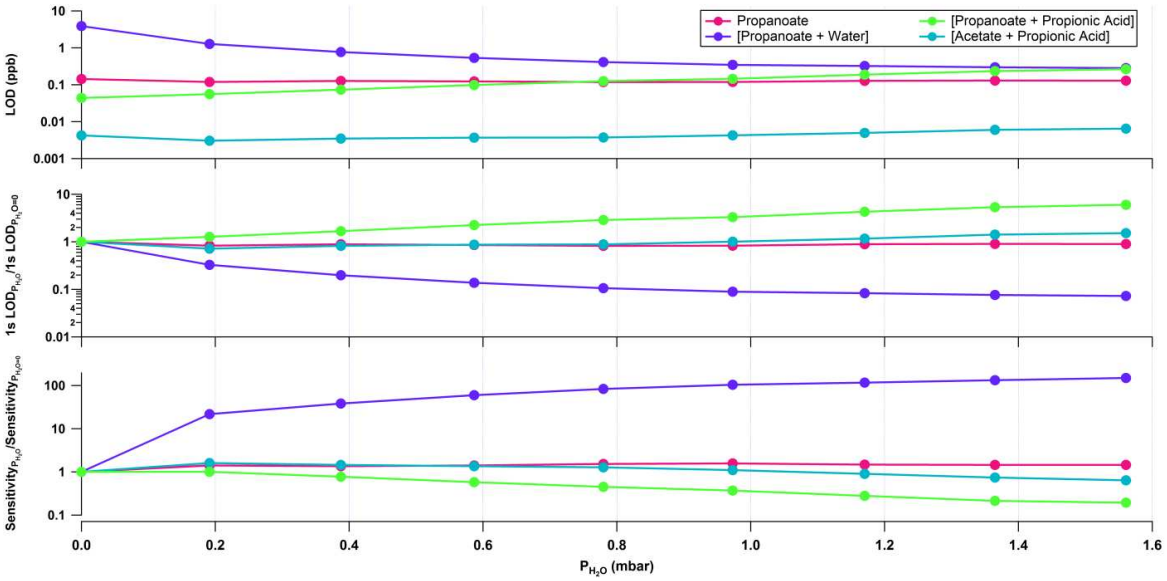

FIGURE 3.7 RH DEPENDENCE ON SENSITIVITY AND LOD UNDER CLUSTER SETTINGS:

The propionic acid data used in Figure 3.6 at a dV=2 is replotted as a function water vapor content in the IMR. Top: The calculated values for the limit of detection for propionic acid related ions (S/N=3, 1 s integration). Middle: the limit of detection (S/N=3, 1 s integration) relative to the limit of detection under dry conditions. Bottom: the change in sensitivity relative to the sensitivity under dry conditions.

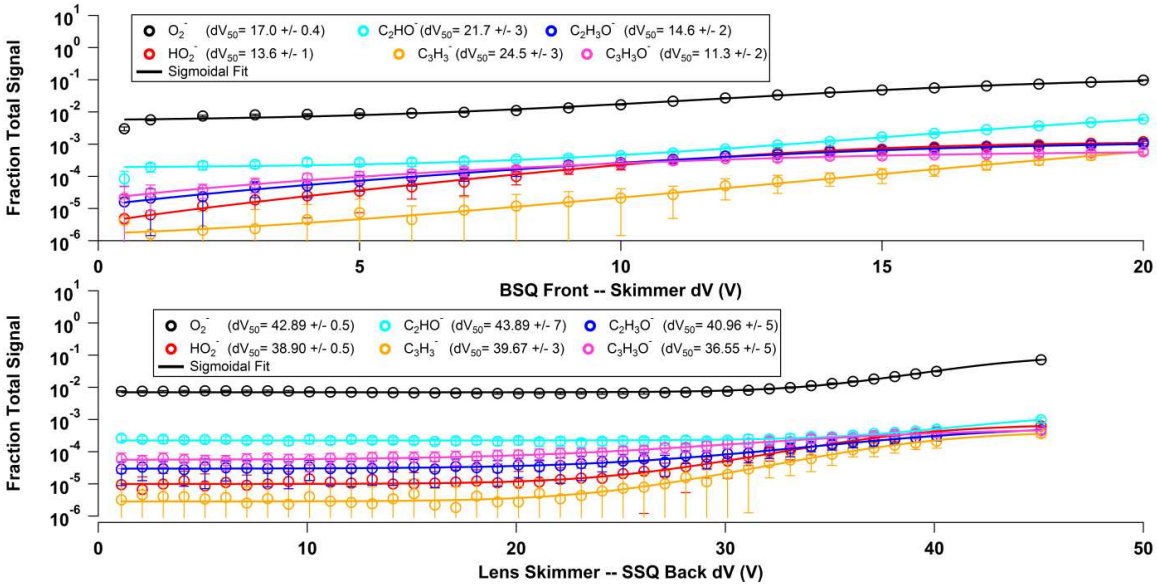

FIGURE 3.8 EVIDENCE OF FRAGMENTATION:

Voltage scanning experiments for a variety of potential fragment ions. Top: Component relation 5. Bottom: Component relation 3.

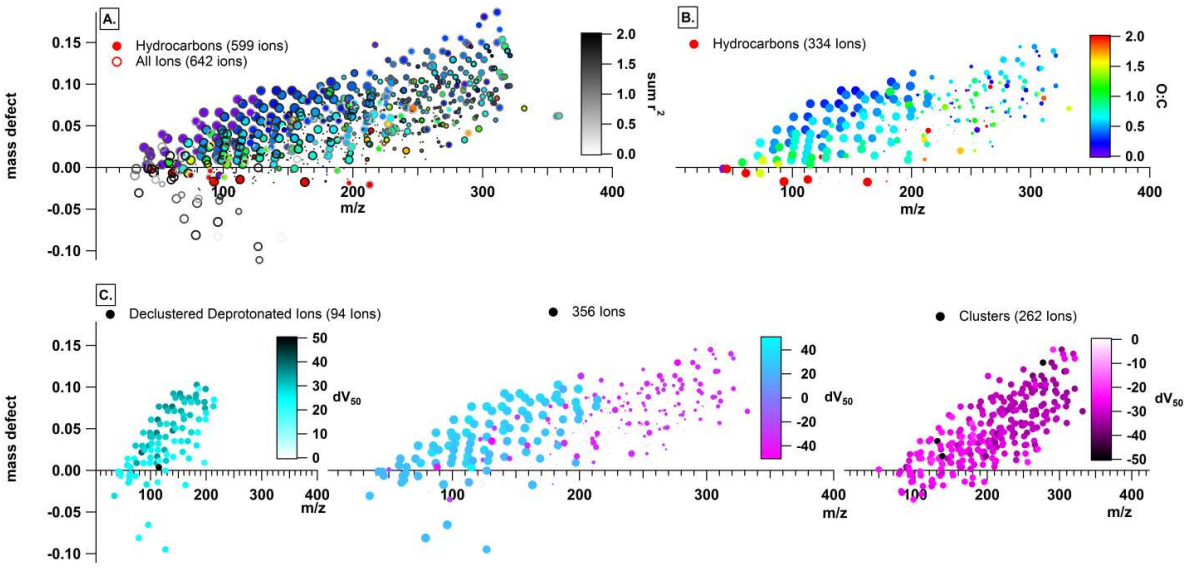

FIGURE 3.9 CLUSTER DETECTION IN COMPLEX MATRIX:

Mass defect plots from scanning component relation 3 during the a-pinene PAM chamber experiment: A. All species (642 ions) are plotted as open circles and colored by the sum correlation coefficient (grey color-scale). Hydrocarbons (599 ions) are plotted as solid circles and colored by the calculated oxygen to carbon ratio (rainbow color-scale). Both the open circles and solid circles are sized by the percent change during the scanning experiment. Small circles are decreasing as a function of increasing electric field strength while large circles are increasing. B. Hydrocarbons that meet the scanning criteria (334 ions) are plotted as solid circles colored by their oxygen to carbon ratio (rainbow color-scale); these are also sized by the percent change during the scanning experiment. C. (Left) Ions (94 non-clusters) which meet the scanning criteria and increase during a voltage scan (+dV_{50}) are plotted as solid circles (Cyan color-scale). (Middle) Ions which meet the scanning criteria (334 ions) are colored by dV_{50} (cyan-magenta color-scale). (Right) ions (262 clusters) which meet the scanning criteria and decrease during a voltage scan (-dV_{50}) are plotted as solid circles (magenta color-scale).

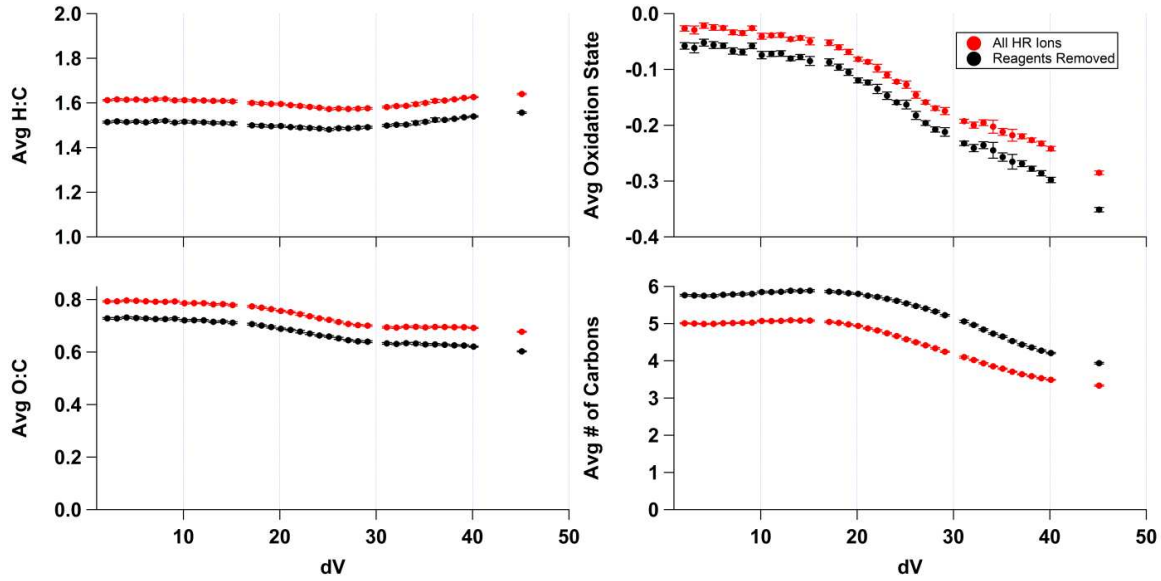

FIGURE 3.10 BULK PROPERTIES DURING DECLUSTER SCANS:

Bulk properties calculated in Tofware during the α-pinene PAM chamber experiment are plotted as a function of dV (component relation 3)

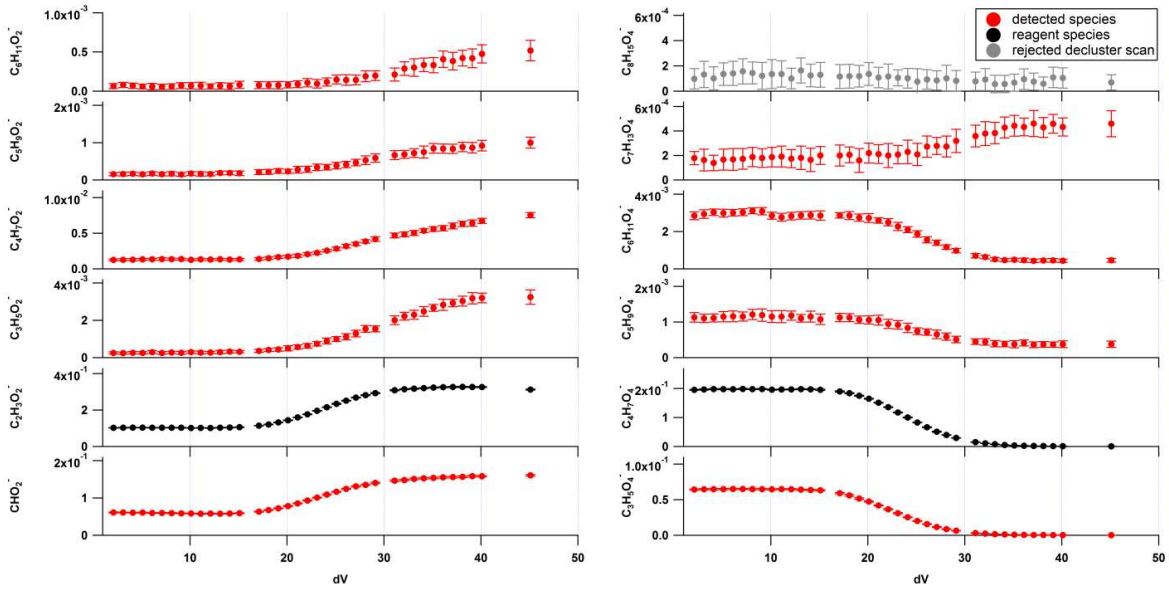

FIGURE 3.11 COMPARISON OF ALKANOIC ACIDS DURING AUTHENTIC STANDARD DECLUSTERING SCANS AND COMPLEX MATRIX DECLUSTERING SCANS:

Individual alkanoic acid scans obtained during the scanning PAM chamber experiment (left) and [alkanoic acid + acetate] clusters scans (right).

3.8 Chapter 3 Supplemental Information (SI3)

SI 3.8.1: Experimental Setup

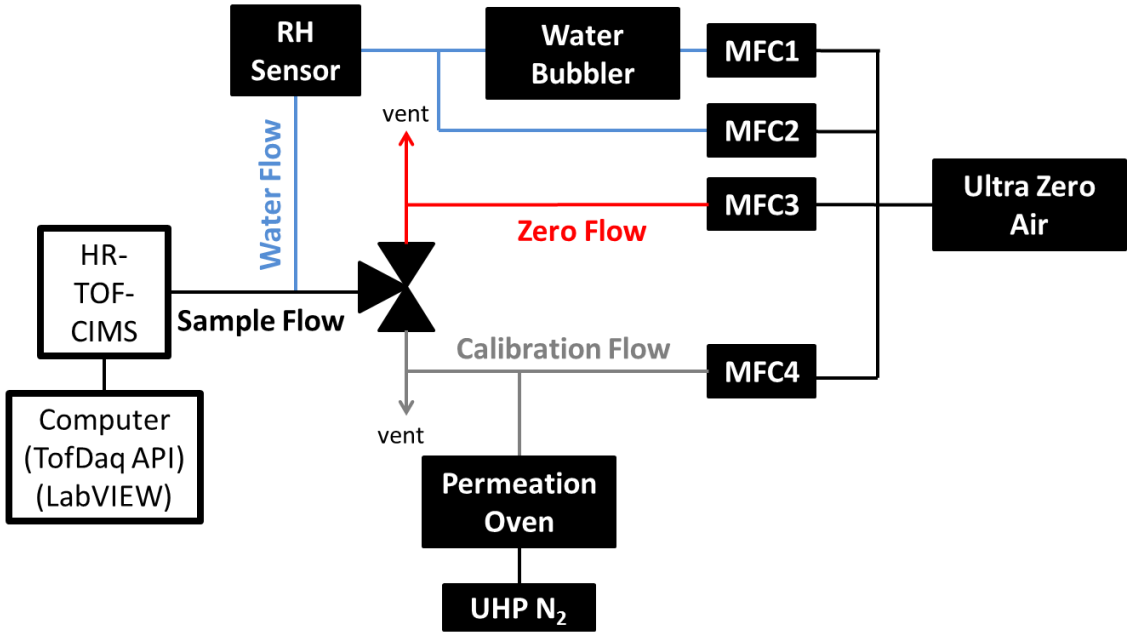

FIGURE SI3.1 EXPERIMENTAL SETUP:

Schematic diagram of the automated experimental setup for used calibrating the HR-TOF-CIMS under different voltage and humidity conditions.

SI 3.8.2: Thuner determined voltage configuration starting point

TABLE SI3.1 INITIAL VOLTAGE CONFIGURATION (THUNER DERIVED)

Component	Voltage
IMR Vacuum Region (100 mbar) SH-112 Agilent Single Scroll Pump	
IMR	-22
Short Segmented Quadrupole Region (2 mbar) Agilent TriScroll 600	
Nozzle	1.768
SSQ Entrance Plate	-2.766
SSQ Front	6.492
SSQ Back	4.196
Lens Skimmer	5.303
Skimmer	12
Big Segmented Quadrupole Region (1.3×10^{-3} mbar) Split Flow Pfeiffer Turbo Pump Stage 1	
BSQ Front	13
BSQ Back	13
Skimmer	20.194
Primary Beam Region (1.12×10^{-4}) Split Flow Pfeiffer Turbo Pump Stage 2	
Ref. (Bias)	56.617
Ion Lens	91.604
Deflector Flange	91.35
Deflector	95.25
Time-of-Flight Region (7.5×10^{-7} mbar) Split Flow Pfeiffer Turbo Pump Stage 3	
TOF Pulse	700
TOF Reference	43.895
TOF Extraction 1	30
TOF Extraction 2	700
TOF Lens	0
Drift	3000
Reflectron Grid	645.247
Reflectron Back	700
Post Acceleration	2800

SI 3.8.2.1: Thuner Method General Setup

The HR-TOF-CIMS continuously samples Ultra Zero Grade Air (Airgas, Inc.) to maintain stable signal across the mass range used for the Thuner experiments. Two zero air systems were also investigated (Environics, Inc. and Aadco Instruments, Inc.), but these systems cause instabilities and are not suitable for long Thuner experiments (or most CIMS work in general). The set of voltages chosen to create all subsequent voltage configurations are shown in Table SI3.1.

The approach to these Thuner experiments is to control clustering while optimizing the voltage configurations to maximize ion transmission efficiency. All of the controlling factors are summarized in Table SI3.2. All of the ions used for responses are summarized in Table SI3.3. The summary of results is presented in Figure SI3.1. Cluster control is primarily accomplished by controlling the voltage difference between the BSQ front and last skimmer in the SSQ (component relation 5) because this set of components is most sensitive towards controlling cluster transmission. The ions used to track sensitivity are all deprotonated-declustered ions. The idea is that cluster transmission is essentially held constant at each tuning step by constraining the system at component relation 5. Then the absolute ion transmission efficiency can be improved by monitoring the chosen ions. This is not exactly correct because other components can float to high or low voltage differences leading to more or less declustered operation; this can be overcome by more constrained control over the various API component relations. This effect is practically dealt with by simply post-processing the Thuner results and using the ratio between the signal of the [acetate + acetic acid] cluster and the acetate ion as the filtering criteria for choosing the voltage files.

Figure SI3.1 (top) shows all the voltage experiments for the complete Thuner experiment. Each step is repeated 10 times with small allowable voltage ranges applied to each component. This allows Thuner to test voltage sets within a fairly small voltage space where optimizations are better constrained. The skimmer to BSQ voltage difference is changed after tuning the SSQ, BSQ, and TOF voltages using a single voltage range. Seven voltage ranges are used (0-3 V, 4-6 V, 7-9 V, 10-12 V, 13-15 V, 16-18 V, and 19-21 V).

The observed decrease in average ion signal at high clustering ratios arises from the choice of response ions being deprotonated-declustered ions. Much less acetate makes it through the API because a large fraction of the acetate ion is bound up in clustering reactions. This can be seen in the Figure SI3.1 (bottom panel) specifically examining the [acetate + acetic acid] cluster and acetate. At low voltage differences (high acetate cluster ratio) there is a huge signal from [acetate + acetic acid] cluster which rapidly decreases as a function of voltage difference. The opposite trend is true for acetate.

These considerations highlight the difficulty of tuning the API with Thuner. Two possible approaches exist for future investigations: highly constrained tuning and highly targeted tuning. This manuscript (main paper) shows that the various components in the API have knowable relationships, and their effects are only observed under certain voltage differences. Thus, it seems possible to tune while keeping all these voltage differences within certain ranges that will not significantly contribute to either relative ion transmission effects (e.g. voltage differences across the quadrupoles) or declustering effects. Then a single component relationship (skimmer to BSQ front) may be used to control clustering. The other, and probably simpler option, is to let Thuner to the work by targeting certain performance criteria. Acetate, formate, and chloride are used as response variables in the work discussed here. Alternatively, one could define the acetate

cluster ratio and use this number as a specific target. Key components can still be constrained using this targeted mode of tuning.

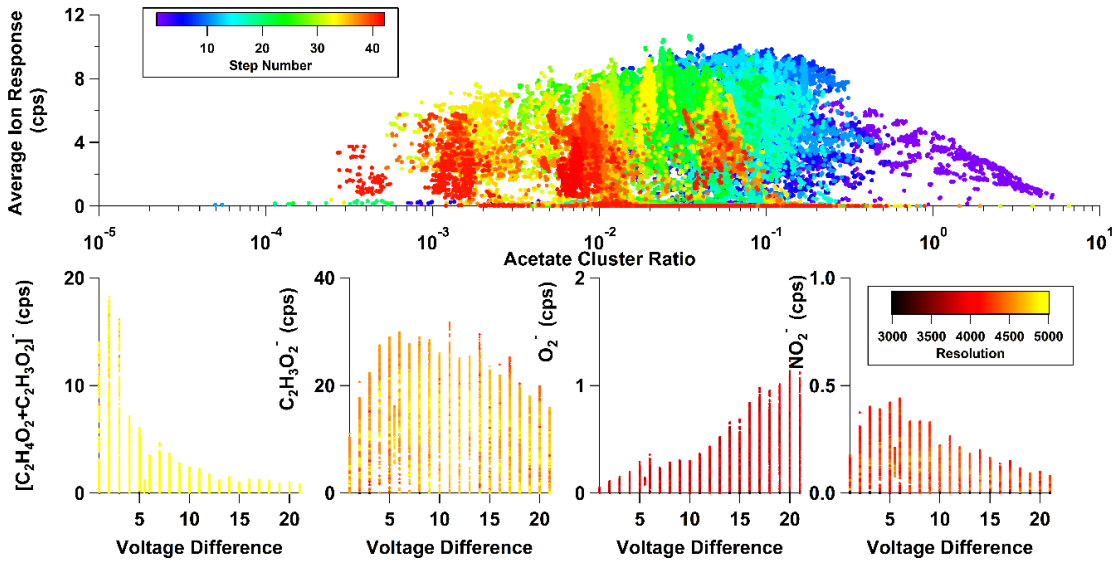

FIGURE SI3.2 THUNER RESULTS:

Thuner results of various ions and average response. Each point is one voltage configuration. Top: the average ion response is colored by the Thuner step number and plotted as a function of the acetate cluster ratio. Bottom: The average ion response of individual species is plotted as a function of applied voltage difference between the last skimmer of the SSQ vacuum region and the BSQ entrance. These data are colored by the resolution of the detected peak.

TABLE SI3.2 THUNER API VOLTAGE RELATIONS:

Step 1: SSQ Tuning Step			
Relationship Name	Components	Vacuum Region	Comments
IMR	IMR	IMR	
Nozzle	Nozzle	IMR to SSQ	
SSQ Entrance Plate	SSQ Entrance Plate	SSQ	
SSQ Average	(SSQ front + SSQ Back)/2	SSQ	Average voltage of SSQ
SSQ Difference	SSQ Back – SSQ Front	SSQ	Voltage drop across SSQ
Lens Skimmer	Lens Skimmer	SSQ	
SSQ-BSQ Transition	BSQ Front – Skimmer	SSQ to BSQ	Voltage drop from last SSQ region skimmer to BSQ front
BSQ Average	(BSQ front + BSQ Back)/2	BSQ	Average voltage of BSQ
BSQ Difference	BSQ Back – BSQ Front	BSQ	Voltage drop across BSQ
Step 2: BSQ/PB Tuning Step			
Lens Skimmer	Lens Skimmer	SSQ	
SSQ-BSQ Transition	BSQ Front – Skimmer	SSQ-BSQ	Voltage drop from last SSQ region skimmer to BSQ front
BSQ Average	(BSQ front + BSQ Back)/2	BSQ	Average voltage of BSQ
BSQ Difference	BSQ Back – BSQ Front	BSQ	Voltage drop across BSQ
Skimmer 2	Skimmer 2	BSQ	
Reference	Reference	PB	
Deflector Average	(deflector + deflector flange)/2	PB	Average voltage of lens stack
Deflector Difference	deflector flange – deflector	PB	Difference of lens stack
Lens	Lens	TOF	
Step 3: PB/TOF Tuning			
Reference	Reference	PB	
Deflector Average	(deflector + deflector flange)/2	PB	Average voltage of lens stack
Deflector Difference	deflector flange – deflector	PB	Difference of lens stack
Lens	Lens	TOF	
TOF Extraction Pulse 1	TOF Extraction Pulse 1	TOF	
TOF Extraction Reference	TOF Extraction Reference	TOF	
Reflectron Grid	Reflectron Grid	TOF	

TABLE SI3.3 THUNER IONS:

All Tuning Steps		
Ion	Used for m/z calibration	Used for sensitivity response
O_2^-	Yes	No
Cl^-	Yes	Yes
CHO_2^-	Yes	Yes
NO_2^-	Yes	No
$CH_3CO_2^-$ (Acetate Reagent Ion)	Yes	Yes
NO_3^-	Yes	No
$C_4H_7O_4^-$ (Acetate Reagent Cluster)	Yes	No

SI 3.8.3: Proposed mechanism for observed [•$C_2H_3O_5$ + Acetate]$^-$ cluster

Alpha-particle emission from ^{210}Po

$^{210}Po \rightarrow \alpha + {}^{206}Pb$ (SI R3.1)

$\alpha + N_2 \rightarrow \alpha + N_2^+ + e^-$ (SI R3.2)

Electron capture and dissociation of Acetic Anhydride

$H_3CC(O)O(O)CCH_3 + e^- \rightarrow H_3CC(O)O(O)CCH_3^-$ (SI R3.3)

$H_3CC(O)O(O)CCH_3^- + M \rightarrow H_3CC(O)O^- + \bullet(O)CCH_3^-$ (SI R3.4)

Auto-oxidation of radical fragment

$\bullet(O)CCH_3^- + 2O_2 \rightarrow \bullet C_2H_3O_5$ (SI R3.5)

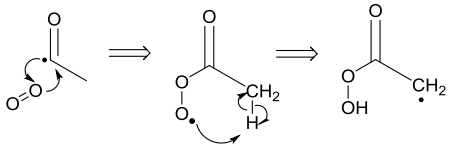

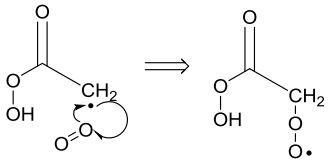

Cluster Formation of Radical

$CH_3C(O)O^- + \bullet C_2H_3O_5 \rightarrow [CH_3C(O)O + \bullet C_2H_3O_5]^-$ (SI R3.6)

SI 3.8.4: Effect of [acetic anhydride] on observed background spectra and reagent ions

Bertram *et al.* (2011) show a mass spectrum with an [acetate + acetic acid]/acetate ratio of 5.54 and an [acetate + 2(acetic acid)]/acetate ratio of 0.83. Both of these clusters are in much higher abundance in that study than has ever been observed on our instrument. Additionally, the peak at m/z 166 corresponds to $[CH_3C(O)O^- + \bullet C_2H_3O_5]^-$ in our system. This peak is observed by Bertram *et al.* (2011), but is very small compared to the [acetate + 2(acetic acid)] cluster. Thus, API tuning alone probably does not explain the differences observed between our instruments because one would assume that the $[CH_3C(O)O^- + \bullet C_2H_3O_5]^-$ cluster would be transmitted easily given the abundance of the higher order cluster.

The amount of acetic anhydride added to these systems remains a difficult number to constrain because liquid filled reservoirs are routinely used to generate acetate reagent ions. We attempted heating and cooling experiments that show subtle changes in the abundance and ratio of the dominate species produced from acetate CIMS. Figure SI3.3 shows the experimental results. Briefly, the acetic anhydride glass reservoir, stainless steel transfer lines, and Po-210 ionizer are constantly heated using heating rope and a PID temperature controller during normal operation. This entire heating system is turned off during this experiment and allowed to cool while the HR-TOF-CIMS continues acquiring mass spectra. This experiment is conducted under two voltage configurations (high declustering mode dV=20 and cluster mode dV=2) and two relative humidity settings (0% and 80% RH).

No change is observed under declustered settings further highlighting the importance of running this instrument in cluster mode to understand the underlying ion-neutral chemistry occurring in the IMR. Operation under cluster mode shows significant changes. Under dry conditions, the [acetate + 2(acetic acid)] cluster and the [acetate + water] cluster are observable

but very small. Increasing the temperature (more acetic anhydride) leads to an increase in both the [acetate + acetic acid] and [acetate + 2(acetic acid)] clusters while slightly decreasing the [$CH_3C(O)O$ + •$C_2H_3O_5$] cluster. Under high relative humidity conditions, the [acetate + 2(acetic acid)] is very small and barely detectable. The [acetate + water] and [$CH_3C(O)O$ + •$C_2H_3O_5$] clusters decreases as more acetic anhydride is added to the Po-210 ionizer. It is not expected that adding huge amounts of acetic anhydride will ever be sufficient to titrate out the [acetate+water] cluster because it makes up a very large fraction of the total signal.

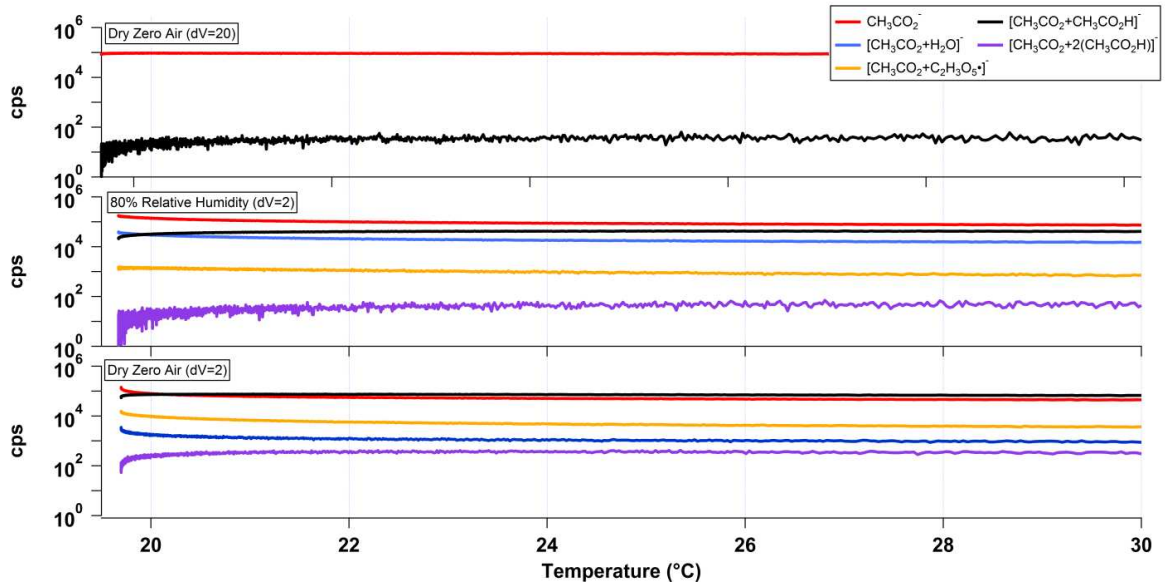

FIGURE SI3.3 EFFECT OF ACETIC ANHYDRIDE CONCENTRATION:

The effect of heating and cooling the acetic anhydride reservoir and transfer lines on the observed reagent ion signals. The heating/cooling cycle is conducted under declustered settings (top) and clustered settings (middle and bottom). Relative humidity is set to 80% under cluster mode (middle) for comparison to dry experiments under cluster mode (bottom).

SI 3.8.5: Other calibrations and additional data

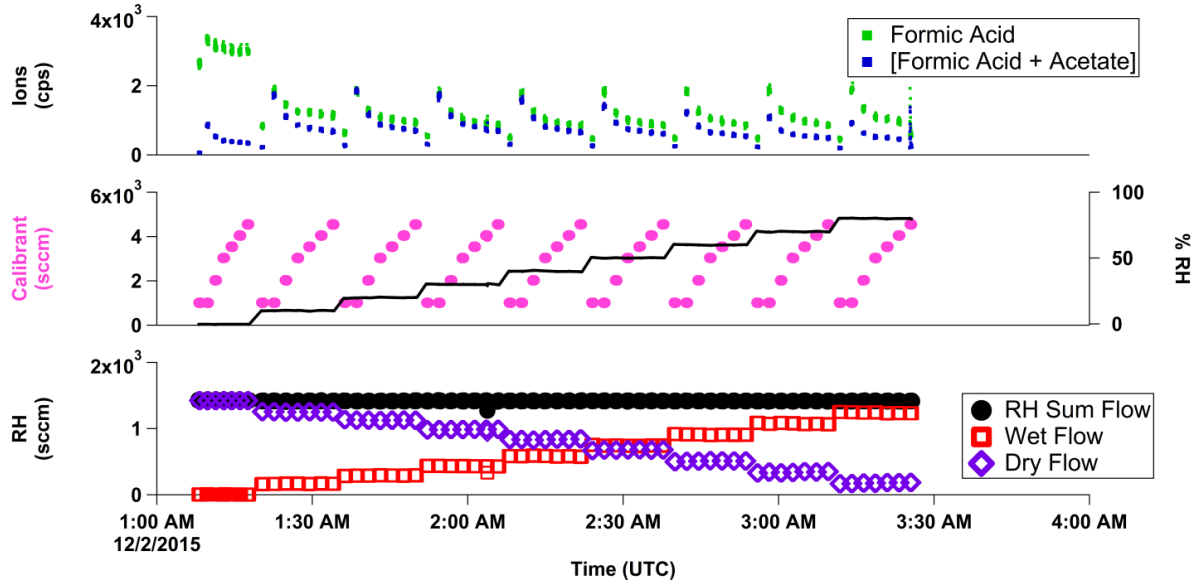

FIGURE SI3.4 EXPERIMENTAL SUMMARY:

Detailed summary of experimental calibration procedure for voltage and relative humidity dependent calibrations. (Bottom) Relative humidity control system: the flow from the MFC pushing ultra zero air through a series of water filled glass bubblers and the flow from the MFC controlling the dry air flow. The sum of these two controllers is held constant. (Middle) The resulting relative humidity generated from the relative humidity control system measured from the inline relative humidity sensor is plotted on the right axis. The MFC controlling the dilution flow of the calibration source is plotted on the left axis. (Top) The ion signal is shown for formic acid and the [acetate + formic acid] cluster during the calibration experiment.

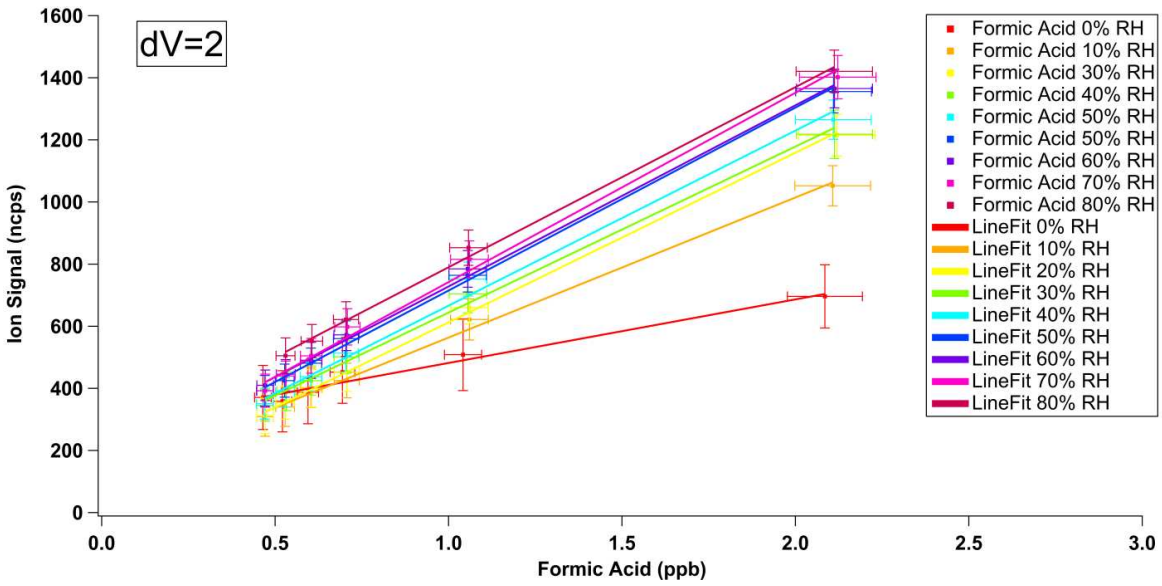

FIGURE SI3.5 CALIBRATION CURVE EXAMPLE:

Normalized and background subtracted calibration curves colored by relative humidity and collected under a single voltage configuration using the experimental setup graphically described in Figure SI3. These data are automatically generated for all species investigated. Deprotonated-declustered formic acid is shown here.

SI 3.8.5.1 Sensitivity

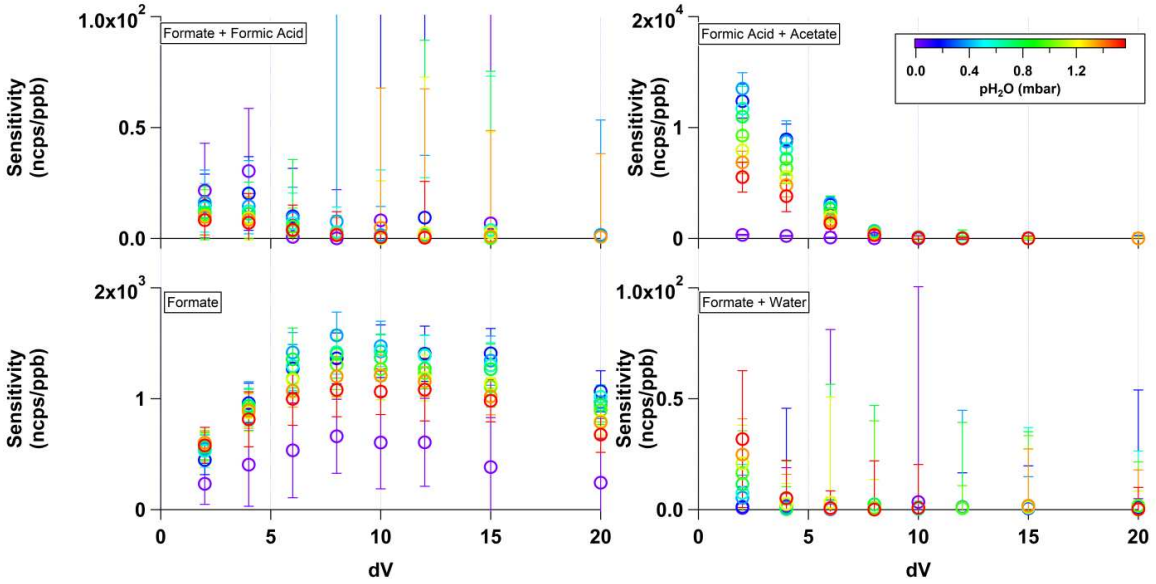

FIGURE SI3.6 SENSITIVITY TO FORMIC ACID:

The sensitivity to formic acid and related clusters is plotted against the voltage difference applied between the skimmer and BSQ front (component relation 5). The points are colored by the calculated partial pressure of water in the IMR corresponding to changing the relative humidity from 0% to 80% under laboratory conditions. Sensitivity drops off at higher dV values for clustered species but is maintained for declustered-deprotonated ions.

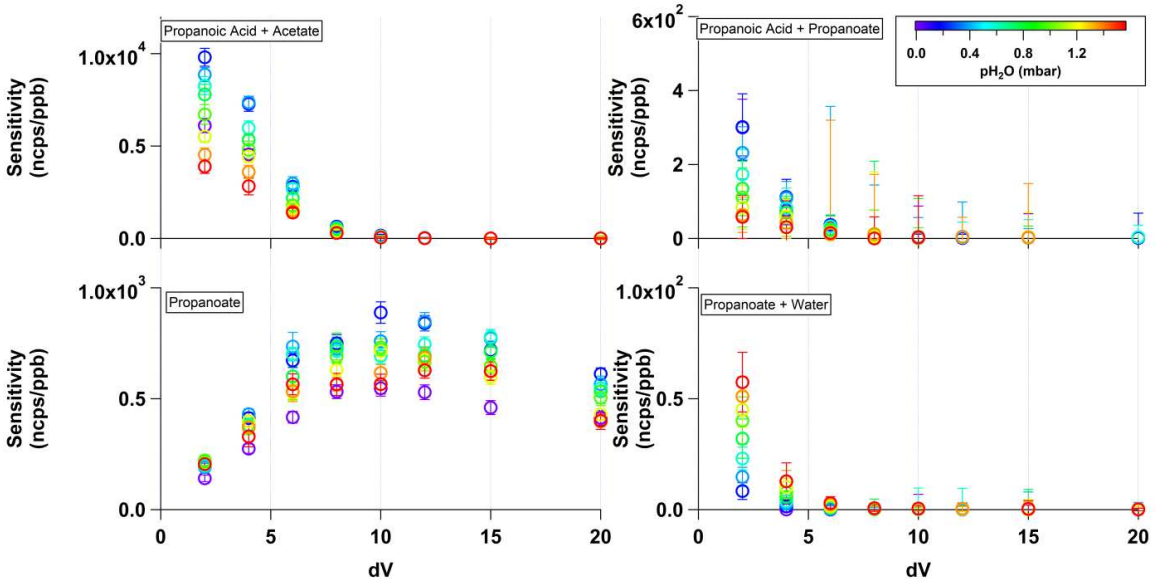

FIGURE SI3.7 SENSITIVITY TO PROPANOIC ACID:

The sensitivity to propanoic acid and related clusters is plotted against the voltage difference applied between the skimmer and BSQ front (component relation 5). The points are colored by the calculated partial pressure of water in the IMR corresponding to changing the relative humidity from 0% to 80% under laboratory conditions. Sensitivity drops off at higher dV values for clustered species but is maintained for declustered-deprotonated ions.

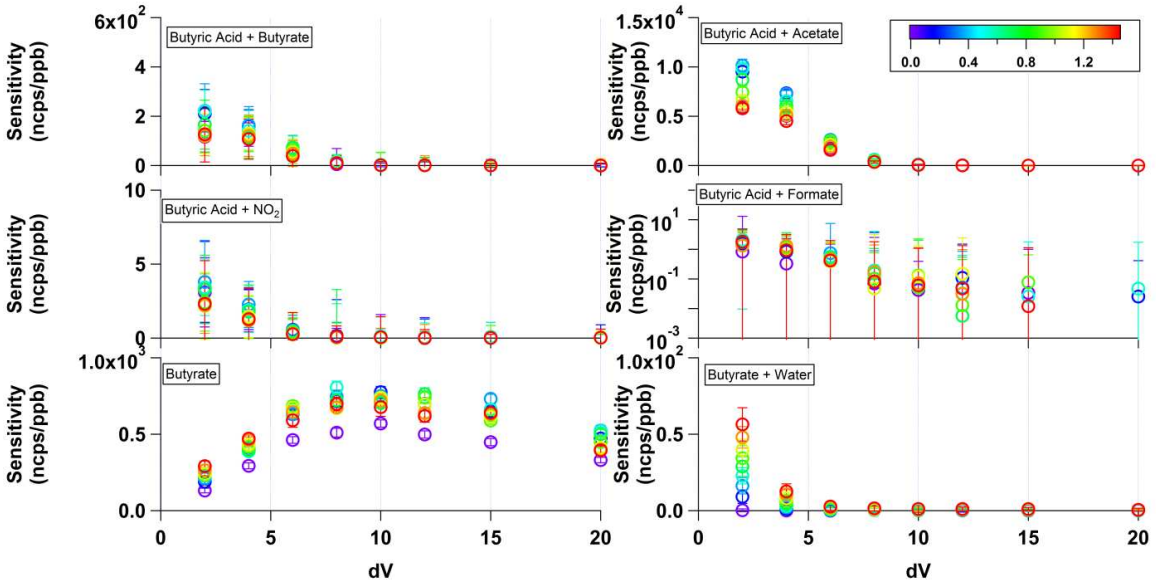

FIGURE SI3.8 SENSITIVITY TO BUTYRIC ACID:

The sensitivity to butyric acid and related clusters is plotted against the voltage difference applied between the skimmer and BSQ front (component relation 5). The points are colored by the calculated partial pressure of water in the IMR corresponding to changing the relative humidity from 0% to 80% under laboratory conditions. Sensitivity drops off at higher dV values for clustered species but is maintained for declustered-deprotonated ions.

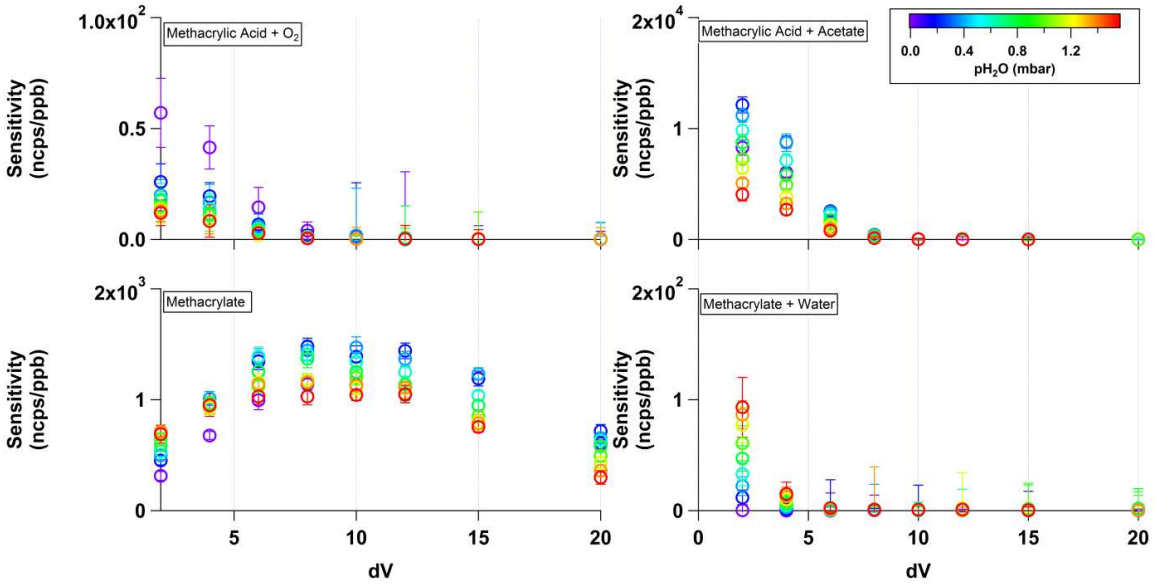

FIGURE SI3.9 SENSITIVITY TO METHACRYLIC ACID:

The sensitivity to methacrylic acid and related clusters is plotted against the voltage difference applied between the skimmer and BSQ front (component relation 5). The points are colored by the calculated partial pressure of water in the IMR corresponding to changing the relative humidity from 0% to 80% under laboratory conditions. Sensitivity drops off at higher dV values for clustered species but is maintained for declustered-deprotonated ions.

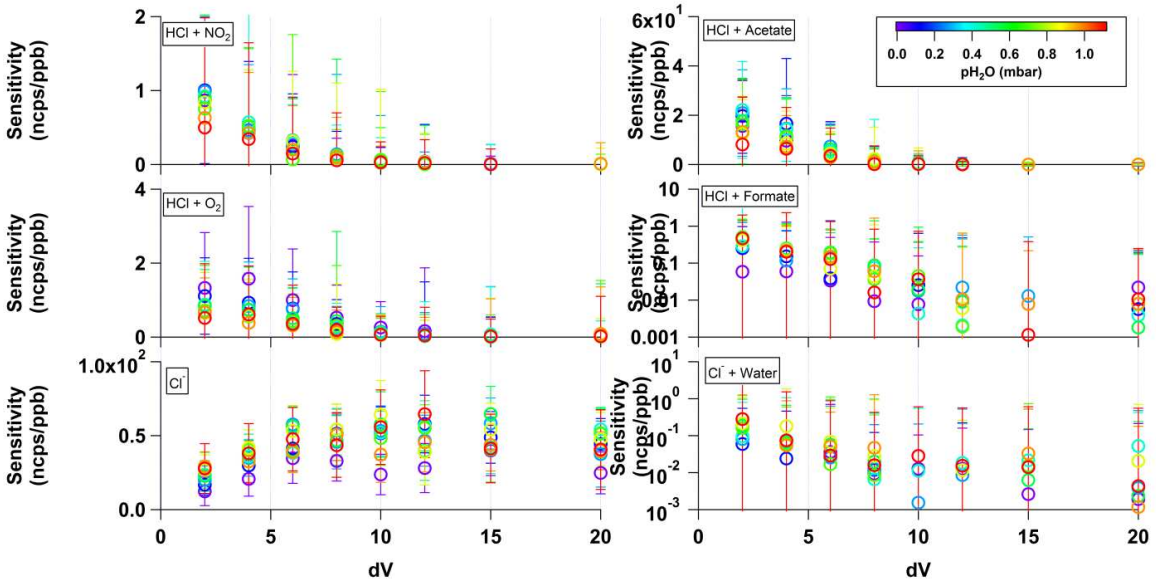

FIGURE SI3.10 SENSITIVITY TO HYDROCHLORIC ACID:

The sensitivity to hydrochloric acid and related clusters is plotted against the voltage difference applied between the skimmer and BSQ front (component relation 5). The points are colored by the calculated partial pressure of water in the IMR corresponding to changing the relative humidity from 0% to 80% under laboratory conditions. Sensitivity drops off at higher dV values for clustered species but is maintained for declustered-deprotonated ions.

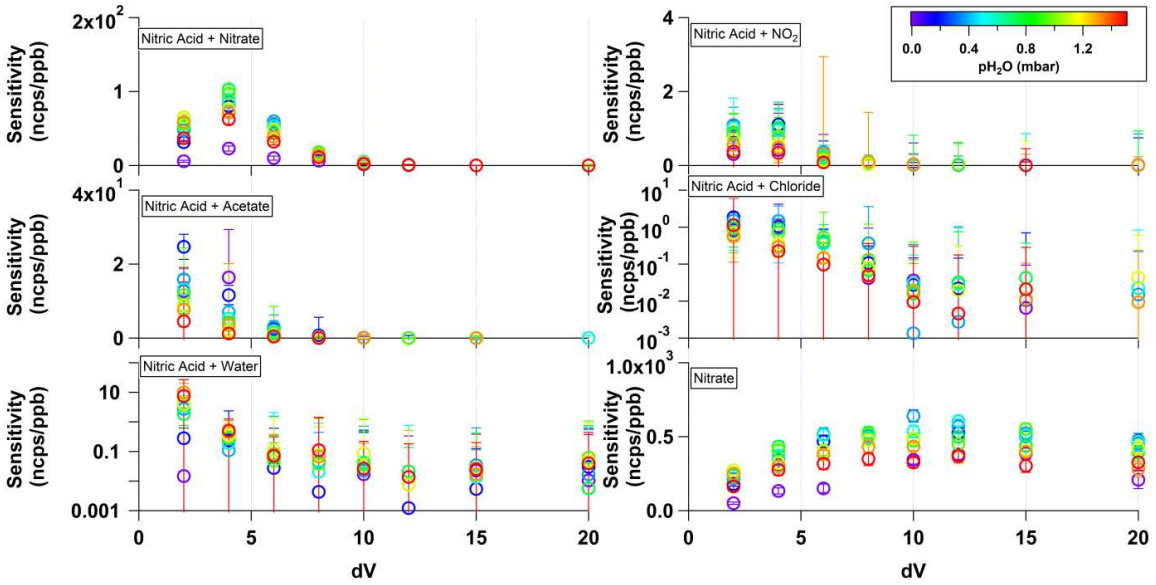

FIGURE SI3.11 SENSITIVITY TO NITRIC ACID:

The sensitivity to nitric acid and related clusters is plotted against the voltage difference applied between the skimmer and BSQ front (component relation 5). The points are colored by the calculated partial pressure of water in the IMR corresponding to changing the relative humidity from 0% to 80% under laboratory conditions. Sensitivity drops off at higher dV values for clustered species but is maintained for declustered-deprotonated ions.

SI 3.8.5.2 Sensitivity Ratios

Sensitivity Ratio = $\frac{S_{RH,dV}[RC(O)OH+X]}{S_{RH,dV}(RC(O)O^{-})}$ (SI Eqn. 3.1)

The sensitivity ratio is defined as the sensitivity at some relative humidity and voltage configuration ($S_{RH,dV}$) of some cluster [RC(O)OH+X] divided by the sensitivity at the same relative humidity and voltage configuration ($S_{RH,dV}$) of the deprotonated-declustered ion during the calibration [RC(O)O$^-$]. These plots (along with the LOD plots SI3.8.5.3) show another way of examining how much a cluster can contribute to an observed signal relative to the signal of the identified deprotonated-declustered ion. It should be noted that if linear regression converges in the automated calibration curve processing script, it is included in this plot to provide an estimate of a calibration factor. At high dV values, many of the cluster calibration curves show poor r^2 values and the trend of decreasing sensitivity ratio as a function of dV will weaken.

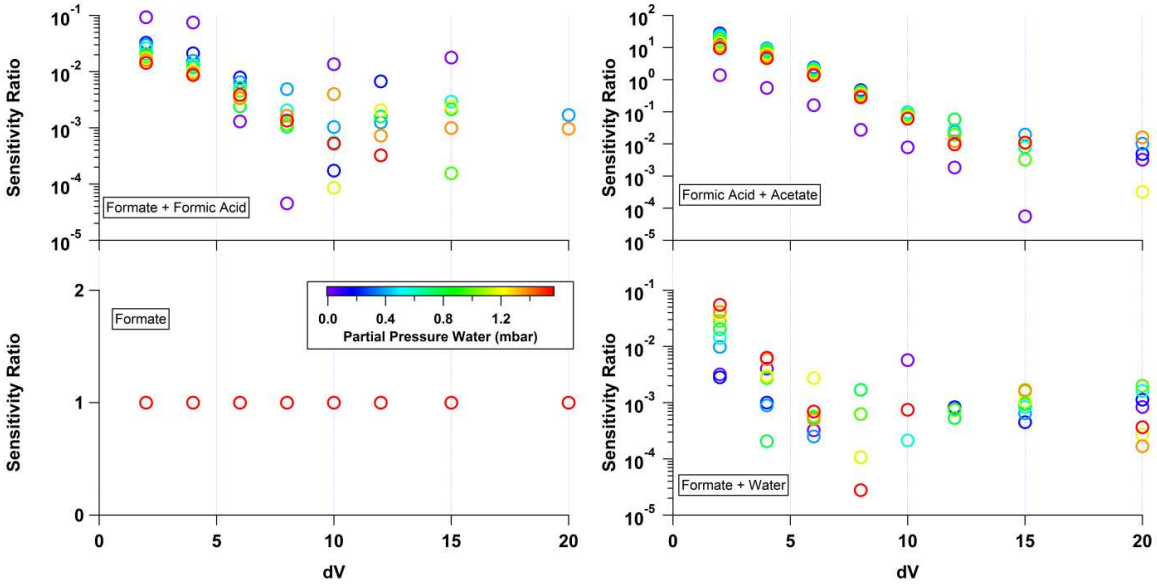

FIGURE SI3.12 SENSITIVITY RATIOS OF FORMIC ACID:

Sensitivity ratios of various formic acid clusters relative to the sensitivity of formic acid under a variety of relative humidity conditions and voltage configurations. The contribution of the formic acid clusters to the observed mass spectrum decreases relative to the contribution at the deprotonated-declustered mass as dV increases.

.

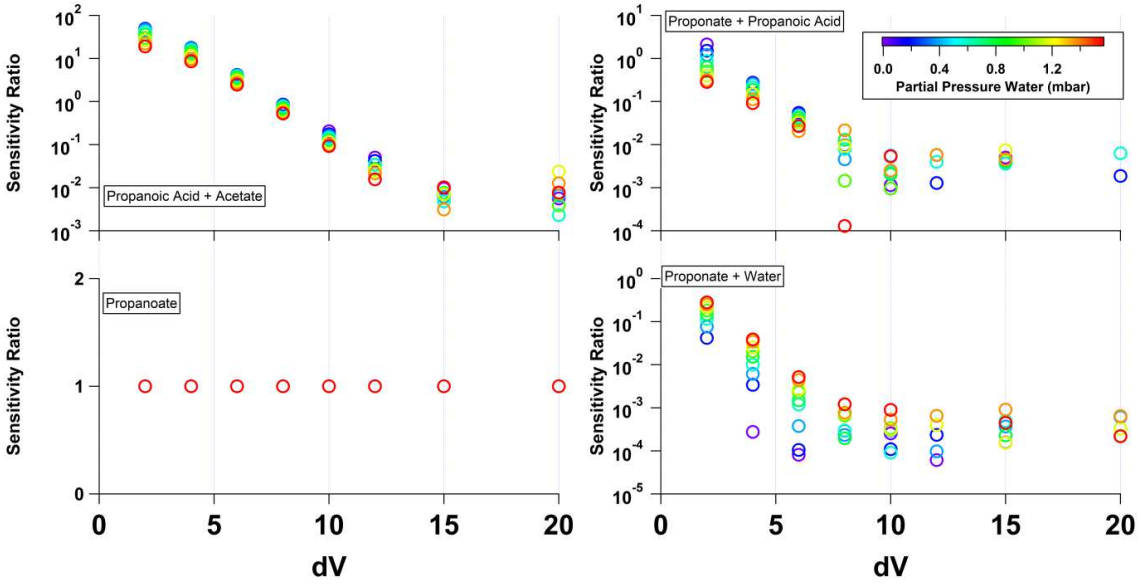

FIGURE SI3.13 SENSITIVITY RATIOS OF PROPANOIC ACID:

Sensitivity ratios of various propanoic acid clusters relative to the sensitivity of propanoic acid under a variety of relative humidity conditions and voltage configurations. The contribution of the propanoic acid clusters to the observed mass spectrum decreases relative to the contribution at the deprotonated-declustered mass as dV increases.

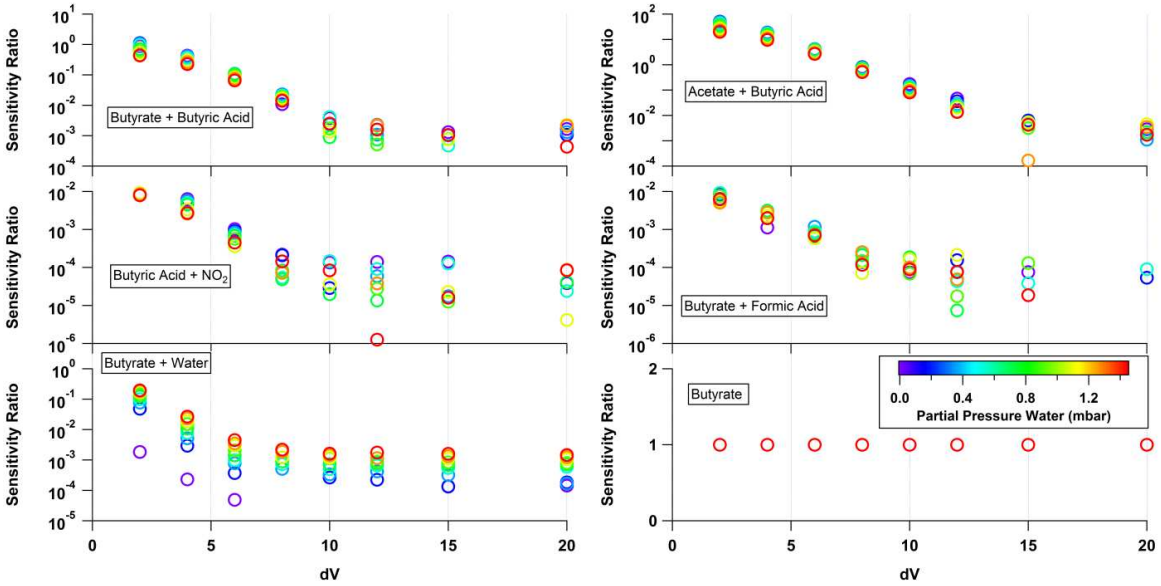

FIGURE SI3.14 SENSITIVITY RATIOS OF VARIOUS BUTYRIC ACID:

Sensitivity ratios of various butyric acid clusters relative to the sensitivity of butyric acid under a variety of relative humidity conditions and voltage configurations. The contribution of the butyric acid clusters to the observed mass spectrum decreases relative to the contribution at the deprotonated-declustered mass as dV increases.

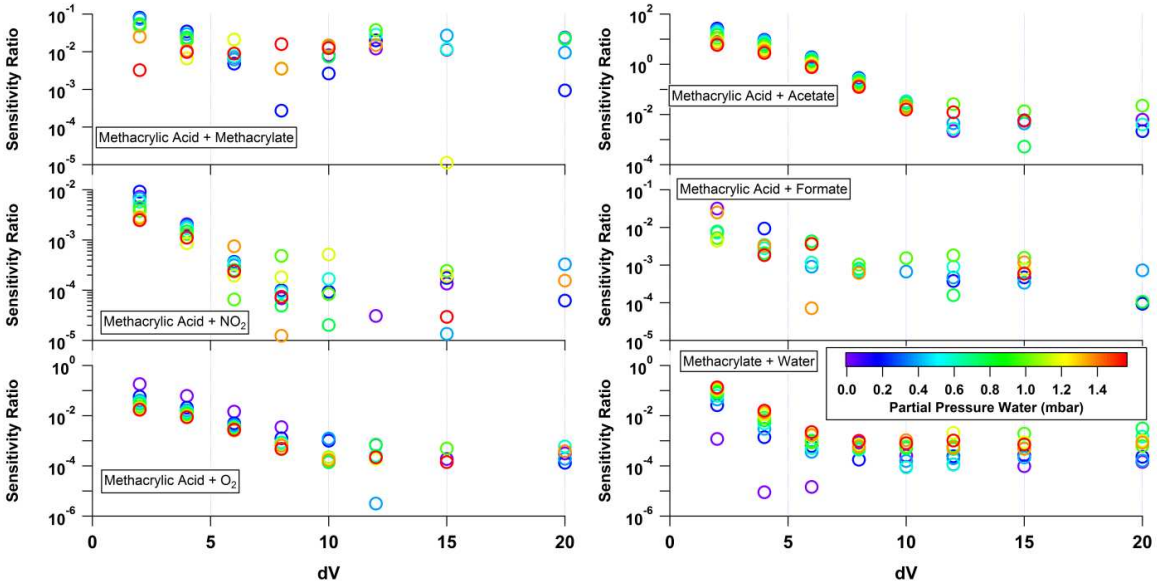

FIGURE SI3.15 SENSITIVITY RATIOS OF METHACRYLIC ACID:

Sensitivity ratios of various methacrylic acid clusters relative to the sensitivity of methacrylic acid under a variety of relative humidity conditions and voltage configurations. The contribution of the methacrylic acid clusters to the observed mass spectrum decreases relative to the contribution at the deprotonated-declustered mass as dV increases. Here, the deprotonated-declustered methacrylate ion is removed (it always equals 1), and the methacrylic acid self-cluster is included.

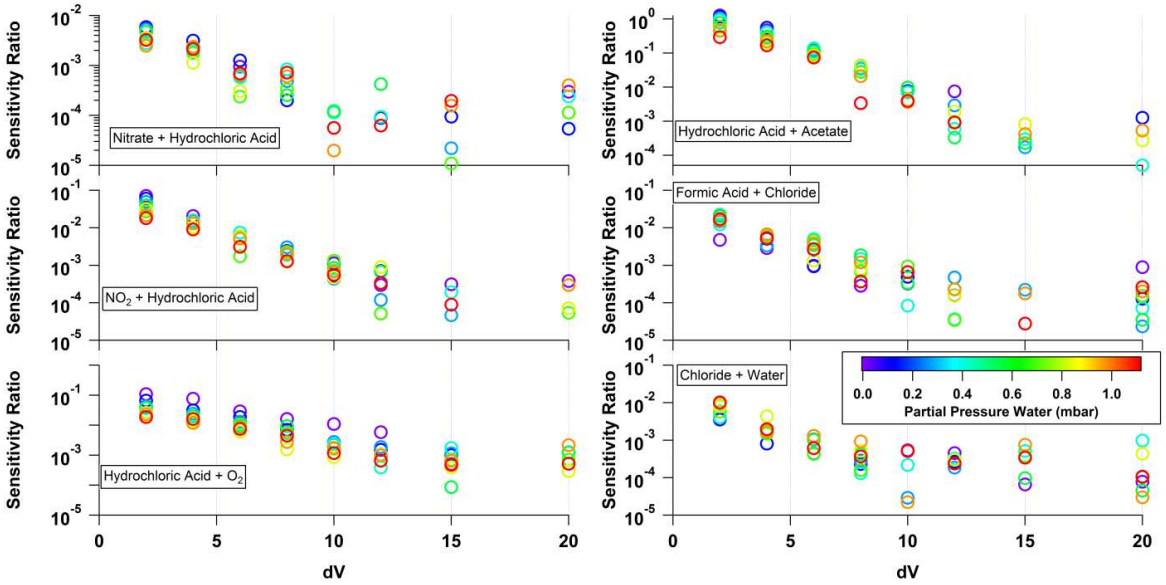

FIGURE SI3.16 SENSITIVITY RATIOS OF HYDROCHLORIC ACID:

Sensitivity ratios of various hydrochloric acid clusters relative to the sensitivity of hydrochloric acid under a variety of relative humidity conditions and voltage configurations. The contribution of the hydrochloric acid clusters to the observed mass spectrum decreases relative to the contribution at the deprotonated-declustered mass as dV increases. Here, the deprotonated-declustered chloride ion is removed (it always equals 1), and the [nitrate+hydrochloric acid] cluster is included.

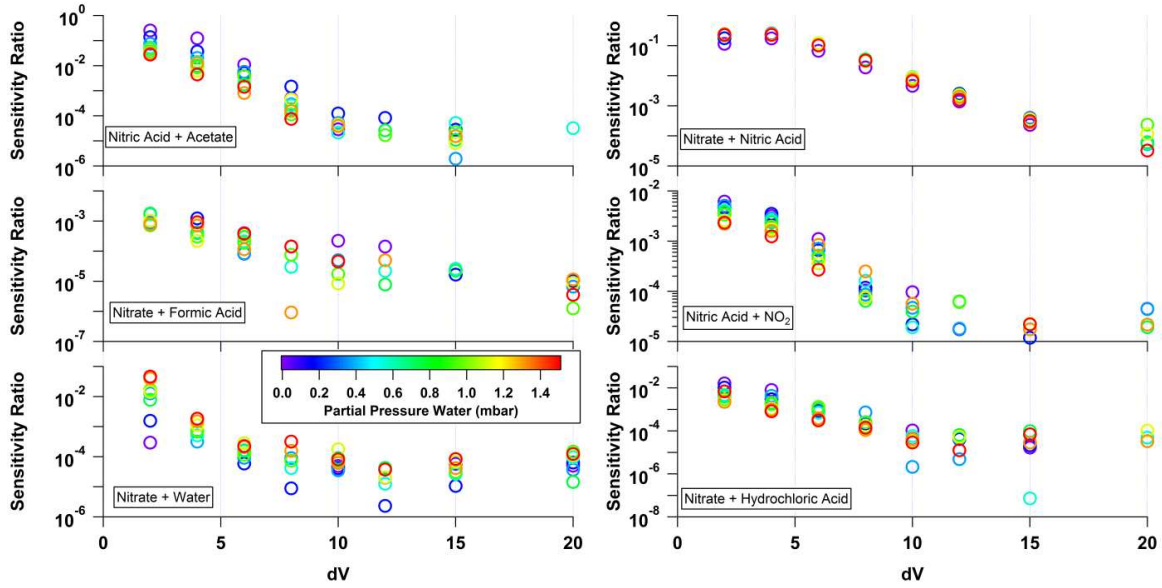

FIGURE SI3.17 SENSITIVITY RATIOS OF NITRIC ACID:

Sensitivity ratios of various nitric acid clusters relative to the sensitivity of nitric acid under a variety of relative humidity conditions and voltage configurations. The contribution of the nitric acid clusters to the observed mass spectrum decreases relative to the contribution at the deprotonated-declustered mass as dV increases. Here, the deprotonated-declustered nitrate ion is removed (it always equals 1), and the [nitrate+formic] acid self-cluster is included.

SI 3.8.5.3 Limit of Detection

LOD: S/N=3

$$\frac{S}{N} = \frac{C_f[x]t}{\sqrt{C_f[x]t+2Bt}} \qquad \text{(SI Eqn. 3.2)}$$

The limit of detection (LOD) is calculated via SI Eqn. 3.2 following the work of Bertram *et al.* (2011) and application by Brophy and Farmer (2015). S/N is the signal-to-noise ratio, C_f is the calibration factor, [x] is the mixing ratio, t is the integration time, and B is the background count rate. This derivation assumes Poisson statistics. These plots show at what concentration clustering is going to contribute to the observed mass spectrum with statistical significance.

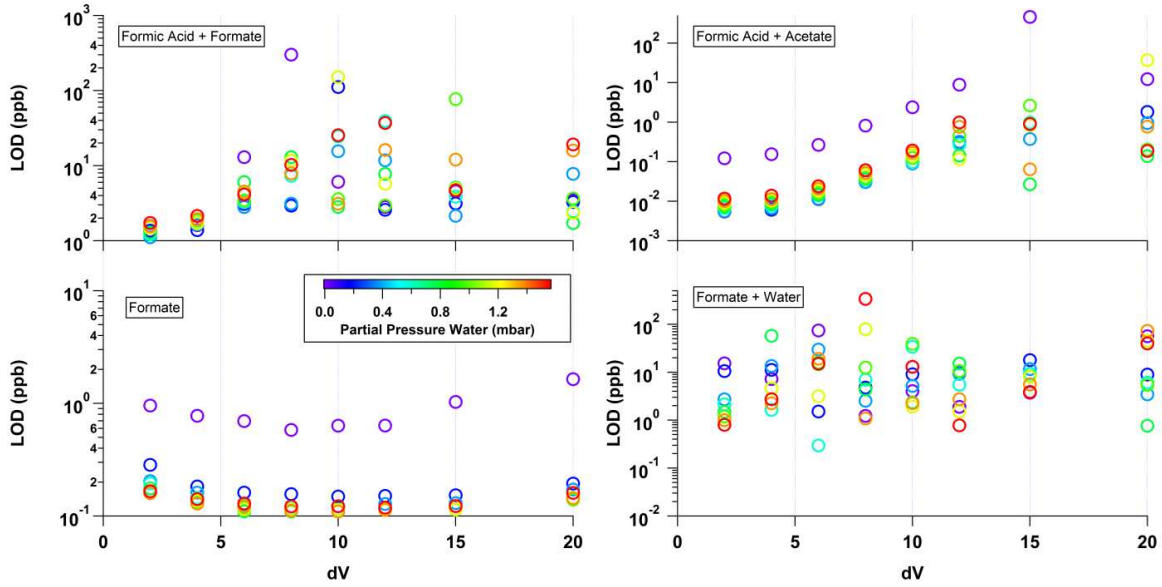

FIGURE SI3.18 LIMIT OF DETECTION OF FORMIC ACID:

The calculated 1 s (S/N=3) limit of detection of formic acid and related clusters is plotted against the voltage difference applied between the skimmer and BSQ front (component relation 5). The points are colored by the calculated partial pressure of water in the IMR corresponding to changing the relative humidity from 0% to 80% under laboratory conditions. The limit of detection is observed to increase or become sporadic at higher dV values for clusters while declustered-deprotonated species remain detectable at low concentrations.

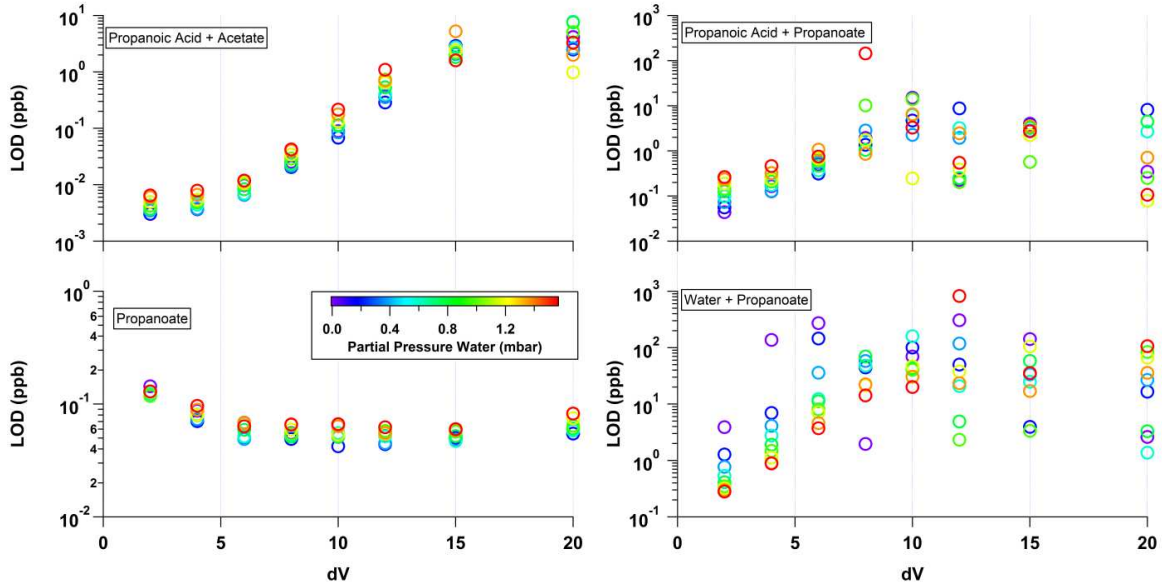

FIGURE SI3.19 LIMIT OF DETECTION OF PROPANOIC ACID:

The calculated 1 s (S/N=3) limit of detection of propanoic acid and related clusters is plotted against the voltage difference applied between the skimmer and BSQ front (component relation 5). The points are colored by the calculated partial pressure of water in the IMR corresponding to changing the relative humidity from 0% to 80% under laboratory conditions. The limit of detection is observed to increase or become sporadic at higher dV values for clusters while declustered-deprotonated species remain detectable at low concentrations.

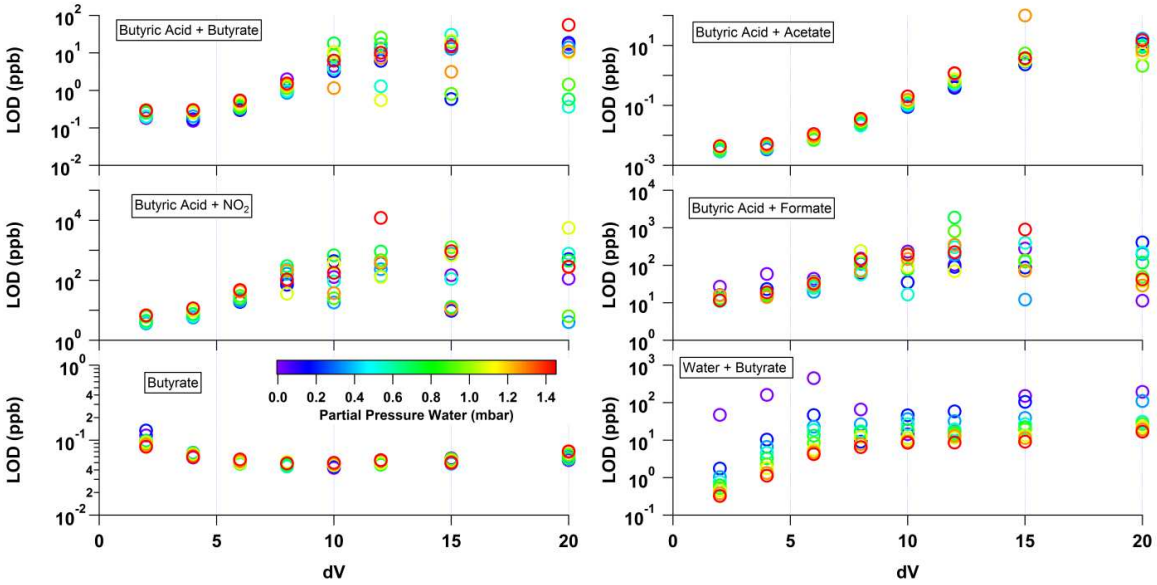

FIGURE SI3.20 LIMIT OF DETECTION OF BUTYRIC ACID:

The calculated 1 s (S/N=3) limit of detection of butyric acid and related clusters is plotted against the voltage difference applied between the skimmer and BSQ front (component relation 5). The points are colored by the calculated partial pressure of water in the IMR corresponding to changing the relative humidity from 0% to 80% under laboratory conditions. The limit of detection is observed to increase or become sporadic at higher dV values for clusters while declustered-deprotonated species remain detectable at low concentrations.

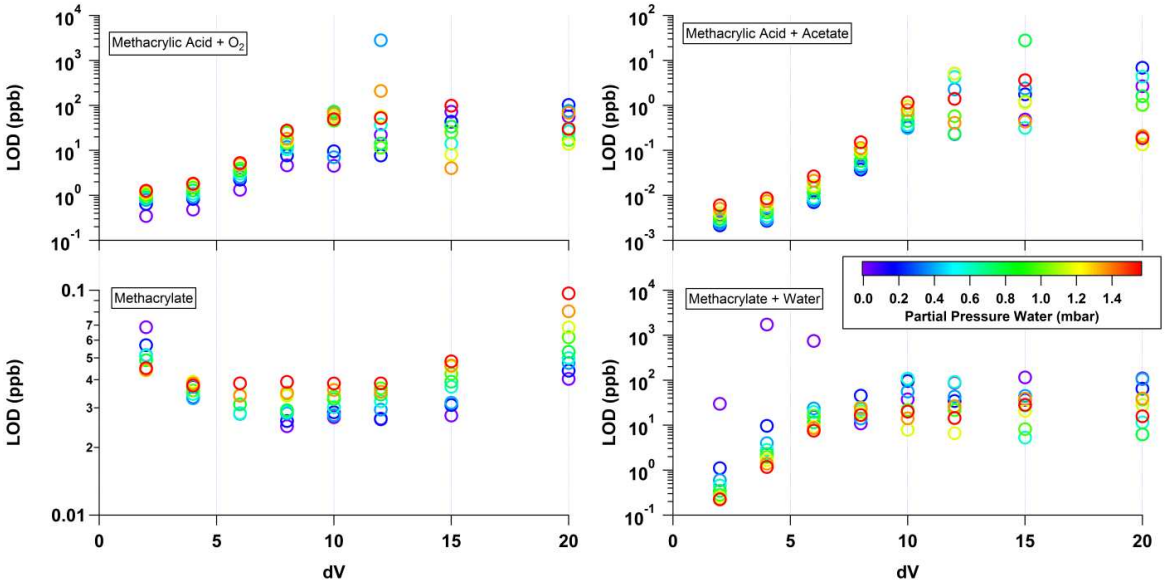

FIGURE SI3.21 LIMIT OF DETECTION OF METHACRYLIC ACID:

The calculated 1 s (S/N=3) limit of detection of methacrylic acid and related clusters is plotted against the voltage difference applied between the skimmer and BSQ front (component relation 5). The points are colored by the calculated partial pressure of water in the IMR corresponding to changing the relative humidity from 0% to 80% under laboratory conditions. The limit of detection is observed to increase or become sporadic at higher dV values for clusters while declustered-deprotonated species remain detectable at low concentrations.

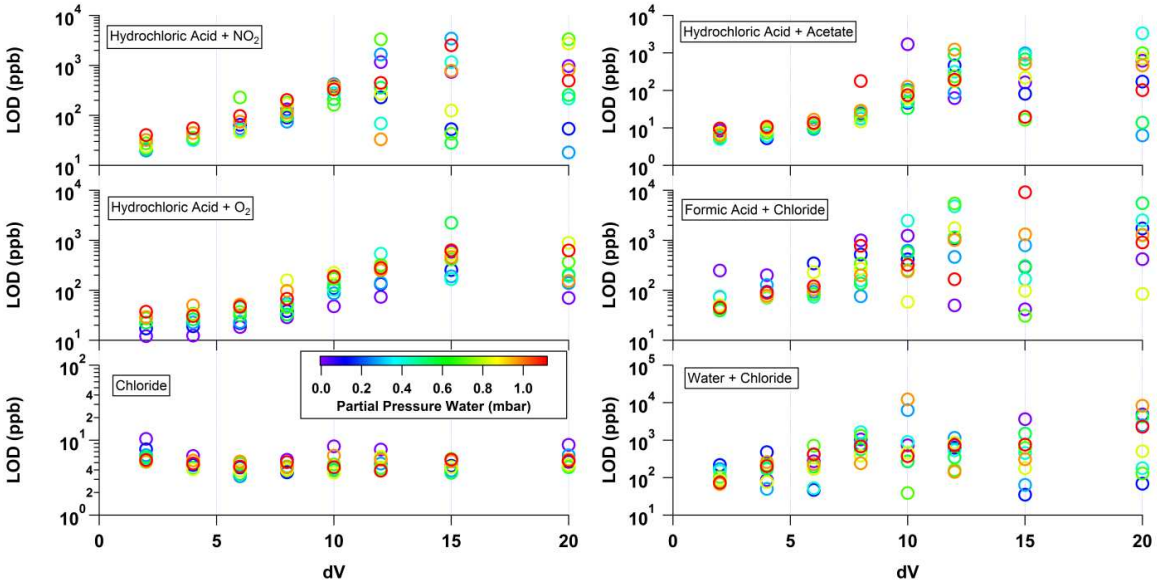

FIGURE SI3.22 LIMIT OF DETECTION OF HYDROCHLORIC ACID:

The calculated 1 s (S/N=3) limit of detection of hydrochloric acid and related clusters is plotted against the voltage difference applied between the skimmer and BSQ front (component relation 5). The points are colored by the calculated partial pressure of water in the IMR corresponding to changing the relative humidity from 0% to 80% under laboratory conditions. The limit of detection is observed to increase or become sporadic at higher dV values for clusters while declustered-deprotonated species remain detectable at low concentrations.

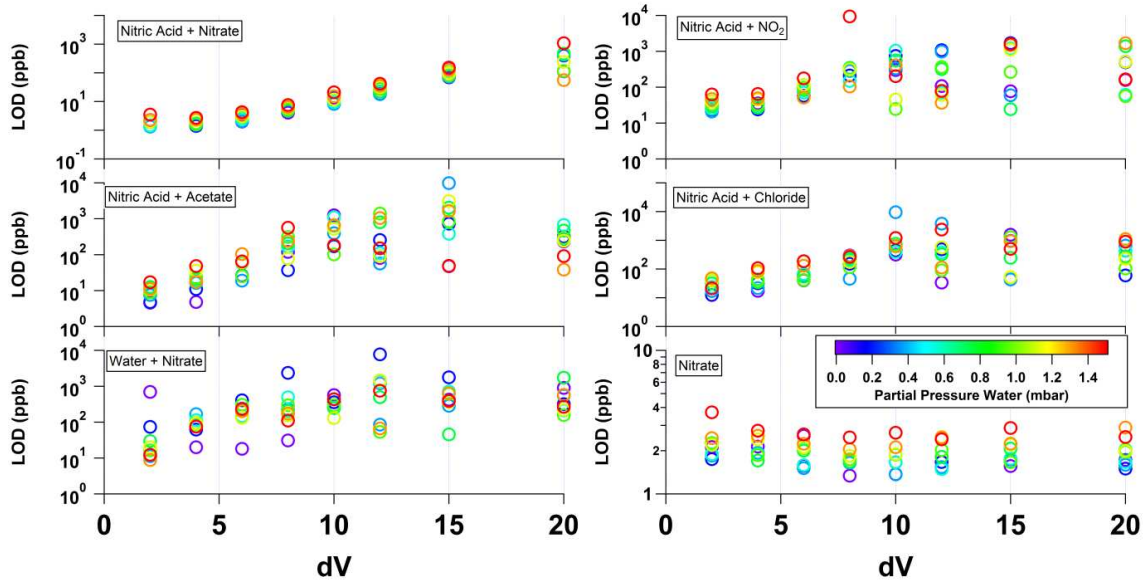

FIGURE SI3.23 LIMIT OF DETECTION OF NITRIC ACID:

The calculated 1 s (S/N=3) limit of detection of nitric acid and related clusters is plotted against the voltage difference applied between the skimmer and BSQ front (component relation 5). The points are colored by the calculated partial pressure of water in the IMR corresponding to changing the relative humidity from 0% to 80% under laboratory conditions. The limit of detection is observed to increase or become sporadic at higher dV values for clusters while declustered-deprotonated species remain detectable at low concentrations.

SI3.8.6: Evaluation of Chhabra Method for Dealing with Cluster Contributions

Chhabra et al. (2015) formulate the expression that the clustered mass intensity ($I_{i+acetate}$) is equal to the sum of the cluster ($I_{i'}$) plus a non-clustered ion with the same exact mass (I_j). Thus:

$$I_{i+acetate} = I_{i'} + I_j \qquad \text{(SI Eqn. 3.3)}$$

Next, the authors assume that the ratio between $I_{i'}$ and I_i is constant and no more than the acetate ratio of 0.2 in their study. Either the $I_{i+acetate}$ to I_i ratio, or 0.2 is used (whichever value is smaller) to determine the contribution of the clustered species to the mass $I_{i+acetate}$.

$$I_{i'} \approx (I_{i+acetate}/I_i) \times I_j \quad \text{OR} \quad I_{i'} \approx 0.2 \times I_j \qquad \text{(SI Eqn. 3.4)}$$

An acetate ratio of 0.2 in our system corresponds to operating component relation 5 at a dV of ~6 V (actual acetate ratio of 0.16). Here, the relative contribution of propionic acid to the [propionic acid + acetate]$^-$ cluster ranges between 2.47 and 4.15 depending on the relative humidity. The relative contribution of formic acid to the [formic acid + acetate]$^-$ cluster ranges between 0.16 to 2.38. The relative contribution of butyric acid to the [butyric acid + acetate]$^-$ cluster ranges between 2.67 and 4.1. The relative contribution of methacrylic acid to the [methacrylic acid + acetate]$^-$ cluster ranges between 0.77 and 1.89. The self-cluster of propionic acid contributes only 0.054 and the water-cluster contributes an order of magnitude less relative to the deprotonated-declustered sensitivity. This is a consistent story for all the alkanoic acids evaluated. Nitric acid provides an interesting example. The [nitric acid + acetate]$^-$ cluster contributes between 0.011 and 0.008 relative to the nitrate signal while the nitric acid self-cluster contributes between 0.12 and 0.06 relative to nitrate. This self-cluster is not addressed by these recommendations.

REFERENCES

Aljawhary, D., Lee, A. K. Y. and Abbatt, J. P. D.: High-resolution chemical ionization mass spectrometry (ToF-CIMS): application to study SOA composition and processing, Atmospheric Measurement Techniques, 6(11), 3211, doi:10.5194/amt-6-3211-2013, 2013.

Bertram, T. H., Kimmel, J. R., Crisp, T. A., Ryder, O. S., Yatavelli, R. L. N., Thornton, J. A., Cubison, M. J., Gonin, M. and Worsnop, D. R.: A field-deployable, chemical ionization time-of-flight mass spectrometer, Atmospheric Measurement Techniques, 4(7), 1471, doi:10.5194/amt-4-1471-2011, 2011.

Brophy, P. and Farmer, D. K.: A switchable reagent ion high resolution time-of-flight chemical ionization mass spectrometer for real-time measurement of gas phase oxidized species: characterization from the 2013 southern oxidant and aerosol study, Atmospheric Measurement Techniques, 8(7), 2945, doi:10.5194/amt-8-2945-2015, 2015.

Budisulistiorini, S. H., Li, X., Bairai, S. T., Renfro, J., Liu, Y., Liu, Y. J., McKinney, K. A., Martin, S. T., McNeill, V. F., Pye, H. O. T., Nenes, A., Neff, M. E., Stone, E. A., Mueller, S., Knote, C., Shaw, S. L., Zhang, Z., Gold, A. and Surratt, J. D.: Examining the effects of anthropogenic emissions on isoprene-derived secondary organic aerosol formation during the 2013 Southern Oxidant and Aerosol Study (SOAS) at the Look Rock, Tennessee ground site, Atmospheric Chemistry and Physics, 15(15), 8871, doi:10.5194/acp-15-8871-2015, 2015.

Chhabra, P. S., Lambe, A. T., Canagaratna, M. R., Stark, H., Jayne, J. T., Onasch, T. B., Davidovits, P., Kimmel, J. R. and Worsnop, D. R.: Application of high-resolution time-of-flight chemical ionization mass spectrometry measurements to estimate volatility distributions of α-pinene and naphthalene oxidation products, Atmospheric Measurement Techniques, 8(1), 1, doi:10.5194/amt-8-1-2015, 2015.

Cubison, M. J. and Jimenez, J. L.: Statistical precision of the intensities retrieved from constrained fitting of overlapping peaks in high-resolution mass spectra, Atmospheric Measurement Techniques, 8(6), 2333, doi:10.5194/amt-8-2333-2015, 2015.

DeCarlo, P. F., Kimmel, J. R., Trimborn, A., Northway, M. J., Jayne, J. T., Aiken, A. C., Gonin, M., Fuhrer, K., Horvath, T., Docherty, K. S., Worsnop, D. R. and Jimenez, J. L.: Field-deployable, high-resolution, time-of-flight aerosol mass spectrometer, Anal Chem, 78(24), 8281–8289, doi:10.1021/ac061249n, 2006.

Ehn, M., Junninen, H., Petäjä, T., Kurtén, T., Kerminen, V. M., Schobesberger, S., Manninen, H. E., Ortega, I. K., Vehkamäki, H., Kulmala, M. and Worsnop, D. R.: Composition and temporal behavior of ambient ions in the boreal forest, Atmospheric Chemistry and Physics, 10(17), 8513, doi:10.5194/acp-10-8513-2010, 2010.

Ehn, M., Junninen, H., Schobesberger, S., Manninen, H. E., Franchin, A., Sipilä, M., Petäjä, T., Kerminen, V.-M., Tammet, H., Mirme, A., Mirme, S., Hõrrak, U., Kulmala, M. and Worsnop, D. R.: An Instrumental Comparison of Mobility and Mass Measurements of Atmospheric Small Ions, Aerosol Science and Technology, 45(4), 522, doi:10.1080/02786826.2010.547890, 2011.

Ehn, M., Thornton, J. A., Kleist, E., Sipilä, M., Junninen, H., Pullinen, I., Springer, M., Rubach, F., Tillmann, R., Lee, B., Lopez-Hilfiker, F., Andres, S., Acir, I.-H., Rissanen, M., Jokinen, T., Schobesberger, S., Kangasluoma, J., Kontkanen, J., Nieminen, T., Kurtén, T., Nielsen, L. B., Jørgensen, S., Kjaergaard, H. G., Canagaratna, M., Maso, M. D., Berndt, T., Petäjä, T., Wahner, A., Kerminen, V.-M., Kulmala, M., Worsnop, D. R., Wildt, J. and Mentel, T. F.: A large source of low-volatility secondary organic aerosol, Nature, 506(7489), 476–479, doi:10.1038/nature13032, 2014.

Eisele, F. L.: Identification of tropospheric ions, Journal of Geophysical Research: Atmospheres, 91(D7), 7897, doi:10.1029/jd091id07p07897, 1986.

Faust, J. A., Junninen, H., Ehn, M., Chen, X., Ruusuvuori, K., Kieloaho, A.-J., Bäck, J., Ojala, A., Jokinen, T., Worsnop, D. R., Kulmala, M. and Petäjä, T.: Real-Time Detection of Arsenic Cations from Ambient Air in Boreal Forest and Lake Environments, Environmental Science & Technology Letters, 3(2), 42, doi:10.1021/acs.estlett.5b00308, 2016.

Friedman, B., Brophy, P., Brune, W. H. and Farmer, D. K.: Anthropogenic Sulfur Perturbations on Biogenic Oxidation: SO2 Additions Impact Gas-Phase OH Oxidation Products of α- and β-Pinene, Environmental Science & Technology, 50(3), 1269–1279, doi:10.1021/acs.est.5b05010, 2016.

Heinritzi, M., Simon, M., Steiner, G., Wagner, A. C., Kürten, A., Hansel, A. and Curtius, J.: Characterization of the mass-dependent transmission efficiency of a CIMS, Atmospheric Measurement Techniques, 9(4), 1449, doi:10.5194/amt-9-1449-2016, 2016.

Huey, L. G.: Measurement of trace atmospheric species by chemical ionization mass spectrometry: speciation of reactive nitrogen and future directions, Mass Spectrom Rev, 26(2), 166–184, doi:10.1002/mas.20118, 2007.

Iyer, S., Lopez-Hilfiker, F., Lee, B. H., Thornton, J. A. and Kurtén, T.: Modeling the Detection of Organic and Inorganic Compounds Using Iodide-Based Chemical Ionization, J Phys Chem A, 120(4), 576–587, doi:10.1021/acs.jpca.5b09837, 2016.

Jokinen, T., Sipilä, M., Junninen, H., Ehn, M., Lönn, G., Hakala, J., Petäjä, T., Mauldin, R. L., Kulmala, M. and Worsnop, D. R.: Atmospheric sulphuric acid and neutral cluster measurements using CI-APi-TOF, Atmospheric Chemistry and Physics, 12(9), 4117, doi:10.5194/acp-12-4117-2012, 2012.

Junninen, H., Ehn, M., Petäjä, T., Luosujärvi, L., Kotiaho, T., Kostiainen, R., Rohner, U., Gonin, M., Fuhrer, K., Kulmala, M. and Worsnop, D. R.: A high-resolution mass spectrometer to measure atmospheric ion composition, Atmospheric Measurement Techniques, 3(4), 1039, doi:10.5194/amt-3-1039-2010, 2010.

Kim, S., Karl, T., Helmig, D., Daly, R., Rasmussen, R. and Guenther, A.: Measurement of atmospheric sesquiterpenes by proton transfer reaction-mass spectrometry (PTR-MS), Atmospheric Measurement Techniques, 2(1), 99, doi:10.5194/amt-2-99-2009, 2009.

Krechmer, J. E., Coggon, M. M., Massoli, P., Nguyen, T. B., Crounse, J. D., Hu, W., Day, D. A., Tyndall, G. S., Henze, D. K., Rivera-Rios, J. C., Nowak, J. B., Kimmel, J. R., Mauldin, R. L., Stark, H., Jayne, J. T., Sipilä, M., Junninen, H., Clair, J. M. S., Zhang, X., Feiner, P. A., Zhang, L., Miller, D. O., Brune, W. H., Keutsch, F. N., Wennberg, P. O., Seinfeld, J. H., Worsnop, D. R., Jimenez, J. L. and Canagaratna, M. R.: Formation of Low Volatility Organic Compounds and Secondary Organic Aerosol from Isoprene Hydroxyhydroperoxide Low-NO Oxidation, Environmental Science & Technology, 49(17), 10330–10339, doi:10.1021/acs.est.5b02031, 2015.

Lee, B. H., Lopez-Hilfiker, F. D., Mohr, C., Kurtén, T., Worsnop, D. R. and Thornton, J. A.: An iodide-adduct high-resolution time-of-flight chemical-ionization mass spectrometer: application to atmospheric inorganic and organic compounds, Environmental Science & Technology, 48(11), 6309–6317, doi:10.1021/es500362a, 2014.

Lopez-Hilfiker, F. D., Iyer, S., Mohr, C., Lee, B. H., DaposAmbro, E. L., Kurtén, T. and Thornton, J. A.: Constraining the sensitivity of iodide adduct chemical ionization mass spectrometry to multifunctional organic molecules using the collision limit and thermodynamic stability of iodide ion adducts, Atmospheric Measurement Techniques, 9(4), 1505, doi:10.5194/amt-9-1505-2016, 2016.

Lopez-Hilfiker, F. D., Mohr, C., Ehn, M., Rubach, F., Kleist, E., Wildt, J., Mentel, T. F., Carrasquillo, A. J., Daumit, K. E., Hunter, J. F., Kroll, J. H., Worsnop, D. R. and Thornton, J. A.: Phase partitioning and volatility of secondary organic aerosol components formed from α-pinene ozonolysis and OH oxidation: the importance of accretion products and other low volatility compounds, Atmospheric Chemistry and Physics, 15(14), 7765, doi:10.5194/acp-15-7765-2015, 2015.

Lopez-Hilfiker, F. D., Mohr, C., Ehn, M., Rubach, F., Kleist, E., Wildt, J., Mentel, T. F., Lutz, A., Hallquist, M., Worsnop, D. and Thornton, J. A.: A novel method for online analysis of gas and particle composition: description and evaluation of a Filter Inlet for Gases and AEROsols (FIGAERO), Atmospheric Measurement Techniques, 7(4), 983, doi:10.5194/amt-7-983-2014, 2014.

Mohr, C., Lopez-Hilfiker, F. D., Zotter, P., Prévôt, A. S. H., Xu, L., Ng, N. L., Herndon, S. C., Williams, L. R., Franklin, J. P., Zahniser, M. S., Worsnop, D. R., Knighton, W. B., Aiken, A. C., Gorkowski, K. J., Dubey, M. K., Allan, J. D. and Thornton, J. A.: Contribution of nitrated phenols to wood burning brown carbon light absorption in Detling, United Kingdom during winter time, Environmental Science & Technology, 47(12), 6316–6324, doi:10.1021/es400683v, 2013.

Olenius, T., Schobesberger, S., Kupiainen-Määttä, O., Franchin, A., Junninen, H., Ortega, I. K., Kurtén, T., Loukonen, V., Worsnop, D. R., Kulmala, M. and Vehkamäki, H.: Comparing simulated and experimental molecular cluster distributions, Faraday Discussions, 165, 75, doi:10.1039/c3fd00031a, 2013.

Rivera-Rios, J. C., Nguyen, T. B., Crounse, J. D., Jud, W., Saint Clair, J. M., Mikoviny, T., Gilman, J. B., Lerner, B. M., Kaiser, J. B., de Gouw, J., Wisthaler, A., Hansel, A., Wennberg, P. O., Seinfeld, J. H. and Keutsch, F. N.: Conversion of hydroperoxides to carbonyls in field and laboratory instrumentation: Observational bias in diagnosing pristine versus anthropogenically controlled atmospheric chemistry, Geophysical research letters, 41(23), 8645, doi:10.1002/2014gl061919, 2014.

Schobesberger, S., Franchin, A., Bianchi, F., Rondo, L., Duplissy, J., Kürten, A., Ortega, I. K., Metzger, A., Schnitzhofer, R., Almeida, J., Amorim, A., Dommen, J., Dunne, E. M., Ehn, M., Gagné, S., Ickes, L., Junninen, H., Hansel, A., Kerminen, V. M., Kirkby, J., Kupc, A., Laaksonen, A., Lehtipalo, K., Mathot, S., Onnela, A., Petäjä, T., Riccobono, F., Santos, F. D., Sipilä, M., Tomé, A., Tsagkogeorgas, G., Viisanen, Y., Wagner, P. E., Wimmer, D., Curtius, J., Donahue, N. M., Baltensperger, U., Kulmala, M. and Worsnop, D. R.: On the composition of ammonia–sulfuric-acid ion clusters during aerosol particle formation, Atmospheric Chemistry and Physics, 15(1), 55, doi:10.5194/acp-15-55-2015, 2015.

Sipilä, M., Sarnela, N., Jokinen, T., Junninen, H., Hakala, J., Rissanen, M. P., Praplan, A., Simon, M., Kürten, A., Bianchi, F., Dommen, J., Curtius, J., Petäjä, T. and Worsnop, D. R.: Bisulfate – cluster based atmospheric pressure chemical ionization mass spectrometer for high-sensitivity (, Atmospheric Measurement Techniques, 8(10), 4001, doi:10.5194/amt-8-4001-2015, 2015.

Stark, H., Yatavelli, R. L. N., Thompson, S. L., Kimmel, J. R., Cubison, M. J., Chhabra, P. S., Canagaratna, M. R., Jayne, J. T., Worsnop, D. R. and Jimenez, J. L.: Methods to extract molecular and bulk chemical information from series of complex mass spectra with limited mass resolution, International Journal of Mass Spectrometry, 389, 26, doi:10.1016/j.ijms.2015.08.011, 2015.

Veres, P., Roberts, J. M., Warneke, C., Welsh-Bon, D., Zahniser, M., Herndon, S., Fall, R. and de Gouw, J.: Development of negative-ion proton-transfer chemical-ionization mass

spectrometry (NI-PT-CIMS) for the measurement of gas-phase organic acids in the atmosphere, International Journal of Mass Spectrometry, 274(1-3), 48, doi:10.1016/j.ijms.2008.04.032, 2008.

Viidanoja, J., Reiner, T. and Arnold, F.: Laboratory investigations of negative ion molecule reactions of formic and acetic acids: implications for atmospheric measurements by ion-molecule reaction …, International Journal of Mass Spectrometry, 1998.

Warneke, C., Veres, P., Murphy, S. M., Soltis, J., Field, R. A., Graus, M. G., Koss, A., Li, S. M., Li, R., Yuan, B., Roberts, J. M. and de Gouw, J. A.: PTR-QMS versus PTR-TOF comparison in a region with oil and natural gas extraction industry in the Uintah Basin in 2013, Atmospheric Measurement Techniques, 8(1), 411, doi:10.5194/amt-8-411-2015, 2015.

Wentzell, J. J. B., Liggio, J., Li, S.-M., Vlasenko, A., Staebler, R., Lu, G., Poitras, M.-J., Chan, T. and Brook, J. R.: Measurements of gas phase acids in diesel exhaust: a relevant source of HNCO? Environmental Science & Technology, 47(14), 7663–7671, doi:10.1021/es401127j, 2013.

Yatavelli, R. L. N., Lopez-Hilfiker, F., Wargo, J. D., Kimmel, J. R., Cubison, M. J., Bertram, T. H., Jimenez, J. L., Gonin, M., Worsnop, D. R. and Thornton, J. A.: A Chemical Ionization High-Resolution Time-of-Flight Mass Spectrometer Coupled to a Micro Orifice Volatilization Impactor (MOVI-HRToF-CIMS) for Analysis of Gas and Particle-Phase Organic Species, Aerosol Science and Technology, 46(12), 1313, doi:10.1080/02786826.2012.712236, 2012.

Yatavelli, R. L. N., Stark, H., Thompson, S. L., Kimmel, J. R., Cubison, M. J., Day, D. A., Campuzano-Jost, P., Palm, B. B., Hodzic, A., Thornton, J. A., Jayne, J. T., Worsnop, D. R. and Jimenez, J. L.: Semicontinuous measurements of gas–particle partitioning of organic acids in a ponderosa pine forest using a MOVI-HRToF-CIMS, Atmospheric Chemistry and Physics, 14(3), 1527, doi:10.5194/acp-14-1527-2014, 2014.

Zhao, R., Mungall, E. L., Lee, A. K. Y., Aljawhary, D. and Abbatt, J. P. D.: Aqueous-phase photooxidation of levoglucosan – a mechanistic study using aerosol time-of-flight chemical ionization mass spectrometry (Aerosol ToF-CIMS), Atmospheric Chemistry and Physics, 14(18), 9695, doi:10.5194/acp-14-9695-2014, 2014.

CHAPTER 4

HEADSPACE ANALYSIS OF AQUEOUS LIQUID SAMPLES USING ACETATE IONIZATION WITH A HIGH-RESOLUTION TIME-OF-FLIGHT CHEMICAL IONIZATION MASS SPECTROMETER

4.1 Introduction

Proton transfer reaction mass spectrometry (PTR-MS) is best known as an atmospheric sampling technique that first used quadrupole mass spectrometers for detecting volatile organic compounds (VOCs) in ambient air (Lindinger and Jordan, 1998; Lindinger et al., 1998). Subsequent developments have led to the implementation of PTR drift tubes and ion sources on time-of-flight mass spectrometers (TOF-MS) (Jordan et al., 2009). These PTR-TOF-MS systems have seen continued improvements in sensitivity, limits of detection (LOD), and mass resolution in recent years (Sulzer et al., 2014). PTR-MS and PTR-TOF-MS ionize ambient VOCs through ion-neutral reactions with the hydronium ion (H_3O^+) where VOCs with proton affinities greater than water gain a proton (R4.1). Other reagent ions have, however, been used with the PTR-MS and PTR-TOF-MS systems. The NO^+ and O_2^+ reagent ions were reported early in the PTR-TOF-MS development (Jordan et al., 2009), and later, the Kr^+ ion was also reported for ionizing molecules with proton affinities lower than water via direct charge transfer (R4.2) (Sulzer et al., 2012). These additional reagent ions have seen only limited application.

$$R + H_3O^+ \rightarrow RH^+ + H_2O \quad \text{(R4.1)}$$

$$R + Kr^+ \rightarrow R^+ + Kr \quad \text{(R4.2)}$$

PTR-TOF-MS has simultaneously been successfully developed as a headspace analyzer for food and drink samples with high-resolution (HR) analysis being a particularly powerful tool (Ibáñez et al., 2015). Headspace analysis refers to the analysis of the gas-phase above a liquid sample in a sealed container. The headspace can either be analyzed using static methods where the gas-liquid partitioning is allowed to reach equilibrium such that the gas-phase reaches its equilibrium vapor pressure with the liquid phase. Alternative, dynamic methods continuously remove the gas-phase headspace causing the gas-phase to never reach true equilibrium. Both methods typically require pre-concentration, which is normally not conducted with PTR-MS methodologies allowing for direct, online analysis. The application of mass spectrometers designed for atmospheric measurements to headspace analysis is obvious because the headspace analytes are in the gas phase. Additionally, the various molecules that make up headspace samples are the molecules that participate in creating the perception of the aroma and the taste of a food or drink. The general concept of an "electronic nose" (or more specific to mass spectrometry: "new-generation electronic noses") for detecting food spoilage, origin, species, or impurities has been discussed in the literature, and these online, direct mass spectrometry techniques are generally well suited for this concept (Peris and Escuder-Gilabert, 2009). HR mass spectrometry techniques are particularly useful for these applications where sample complexity and vast numbers of molecules exist in the headspace. These HR headspace techniques are typically coupled with statistical modeling and clustering methods to deal with the complex nature of these data sets (Ibáñez et al., 2015).

Numerous differences between ambient atmospheric sampling and headspace analysis exist. High concentrations of individual species (or high concentrations of many molecules) may be present, and matrix effects can ruin a chemical ionization mass spectrometry (CIMS)

experiment by depleting the reagent ion due to high concentrations of species that react with the reagent. Additionally, the gas sample volume is rarely limited in atmospheric studies but often limited in headspace analysis. Solid foods are typically simpler to analyze with off the shelf PTR-MS systems because of lower gas phase headspace concentrations and limited matrix effects. For example, PTR-TOF-MS has been applied to the study of apple genetics as they relate to volatiles (Cappellin et al., 2015), apple ripening (Soukoulis et al., 2012), chili peppers (Taiti et al., 2014), volatile compounds in olive fruits (Masi et al., 2015a), and the influence of milk storage conditions on Trentingrana cheese (Fabris et al., 2010). Additionally, other techniques have been applied in conjunction with PTR-TOF-MS in a combined approach for the analysis of saffron (Masi et al., 2015b). PTR-TOF-MS was compared to solid-phase micro-extraction followed by GC-MS analysis for studying the effects of storing dried porcini mushrooms (Aprea et al., 2015). The analysis of solid foods described above use PTR-MS with little to no modification.

Liquids, particularly alcoholic beverages with high ethanol concentrations, pose difficult problems for PTR-MS because ethanol can deplete the H_3O^+ primary reagent. This problem was exploited by diluting the headspace of wine samples with a saturated ethanol-N_2 mixture, such that protonated ethanol was observed as the primary reagent ion (Boscaini et al., 2004). This dilution approach created numerous ethanol clusters $[(CH_3CH_2OH)_n + CH_3CH_2OH_2]^+$ and led to difficulties interpreting the mass spectrum (Boscaini et al., 2004). Dilution of the headspace 40x with N_2 was also investigated with PTR-MS using principal component analysis (PCA) (Spitaler et al., 2007). Here, the authors observe a simplified spectra with the anticipated H_3O^+ primary reagent ion chemistry and minimal clustering, but it is possible that the large dilution factor leads to certain compounds being below the instrument's LOD (Spitaler et al., 2007). Subsequent

investigations suggested operating the drift tube under higher electric field strengths to break apart ethanol clusters (E/N) (Fiches et al., 2013), and the method was applied to brandy samples (Fiches et al., 2014). High E/N (electric field strength, E, normalized to the number density, N) drift tube operating conditions will lead to increased fragmentation that can increase the complexity of an observed spectrum as protonated ions coexist with lower molecular weight fragments. Potentially valuable information can also be lost via fragmentation with the destruction of large molecules. Gas chromatography coupled to PTR-MS has been used for wine analysis using the fastGC-PTR-TOF-MS to overcome the limitations posed by the aforementioned direct PTR-MS techniques (Romano et al., 2014). Very recent methodologies have been proposed using argon as a diluting gas to minimize fragmentation while simultaneously optimizing E/N conditions (Campbell-Sills et al., 2016). The difficulties in analyzing alcohol containing beverages have led to substantial methods development that was not necessary for the headspace analysis of solid foods.

These alcoholic beverage methodology studies aim to overcome the obvious problem: ethanol reacts with H_3O^+ and creates numerous ethanol containing clusters that disrupt the anticipated ion chemistry; this is a classic chemical ionization (CI) MS problem. The typical goal of CIMS is to ionize only select components of a complex mixture in order to simplify the number of molecules detected in the mass spectrometer. For CIMS, the H_3O^+ reagent ion is a poor choice in headspace analysis for liquids with high alcohol concentrations and has, thus, required extensive method development. While H_3O^+ is sensitive to numerous VOCs, many of which are of interest for headspace analysis in the food and beverage industry, ethanol not only interferes with the desired ionization pathways, but also results in overlapping HR peaks challenging interpretation and analysis of HR mass spectra.

Numerous other CIMS reagent ions exist and have been reviewed (Huey, 2007). Acetate is an emerging reagent ion for CIMS and was developed using quadrupole based instruments (Veres et al., 2008). The emergence of TOF-MS with an atmospheric pressure interface for atmospheric sampling has made extensive use of the acetate reagent ion (Bertram et al., 2011; Brophy and Farmer, 2015; Budisulistiorini et al., 2015; Mohr et al., 2013; Wentzell et al., 2013; Yatavelli et al., 2012; 2014). The details of acetate CIMS are complex but TOF-MS has helped to elucidate the underlying chemistry (Bertram et al., 2011; Brophy and Farmer, 2015). The most commonly used API-TOF (Aerodyne Resaerch, Inc. and Tofwerk AG) is extensively discussed in the literature (Junninen et al., 2010; Lee et al., 2014; Yatavelli et al., 2012). Briefly, acetate CIMS deprotonates carboxylic acids which are detected as deprotonated-declustered ions if sufficient collisional dissociation is performed (see Chapter 3). The reaction proceeds via proton abstraction R4.3, clustering R4.4, and collision induced dissociation R4.5 (see Chapter 3 for details).

Proton Abstraction:

$$CH_3C(O)O^- + R\text{-}C(O)OH \rightarrow CH_3C(O)O + R\text{-}C(O)O^- \quad (R4.3)$$

Clustering:

$$CH_3C(O)O^- + R\text{-}C(O)OH \rightarrow [CH_3C(O)OH + R\text{-}C(O)O]^- \quad (R4.4)$$

Collision induced dissociation (CID):

$$[CH_3C(O)O + R\text{-}C(O)O]^- + E_{CID} \rightarrow CH_3C(O)OH + R\text{-}C(O)O^- \quad (R4.5)$$

All the PTR-TOF-MS studies cited above use statistical modeling techniques to classify, group, or differentiate samples based on HR mass spectral data. Thus, the exact compounds one observes are not necessarily that important as long as they exist in distinct quantities or distributions such that statistical models (cluster or factor methods, for example) can distinguish

statistically significant differences. As such, the oxygenated carboxylic acids represent an entire class of compounds that PTR-MS fails to capture as well as other negative ion mode CIMS methods (such as acetate CIMS) (Aljawhary et al., 2013). We present the first report of headspace analysis with a high-resolution time-of-flight chemical ionization mass spectrometer (HR-TOF-CIMS) operated with acetate reagent ions. Four beer samples from New Belgium Brewing are analyzed for carboxylic acids in the headspace using a simple experimental setup that integrates directly into preexisting HR-TOF-CIMS configurations for atmospheric sampling.

4.2 Methods

A HR-TOF-CIMS (Tofwerk AG, Aerodyne Research, Inc.) operating with acetate reagent ion chemistry is configured for dynamically analyzing the headspace of aqueous solutions without pre-concentration or pre-separation. The HR-TOF-CIMS is normally configured for atmospheric sampling and operates at high flow rates (~2 SLPM) for the detection of ultra-trace species (routinely < 1 ppbv) (Brophy and Farmer, 2015; Lee et al., 2014). As such, two possibilities exist for modifying this instrument for headspace analysis where concentrations are expected to be much higher and where available gas volumes are much smaller (< 100 mL). (1) The orifice size of the ion molecule reactor (IMR) can be reduced to decrease the sample flowrate into the CI region of the mass spectrometer. This is complicated by downstream fluid dynamics and preexisting CI source design. Mass flow through the instrument needs to be maintained in order to maintain sufficient sensitivity, and this is accomplished by replacing the second orifice between the IMR and the first quadrupole region. Additionally, the CI reagent flow into the IMR is normally configured for ambient sampling at ~2 SLPM. This is another consideration that needs to be addressed if the sample flow is reduced. (2) Dilution methods can be employed for high concentration samples where gas volumes are limited (Spitaler et al.,

2007). This second approach does not require precise machining of metal orifices, connects directly onto the front end of a preexisting instrument at the ambient sampling flow rate, and has the added benefit of being able to rapidly change the extent to which the sample is diluted. The headspace concentrations of various analytes detected by acetate CIMS are expected to vary extensively depending on the sample type making this feature highly desirable despite its complexity. We choose the dilution method for these reasons.

4.2.1 Headspace Setup for the HR-TOF-CIMS

A sealed, clean glass vial (~250 mL) with a septum cap holds the sample solution (~50 mL). A low flow (~50 sccm) of either ultra-high purity (UHP) N_2 or ultra zero air is delivered through the septum using 1/8'' instrument grade stainless steel lines connected to a 1/16'' stainless steel needle (Restek, Inc.) and an analogue mass flow controller (MKS Instruments, Inc.). A separate 1/16'' PEEK line (Vici Metronics, Inc.) is directly inserted through the septum without a needle to prevent surface reactions and sample coating on stainless steel surfaces. The 1/16'' PEEK line is inserted into a 1/8'' outer diameter PEEK tube with a 1/16'' inner diameter to provide 1/8'' PFA Swagelok connections. A vent is installed downstream from the sample on the PEEK line to maintain, approximately, atmospheric pressure in the sample vial. This flow mixes with a large volume makeup flow of either UHP N_2 or ultra zero air controlled by mass flow controllers such that a few sccm (~10 sccm) of the sample vents to the room from the PEEK line (Figure 4.1).

4.2.2 Headspace Procedure

Acetate CI methods are characterized by high background count rates at nearly every mass-to-charge ratio (m/z) observed in the HR mass spectrum. It is extremely important to measure a representative background spectrum for both normalization and data quality control

and assurance (Brophy and Farmer, 2015). The normalized signal $\left(S_{m/z}^{Norm}\right)$ is calculated by multiplying the HR signal of interest $\left(S_{m/z}^{sample}\right)$ by the ratio of the acetate reagent ion (or total ion signal) in the background $\left(S_{Ac^-}^{bkg}\right)$ to acetate reagent ion (or total ion signal) while sampling $\left(S_{Ac^-}^{sample}\right)$ (Eqn. 4.1) (Bertram et al., 2011). The background of the headspace apparatus and HR-TOF-CIMS is determined by operating the whole system without any solution in the sample vial and flowing carrier gas through the system. Next, the sample can be injected via a syringe into the sample vial and allowed to settle. This will produce two distinct headspace experiments: turbulent headspace (measured directly after injection) and tranquil headspace (measured once the observed signals stabilize after sample injection). Both phases of the experiment are considered dynamic headspace sampling techniques because equilibrium vapor pressure conditions are never reached due to continually blowing off the headspace with either the UHP N_2 ultra zero air flow. Turbulent headspace sampling produces higher concentrations of analytes in the headspace, but the usefulness of this portion of the experiment is questionable because the signals are constantly changing until the liquid volume becomes static (i.e. no bubbling, mixing, etc.). Reproducibility issues with turbulent headspace are expected.

$$S_{m/z}^{Norm} = \left(S_{m/z}^{sample}\right) \times \frac{\left(S_{Ac^-}^{bkg}\right)}{\left(S_{Ac^-}^{sample}\right)} \qquad \text{(Eqn. 4.1)}$$

4.2.3 Data Analysis

Mass spectral data are processed in Tofware (Aerodyne Research Inc., Tofwerk AG), and subsequent analysis is conducted using Igor Pro (Wavemetrics, Inc.). The mass spectrum is acquired as a single Hierarchical Data Format (HDF5, HDF Group) file at 1 s time resolution. The data acquired after injecting the sample is collected using the same instrument configuration settings but is broken up into short (1-5 minutes) data files for processing. Tofware integrates the

HR peak fits into individual HR time series. These time series are then processed into mass defect enhancement plots, which eliminate signals that increase by <5% and have a signal-to-noise ratio (S/N) <3. Here, S/N is defined as the normalized signal during sampling divided by the standard deviation of the normalized signal in the background. This data analysis procedure is described by Brophy and Farmer (2015) for the non-targeted analysis of carboxylic acids in the atmosphere and provides a robust route for non-targeted analysis with the HR-TOF-CIMS. Last, the ion signals are colored by percent change from background and size by S/N after applying the aforementioned criteria.

Principal component analysis (PCA) is also used to differentiate the four beer samples. We used Igor Pro to prepare data, for PCA analysis by R (Version 3.3.0) and RStudio (Version 0.99.902). First, we apply the criteria used to make the mass defect enhancement plots and calculate the signals into percent change from background. Next, HR fits that contain NANs due to the application of criteria cutoffs and percent change calculations are set to zero. If a HR fit for all samples contain only zeros, the HR fit is eliminated from further analysis. This reduces the number of measured ions from 621 to 601. Next, PCA is run by centering the values on zero and scaling the values to have unit variance prior to model fitting. PCA is run "out of the box" within R. PCA is a good choice for handling the data calculated as percent change from background because signals both increase and decrease. Thus, principal components are generated that contain increasing signals and others contain primarily decreasing signals.

4.3 Beer Samples and Sample Handling

Four beer samples from the New Belgium Brewery (Fort Collins, CO) are analyzed for carboxylic acids in the headspace. Table 1 describes relevant features of the various beer samples which are substantially different in style and ingredients. The beer sample is first transferred into

a clean vial and allowed to warm to room temperature. Next, a clean syringe is used to transfer ~50 mL of beer into a clean, dry headspace analysis vial after sampling the background. The beer is injected into the headspace analysis vial and sampling begins immediately; a large amount of bubbling occurs during the turbulent headspace phase. Here, we define turbulent headspace as the condition where bubbling, mixing, and other processes can increase the gas-phase concentration of analytes and cannot be described with equilibrium vapor pressures. After a few minutes (<5), the liquid becomes tranquil and the observed signals stabilize. Here, the tranquil headspace is defined as the condition where equilibrium vapor pressures can be established if dynamic headspace analysis was not being conducted. Sampling continues (~5 minutes) and a stable portion of the experiment is chosen to be compared to the background measurement period to produce mass defect enhancement plots.

4.4 Results and Discussion

The mass defect enhancement plots for the four beer samples are shown in figure 4.2. Visual inspection of these four plots shows substantial differences between each sample. Abby contains 517 peaks, Rampant contains 491 peaks, Trippel contains 416 peaks, and Yuzu contains 358 peaks above the threshold limits. The calculated average O:C and average H:C ratio varies for each sample. Yuzu has the largest O:C ratio of 0.79, followed by Abby (0.62), Trippel (0.57), and Rampant (0.35). H:C ratios show less variability. Yuzu has the highest H:C ratio of 1.9 followed by Trippel and Rampant (1.8) and lastly Abby (1.7). These data are also plotted as Kroll diagrams (Figures 4.3-4.6) that are commonly used in atmospheric chemistry and plot the HR peak areas in oxidation state space vs carbon number. This shows how oxidation occurs as a function of carbon number and can help elucidate trends such as fragmentation, oligomerization, and functionalization (Kroll et al., 2011). The oxidation state can be approximated by equation

4.2 where O_sC is the oxidation state of some compound whose molecular formula is known, O:C is the oxygen to carbon ratio, and H:C is the hydrogen to carbon ratio (Kroll et al., 2011).

$$O_sC=2(O:C)-(H:C) \quad \text{(Eqn 4.2)}$$

The O:C numbers are consistent with the brewing process of each beer. Yuzu contains Schultheiss, Lactobacillus, Breattanomyces, Bruxellensis yeast strains. Lactobacillus is known to produce lactic acid, and Breattanomyces and Bruxellensis both produce large amounts of acetic acid. Abby has a slightly lower O:C ratio and is brewed with "Belgian Yeast", which will contain substantial numbers of Breattanomyces and, thus, will produce large quantities of acetic acid during the brewing process. Next, Trippel is brewed as a split fermentation using half Belgian Yeast and half lager yeast. Lagers typically do not have a strong acidic character and the yeast does not produce substantial amounts of acetic or lactic acids. Rampant has the lowest O:C ratio and is brewed solely with ale yeast which will not produce much acetic or lactic acids. Acetate as a reagent ion is, thus, blind to the two most prevalent substituents of these beers: acetic acid and ethanol. This highlights the importance of the choice of reagent ion for headspace analysis relative to the sample: reagent ions can be overwhelmed by the dominant components introducing unanticipated chemistries, or they can be blind to them. Measurements excluding the dominant beverage components – in the case of beer, acetic acid and ethanol – have the advantage of focusing the measurement on the lower concentration constituents that are thought to dominate the flavor and fragrance profile.

The large amount of data acquired from the HR-TOF-CIMS necessitates statistical treatment of the data set. PCA produces four principal components with 44.3% of the variance explained in the first principal component, 35.6% explained in the second principal component, and 20% explained by the third principal component. The fourth principal component explains

<1% of the variance. The first two principal components can separate the four beer samples by plotting the first principal component against the second principal component (Figure 4.7). Each ion is also displayed in figure 4.7 as arrows showing the relative loading of each ion onto each principal component. Unfortunately, additional explanatory data do not exist for these beer samples, limiting additional interpretation of the PCA results.

4.5 Conclusion

Headspace analysis conducted using novel CIMS reagent ions is a promising route to ionizing select species or classes of species in the gas phase, but the choice of reagent ion is something that has seen little attention outside of the atmospheric measurement community where selectivity is extremely important. We demonstrate that substantial variation exists in the mass spectra observed for four beers using the acetate reagent ion. Mass defect enhancement plots developed for non-targeted analysis of atmospheric high-resolution CIMS data show obvious differences between each sample. PCA confirms that these differences are sufficient to differentiate each beer by simply applying PCA. Future work should focus on the effect of high concentrations of ethanol and acetic acid when using acetate CIMS as these are suspected to be the primary interferences for this system due to their large concentrations. Additionally, quantification remains a nebulous topic for HR-TOF-CIMS in both the atmosphere where the technique was developed and in the work presented here. Absolute quantification of carboxylic acids could be of great use to analysts for rapidly screening beer headspace to determine the extent of fermentation, and this could be used in both process monitoring and end product quality control and assurance. Lastly, chromatographic separations are routinely used in the industrial production of alcoholic beverages, but these techniques are time consuming and often targeted. Comparisons between the ability to distinguish differences between samples or detect unwanted

byproducts with HR-TOF-CIMS should be conducted using routine measurements as the benchmark. A great deal of information exists in these mass spectra and extends the analytical capabilities of headspace analysis by rapidly analyzing complex samples without pre-separation, pre-concentration, sample prep, or targeting individual compounds making this technique, despite the complexity of data produced, extremely promising.

4.6 Figures

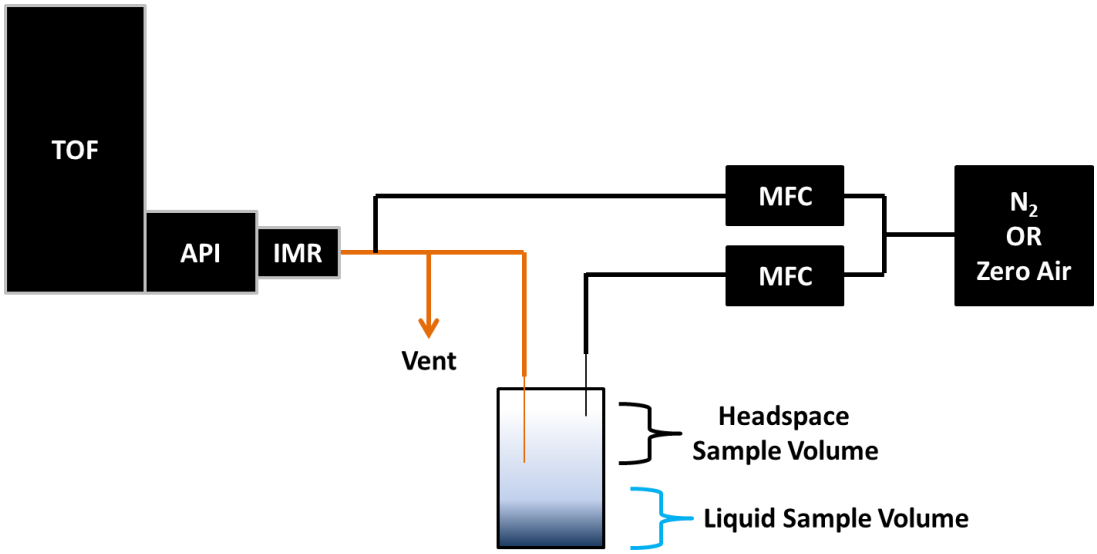

FIGURE 4.1 EXPERIMENTAL SETUP:

Headspace analysis dilution and sampling setup for aqueous samples.

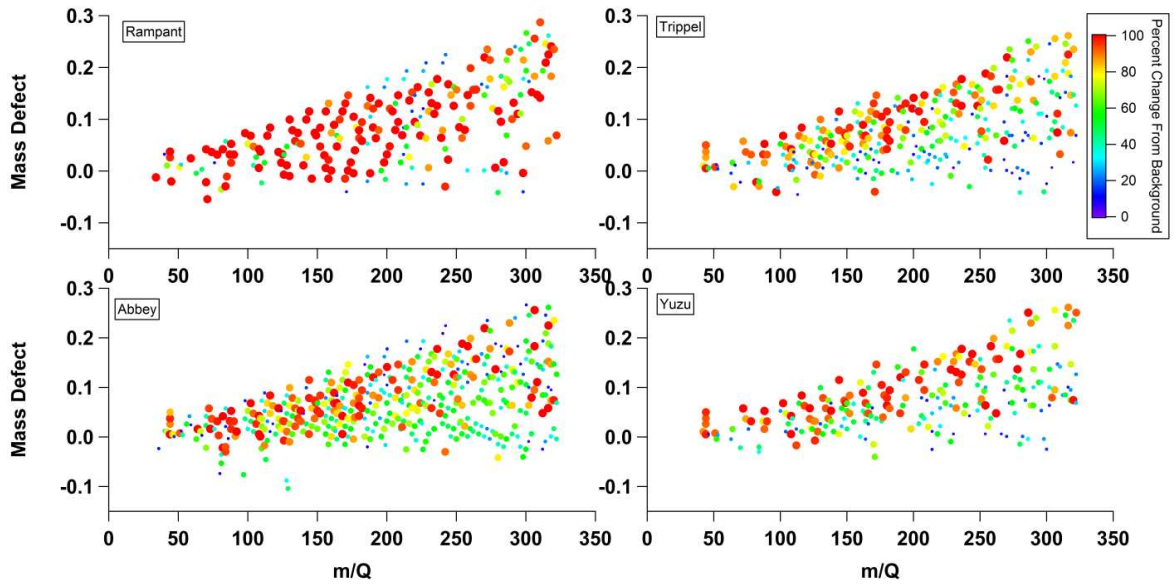

FIGURE 4.2 MASS DEFECT ENHANCEMENT PLOT:

Mass defect enhancement plots of the filtered mass spectrum for the four beer samples analyzed. Each point is a high-resolution ion fit colored by percent change from background and sized by signal to noise.

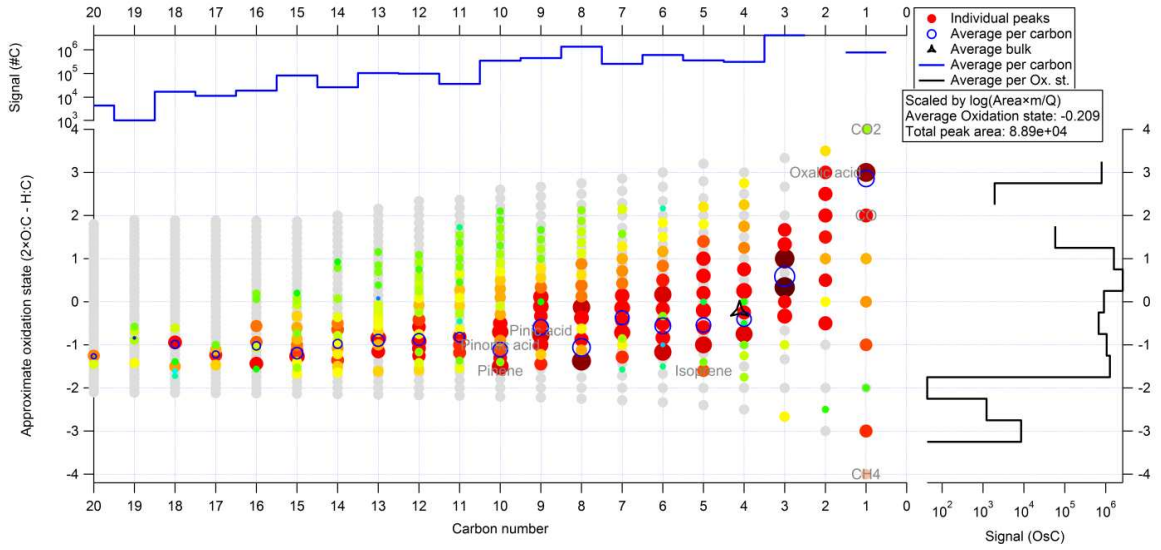

FIGURE 4.3 KROLL DIAGRAM ABBY:

(Main) Kroll diagram of Abby where oxidation state is plotted as a function of carbon number. (Top) Signal contribution from each set of compounds grouped by carbon number is plotted as a blue trace. (Right) Contribution to the average oxidation state binned by oxidation state bins is plotted as a black trace.

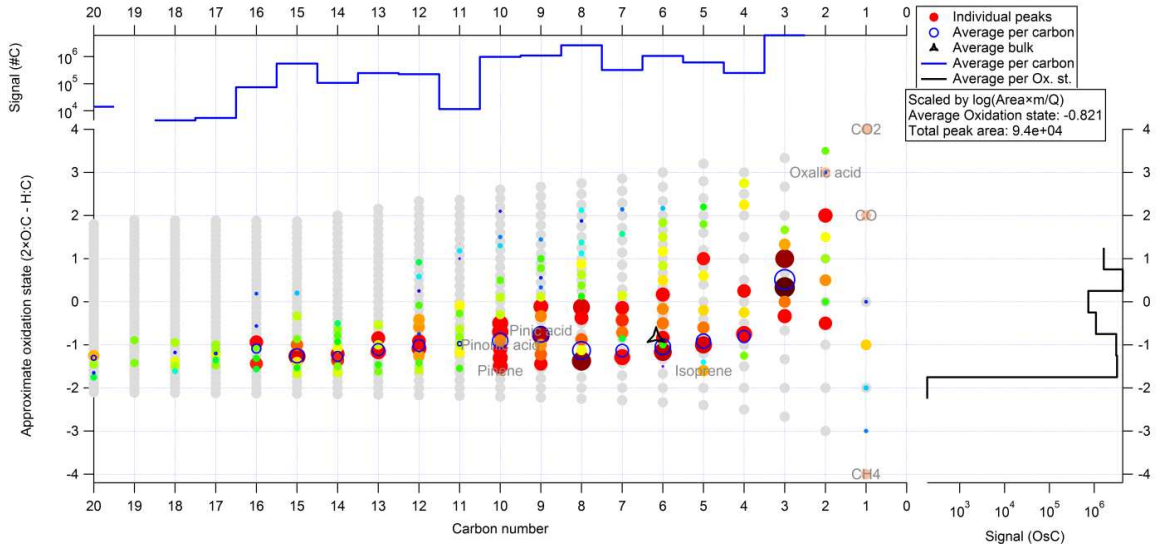

FIGURE 4.4 KROLL DIAGRAM RAMPANT:

(Main) Kroll diagram of Rampant where oxidation state is plotted as a function of carbon number. (Top) Signal contribution from each set of compounds grouped by carbon number is plotted as a blue trace. (Right) Contribution to the average oxidation state binned by oxidation state bins is plotted as a black trace.

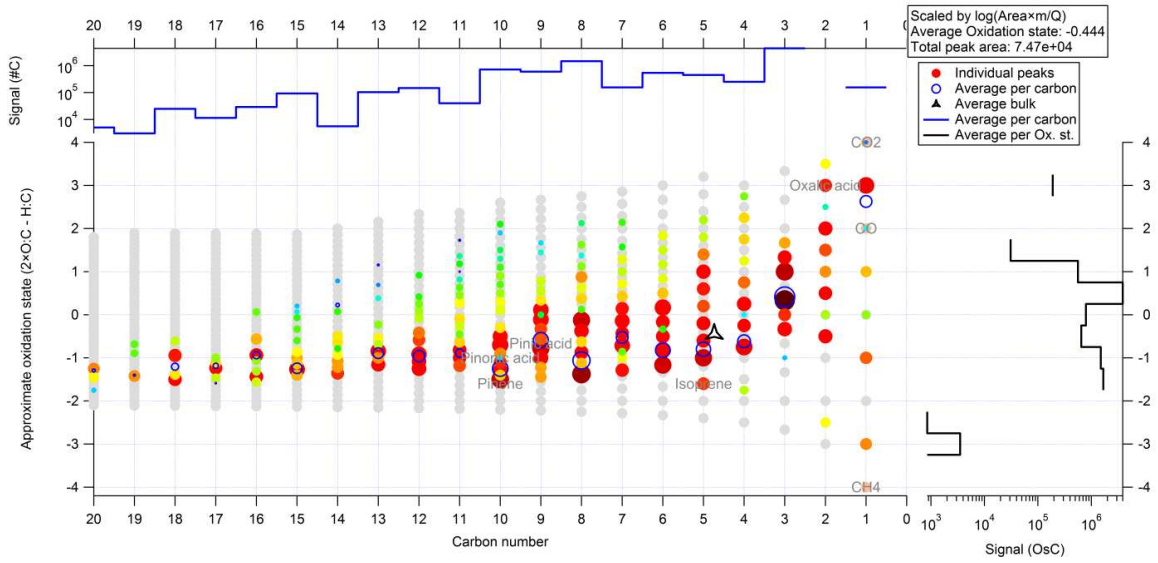

FIGURE 4.5 KROLL DIAGRAM TRIPPEL:

(Main) Kroll diagram of trippel where oxidation state is plotted as a function of carbon number. (Top) Signal contribution from each set of compounds grouped by carbon number is plotted as a blue trace. (Right) Contribution to the average oxidation state binned by oxidation state bins is plotted as a black trace.

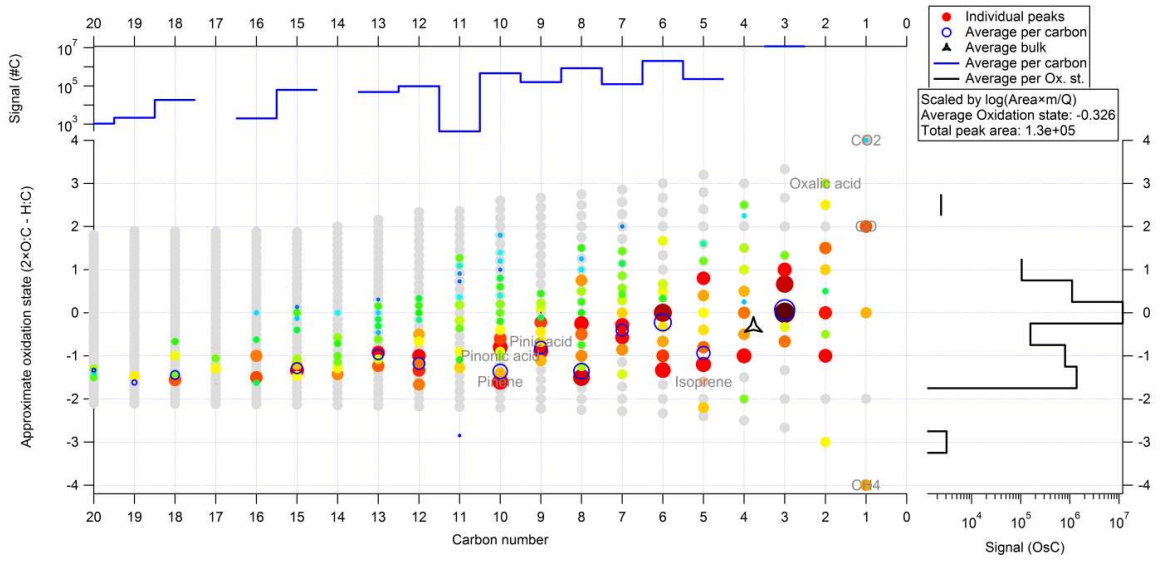

FIGURE 4.6 KROLL DIAGRAM YUZU:

(Main) Kroll diagram of Yuzu where oxidation state is plotted as a function of carbon number. (Top) Signal contribution from each set of compounds grouped by carbon number is plotted as a blue trace. (Right) Contribution to the average oxidation state binned by oxidation state bins is plotted as a black trace.

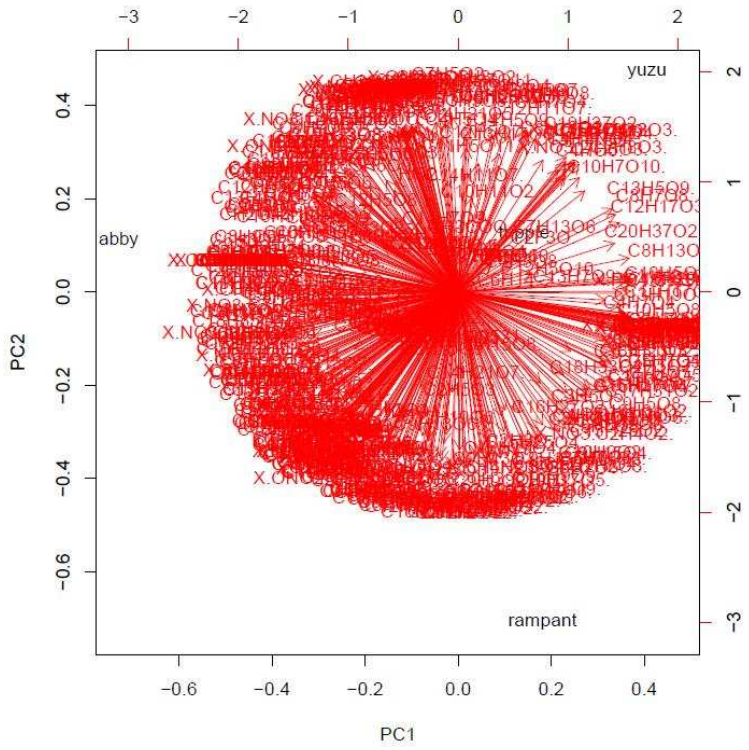

FIGURE 4.7 PCA RESULTS:

The red arrows labeled with the assigned ion formula show the loading of each ion signal onto each principal component. The sample names are also plotted to show differentiation of each sample type by the first two principal components.

4.7 Tables

TABLE 4.1 BEER SAMPLES:

	Rampant	**Abby**	**Yuzu**	**Trippel**
Beer Type	Imperial IPA	Belgian-style dubbel	Imperial Berliner Weisse Style Ale	Belgian-style Ale
ABV	8.5%	7%	8%	8.5%
IBU	85	20	6	43
Yeast	Ale Yeast	Belgian yeast	Schultheiss, Lactobacillus, Breattanomyces Bruxellensis	Split Fermentation (½ lager yeast, ½ Belgian yeast)
Hops	Mosaic, Calypso, Centennial	Willamette, Nugget, Liberty	NONE	Target, Hallertau Mittelfruh, Saaz, Liberty
Malts	Pale, Black	Pale, Chocolate, Caramel Munich, Special W, Black Barley, Oats	Pale, Wheat	Pale, Munich, Plilsner
Other			Yuzu Juice	Coriander

REFERENCES

Aljawhary, D., Lee, A. K. Y. and Abbatt, J. P. D.: High-resolution chemical ionization mass spectrometry (ToF-CIMS): application to study SOA composition and processing, Atmospheric Measurement Techniques, 6(11), 3211, doi:10.5194/amt-6-3211-2013, 2013.

Aprea, E., Romano, A., Betta, E., Biasioli, F., Cappellin, L., Fanti, M. and Gasperi, F.: Volatile compound changes during shelf life of dried Boletus edulis: comparison between SPME-GC-MS and PTR-ToF-MS analysis, J Mass Spectrom, 50(1), 56–64, doi:10.1002/jms.3469, 2015.

Bertram, T. H., Kimmel, J. R., Crisp, T. A., Ryder, O. S., Yatavelli, R. L. N., Thornton, J. A., Cubison, M. J., Gonin, M. and Worsnop, D. R.: A field-deployable, chemical ionization time-of-flight mass spectrometer, Atmospheric Measurement Techniques, 4(7), 1471, doi:10.5194/amt-4-1471-2011, 2011.

Boscaini, E., Mikoviny, T., Wisthaler, A., Hartungen, von, E. and Märk, T. D.: Characterization of wine with PTR-MS, International Journal of Mass Spectrometry, 239(2-3), 215, doi:10.1016/j.ijms.2004.07.023, 2004.

Brophy, P. and Farmer, D. K.: A switchable reagent ion high resolution time-of-flight chemical ionization mass spectrometer for real-time measurement of gas phase oxidized species: characterization from the 2013 southern oxidant and aerosol study, Atmospheric Measurement Techniques, 8(7), 2945, doi:10.5194/amt-8-2945-2015, 2015.

Budisulistiorini, S. H., Li, X., Bairai, S. T., Renfro, J., Liu, Y., Liu, Y. J., McKinney, K. A., Martin, S. T., McNeill, V. F., Pye, H. O. T., Nenes, A., Neff, M. E., Stone, E. A., Mueller, S., Knote, C., Shaw, S. L., Zhang, Z., Gold, A. and Surratt, J. D.: Examining the effects of anthropogenic emissions on isoprene-derived secondary organic aerosol formation during the 2013 Southern Oxidant and Aerosol Study (SOAS) at the Look Rock, Tennessee ground site, Atmospheric Chemistry and Physics, 15(15), 8871, doi:10.5194/acp-15-8871-2015, 2015.

Campbell-Sills, H., Capozzi, V., Romano, A., Cappellin, L., Spano, G., Breniaux, M., Lucas, P. and Biasioli, F.: Advances in wine analysis by PTR-ToF-MS: Optimization of the method and discrimination of wines from different geographical origins and fermented with different malolactic starters, International Journal of Mass Spectrometry, 397-398, 42, doi:10.1016/j.ijms.2016.02.001, 2016.

Cappellin, L., Costa, F., Aprea, E., Betta, E., Gasperi, F. and Biasioli, F.: Double clustering of PTR-ToF-MS data enables the mapping of QTLs related to apple fruit volatilome, Scientia Horticulturae, 197, 24, doi:10.1016/j.scienta.2015.10.043, 2015.

Fabris, A., Biasioli, F., Granitto, P. M. and Aprea, E.: PTR-TOF-MS and data-mining methods for rapid characterisation of agro-industrial samples: influence of milk storage conditions on the volatile compounds profile of …, Journal of mass …, 2010.

Fiches, G., Déléris, I., Saint-Eve, A., Brunerie, P. and Souchon, I.: Modifying PTR-MS operating conditions for quantitative headspace analysis of hydro-alcoholic beverages. 2. Brandy characterization and discrimination by PTR-MS, International Journal of Mass Spectrometry, 360, 15, doi:10.1016/j.ijms.2013.11.010, 2014.

Fiches, G., Déléris, I., Saint-Eve, A., Pollet, B., Brunerie, P. and Souchon, I.: Modifying PTR-MS operating conditions for quantitative headspace analysis of hydro-alcoholic beverages. 1. Variation of the mean collision energy to control ionization processes occurring during PTR-MS analyses of 10–40% (v/v) ethanol–water solutions, International Journal of Mass Spectrometry, 356, 41, doi:10.1016/j.ijms.2013.10.001, 2013.

Huey, L. G.: Measurement of trace atmospheric species by chemical ionization mass spectrometry: speciation of reactive nitrogen and future directions, Mass Spectrom Rev, 26(2), 166–184, doi:10.1002/mas.20118, 2007.

Ibáñez, C., Simó, C., García-Cañas, V., Acunha, T. and Cifuentes, A.: The role of direct high-resolution mass spectrometry in foodomics, Anal Bioanal Chem, 407(21), 6275–6287, doi:10.1007/s00216-015-8812-1, 2015.

Jordan, A., Haidacher, S., Hanel, G., Hartungen, E., Herbig, J., Märk, L., Schottkowsky, R., Seehauser, H., Sulzer, P. and Märk, T. D.: An online ultra-high sensitivity Proton-transfer-reaction mass-spectrometer combined with switchable reagent ion capability (PTR+SRI−MS), International Journal of Mass Spectrometry, 286(1), 32, doi:10.1016/j.ijms.2009.06.006, 2009.

Junninen, H., Ehn, M., Petäjä, T., Luosujärvi, L., Kotiaho, T., Kostiainen, R., Rohner, U., Gonin, M., Fuhrer, K., Kulmala, M. and Worsnop, D. R.: A high-resolution mass spectrometer to measure atmospheric ion composition, Atmospheric Measurement Techniques, 3(4), 1039, doi:10.5194/amt-3-1039-2010, 2010.

Kroll, J. H., Donahue, N. M., Jimenez, J. L., Kessler, S. H., Canagaratna, M. R., Wilson, K. R., Altieri, K. E., Mazzoleni, L. R., Wozniak, A. S., Bluhm, H., Mysak, E. R., Smith, J. D., Kolb, C. E. and Worsnop, D. R.: Carbon oxidation state as a metric for describing the chemistry of atmospheric organic aerosol, Nature Chemistry, 3(2), 133–139, doi:10.1038/nchem.948, 2011.

Lee, B. H., Lopez-Hilfiker, F. D., Mohr, C., Kurtén, T., Worsnop, D. R. and Thornton, J. A.: An iodide-adduct high-resolution time-of-flight chemical-ionization mass spectrometer: application to atmospheric inorganic and organic compounds, Environmental Science & Technology, 48(11), 6309–6317, doi:10.1021/es500362a, 2014.

Lindinger, W. and Jordan, A.: Proton-transfer-reaction mass spectrometry (PTR–MS): on-line monitoring of volatile organic compounds at pptv levels, Chem Soc Rev, 27(5), 347, doi:10.1039/a827347z, 1998.

Lindinger, W., Hansel, A. and Jordan, A.: On-line monitoring of volatile organic compounds at pptv levels by means of proton-transfer-reaction mass spectrometry (PTR-MS) medical applications, food control and environmental research, International Journal of Mass Spectrometry and Ion Processes, 173(3), 191, doi:10.1016/s0168-1176(97)00281-4, 1998.

Masi, E., Romani, A. and Pandolfi, C.: PTR-TOF-MS analysis of volatile compounds in olive fruits, Journal of the …, 2015a.

Masi, E., Taiti, C., Heimler, D., Vignolini, P., Romani, A. and Mancuso, S.: PTR-TOF-MS and HPLC analysis in the characterization of saffron (Crocus sativus L.) from Italy and Iran, Food Chemistry, 192, 75–81, doi:10.1016/j.foodchem.2015.06.090, 2015b.

Mohr, C., Lopez-Hilfiker, F. D., Zotter, P., Prévôt, A. S. H., Xu, L., Ng, N. L., Herndon, S. C., Williams, L. R., Franklin, J. P., Zahniser, M. S., Worsnop, D. R., Knighton, W. B., Aiken, A. C., Gorkowski, K. J., Dubey, M. K., Allan, J. D. and Thornton, J. A.: Contribution of nitrated phenols to wood burning brown carbon light absorption in Detling, United Kingdom during winter time, Environmental Science & Technology, 47(12), 6316–6324, doi:10.1021/es400683v, 2013.

Peris, M. and Escuder-Gilabert, L.: A 21st century technique for food control: electronic noses, Anal Chim Acta, 638(1), 1–15, doi:10.1016/j.aca.2009.02.009, 2009.

Romano, A., Fischer, L., Herbig, J., Campbell-Sills, H., Coulon, J., Lucas, P., Cappellin, L. and Biasioli, F.: Wine analysis by FastGC proton-transfer reaction-time-of-flight-mass spectrometry, International Journal of Mass Spectrometry, 369, 81, doi:10.1016/j.ijms.2014.06.006, 2014.

Soukoulis, C., Cappellin, L., Aprea, E., Costa, F., Viola, R., Märk, T. D., Gasperi, F. and Biasioli, F.: PTR-ToF-MS, A Novel, Rapid, High Sensitivity and Non-Invasive Tool to Monitor Volatile Compound Release During Fruit Post-Harvest Storage: The Case Study of Apple Ripening, Food and Bioprocess Technology, 6(10), 2831, doi:10.1007/s11947-012-0930-6, 2012.

Spitaler, R., Araghipour, N., Mikoviny, T., Wisthaler, A., Via, J. D. and Märk, T. D.: PTR-MS in enology: Advances in analytics and data analysis, International Journal of Mass Spectrometry, 266(1-3), 1, doi:10.1016/j.ijms.2007.05.013, 2007.

Sulzer, P., Edtbauer, A., Hartungen, E., Jürschik, S., Jordan, A., Hanel, G., Feil, S., Jaksch, S., Märk, L. and Märk, T. D.: From conventional proton-transfer-reaction mass spectrometry (PTR-MS) to universal trace gas analysis, International Journal of Mass Spectrometry, 321-322, 66, doi:10.1016/j.ijms.2012.05.003, 2012.

Sulzer, P., Hartungen, E., Hanel, G., Feil, S., Winkler, K., Mutschlechner, P., Haidacher, S., Schottkowsky, R., Gunsch, D., Seehauser, H., Striednig, M., Jürschik, S., Breiev, K., Lanza, M., Herbig, J., Märk, L., Märk, T. D. and Jordan, A.: A Proton Transfer Reaction-Quadrupole interface Time-Of-Flight Mass Spectrometer (PTR-QiTOF): High speed due to extreme sensitivity, International Journal of Mass Spectrometry, 368, 1, doi:10.1016/j.ijms.2014.05.004, 2014.

Taiti, C., Costa, C., Menesatti, P., Comparini, D., Bazihizina, N., Azzarello, E., Masi, E. and Mancuso, S.: Class-modeling approach to PTR-TOFMS data: a peppers case study, J Sci Food Agric, 95(8), 1757–1763, doi:10.1002/jsfa.6761, 2014.

Veres, P., Roberts, J. M., Warneke, C., Welsh-Bon, D., Zahniser, M., Herndon, S., Fall, R. and de Gouw, J.: Development of negative-ion proton-transfer chemical-ionization mass spectrometry (NI-PT-CIMS) for the measurement of gas-phase organic acids in the atmosphere, International Journal of Mass Spectrometry, 274(1-3), 48, doi:10.1016/j.ijms.2008.04.032, 2008.

Wentzell, J. J. B., Liggio, J., Li, S.-M., Vlasenko, A., Staebler, R., Lu, G., Poitras, M.-J., Chan, T. and Brook, J. R.: Measurements of gas phase acids in diesel exhaust: a relevant source of HNCO? Environmental Science & Technology, 47(14), 7663–7671, doi:10.1021/es401127j, 2013.

Yatavelli, R. L. N., Lopez-Hilfiker, F., Wargo, J. D., Kimmel, J. R., Cubison, M. J., Bertram, T. H., Jimenez, J. L., Gonin, M., Worsnop, D. R. and Thornton, J. A.: A Chemical Ionization High-Resolution Time-of-Flight Mass Spectrometer Coupled to a Micro Orifice Volatilization Impactor (MOVI-HRToF-CIMS) for Analysis of Gas and Particle-Phase Organic Species, Aerosol Science and Technology, 46(12), 1313, doi:10.1080/02786826.2012.712236, 2012.

Yatavelli, R. L. N., Stark, H., Thompson, S. L., Kimmel, J. R., Cubison, M. J., Day, D. A., Campuzano-Jost, P., Palm, B. B., Hodzic, A., Thornton, J. A., Jayne, J. T., Worsnop, D. R. and Jimenez, J. L.: Semicontinuous measurements of gas–particle partitioning of organic acids in a ponderosa pine forest using a MOVI-HRToF-CIMS, Atmospheric Chemistry and Physics, 14(3), 1527, doi:10.5194/acp-14-1527-2014, 2014.

CHAPTER 5

FUTURE DIRECTIONS FOR ACETATE CI AND HR-TOF-CIMS

5.1 The Quantification Challenge

Acetate chemical ionization (CI) as applied to high-resolution time-of-flight chemical ionization mass spectrometry (HR-TOF-CIMS) is a quantitative mass spectrometry technique, but determining linear range, sensitivity, matrix effects, and the underlying ionization mechanisms for all observed compounds remains a distant goal (Bertram et al., 2011; Veres et al., 2008). The number of authentic carboxylic acid standards greatly limits one's ability to directly calibrate the instrument. Few acids are available as authentic standards and most exist as solids at room temperature, challenging the preparation of permeation tubes for direct calibration. Moreover, commercially available authentic standards do not contain sufficiently complex functional groups (peroxy acids, polyfunctional oxygenates, etc) to represent the chemical diversity of molecules observed in the atmosphere. Thus, direct, gas-phase calibrations are possible for only a select number of alkanoic acids, simple keto- and hydroxy-acids, and a few di-acids (Veres et al., 2010; Washenfelder et al., 2003).

An alternative approach to calibration with authentic standards uses the filter inlet for gases and aerosols (FIGAERO) (Lopez-Hilfiker et al., 2014). This inlet uses a linearly actuated front plate to switch between a Teflon filter for particle collection and pre-concentration, a gas-phase inlet for ambient gas measurement, and a heated nitrogen flow for desorbing collected particulate matter from the filter. Calibrations have been conducted with this inlet by injecting a solution of authentic standards onto the Teflon filter and then desorbing the injected mass with a

heated nitrogen flow (Lee et al., 2014; Lopez-Hilfiker et al., 2014; 2015). Similar methods have been applied to the FIGAERO's precursor: the micro orifice volatilization impactor (MOVI) (Mohr et al., 2013; Yatavelli et al., 2012). Both these inlets (FIGAERO and MOVI) require heating an injected liquid volume which can lead to the degradation of the authentic standards and incomplete desorption. Additionally, the injection of organic solvents (such as acetone) can produce unanticipated reagent ion clusters that may change the sensitivity of the system by introducing matrix effects.

Comprehensive calibrations using the injection and permeation tube methods provide numerous calibration factors for a variety of compounds, but peroxy-acids and other molecules with very high O:C ratios are not available as authentic standards. The recent discovery of highly oxygenated molecules (HOMs) from both alpha-pinene (Ehn et al., 2014; Mentel et al., 2015) and isoprene (Krechmer et al., 2015) highlight this challenge as these molecules are currently impossible to synthesize and isolate as pure compounds, due to their complexity and potentially explosive behavior in the large concenetrations required for permeation tubes. These challenges have motivated recent laboratory (Lopez-Hilfiker et al., 2016) and computational (Iyer et al., 2016) work aimed at determining the sensitivity of iodide-adduct CI using voltage scanning in the atmospheric pressure interface (API) of the HR-TOF-CIMS and theoretical modeling. Voltage scanning the API causes iodide-adducts formed in the ion source to fall apart, and the voltage at which adducts disappear is related to the binding energy of the molecule with iodide (Lopez-Hilfiker et al., 2016). Iodide-adduct CI is, however, a rather simple system because iodide is both a very electronegative and a very strong acid. Thus, neither charge transfer nor proton transfer reactions are anticipated to occur to an appreciable extent (Iyer et al., 2016). This is further simplified by simply ignoring all of the ions that are not clustered with iodide; HR-

TOF-CIMS enables this because iodide has a large, negative mass defect and is easily identified in the high-resolution (HR) mass spectrum (Lee et al., 2014).

The types of product ions observed using a HR-TOF-CIMS with the acetate reagent ion highlight the complexity of this chemistry (Figure 5.1). Both deprotonation reactions products and clustering reactions products are observed depending on the extent of collision induced dissociation in the API (Bertram et al., 2011). These details are best described in comparison with iodide-adduct CI, which from first principals and experimental studies appears to be a much simpler system (Iyer et al., 2016; Lopez-Hilfiker et al., 2016). First, acetate containing clusters are impossible to identify from declustered-deprotonated ions by only inspecting the mass spectrum. For example, formic acid (CH_2O_2) clustered with acetate ($C_2H_3O_2^-$) produces an ion that is observed as ($C_3H_5O_4^-$) that shows up at an odd mass consistent with deprotonation of glyceric acid ($C_3H_6O_4$). Voltage scanning is essential for unambiguously identifying the contribution of clustering to the mass spectrum (see Chapter 3). Second, little is known about the exact mechanism of clustering or deprotonation reactions. Figure 5.1 shows multiple paths to observing the same ions via totally different ionization mechanisms and gas-phase chemical reactions. Third, the desired mass spectrum containing only deprotonated-declustered ions relies on CID in the API; this process is extremely complex. For example, figure 5.1 shows the formation of the [acetate+formic acid] cluster via reaction pathway b. Upon entering the API, the cluster will undergo some degree of CID leading to either the destruction of the cluster or the transmission of the cluster if sufficiently strong collisions do not occur. Then, the question is: which species gets the proton, and to what extent? It is possible the CID simply breaks up the acetate formic acid cluster back into its original constituents, but it is also possible that formic acid is deprotonated and then detected. A fourth possibility also exists where CID is strong

enough to dissociate the cluster in such a way that the ion is ejected from a stable trajectory in the ion beam and neither the cluster nor either of the possible deprotonated-declustered ions are observed.

These complications have been known since the early development of atmospheric pressure CI sources with respect to understanding ion composition (Eisele, 1986), the effects of clustering on sensitivity (Jost et al., 2003), and the clustering behavior of various negative ions (Viidanoja et al., 1998). Recent, detailed investigations have examined cluster formation and control in atmospheric pressure ion sources and transfer optics in time-of-flight mass spectrometers (Albrecht et al., 2014; Klee et al., 2014); these studies detect ions formed in the ion source by maintaining the thermal distribution of clusters through the custom built API. The major difference between our current predicament and the early investigations of these processes is that HR analysis enables the identification of previously uninvestigated ions. Thus, the ability to know the elemental composition of measured ions across the entire mass spectrum has produced the lofty goal of "quantifying everything". One major complicating factor to understanding ion source chemistry is that the observed mass spectrum is not necessarily representative of reactions occurring in the ion source unless great care is taken, as is the case with the study by Albrecht *et al.* (2014).

The idea of "quantifying everything" is broadly motivated from previous ideas put forth in the literature. For example, the proton-transfer reaction mass spectrometer (PTR-MS) was designed with the intent of being able to quantify gas-phase species by knowing their gas-phase proton affinities, but water clustering reactions (Lau et al., 1982) complicate this assumption because some compounds react with these clusters (Midey et al., 2000). As such, PTR-MS is routinely calibrated by static cylinder methods despite years of kinetic study and experimentally

determining proton affinities of various molecules (de Gouw and Warneke, 2006). The extensively deployed aerosol mass spectrometer (AMS) (Zhang et al., 2007) has also been developed for the quantitative measurement of atmospheric aerosols (Aiken et al., 2008; Drewnick et al., 2009; Mohr et al., 2012; Zhang et al., 2005). HR-TOF-CIMS and PTR-TOF instruments observe numerous compounds where the molecular formula is known but the structure is unknown. Molecular formula alone is insufficient for determining key parameters for the PTR-TOF-MS and HR-TOF-CIMS (e.g. polarizability, dipole moment, proton affinity, reactivity with H_3O^+ and/or $H_3O(H_2O)_n^+$ or other reagent ion/ion-clusters). With these considerations and the acknowledgement of the complexity of ion chemistry, even in the well understood and highly studied case of PTR-MS, quantification of everything remains a distant goal.

5.2 Responses to the Quantification Challenge

Three paths forward exist for acetate CIMS: (1) laboratory studies aimed at understanding the kinetics, clustering reactions, and elucidating the actual mechanisms for deprotonation, (2) continued efforts to quantify targeted species that are easily calibrated via the methods described above, or (3) avoidance of the problem by asking different questions or coupling the measurement to additional measurements such that useful data products can be produced.

5.2.1 Laboratory Studies

The CF_3O^- reagent ion provides an example of how to characterize acetate CIMS as the observed clustering chemistry, fluoride transfer reactions, and proton transfer reactions are complex and occur simultaneously in the reaction chamber. Further, the study of CF_3O^- may provide a better roadmap for future laboratory studies than iodide-adduct CIMS because of the

multitude of reactions that occur with CF_3O^-. The first report of CF_3O^- CIMS (Huey et al., 1996b) was used to measure $ClNO_2$, HNO_3, HCl, N_2O_5, SO_2, HI, and H_2O. Early characterization relied heavily on the flowing afterglow technique (Ferguson et al., 1969) to determine rate coefficients and product yields (Huey et al., 1996b) as well as the gas-phase acidity of CF_3OH (Huey et al., 1996a). Further investigations with the flowing afterglow technique determined the rate coefficients of CF_3O^-, CF_3O^-HF, and $CF_3O^-H_2O$ reactions with HNO_3, HCOOH, CH_3COOH, which proceed at the collisional limit (Amelynck et al., 2000a). HCl was also studied using CF_3O^-, CF_3O^-HF, and $CF_3O^-H_2O$ reagent ions with the same flowing afterglow setup, and the reactions were also found to proceed at the collisional limit (Amelynck et al., 2000b). More recent work has focused on applied measurements of CF_3O^- by the Wenberg Group at CalTech using both TOF-MS (Crounse et al., 2006) and tandem mass spectrometry (Clair et al., 2010; Saint Clair et al., 2014).

Ion-neutral reactions proceeding at the collisional limit is a predominant, but not omnipresent, feature of these chemistries. The reaction I^- with N_2O_5 also proceeds at the collisional rate and was first reported by Huey *et al.* (Huey et al., 1995); this fact was recently taken advantage of by simply applying the collisional limit to all species measured with iodide-adduct CIMS producing excellent agreement between AMS and FIGAERO data (Lopez-Hilfiker et al., 2016). Acetate CIMS reactions may proceeded at the collisional limit, but detailed investigations via flowing afterglow (Ferguson et al., 1969) or selected ion flow tube (SIFT) measurements (Adams and Smith, 1976) are an obvious next step.

The primary problem with acetate CIMS is that there are many possible reagent ions and ion-neutral (or ion-radical) clusters that flowing afterglow techniques may suffer from simultaneously creating numerous reagent ion species in the ion source. Thus, the more complex

but controlled approach of SIFT measurements are a promising route towards understanding these reaction mechanisms. Acetate (CH_3COO^-) and its most prevalent clusters ([$(CH_3COOH)_n$ + $CH3COO^-$] and [H_2O + $CH3COO^-$]) can be directly selected via quadrupole mass filters before entering the flow tube and reacting with neutral species. Understanding the kinetics of the reactions of acetate and acetate clusters with neutral acids is a key, fundamental gap in our understanding of this ionization chemistry. Knowing how this chemistry proceeds is of great importance for both interpreting atmospheric CIMS data and tuning important system variables (such as the amount of acetic anhydride added to the system, as this likely controls the extent and distribution of acetate related clusters).

5.2.2 Alternative Approaches

The most obvious application of these HR-TOF-CIMS measurements is eddy covariance (EC) flux measurements where absolute quantification is unnecessary for determining the exchange velocity of every species in the HR mass spectrum. Fast (~10 Hz) and sensitive (<1 ppb limit of quantification) mass spectrometry instrumentation and electronics (Kimmel et al., 2011) have enabled the possibility of measuring a vast suite of compounds with the EC flux method (Müller et al., 2010). This is of particular interest for semi- and low-volatility, gas-phase oxygenated compounds which dominate secondary organic aerosol (SOA) production (Jimenez et al., 2009). Only limited EC measurements of these compounds are reported (Langford et al., 2010; Misztal et al., 2011; Nguyen et al., 2015). The lack of wet and dry deposition measurements is noted as a key knowledge-gap in a recent review of atmospheric organic chemistry (Glasius and Goldstein, 2016).

Modeling studies investigating the role of wet and dry deposition highlight the importance of constraining and accounting for deposition processes when calculating SOA

concentrations (Bessagnet et al., 2010). This is especially true for semivolatile gas-phase species, for which including wet and dry deposition can reduce both anthropogenic and biogenic SOA concentrations by 48% and 63% respectively (Knote et al., 2015). Additionally, organic acids have been shown to exhibit interesting and unexpected ambient temporal behavior, suggesting these compounds are rapidly produced and deposited in various environments (Brophy and Farmer, 2015; Veres et al., 2011). Recent modeling studies completely fail to recreate both the general trend and absolute concentrations of formic acid in the South Eastern United States pointing to a fundamental gap in our knowledge of atmospheric oxidation and deposition processes (Millet et al., 2015). Direct ecosystem scale EC flux measurements need to be conducted to help constrain SOA models that include deposition processes. Determining the flux of these species requires absolute quantification. At this point, however, the lack of direct measurements of semi- and low-volatility species needs to be addressed, and exchange velocities in which fluxes are normalized by concentrations and thus independent of the calibration are an obvious route when quantification remains challenging.

Ongoing seasonal flux measurements conducted by the Farmer Group at the Manitou Experimental Forest (Ortega et al., 2014) flux site near Woodland Park, Colorado has produced promising preliminary results. Online calibrations of formic, propionic, butyric, methacrylic, and lactic acids will provide quantitative EC flux measurements, but hundreds of other species exhibit obvious flux profiles where exchange velocities can be calculated (Figure 5.2). This work is a direct extension of the measurement system developed during the Southern Oxidant and Aerosol Study during the Summer of 2013 (Brophy and Farmer, 2015).

5.2.3 Quantification, Who Needs It?

The inability to model tropospheric formic acid concentrations and temporal behavior during the Southern Oxidant and Aerosol Study in the summer of 2013 (Millet et al., 2015) points to some serious problems with current modeling approaches and calls into question the need for quantitative measurements of all species detected by CIMS measurements. Namely, how can the concentration time series of hundreds of oxygenated hydrocarbons, carboxylic acids, and organic peroxides meaningfully be integrated into current modeling schemes? This question is particularly concerning when evaluated with the understanding that we cannot get the simplest carboxylic acid, formic acid, correct (concentration, spatial and temporal distributions) even when the modeling attempt is constrained with, arguably, the most comprehensive set of co-located measurements conducted to date. Moreover, even if this can be incorporated into tropospheric chemistry modeling schemes, we lack the fundamental knowledge about the nature of these compounds (e.g. structure, volatility, OH reactivity, subsequent SOA chemistry, gas-phase acidity, polarizability, etc.).

These challenges are highlighted in a previous review by Goldstein and Galbally (2007) and in a more recent review by Glasius and Goldstein (2016). They argue that future work should focus on many of the issues raised above regarding the nature and concentration of recently identified low-volatility species, but they also raise the concern of how much more information is really needed (Glasius and Goldstein, 2016; Goldstein and Galbally, 2007); is it really necessary to quantify everything? The answers to these questions may rely on the types of next-generation models that are produced in the future. Early air quality models relied on available measurements as the focus of inputs and data outputs for testing model validity and predicting key parameters (e.g. ozone, NO_x, etc.). Now, the number and diversity of

measurements makes the task of comprehensive data integration into modeling schemes nearly impossible. Thus, if the end result is to reduce the complexity of actual measurements (perhaps hundreds of measured compounds from a single instrument) into a single numerical value, how important is it that we know the absolute structure and concentration of every semi- or low-volatility species?

The complexity and volume of data produced from a single HR-TOF-CIMS is astounding, and we need to be careful that the correct questions are being asked such that meaningful conclusions can be derived from this unprecedented amount of data. Qualitative measurements of SO_2 perturbations to the oxidation of a- and b-pinene show that the bulk oxidation chemistry drastically changes as a result of SO_2 mixing ratios (Friedman et al., 2016). Perhaps, this type of study provides a more useful set of information where modelers can be guided to relevant processes and gaps in the knowledge based on relatively simple experiments and questions. The treatment of oxidation schemes as non-interacting (i.e. a-pinene oxidation follows the anticipated oxidation chemistry of a-pinene in an atmospheric simulation chamber without interacting with other oxidation schemes) is another complexity reducing assumption that is currently under investigation by the Farmer group. This question is answerable without knowing the absolute concentrations of each oxidation product detected by HR-TOF-CIMS instruments. Another example of non-quantified analysis guiding modeling concepts shows that the gas and particle phase track each other during photochemical oxidation of diesel exhaust (Friedman, *et al. 2016 Submitted)*. Here, we show that by grouping gas-phase species detected with the HR-TOF-CIMS into volatility bins (e.g. volatile, semi-volatile, low-volatile, etc) clear changes in oxidation state occur in each volatility bin and track particle oxidation state determined by TOF-AMS measurements. Again, this demonstrates a key concept: bulk gas-

phase carbon oxidation occurs simultaneously with SOA aging and production. This becomes especially clear when implementing volatility binning schemes that are often used in SOA models and descriptors (Donahue et al., 2011; Heald et al., 2010; Kroll et al., 2011). These limited examples ask clear questions that are answerable using the entire HR mass spectrum collected from the HR-TOF-CIMS, and the questions test hypothesis and paradigms that exist in the literature.

Recent ambient ion measurements have shown that HOMs and mixes of sulfuric acid and ammonia are observed during nucleation events in the free troposphere (Bianchi et al., 2016). Four distinct events are categorized without quantification: non-event days, cloudy days, new particle formation days with average sulfuric acid concentrations, and new particle formation days with enhanced sulfuric acid concentrations. The API-TOF (also referred to in the literature as APi-TOF) (Junninen et al., 2010) provides a qualitative mass defect plot of each day, clearly showing the growth of large clusters into the nanometer size range corresponding to nearly 1000 m/z (Bianchi et al., 2016). This work provides *in situ* verification of the types of chemistry observed during the Cosmics Leaving OUtdoor Droplets (CLOUD) chamber study at the European Organization for Nuclear Research (CERN) (Kirkby et al., 2016; Schobesberger et al., 2015; Tröstl et al., 2016).

5.3 Atmospheric Nucleation and Voltage Scanning

The CLOUD chamber study has identified a major source of atmospheric particles using numerous HR-TOF-MS systems and the CLOUD chamber. It should be noted that the Tofwerk HR-TOF-CIMS has been absolutely necessary for these studies. The details of these experiments are not particularly important with respect to future directions for the work presented in this dissertation, but the voltage scanning methodologies (See Chapter 3) are directly applicable to

the CLOUD chamber data for every HR-TOF-CIMS and numerous results that have very recently been published (Kirkby et al., 2016; 2011; Kürten et al., 2014; Lehtipalo et al., 2016; Schobesberger et al., 2015; Tröstl et al., 2016).

One of the fundamental gaps in our understanding lies at the interface between gas-phase molecules and 1-5 nm particles. Numerous arguments are made regarding the limits of how well HOMs and low-volatility compound partition to small particles or clusters based on the application of the Kelvin effect and Köhler theory. The Kelvin effect describes changes in vapor pressure as a function of droplet curvature and Köhler theory extends this description with Raoult's law. This theoretical structure as a description of initial clustering and particle formation from gas-phase species is explicitly stated to be ambiguous (Tröstl et al., 2016). *A priori*, the application of these theories below 5 nm makes little sense because of the recent HR-TOF-CIMS measurements of HOMs and API-TOF measurements of ambient ion-clusters. The HOM system consists of very large, organic, gas-phase molecules that weigh in excess of ~600 amu (Ehn et al., 2014; 2012; Mentel et al., 2015). These molecules, along with sulfuric acid and ammonia, can cluster to form stable particles or clusters (Kirkby et al., 2011; Schobesberger et al., 2015). Thus, this system is absolutely not bulk phase as two a-pinene ($C_{10}H_{16}$) derived HOM dimers ($C_{20}H_xO_z$) will produce a 1.7 nm (mobility diameter) cluster with a m/z of ~1200 (Kirkby et al., 2016). First, these clusters are not spheres and likely exist through non-covalent bonding intermolecular forces. Second, volatility should not be used to describe the possibility of two molecules clustering together. Thus, it is this interesting chemical space where our binary description of matter existing as either molecules and atoms or bulk phase matter fails to adequately describe the initial nucleation phenomenon.

Voltage scanning methodologies (Chapter 3) can directly determine if these <5 nm clusters behave as individually clustered molecules or as bulk-phase matter. Additionally, the strength (or stability) of these clusters can be determined via voltage scanning methods and, potentially, quantified. The diversity of the clusters observed <1000 m/z in the ambient atmosphere makes identifying precursors or early stage nucleating clusters very difficult (Bianchi et al., 2016). Moreover, reconciling why these clusters are omnipresent in the free troposphere while nucleation events are not may be explained by the difference between cluster formation and evaporation rates, which are likely based on cluster stability and binding energy. Cluster evaporation is expected to become negligible at 1.7 nm (Kirkby et al., 2016) and this hypothesis can be answered by voltage scanning. The ambient measurements also exhibit numerous unidentified HR ions in the mass defect plot (Bianchi et al., 2016). The binding energies of these unidentified clusters can be determined even though the molecular formula is unknown.

Other interesting features exist in the ambient ion measurements in the CLOUD chamber. The periodic structure of the positive ion mass spectrum is not observed to the same extent in the negative ion mass spectrum, and this is explained by positive ions primarily clustering with HOM dimers ($C_{20}H_xO_z$) while negative ions cluster with both dimers and monomers ($C_{10}H_xO_z$) (Kirkby et al., 2016). This claim describes the observed mass spectrum, but the reason for this is difficult to reconcile. Signal exists in the positive ion mass spectrum between the periodic maximums, and voltage scanning may show that these periodic minimums have lower cluster stability than the high intensity periodic maximums. Numerous details emerging from CLOUD should be fairly easy to clarify with these proposed voltage scanning methodologies.

5.4 Major Conclusions

Immediate and pressing questions exist for ongoing acetate CIMS characterization. Namely, the determination of the actual ion-neutral mechanism(s) leading to the formation of deprotonated carboxylic acids is a fundamental gap in our knowledge. This information is extremely important for understanding the types of molecules detected with acetate CIMS using an HR-TOF-CIMS for non-targeted studies. This can be accomplished with SIFT measurements and the kinetics of the various reactions can be determined.

The relative ease of EC flux measurements during our recent deployments with acetate HR-TOF-CIMS is another obvious area of exploration that is of great importance to atmospheric chemistry. Comparisons of acetate-derived EC flux measurements with PTR-TOF-MS and iodide-adduct HR-TOF-CIMS methodologies should be conducted. Luckily, the instrument that is currently deployed at the Manitou Experiential Forest has reagent ion switching capabilities and has been previously described (Brophy and Farmer, 2015). Comparisons with iodide adduct CIMS are ongoing. Voltage scanning in the ambient atmosphere will also provide an additional level of quality control to ensure that measured ions are, in fact, individual ions and not ion-neutral clusters (i.e. reagent ion-neutral clusters).

Lastly, the CLOUD chamber studies examining the behavior of ambient ions and the various associated field studies should begin to conduct voltage scanning experiments. These methodologies may provide clear insights to the nature of <1 nm clusters and, potentially, provide insight into the nature of <5 nm clusters if sufficiently strong declustering fields can be applied. This is new and emerging science regarding previously unidentified processes governing SOA formation and cloud condensation nuclei formation with direct implications for climate

forcing. The nature of the initial stages of particle nucleation need to be addressed, and the tools already exist; it is simply a matter of writing a bit of code.

The power of HR-TOF-MS is only beginning to emerge, and HR-TOF-MS already dominates atmospheric chemistry measurements despite its relatively recent emergence. Long term trends suggest that instrument sensitivity will continue to increase along with mass resolution and acquisition rates. It remains nebulous, however, how further increases to mass resolution and sensitivity will provide further insights to atmospheric chemical processes. Modeling attempts at integrating the complexities elucidated by recent instrumental advances appear to be a key liming step. This is, however, contrasted by the limited number of *in situ* field measurement campaigns with respect to global coverage, seasonal coverage, ecosystem scale measurements, and the co-location of related measurements. Remote sensing platforms are playing an increasingly important role, but these techniques still lack the chemical complexity of *in situ* mass spectrometry methods. Satellite retrievals of compound classes such as HOMs appear to be far in the future. Despite all of this, it does appear that we have reached the point in time where sufficient (albeit nowhere near perfect) measurements exist to answer many of the uncertainties related to the earth and the climate systems. Now, it is a matter of global policy directions for funding and intellectual effort that likely provides the greatest hurdle to be overcome.

5.5 Chapter 5 Figures

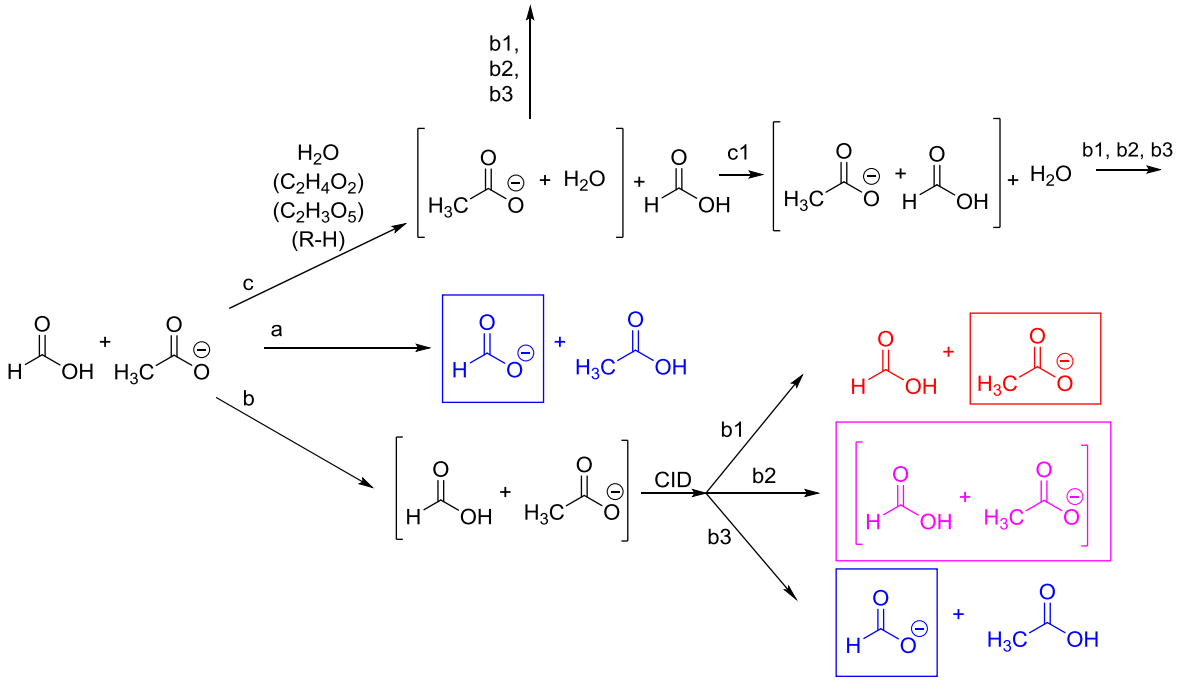

FIGURE 5.1 ACETATE CI POSSIBLE REACTIONS:

Acetate ions are formed in large abundance from the Po-210 ion source and will react with some neutral species (formic acid is shown here). (a) Direct deprotonation can occur in the IMR and lead to formate and acetic acid (Blue Products). These products will either continue to react in the IMR or enter the API and be detected (Blue Products). (b-c) Clustering reactions also occur to form ion-neutral adducts that will either enter the API and undergo CID (b1-b3) or undergo a ligand switch reaction with some other species in the IMR (c1). The product of c1 then either continues to ligand switch with other available neutral species, fall apart, or enters the API and undergoes CID (b1-b3) to be detected as either blue, pink, or red products.

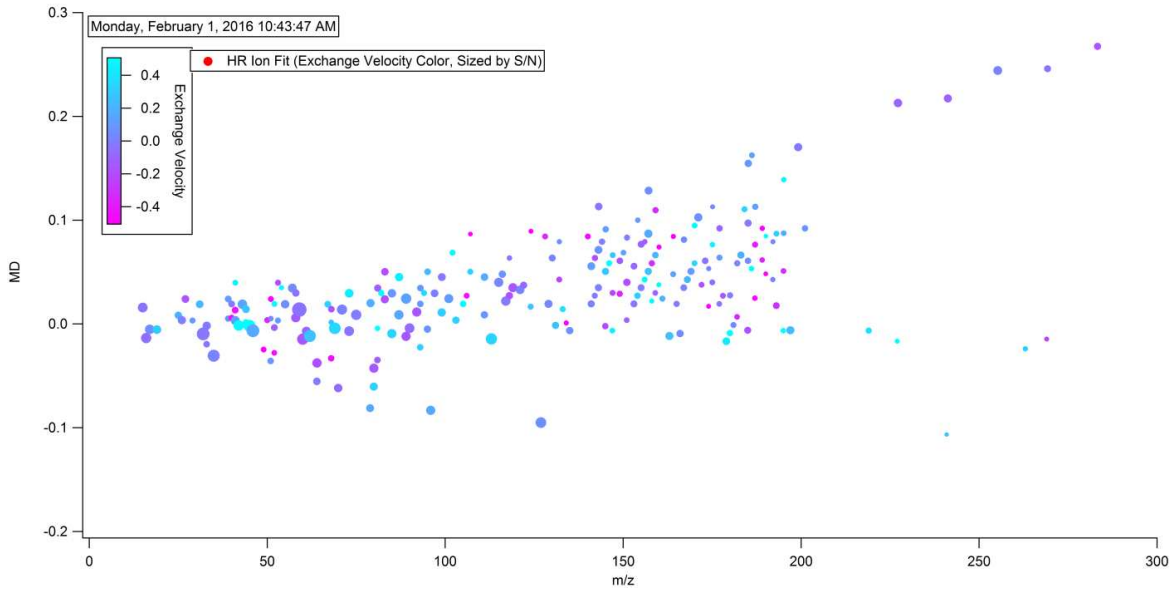

FIGURE 5.2 MASS DEFECT PLOT OF EXCHANGE VELOCITIES:

The exchange velocity determined in the EC flux algorithm is plotted in mass defect space as a function of mass-to-charge ratio. These data were acquired beginning on February 1at 10:43 AM at the Manitou Experimental Forest. Ryan Fulgham was responsible for running the experiment and wrote the majority of the base flux analysis code (Preliminary data).

REFERENCES

Adams, N. G. and Smith, D.: The selected ion flow tube (SIFT); a technique for studying ion-neutral reactions, International journal of mass spectrometry and ion …, 1976.

Aiken, A. C., DeCarlo, P. F., Kroll, J. H., Worsnop, D. R., Huffman, J. A., Docherty, K. S., Ulbrich, I. M., Mohr, C., Kimmel, J. R., Sueper, D., Sun, Y., Zhang, Q., Trimborn, A., Northway, M., Ziemann, P. J., Canagaratna, M. R., Onasch, T. B., Alfarra, M. R., Prévôt, A. S. H., Dommen, J., Duplissy, J., Metzger, A., Baltensperger, U. and Jimenez, J. L.: O/C and OM/OC Ratios of Primary, Secondary, and Ambient Organic Aerosols with High-Resolution Time-of-Flight Aerosol Mass Spectrometry, Environmental Science & Technology, 42(12), 4478, doi:10.1021/es703009q, 2008.

Albrecht, S., Klopotowski, S., Derpmann, V., Klee, S., Brockmann, K. J., Stroh, F. and Benter, T.: Studies of the mechanism of the cluster formation in a thermally sampling atmospheric pressure ionization mass spectrometer, Rev Sci Instrum, 85(1), 014102, doi:10.1063/1.4854855, 2014.

Amelynck, C., Schoon, N. and Arijs, E.: Gas phase reactions of CF3O− and CF3O−H2O with nitric, formic, and acetic acid, International Journal of Mass Spectrometry, 203(1-3), 165, doi:10.1016/s1387-3806(00)00321-3, 2000a.

Amelynck, C., Van, A. M., Schoon, B. N. and Arijs, E.: Gas phase reactions of CF 3 O− and CF 3 O−· H 2 O and their relevance to the detection of stratospheric HCl, International Journal of Mass …, 2000b.

Bertram, T. H., Kimmel, J. R., Crisp, T. A., Ryder, O. S., Yatavelli, R. L. N., Thornton, J. A., Cubison, M. J., Gonin, M. and Worsnop, D. R.: A field-deployable, chemical ionization time-of-flight mass spectrometer, Atmospheric Measurement Techniques, 4(7), 1471, doi:10.5194/amt-4-1471-2011, 2011.

Bessagnet, B., Seigneur, C. and Menut, L.: Impact of dry deposition of semi-volatile organic compounds on secondary organic aerosols, Atmospheric Environment, 44(14), 1781, doi:10.1016/j.atmosenv.2010.01.027, 2010.

Bianchi, F., Tröstl, J., Junninen, H., Frege, C., Henne, S., Hoyle, C. R., Molteni, U., Herrmann, E., Adamov, A., Bukowiecki, N., Chen, X., Duplissy, J., Gysel, M., Hutterli, M., Kangasluoma, J., Kontkanen, J., Kürten, A., Manninen, H. E., Munch, S., Perakyla, O., Petäjä, T., Rondo, L., Williamson, C., Weingartner, E., Curtius, J., Worsnop, D. R., Kulmala, M., Dommen, J. and Baltensperger, U.: New particle formation in the free troposphere: A question of chemistry and timing, Science, 352(6289), 1109, doi:10.1126/science.aad5456, 2016.

Brophy, P. and Farmer, D. K.: A switchable reagent ion high resolution time-of-flight chemical ionization mass spectrometer for real-time measurement of gas phase oxidized species: characterization from the 2013 southern oxidant and aerosol study, Atmospheric Measurement Techniques, 8(7), 2945, doi:10.5194/amt-8-2945-2015, 2015.

Clair, J. M. S., McCabe, D. C., Crounse, J. D., Steiner, U. and Wennberg, P. O.: Chemical ionization tandem mass spectrometer for the in situ measurement of methyl hydrogen peroxide, Rev Sci Instrum, 81(9), 094102, doi:10.1063/1.3480552, 2010.

Crounse, J. D., McKinney, K. A., Kwan, A. J. and Wennberg, P. O.: Measurement of gas-phase hydroperoxides by chemical ionization mass spectrometry, Anal Chem, 78(19), 6726–6732, doi:10.1021/ac0604235, 2006.

Donahue, N. M., Epstein, S. A., Pandis, S. N. and Robinson, A. L.: A two-dimensional volatility basis set: 1. organic-aerosol mixing thermodynamics, Atmospheric Chemistry and Physics, 11(7), 3303, doi:10.5194/acp-11-3303-2011, 2011.

Drewnick, F., Hings, S. S., Alfarra, M. R., Prévôt, A. S. H. and Borrmann, S.: Aerosol quantification with the Aerodyne Aerosol Mass Spectrometer: detection limits and ionizer background effects, Atmospheric Measurement Techniques, 2(1), 33, doi:10.5194/amt-2-33-2009, 2009.

Ehn, M., Kleist, E., Junninen, H., Petäjä, T., Lönn, G., Schobesberger, S., Maso, M. D., Trimborn, A., Kulmala, M., Worsnop, D. R., Wahner, A., Wildt, J. and Mentel, T. F.: Gas phase formation of extremely oxidized pinene reaction products in chamber and ambient air, Atmospheric Chemistry and Physics, 12(11), 5113, doi:10.5194/acp-12-5113-2012, 2012.

Ehn, M., Thornton, J. A., Kleist, E., Sipilä, M., Junninen, H., Pullinen, I., Springer, M., Rubach, F., Tillmann, R., Lee, B., Lopez-Hilfiker, F., Andres, S., Acir, I.-H., Rissanen, M., Jokinen, T., Schobesberger, S., Kangasluoma, J., Kontkanen, J., Nieminen, T., Kurtén, T., Nielsen, L. B., Jørgensen, S., Kjaergaard, H. G., Canagaratna, M., Maso, M. D., Berndt, T., Petäjä, T., Wahner, A., Kerminen, V.-M., Kulmala, M., Worsnop, D. R., Wildt, J. and Mentel, T. F.: A large source of low-volatility secondary organic aerosol, Nature, 506(7489), 476–479, doi:10.1038/nature13032, 2014.

Eisele, F. L.: Identification of tropospheric ions, Journal of Geophysical Research: Atmospheres, 91(D7), 7897, doi:10.1029/jd091id07p07897, 1986.

Ferguson, E. E., Fehsenfeld, F. C. and Schmeltekopf, A. L.: Flowing Afterglow Measurements of Ion-Neutral Reactions. 1969.

Friedman, B., Brophy, P., Brune, W. H. and Farmer, D. K.: Anthropogenic Sulfur Perturbations on Biogenic Oxidation: SO2 Additions Impact Gas-Phase OH Oxidation Products of α- and β-

Pinene, Environmental Science & Technology, 50(3), 1269–1279, doi:10.1021/acs.est.5b05010, 2016.

Glasius, M. and Goldstein, A. H.: Recent Discoveries and Future Challenges in Atmospheric Organic Chemistry, Environmental Science & Technology, 50(6), 2754–2764, doi:10.1021/acs.est.5b05105, 2016.

Goldstein, A. H. and Galbally, I. E.: Known and Unexplored Organic Constituents in the Earth's Atmosphere, Environmental Science & Technology, 41(5), 1514, doi:10.1021/es072476p, 2007.

Heald, C. L., Kroll, J. H., Jimenez, J. L., Docherty, K. S., DeCarlo, P. F., Aiken, A. C., Chen, Q., Martin, S. T., Farmer, D. K. and Artaxo, P.: A simplified description of the evolution of organic aerosol composition in the atmosphere, Geophysical research letters, 37(8), n/a, doi:10.1029/2010gl042737, 2010.

Huey, L. G., Dunlea, E. J. and Howard, C. J.: Gas-Phase Acidity of CF3OH, The Journal of Physical …, 1996a.

Huey, L. G., Hanson, D. R. and Howard, C. J.: Reactions of SF6- and I- with Atmospheric Trace Gases, The Journal of Physical Chemistry, 99(14), 5001, doi:10.1021/j100014a021, 1995.

Huey, L. G., Villalta, P. W. and Dunlea, E. J.: Reactions of CF3O-with atmospheric trace gases, The Journal of …, 1996b.

Iyer, S., Lopez-Hilfiker, F., Lee, B. H., Thornton, J. A. and Kurtén, T.: Modeling the Detection of Organic and Inorganic Compounds Using Iodide-Based Chemical Ionization, J Phys Chem A, 120(4), 576–587, doi:10.1021/acs.jpca.5b09837, 2016.

Jimenez, J. L., Canagaratna, M. R., Donahue, N. M., Prévôt, A. S. H., Zhang, Q., Kroll, J. H., DeCarlo, P. F., Allan, J. D., Coe, H., Ng, N. L., Aiken, A. C., Docherty, K. S., Ulbrich, I. M., Grieshop, A. P., Robinson, A. L., Duplissy, J., Smith, J. D., Wilson, K. R., Lanz, V. A., Hueglin, C., Sun, Y. L., Tian, J., Laaksonen, A., Raatikainen, T., Rautiainen, J., Vaattovaara, P., Ehn, M., Kulmala, M., Tomlinson, J. M., Collins, D. R., Cubison, M. J., Dunlea, E. J., Huffman, J. A., Onasch, T. B., Alfarra, M. R., Williams, P. I., Bower, K., Kondo, Y., Schneider, J., Drewnick, F., Borrmann, S., Weimer, S., Demerjian, K., Salcedo, D., Cottrell, L., Griffin, R., Takami, A., Miyoshi, T., Hatakeyama, S., Shimono, A., Sun, J. Y., Zhang, Y. M., Dzepina, K., Kimmel, J. R., Sueper, D., Jayne, J. T., Herndon, S. C., Trimborn, A. M., Williams, L. R., Wood, E. C., Middlebrook, A. M., Kolb, C. E., Baltensperger, U. and Worsnop, D. R.: Evolution of organic aerosols in the atmosphere, Science, 326(5959), 1525–1529, doi:10.1126/science.1180353, 2009.

Jost, C., Sprung, D., Kenntner, T. and Reiner, T.: Atmospheric pressure chemical ionization mass spectrometry for the detection of tropospheric trace gases: the influence of clustering on sensitivity and precision, International Journal of Mass Spectrometry, 223-224, 771, doi:10.1016/s1387-3806(02)00963-6, 2003.

Junninen, H., Ehn, M., Petäjä, T., Luosujärvi, L., Kotiaho, T., Kostiainen, R., Rohner, U., Gonin, M., Fuhrer, K., Kulmala, M. and Worsnop, D. R.: A high-resolution mass spectrometer to measure atmospheric ion composition, Atmospheric Measurement Techniques, 3(4), 1039, doi:10.5194/amt-3-1039-2010, 2010.

Kimmel, J. R., Farmer, D. K., Cubison, M. J., Sueper, D., Tanner, C., Nemitz, E., Worsnop, D. R., Gonin, M. and Jimenez, J. L.: Real-time aerosol mass spectrometry with millisecond resolution, International Journal of Mass Spectrometry, 303(1), 15, doi:10.1016/j.ijms.2010.12.004, 2011.

Kirkby, J., Curtius, J., Almeida, J., Dunne, E., Duplissy, J., Ehrhart, S., Franchin, A., Gagné, S., Ickes, L., Kürten, A., Kupc, A., Metzger, A., Riccobono, F., Rondo, L., Schobesberger, S., Tsagkogeorgas, G., Wimmer, D., Amorim, A., Bianchi, F., Breitenlechner, M., David, A., Dommen, J., Downard, A., Ehn, M., Flagan, R. C., Haider, S., Hansel, A., Hauser, D., Jud, W., Junninen, H., Kreissl, F., Kvashin, A., Laaksonen, A., Lehtipalo, K., Lima, J., Lovejoy, E. R., Makhmutov, V., Mathot, S., Mikkilä, J., Minginette, P., Mogo, S., Nieminen, T., Onnela, A., Pereira, P., Petäjä, T., Schnitzhofer, R., Seinfeld, J. H., Sipilä, M., Stozhkov, Y., Stratmann, F., Tomé, A., Vanhanen, J., Viisanen, Y., Vrtala, A., Wagner, P. E., Walther, H., Weingartner, E., Wex, H., Winkler, P. M., Carslaw, K. S., Worsnop, D. R., Baltensperger, U. and Kulmala, M.: Role of sulphuric acid, ammonia and galactic cosmic rays in atmospheric aerosol nucleation, Nature, 476(7361), 429–433, doi:10.1038/nature10343, 2011.

Kirkby, J., Duplissy, J., Sengupta, K., Frege, C., Gordon, H., Williamson, C., Heinritzi, M., Simon, M., Yan, C., Almeida, J., Tröstl, J., Nieminen, T., Ortega, I. K., Wagner, R., Adamov, A., Amorim, A., Bernhammer, A.-K., Bianchi, F., Breitenlechner, M., Brilke, S., Chen, X., Craven, J., Dias, A., Ehrhart, S., Flagan, R. C., Franchin, A., Fuchs, C., Guida, R., Hakala, J., Hoyle, C. R., Jokinen, T., Junninen, H., Kangasluoma, J., Kim, J., Krapf, M., Kürten, A., Laaksonen, A., Lehtipalo, K., Makhmutov, V., Mathot, S., Molteni, U., Onnela, A., Peräkylä, O., Piel, F., Petäjä, T., Praplan, A. P., Pringle, K., Rap, A., Richards, N. A. D., Riipinen, I., Rissanen, M. P., Rondo, L., Sarnela, N., Schobesberger, S., Scott, C. E., Seinfeld, J. H., Sipilä, M., Steiner, G., Stozhkov, Y., Stratmann, F., Tomé, A., Virtanen, A., Vogel, A. L., Wagner, A. C., Wagner, P. E., Weingartner, E., Wimmer, D., Winkler, P. M., Ye, P., Zhang, X., Hansel, A., Dommen, J., Donahue, N. M., Worsnop, D. R., Baltensperger, U., Kulmala, M., Carslaw, K. S. and Curtius, J.: Ion-induced nucleation of pure biogenic particles, Nature, 533(7604), 521, doi:10.1038/nature17953, 2016.

Klee, S., Derpmann, V., Wißdorf, W., Klopotowski, S., Kersten, H., Brockmann, K. J., Benter, T., Albrecht, S., Bruins, A. P., Dousty, F., Kauppila, T. J., Kostiainen, R., O'Brien, R., Robb, D. B. and Syage, J. A.: Are clusters important in understanding the mechanisms in atmospheric pressure ionization? Part 1: Reagent ion generation and chemical control of ion populations, J Am Soc Mass Spectrom, 25(8), 1310–1321, doi:10.1007/s13361-014-0891-2, 2014.

Knote, C., Hodzic, A. and Jimenez, J. L.: The effect of dry and wet deposition of condensable vapors on secondary organic aerosols concentrations over the continental US, Atmospheric Chemistry and Physics, 15(1), 1, doi:10.5194/acp-15-1-2015, 2015.

Krechmer, J. E., Coggon, M. M., Massoli, P., Nguyen, T. B., Crounse, J. D., Hu, W., Day, D. A., Tyndall, G. S., Henze, D. K., Rivera-Rios, J. C., Nowak, J. B., Kimmel, J. R., Mauldin, R. L., Stark, H., Jayne, J. T., Sipilä, M., Junninen, H., Clair, J. M. S., Zhang, X., Feiner, P. A., Zhang, L., Miller, D. O., Brune, W. H., Keutsch, F. N., Wennberg, P. O., Seinfeld, J. H., Worsnop, D. R., Jimenez, J. L. and Canagaratna, M. R.: Formation of Low Volatility Organic Compounds and Secondary Organic Aerosol from Isoprene Hydroxyhydroperoxide Low-NO Oxidation, Environmental Science & Technology, 49(17), 10330–10339, doi:10.1021/acs.est.5b02031, 2015.

Kroll, J. H., Donahue, N. M., Jimenez, J. L., Kessler, S. H., Canagaratna, M. R., Wilson, K. R., Altieri, K. E., Mazzoleni, L. R., Wozniak, A. S., Bluhm, H., Mysak, E. R., Smith, J. D., Kolb, C. E. and Worsnop, D. R.: Carbon oxidation state as a metric for describing the chemistry of atmospheric organic aerosol, Nature Chemistry, 3(2), 133–139, doi:10.1038/nchem.948, 2011.

Kürten, A., Jokinen, T., Simon, M., Sipilä, M., Sarnela, N., Junninen, H., Adamov, A., Almeida, J., Amorim, A., Bianchi, F., Breitenlechner, M., Dommen, J., Donahue, N. M., Duplissy, J., Ehrhart, S., Flagan, R. C., Franchin, A., Hakala, J., Hansel, A., Heinritzi, M., Hutterli, M., Kangasluoma, J., Kirkby, J., Laaksonen, A., Lehtipalo, K., Leiminger, M., Makhmutov, V., Mathot, S., Onnela, A., Petäjä, T., Praplan, A. P., Riccobono, F., Rissanen, M. P., Rondo, L., Schobesberger, S., Seinfeld, J. H., Steiner, G., Tomé, A., Tröstl, J., Winkler, P. M., Williamson, C., Wimmer, D., Ye, P., Baltensperger, U., Carslaw, K. S., Kulmala, M., Worsnop, D. R. and Curtius, J.: Neutral molecular cluster formation of sulfuric acid-dimethylamine observed in real time under atmospheric conditions, Proc Natl Acad Sci USA, 111(42), 15019–15024, doi:10.1073/pnas.1404853111, 2014.

Langford, B., Misztal, P. K., Nemitz, E., Davison, B., Helfter, C., Pugh, T. A. M., MacKenzie, A. R., Lim, S. F. and Hewitt, C. N.: Fluxes and concentrations of volatile organic compounds from a South-East Asian tropical rainforest, Atmospheric Chemistry and Physics, 10(17), 8391, doi:10.5194/acp-10-8391-2010, 2010.

Lau, Y. K., Ikuta, S. and Kebarle, P.: Thermodynamics and kinetics of the gas-phase reactions H3O+(H2O)n-1 + water = H3O+(H2O)n, Journal of the American Chemical Society, 104(6), 1462, doi:10.1021/ja00370a002, 1982.

Lee, B. H., Lopez-Hilfiker, F. D., Mohr, C., Kurtén, T., Worsnop, D. R. and Thornton, J. A.: An iodide-adduct high-resolution time-of-flight chemical-ionization mass spectrometer: application to atmospheric inorganic and organic compounds, Environmental Science & Technology, 48(11), 6309–6317, doi:10.1021/es500362a, 2014.

Lehtipalo, K., Rondo, L., Kontkanen, J., Schobesberger, S., Jokinen, T., Sarnela, N., Kürten, A., Ehrhart, S., Franchin, A., Nieminen, T., Riccobono, F., Sipilä, M., Yli-Juuti, T., Duplissy, J., Adamov, A., Ahlm, L., Almeida, J., Amorim, A., Bianchi, F., Breitenlechner, M., Dommen, J., Downard, A. J., Dunne, E. M., Flagan, R. C., Guida, R., Hakala, J., Hansel, A., Jud, W., Kangasluoma, J., Kerminen, V.-M., Keskinen, H., Kim, J., Kirkby, J., Kupc, A., Kupiainen-Määttä, O., Laaksonen, A., Lawler, M. J., Leiminger, M., Mathot, S., Olenius, T., Ortega, I. K., Onnela, A., Petäjä, T., Praplan, A., Rissanen, M. P., Ruuskanen, T., Santos, F. D., Schallhart, S., Schnitzhofer, R., Simon, M., Smith, J. N., Tröstl, J., Tsagkogeorgas, G., Tomé, A., Vaattovaara, P., Vehkamäki, H., Vrtala, A. E., Wagner, P. E., Williamson, C., Wimmer, D., Winkler, P. M., Virtanen, A., Donahue, N. M., Carslaw, K. S., Baltensperger, U., Riipinen, I., Curtius, J., Worsnop, D. R. and Kulmala, M.: The effect of acid-base clustering and ions on the growth of atmospheric nano-particles, Nat Commun, 7, 11594, doi:10.1038/ncomms11594, 2016.

Lopez-Hilfiker, F. D., Iyer, S., Mohr, C., Lee, B. H., DaposAmbro, E. L., Kurtén, T. and Thornton, J. A.: Constraining the sensitivity of iodide adduct chemical ionization mass spectrometry to multifunctional organic molecules using the collision limit and thermodynamic stability of iodide ion adducts, Atmospheric Measurement Techniques, 9(4), 1505, doi:10.5194/amt-9-1505-2016, 2016.

Lopez-Hilfiker, F. D., Mohr, C., Ehn, M., Rubach, F., Kleist, E., Wildt, J., Mentel, T. F., Carrasquillo, A. J., Daumit, K. E., Hunter, J. F., Kroll, J. H., Worsnop, D. R. and Thornton, J. A.: Phase partitioning and volatility of secondary organic aerosol components formed from α-pinene ozonolysis and OH oxidation: the importance of accretion products and other low volatility compounds, Atmospheric Chemistry and Physics, 15(14), 7765, doi:10.5194/acp-15-7765-2015, 2015.

Lopez-Hilfiker, F. D., Mohr, C., Ehn, M., Rubach, F., Kleist, E., Wildt, J., Mentel, T. F., Lutz, A., Hallquist, M., Worsnop, D. and Thornton, J. A.: A novel method for online analysis of gas and particle composition: description and evaluation of a Filter Inlet for Gases and AEROsols (FIGAERO), Atmospheric Measurement Techniques, 7(4), 983, doi:10.5194/amt-7-983-2014, 2014.

Mentel, T. F., Springer, M., Ehn, M., Kleist, E., Pullinen, I., Kurtén, T., Rissanen, M., Wahner, A. and Wildt, J.: Formation of highly oxidized multifunctional compounds: autoxidation of peroxy radicals formed in the ozonolysis of alkenes – deduced from structure–product relationships, Atmospheric Chemistry and Physics, 15(12), 6745, doi:10.5194/acp-15-6745-2015, 2015.

Midey, A. J., Arnold, S. T. and Viggiano, A. A.: Reactions of H3O+ (H2O) n with Formaldehyde and Acetaldehyde, The Journal of Physical …, 2000.

Millet, D. B., Baasandorj, M., Farmer, D. K., Thornton, J. A., Baumann, K., Brophy, P., Chaliyakunnel, S., de Gouw, J. A., Graus, M., Hu, L., Koss, A., Lee, B. H., Lopez-Hilfiker, F.

D., Neuman, J. A., Paulot, F., Peischl, J., Pollack, I. B., Ryerson, T. B., Warneke, C., Williams, B. J. and Xu, J.: A large and ubiquitous source of atmospheric formic acid, Atmospheric Chemistry and Physics, 15(11), 6283, doi:10.5194/acp-15-6283-2015, 2015.

Misztal, P. K., Nemitz, E., Langford, B., Di Marco, C. F., Phillips, G. J., Hewitt, C. N., MacKenzie, A. R., Owen, S. M., Fowler, D., Heal, M. R. and Cape, J. N.: Direct ecosystem fluxes of volatile organic compounds from oil palms in South-East Asia, Atmospheric Chemistry and Physics, 11(17), 8995, doi:10.5194/acp-11-8995-2011, 2011.

Mohr, C., DeCarlo, P. F., Heringa, M. F., Chirico, R., Slowik, J. G., Richter, R., Reche, C., Alastuey, A., Querol, X., Seco, R., Peñuelas, J., Jimenez, J. L., Crippa, M., Zimmermann, R., Baltensperger, U. and Prévôt, A. S. H.: Identification and quantification of organic aerosol from cooking and other sources in Barcelona using aerosol mass spectrometer data, Atmospheric Chemistry and Physics, 12(4), 1649, doi:10.5194/acp-12-1649-2012, 2012.

Mohr, C., Lopez-Hilfiker, F. D., Zotter, P., Prévôt, A. S. H., Xu, L., Ng, N. L., Herndon, S. C., Williams, L. R., Franklin, J. P., Zahniser, M. S., Worsnop, D. R., Knighton, W. B., Aiken, A. C., Gorkowski, K. J., Dubey, M. K., Allan, J. D. and Thornton, J. A.: Contribution of nitrated phenols to wood burning brown carbon light absorption in Detling, United Kingdom during winter time, Environmental Science & Technology, 47(12), 6316–6324, doi:10.1021/es400683v, 2013.

Müller, M., Graus, M., Ruuskanen, T. M., Schnitzhofer, R., Bamberger, I., Kaser, L., Titzmann, T., Hörtnagl, L., Wohlfahrt, G., Karl, T. and Hansel, A.: First eddy covariance flux measurements by PTR-TOF, Atmospheric Measurement Techniques, 3(2), 387–395, doi:10.5194/amt-3-387-2010, 2010.

Nguyen, T. B., Crounse, J. D., Teng, A. P., Clair, J. M. S., Paulot, F., Wolfe, G. M. and Wennberg, P. O.: Rapid deposition of oxidized biogenic compounds to a temperate forest, Proc Natl Acad Sci USA, 112(5), E392–401, doi:10.1073/pnas.1418702112, 2015.

Ortega, J., Turnipseed, A., Guenther, A. B., Karl, T. G., Day, D. A., Gochis, D., Huffman, J. A., Prenni, A. J., Levin, E. J. T., Kreidenweis, S. M., DeMott, P. J., Tobo, Y., Patton, E. G., Hodzic, A., Cui, Y. Y., Harley, P. C., Hornbrook, R. S., Apel, E. C., Monson, R. K., Eller, A. S. D., Greenberg, J. P., Barth, M. C., Campuzano-Jost, P., Palm, B. B., Jimenez, J. L., Aiken, A. C., Dubey, M. K., Geron, C., Offenberg, J., Ryan, M. G., Fornwalt, P. J., Pryor, S. C., Keutsch, F. N., DiGangi, J. P., Chan, A. W. H., Goldstein, A. H., Wolfe, G. M., Kim, S., Kaser, L., Schnitzhofer, R., Hansel, A., Cantrell, C. A., Mauldin, R. L. and Smith, J. N.: Overview of the Manitou Experimental Forest Observatory: site description and selected science results from 2008 to 2013, Atmospheric Chemistry and Physics, 14(12), 6345, doi:10.5194/acp-14-6345-2014, 2014.

Saint Clair, J. M., Spencer, K. M., Beaver, M. R., Crounse, J. D., Paulot, F. and Wennberg, P. O.: Quantification of hydroxyacetone and glycolaldehyde using chemical ionization mass spectrometry, Atmospheric Chemistry and Physics, 14(8), 4251, doi:10.5194/acp-14-4251-2014, 2014.

Schobesberger, S., Franchin, A., Bianchi, F., Rondo, L., Duplissy, J., Kürten, A., Ortega, I. K., Metzger, A., Schnitzhofer, R., Almeida, J., Amorim, A., Dommen, J., Dunne, E. M., Ehn, M., Gagné, S., Ickes, L., Junninen, H., Hansel, A., Kerminen, V. M., Kirkby, J., Kupc, A., Laaksonen, A., Lehtipalo, K., Mathot, S., Onnela, A., Petäjä, T., Riccobono, F., Santos, F. D., Sipilä, M., Tomé, A., Tsagkogeorgas, G., Viisanen, Y., Wagner, P. E., Wimmer, D., Curtius, J., Donahue, N. M., Baltensperger, U., Kulmala, M. and Worsnop, D. R.: On the composition of ammonia–sulfuric-acid ion clusters during aerosol particle formation, Atmospheric Chemistry and Physics, 15(1), 55, doi:10.5194/acp-15-55-2015, 2015.

Tröstl, J., Chuang, W. K., Gordon, H., Heinritzi, M., Yan, C., Molteni, U., Ahlm, L., Frege, C., Bianchi, F., Wagner, R., Simon, M., Lehtipalo, K., Williamson, C., Craven, J. S., Duplissy, J., Adamov, A., Almeida, J., Bernhammer, A.-K., Breitenlechner, M., Brilke, S., Dias, A., Ehrhart, S., Flagan, R. C., Franchin, A., Fuchs, C., Guida, R., Gysel, M., Hansel, A., Hoyle, C. R., Jokinen, T., Junninen, H., Kangasluoma, J., Keskinen, H., Kim, J., Krapf, M., Kürten, A., Laaksonen, A., Lawler, M., Leiminger, M., Mathot, S., Möhler, O., Nieminen, T., Onnela, A., Petäjä, T., Piel, F. M., Miettinen, P., Rissanen, M. P., Rondo, L., Sarnela, N., Schobesberger, S., Sengupta, K., Sipilä, M., Smith, J. N., Steiner, G., Tomé, A., Virtanen, A., Wagner, A. C., Weingartner, E., Wimmer, D., Winkler, P. M., Ye, P., Carslaw, K. S., Curtius, J., Dommen, J., Kirkby, J., Kulmala, M., Riipinen, I., Worsnop, D. R., Donahue, N. M. and Baltensperger, U.: The role of low-volatility organic compounds in initial particle growth in the atmosphere, Nature, 533(7604), 527, doi:10.1038/nature18271, 2016.

Veres, P. R., Roberts, J. M., Cochran, A. K., Gilman, J. B., Kuster, W. C., Holloway, J. S., Graus, M., Flynn, J., Lefer, B., Warneke, C. and de Gouw, J.: Evidence of rapid production of organic acids in an urban air mass, Geophysical research letters, 38(17), n/a, doi:10.1029/2011gl048420, 2011.

Veres, P., Gilman, J. B., Roberts, J. M., Kuster, W. C., Warneke, C., Burling, I. R. and de Gouw, J.: Development and validation of a portable gas phase standard generation and calibration system for volatile organic compounds, Atmospheric Measurement Techniques, 3(3), 683, doi:10.5194/amt-3-683-2010, 2010.

Veres, P., Roberts, J. M., Warneke, C., Welsh-Bon, D., Zahniser, M., Herndon, S., Fall, R. and de Gouw, J.: Development of negative-ion proton-transfer chemical-ionization mass spectrometry (NI-PT-CIMS) for the measurement of gas-phase organic acids in the atmosphere, International Journal of Mass Spectrometry, 274(1-3), 48, doi:10.1016/j.ijms.2008.04.032, 2008.

Viidanoja, J., Reiner, T. and Arnold, F.: Laboratory investigations of negative ion molecule reactions of formic and acetic acids: implications for atmospheric measurements by ion-molecule reaction …, International Journal of Mass Spectrometry, 1998.

Washenfelder, R. A., Roehl, C. M., McKinney, K. A., Julian, R. R. and Wennberg, P. O.: A compact, lightweight gas standards generator for permeation tubes, Review of Scientific Instruments, 74(6), 3151, doi:10.1063/1.1570949, 2003.

Yatavelli, R. L. N., Lopez-Hilfiker, F., Wargo, J. D., Kimmel, J. R., Cubison, M. J., Bertram, T. H., Jimenez, J. L., Gonin, M., Worsnop, D. R. and Thornton, J. A.: A Chemical Ionization High-Resolution Time-of-Flight Mass Spectrometer Coupled to a Micro Orifice Volatilization Impactor (MOVI-HRToF-CIMS) for Analysis of Gas and Particle-Phase Organic Species, Aerosol Science and Technology, 46(12), 1313, doi:10.1080/02786826.2012.712236, 2012.

Zhang, Q., Alfarra, M. R., Worsnop, D. R., Allan, J. D., Coe, H., Canagaratna, M. R. and Jimenez, J. L.: Deconvolution and Quantification of Hydrocarbon-like and Oxygenated Organic Aerosols Based on Aerosol Mass Spectrometry, Environmental Science & Technology, 39(13), 4938, doi:10.1021/es048568l, 2005.

Zhang, Q., Jimenez, J. L., Canagaratna, M. R., Allan, J. D., Coe, H., Ulbrich, I., Alfarra, M. R., Takami, A., Middlebrook, A. M., Sun, Y. L., Dzepina, K., Dunlea, E., Docherty, K., DeCarlo, P. F., Salcedo, D., Onasch, T., Jayne, J. T., Miyoshi, T., Shimono, A., Hatakeyama, S., Takegawa, N., Kondo, Y., Schneider, J., Drewnick, F., Borrmann, S., Weimer, S., Demerjian, K., Williams, P., Bower, K., Bahreini, R., Cottrell, L., Griffin, R. J., Rautiainen, J., Sun, J. Y., Zhang, Y. M. and Worsnop, D. R.: Ubiquity and dominance of oxygenated species in organic aerosols in anthropogenically-influenced Northern Hemisphere midlatitudes, Geophysical research letters, 34(13), n/a, doi:10.1029/2007gl029979, 2007.

de Gouw, J. and Warneke, C.: Measurements of volatile organic compounds in the earth's atmosphere using proton-transfer-reaction mass spectrometry, Mass Spectrom Rev, 26(2), 223–257, doi:10.1002/mas.20119, 2006.